AN EXPERIMENTAL STUDY OF THE SMALL STRAIN RESPONSE OF SAND

by

DAWIT NEGUSSEY

B.Sc., Southern Illinois University, 1971

M.Sc.C.E., University of Minnesota, 1973

A THESIS SUBMITTED IN PARTIAL FULFILLMENT OF

THE REQUIREMENTS FOR THE DEGREE OF

DOCTOR OF PHILOSOPHY

in

THE FACULTY OF GRADUATE STUDIES

DEPARTMENT OF CIVIL ENGINEERING

We accept this thesis as conforming

to the required standard

THE UNIVERSITY OF BRITISH COLUMBIA

December 1984

Department of Civil Engineering

The University of British Columbia
2075 Wesbrook Place
Vancouver, Canada
V6T 1W5

Date December 28, 1984

ABSTRACT

Fundamental behaviour of Ottawa sand, in the strain range of 1×10^{-2} to 1×10^{-5}, is investigated by direct measurement of deformations in a load controlled conventional triaxial system. Experiments are aimed at examining common concepts and previous experimental justifications for incremental elastic, elasto-plastic and particulate frameworks for characterizing sand behaviour. From fundamental interpretation of test data, an alternative stress-strain relationship is proposed for proportional loading with relative density represented as a separate parameter.

Maximum Young's moduli evaluated from resonant column tests are found to be approximately equal to initial unloading moduli from conventional triaxial tests and initial moduli from virgin loading and subsequent reloadings are much less. Initial unloading moduli are relatively unaffected by the cycle of loading and deviator stress level from which unloading is initiated. The value of Young's modulus at a stress state is not unique but depends on the stress path and strain history.

Nonrecovered strain directions, at small strain, depend on stress direction as opposed to the generally accepted dependence on stress state at large strain. Proportional loading paths are uniquely related to linear strain increment directions and maintain parallel mean normal stress equipotentials in strain space. Energy density increments in two proportional loading paths having identical mean normal stress histories remain proportional. Parallel nonproportional loadings result in a unique strain increment direction, relatively

independent of hydrostatic stress level, with linear stress ratio equipotentials in strain space.

In small strain response, shear strains result mainly from shear stress increments and not from changes in stress ratio. Shear volume response is contractant for both an increasing and decreasing shear stress increment, whereas the sense of shear strain increment alternates with the sense of shear stress increment. When the sense of strain state is opposite to the sense of an applied stress increment, the resulting stress-strain response is softer than when both are of the same sense. Strain paths for compression side shear loading are identical to paths of extension side shear unloading and vice versa. More shear and volumetric strains develop on extension side shear loadings and the ratio of volumetric to shear strain is also higher as opposed to comparable compression side shear loadings.

At higher stress ratio states, decreasing mean normal stress at constant shear and increasing stress ratio conditions; extension side volumetric strain responses are associated with contraction following initial swelling and prior to dilation. This contraction phase is not present on the compression side.

Y.P. Vaid

Thesis Supervisor

TABLE OF CONTENTS

LIST OF FIGURES

INDEX OF NOTATIONS

B_t	tangent bulk modulus
D	dilatancy = $1 - \frac{\delta\varepsilon_v}{\delta\varepsilon_a}$
d	energy density ratio per cycle of consolidation stress ratio
D_r	relative density state
δ	increment
E	Young's Modulus
E_i	initial E in loading
E_{ir}	initial E in reloading
E_{iu}	initial E in unloading
E_{max}	maximum E
E_t	tangent E
ε_a	axial strain
ε_r	radial strain
ε_s	shear strain = $\varepsilon_a - \varepsilon_r$
ε_v	volumetric strain = $\varepsilon_a + 2\varepsilon_r$
θ	direction of strain vector
K_{cv}	upper bound of energy increment ratio
K_E	modulus number
K_o	inverse stress ratio for zero lateral deformation
K_μ	lower bound of energy increment ratio
m	slope of the relationship between ε_a/σ_d and ε_a in small strain response
μ	Poisson's ratio

n	modulus exponent, represents an E_i for a confining stress equal to atmospheric pressure and divided by P_a
η	stress ratio = $\frac{q}{p'}$
η_{cv}	stress ratio at critical state and zero rate of volume change
P_a	atmospheric pressure
p'	effective mean normal stress = $\frac{\sigma_1' + 2\sigma_3'}{3}$
q	shear stress = $\sigma_1' - \sigma_3'$
Q	energy density state
R	stress ratio = $\frac{\sigma_a'}{\sigma_r'}$
r	incremental stress ratio = $\frac{\delta\sigma_a'}{\delta\sigma_r'}$
S	slope of the relationship between W_s and ε_s
σ_1'	major effective principal stress
σ_3'	minor effective principal stress
σ_a'	axial effective stress
σ_d	deviator stress = $\sigma_a - \sigma_r$
σ_r'	radial effective stress
ϕ	friction angle
ϕ_μ	a material characteristic interparticle friction angle
ϕ_{cv}	friction angle at critical state and zero volume change
W_s	work done in shear
ψ	gradient of stress equipotentials in strain space.

ACKNOWLEDGEMENTS

I am greatly indebted to my supervisor, Professor Y.P. Vaid, for his guidance, encouragement and enthusiastic interest throughout this research. I would also like to thank Professors P.M. Byrne, R.G. Campanella and W.D.L. Finn for their advice and counsel. My colleagues J.C. Chern, E. Cheung, A. Sayao, M. Zergoun and especially, P. Lui, shared a common active interest in soil mechanics. I thank them all for their helpful discussions and constructive criticisms.

The task of equipment development was made easier by the advice and assistance of Mr. F. Zurkirchen. Ms. S.N. Krunic typed the manuscript with care and the figures were skillfully drafted by Mrs. M. Sayao. I am grateful for their patience and hard work.

Support and assistance provided by the University of British Columbia, the Natural Science and Engineering Research Council of Canada and Golder Geotechnical Consultants is acknowledged with deep appreciation.

A very special thanks go to my wife, Atsede, and my son, Brook; whose encouragement, optimism and support sustained me through stress and strain.

CHAPTER I - INTRODUCTION

The engineering of sand is often associated with boundary value problems that require a rational stress-strain law for satisfactory solution. Sand possesses a relatively high permeability and insignificant creep deformation properties. Essential features of the stress-strain behaviour of sand are considered to be contained within a time independent domain. A number of constitutive models for sand have been proposed. All are founded upon certain assumptions and hypotheses; with guidance and motivation engendered from experimental observations.

For several decades, research interest has focused heavily on the strength behaviour of sand. Because of uncertainties inherent in soil exploration and assessment of strength properties, foundations are usually designed with generous safety factors against failure. Except perhaps along localized stress concentrations, working stress levels are much below failure. For both loose and dense sand subjected to conventional triaxial stress paths, a significant proportion of peak strength is mobilized at small strain. Working stresses under drained conditions generally induce strains that are less than 1 percent. Similarly, tendencies toward volume contraction and the corresponding development of positive pore pressure during undrained loading are phenomena that occur mainly at small strain.

On account of possible errors and experimental limitations, small deformations associated with strains below 1×10^{-5} are difficult to measure directly. Behaviour at such strain levels is relevant for dynamic response and is assessed indirectly through resonance and wave propagation considerations assuming elastic behaviour. With careful equipment design; small strain response, between 1×10^{-5} and 1×10^{-2}, can be investigated through direct measurement of associated deformations. In previous studies of drained response by direct measurement of deformations, interest was mainly concerned with strain levels in excess of 1×10^{-3}.

Shear induced volume change is a distinct characteristic of particulate materials like sand. Such volume change has often been regarded to be synonymous with dilatancy, or shear volume expansion, in many previous considerations. It is, however, widely known that shear induced volume change can either be contractant or dilatant. For stress ratios approaching failure and associated large strain levels, dilatant effects generally predominate. Whereas, for stress ratios normally associated with working stress levels and thus small strain, contractant shear volume change assumes greater importance. Over all, contractancy would appear to be of much more fundamental interest in the study of sand behaviour. In a broader context, generation of positive pore pressure in undrained shearing is a consequence of contractancy.

Current understanding of the contractant behaviour of sand is very limited. Experimental observations relevant to dilatancy may not be applicable to situations of contractant response. Recoverable deformations become negligible in the dilatant region, whereas, both recoverable and nonrecoverable strain components become significant in the region of contractancy. Elastic-plastic separation of strains is usually deemed feasible through a load unload procedure. However, the experimental evidence in support of such separation does not appear to be convincing. The inevitable existence of inelastic strains as a consequence of reverse slip during unloading can not be denied.

This research focuses on a fundamental experimental investigation of the behaviour of sand at small strain. Some common frameworks and experimental justifications for describing the behaviour of sand as incrementally elastic, elasto-plastic and from particulate considerations are critically examined as to their validity in the region of small strains. Through exercise of systematic and precision oriented experimentation, new observations and consistent trends in small strain response of sand are presented. A fundamental interpretation of test data and an alternative description of stress-strain behaviour is attempted.

Sand behaviour is examined predominantly at a relative density of 50 percent in simple stress paths. The study is concerned with drained deformation response. Behavioural effects of stress parameters and relative density state were examined maintaining wide intervals in both stress and relative density such that the effect of the variables can be established with certainty. Test results are presented and compared in conventional stress-strain representation in order to examine common concepts in small strain region. As well, correspondence between states of stress and strain are investigated in strain rather than stress space.

Pursuit of these objectives required, as a prerequisite, reliable data from carefully performed experiments. Small strain observations cannot be reliably extracted from test setups assembled for the study of large strain response. A measurement range and sensitivity suitable for large strain study are generally too coarse and insensitive for reliable observation of small strain phenomena. Experimental procedures and improvements adopted to enhance large strain investigation may not be useful or even be counterproductive for small strain observations. As a result, test equipment and procedures are critically evaluated and overhauled with the explicit intention of optimizing accuracy and fulfillment of necessary assumptions with regards to small strain study. This necessitated improvement in test equipment in order to facilitate precise loading control, including the ability to follow arbitrary stress paths; and a critical evaluation of available methods, and development of alternative rational procedures, for membrane compliance correction.

CHAPTER II - STRESS-STRAIN RESPONSE OF SAND

Until the recent past, the performance of sand was predominantly evaluated solely in terms of failure. In most cases, design was based on limit equilibrium analyses and without regard to associated deformations. However, rapid introduction of computing facilities made possible the use of numerical solutions to many deformation problems in geotechnical engineering. The desire for implementing this newly acquired capability to practical use has imposed a sudden demand for some form of constitutive input.

Over the past several years, a number of researchers have contributed to a fundamental understanding of the stress-strain behaviour of sand through experimental study. The studies ushered in several improvements in test techniques and equipment, including the use of a variety of test apparatus. However, for the most part, interest has focused on large strain response (generally in excess of 1%) and that too under a limited number of stress paths, all leading to failure. The study of small strain phenomena has been very limited.

2.1 Observed Behaviour

Initial interest in examining shear volume change in sands was motivated by a desire to explain experimentally observed phenomena related to shear strength testing (Taylor, 1948; Bishop, 1950). An energy correction concept was introduced to separate work related to dilation or contraction from that due to friction. Closer agreement between strengths of dense and loose sands was obtained following energy correction. Consideration of shear volume change in the prefailure region did not emerge until the introduction of stress dilatancy concepts several years later (Rowe, 1962).

With the objective of describing sand response within a linear elastic framework, earlier experimental investigators attempted to establish the influence of shear and confining stress on moduli and Poisson's ratio (Chen, 1948; Jakobson, 1957; Makhlouf & Stewart, 1965). Although the test equipment and experimental techniques were much less refined, their qualitative observations regarding the strong influence of density or void ratio, shear and confining stress on strain response remain valid. Such observations of nonlinearity and stress level dependence of stress-strain behaviour are features central to empirical representations that are in wide use today.

Further investigations demonstrated that the stress strain behaviour of sand is path dependent and is influenced by stress history (Lade and Duncan, 1976; Lambrechts and Leonards, 1978; Varadarajan et al, 1983). Upon stress reversal from a stress state near failure, anisotropy induced during shear in one direction has been shown to alter shear deformation characteristics in the opposite direction (Arthur, 1971; Thurairajah, 1973). However, when stress reversal was initiated from a stress state significantly below failure, the response was found to be independent of the loading history in the opposite direction (Tatsuoka and Ishihara, 1974). Apart from the strong influence of density on stress-strain response, structure or soil fabric, as determined by predominant grain orientation, has been shown to significantly alter the nature of inherent anisotropy, in otherwise identical specimens (Arthur and

Menzies, 1972; Yamada and Ishihara, 1979; Oda, 1972, 1976). The effect of inherent anisotropy on small strain response has also been demonstrated to be significant, whereas strength properties have been found to be relatively unaffected. These observations have led to the suggestion that inherent anisotropy becomes erased by stress induced anisotropy that develops with shear loading (Yamada and Ishihara, 1979). Pluviated sand samples acquire a preferred grain orientation and as a result have a stiffer response in the direction of deposition. The degree of inherent anisotropy, as inferred from strain response in hydrostatic compression tests, has been shown to diminish with increasing density (El-Sohby and Andrawes, 1972). However, the influence of the densification procedure in changing the nature of inherent anisotropy has not been clarified.

Strain paths under proportional loading and unloading at low stress ratio levels have been found to be linear (El-Sohby, 1969; El-Sohby and Andrawes, 1973) . Changes in mean normal stress were inferred not to alter inherent anisotropy so long as the stress ratio remained constant. Rowe (1971) has pointed out that the linearity of loading and unloading strain paths during proportional loading of sand also implies linearity for the nonrecovered strain paths. This behaviour bears close resemblance to observed linearity of total, recovered and nonrecovered strain paths during proportional loading of metals (Mehan, 1961; Rees, 1981; 1981a)

The strength of sand has been known to be influenced by rate of loading (Whitman, 1957; Horne, 1965). However, reported stress-strain studies invariably dwell in a time independent domain. There is generally no expressed concern relative to procedures adopted to suppress or assess the relative influence of transient response (commonly identified with creep) during previous investigations. Yet, due consideration and minimization of transient effects is essential for quantitative correspondence between test results.

2.2 Idealization of Behaviour as Either Elastic or Plastic

In analyses of material response, it is often convenient to idealize behaviour as either a purely elastic or plastic continuum. The viability of such idealized representation for sand has been examined in previous experimental investigations, and primarily from simple shear and triaxial tests (Cole, 1967; Roscoe, 1970; Frydman and Zeitlen, 1969).

A simple shear test permits a continuous rotation of principal axes of stress and strain, whereas these axes are fixed in a triaxial test. Coincidence of principal axes of strain rate and stress increment would characterize elastic behaviour (Jaeger, 1964); whereas, principal axes of strain rate and stress would coincide for a plastic material (Hill, 1964). Roscoe (1970), in his Rankine Lecture, reported on important experimental findings from simple shear tests on sand regarding orientations of principal axes of stress, stress increment and strain rate. A coincidence of principal axes of stress and total strain increment was noted under monotonic loading but following attainment of a minimum void ratio. This implies that the stress-strain response of sand when subjected to increasing shear stress and beyond a stage of maximum volumetric contraction resembles ideal plastic behaviour. An initial zero rate of volume change invariably coincides with mobilization of shear strength corresponding to a constant volume friction angle of ϕ_{cv} for sand and at relatively large shear strain. Although less convincing, there was also evidence in support of coincidence of principal axes of stress increment and strain rate during unloading and reloading, thus suggesting some basis for an elastic approximation of unloading and reloading response of sand. However, during virgin loading and prior to maximum contraction, coincidence of neither principal axes of stress nor stress increment with principal axes of strain rate could be inferred with certainty. This uncertainty in part reflects the inherent limitations of the simple shear apparatus relative to determination of stress state and measurement of small deformations (Saada et al, 1980; 83; Cole, 1967; Budhu, 1984; Arthur et al, 1980). At the same time, it also reflects the comparable presence of elastic and plastic responses in the early stages of shearing and that behaviour would not be adequately represented as purely elastic or plastic.

Triaxial test results have been used to demonstrate the usefulness of pseudo-elastic idealization for dense sand (Frydman and Zeitlen, 1969). Considerations were restricted to shear stress states below that corresponding to the material friction angle, Φ_μ, and therefore small strain. Experimental results that suggest an absence of shear volume change were shown and this observation was advanced as justification for a purely elastic idealization of stress-strain response. However, contractant shear induced volume changes occur at small stress ratios and all levels of relative density, becoming more pronounced with decreasing density. Consequently, the experimental evidence presented in support of a pseudo elastic characterization of sand would appear to be realistic when considering dense states only. With decreasing relative density, an elastic approximation would become less desirable as both elastic and plastic responses assume relative importance.

2.3 Particulate Considerations

On a visual scale, sand is a particulate material. Its aggregate behaviour is intermediate between a fluid and a solid with the added shear volume change a peculiar characteristic. Under idealized conditions of particle geometry and packing, the load deformation characteristics of a granular mass can be derived from grain contact considerations. Regular packing of spheres have therefore been studied to gain fundamental understanding of deformation response.

At a plane of contact between two spheres within regular packing; torsion, shear and normal stresses can exist. In the absence of torsion and shear; Hertz's contact theory (Timoshenko and Goodier, 1970) predicts a linear relationship between elastic volumetric strain and the 2/3 power of mean normal stress for a set of isotropic elastic equal spheres. Consideration of torsion and shear at grain contact introduce inelasticity (Dereswicz, 1957) and shear volume change of void space. The kind of shear volume change is determined by density of packing. A simple cubic array, which constitutes a loose packing with a void ratio of 0.910, would experience contraction; whereas dense packing, such as in a face centered cubic array (void ratio of 0.351) would dilate. The nature of shear volume change of granular materials can therefore be either contractant or dilatant depending on the state of packing or density.

The study of idealized geometry, packing and material brings out essential deformation response features to focus. It makes possible the qualitative understanding of sand behaviour within a restricted framework. However, its direct extension towards describing sand would fall short of its intended objective (Rowe, 1971). Individual sand particles are irregular shaped and grain sizes vary. Also, some amount of particle crushing would inevitably occur. Slip and rearrangement would take place at all stress levels and stress paths. In such irregular assemblies, the distribution of contact stresses for particles not in limiting equilibrium cannot be determined. Stress-strain parameters would vary with orientation to crystal structures. Because of these limitations, interpretation of sand behaviour within a particulate framework required an emperical approach using alternative assumptions.

Treatment of sand from particulate considerations gained new ground with the introduction of stress dilatancy theory (Rowe, 1962). As pointed out previously, a desire to separate stress ratio into frictional and dilatancy components appears to have motivated initial interest (Rowe et al, 1964, Bishop, 1964). Since the stress ratio, $R=\sigma_1'/\ \sigma_3'$ is associated with assumed slip strain increment ratio, the stress dilatancy equation, R = KD, was suggested to hold real promise of providing a realistic nonassociated flow rule for particulate materials (Rowe, 1971; Barden and Khayatt, 1966; Cole, 1967). However, the association between stress ratio and dilation rate D is not unique. The difference between upper and lower bounds in K, (corresponding to ϕ_{cv} and ϕ_μ) for sand is of the order of 25 percent and cannot be considered small even though proponents of stress dilatancy suggest otherwise (Barden and Khayatt, 1966). Stress dilatancy theory has been considered valid for stress paths of increasing stress ratio (Rowe, 1971) and shown to be path independent (Tatsuoka, 1976; Cole, 1967). However, reported experimental verifications are invariably from large strain response and along paths that ultimately lead to failure.

A separate class of stress paths that do not lead to failure but are nevertheless paths of increasing stress ratio exist (Hardin, 1983). Validity of stress-dilatancy along such paths that have an orientation between $R = 1/K_o$ and a hydrostatic stress path has not been demonstrated. A hydrostatic path would not conform to stress-dilatancy because the associated energy ratio would not be negative (Barden et al, 1969). A singularity would be objectionable on physical grounds and hence there must exist a neighborhood about the hydrostatic axis within which stress dilatancy would not apply. This same argument can be extended to question the suggested validity of stress-dilatancy in constant stress ratio paths.

In an extension to his earlier work, Rowe (1971) made an alternative proposal for incorporating constant stress ratio response within a stress dilatancy framework. He proposed a conceptual uncoupling of stress increments into vertical and radial components and imposed compressional and extensional stress dilatancy relationships to the uncoupled components respectively. For any uncoupled stress increment along a proportional loading path, both uncoupled stress components would not be associated with increasing stress ratio directions simultaneously. Thus, the conceptual uncoupling of stress increments and implied validity of stress-dilatancy in a direction of decreasing stress ratio is contrary to earlier assumptions. Furthermore, the quoted expression for the uncoupled radial stress increment does not appear to be correct, casting further doubt on the merits of Rowe's proposal.

Shearing of sand along a failure path induces contraction up until significant strength mobilization. Most practical deformation problems lie well below failure. Recoverable strains in this small deformation region are relatively significant and thus a pseudo plastic idealization, as would be implied by stress dilatancy, may not be appropriate. Although there has been interest in using a stress dilatancy relationship as a flow rule in stress deformation modelling of sand (Nova and Wood, 1979; Bardet, 1983), its presumed validity and extrapolation to the region of small strain still remains uncertain (Arthur, 1971). Arguments in favour of a different stress dilatancy relationship for small strain response have been put forward (Nova and Wood, 1979). However, this hypothesis has yet to be verified experimentally.

2.4 Decomposition of Strain

In general, neither a pseudo elastic nor plastic representation has been found to fully characterize the small strain response of sand. More appeal has therefore been made to simultaneous but separate elastic-plastic idealization of behaviour, assuming correspondence between recovered and slip deformations to elastic and plastic strains, respectively. The required decomposition of total strains into elastic and plastic components has generally been considered possible through a load unload procedure. Whether such a separation holds true for sand must, however, be demonstrated by comparing presumed strain components against characteristic behaviour.

A given response would need to satisfy set preconditions to justify classifications as either elastic or plastic. The possible elastic character of recoverable deformations was examined by Holubec (1968). He presented experimental results on dense sand that show no hystereisis upon unloading and reloading up to 80 percent of maximum shear strength. Furthermore, he found incremental elastic properties evaluated at stress points to be independent of stress history. These observations in and of themselves are necessary but not sufficient to establish the elastic character of recovered deformations. For an elastic material, integration of incremental stress-strain equations must also be path independent but the test results have been shown not to satisfy this condition (Coon and Evans, 1969). Moreover, the incremental equations used by Holubec were shown to require an additional term (Merkele and Merkele, 1969). Furthermore, the reported experimental results appear to be erroneous in that the reloading curves stiffen instead of soften with strain. Clearly, Holubec's optimistic outlook from examination of dense sand would not be as encouraging if consideration were to focus on loose behaviour. Inspite of its shortcomings, Holubec's work is still widely referred to justify elastic treatment of recovered deformations.

Validity of elastic-plastic strain separation can also be examined from consideration of the nonrecovered deformations. The direction of plastic strain increment would be uniquely determined by the state of stress if the behaviour is plastic. Observations consistent with this criteria have been reported by Poorooshasb, et al, 1966; Lade and Duncan, 1976. Existence of a potential function whose gradient determines the inclination of the plastic strain increment was claimed. The plastic potential curves for a given void ratio were inferred to form a family of geometrically similar curves closing on the failure and hydrostatic lines. A closer examination of the experimental evidence shows that the unique association of stress state and plastic strain increment vector has been demonstrated only for stress states in the proximity of failure and hence at large strain. As such, these findings are re-affirmations of the stress dilatancy theory of Rowe (1962) and evidence from simple shear test results of Cole (1967), both of which were based on total strain response. Slip at particle contacts is the predominant form of deformation at large strain. Since recoverable deformations are relatively small neither their inclusion or omission would have serious implication. However, the situation at small strain is much different in that both recovered and non-recovered deformations assume relative importance. Extrapolation of findings at large stress ratio to encompass response at small stress ratio is therefore unjustified. In a granular mass, slip and reverse slip would occur during loading and unloading. The isolation of elastic deformation of sand grains from slip occurring at grain contacts is virtually impossible.

Aside from attempts to examine recovered and nonrecovered deformations for symptoms of elastic or plastic behaviour, significant effort has also been directed towards modifying established elasto-plastic concepts to suit test results on sand. In this regard, intersecting yield surfaces and uncoupling of strains into two and three components are features that have been adopted to force fit soil within some form of elastic-plastic type of framework. There is as yet no concensus on a criterion for yielding and a nonassociated form of flow rule is often used. Even after radical alteration of established material models, it has been possible to characterize behaviour at only one void ratio and mostly dense states. The number of required parameters is cumbersome, sometimes in excess of 10, and have to be determined from several tests (Desai et al, 1981; Bardet, 1983). Generally, models need to be calibrated with reference to selected experimental data and tend to be less effective when called upon to make predictions under stress paths different from those considered for calibration (NSF/NSERC Workshop, 1980). Undoubtedly, a lot more remains to be done and the future direction and refinement of soil models will require new experimental findings and alternative ideas.

2.5 Trends in the Study of Sand Behaviour

As stated earlier, the small strain response of sand is a relatively unexplored territory. Although there is growing interest in using the stress dilatancy equation as a flow rule, its validity at small strain is uncertain. In some elastic-plastic approaches, yielding has been postulated to start at the onset of loading (Nova and Wood, 1979). This would imply there is no initial region wherein response would be entirely elastic. A concept of normalized work, introduced by Moroto (1976), has inspired new elastic-plastic model proposals for sand (Ghabaussi and Momen, 1984, 1982; Tobita and Yanagisawa, 1980; Varadarajan et al, 1983). In this concept, the relationship between the work intergal due to shear, normalized by the corresponding mean normal effective stress, and shear strain is suggested to be unique. The slope of this relationship has been further observed to represent a material parameter independent of mean normal effective stress and density. The experimental verification and possible implications of this concept do not, however, appear to have been critically examined.

In view of the impossibility of separation of elastic and plastic strains and the observation that total strains may not be adequately represented as elastic, appeal has been made to considering all deformations as plastic (Mroz, 1983; Chang, 1983). This is contrary to previous suggestion that small strain response be represented as pseudo elastic.

A radical departure from current concepts of stress-strain modelling has been proposed by Zytynski, Randolph, Nova and Wroth (1978). They reject the idea of a purely elastic response at any stage and point out that it would be impossible to isolate elastic and plastic strain components. Furthermore, they and subsequently Bardet (1983), have demonstrated inconsistencies in some current assumptions that lead to extraction of work in a cycle of loading. Zytynski et al proposed an alternative conceptual representation of sand as linked springs and frictional blocks. This would allow simultaneous development of elastic and slip deformations at all times. Although such a mechanical idealization may be useful as a conceptual framework, it appears unrealistic for representing actual response. Further progress in this direction has not been reported to date.

In general, developments have advanced progressively from successful prescription of failure to reasonable but qualitative description of large strain behaviour. Study of small strain phenomena and development of procedures for quantitative description of sand appear to be the direction for future progress.

CHAPTER III - EXPERIMENTAL CONSIDERATIONS

An experimental study of a difficult material such as sand requires consideration of a number of important factors. Suitable and reliable test equipment would need to be assembled. The test material and an appropriate sample size must be selected. Testing procedures would need to be improved and developed with the aim of performing consistent and repeatable tests. The study of small strain phenomena requires precise load application and measurement of deformatons with confidence. Considerations given to these important elements of experimentation are discussed in this chapter.

3.1 Test Equipment

Laboratory test equipment should facilitate development of homogenous stress and strain conditions within the sample, allow adequate control of boundary stresses and permit accurate measurement of boundary displacement. The behaviour of sand is stress path dependent. A sand specimen is in general anisotropic and thus the rotation of principal stresses would influence stress strain behaviour. Equipment that allows unlimited stress path control as well as permit rotation of principal axes is ultimately desired. Some attempt and progress in this direction has been reported (Arthur, et al, 1980). For the moment, however, different factors that control soil behaviour would have to be investigated using different test equipments. A useful evaluation and comparison of various test apparatus has been done by (Saada et al, 1980; 1983; Ladd et al, 1977; Budhu, 1984). The existence of potentially serious deficiencies, with regards to specification and homogeneity of stress and strain, in many testing devices is well known.

The conventional triaxial apparatus has been widely used for study of soil behaviour. Its inherent limitations are well recognized. Several modifications to this test have been made in the past and a wealth of background study exists. In comparison to many other testing devices, a restricted but much more rigorous stress-strain analyses is possible for the triaxial test. There is in general a broad familiarity and acceptance of behaviour characterized by conventional triaxial tests. Consequently, a decision was made to investigate small strain phenomena utilizing an improved triaxial testing system. Examination of the influence of rotation of principal axis was set aside for study using torsional hollow cylinder equipment in a separate forthcoming investigation. A resonant column device was also used to test a few triaxial specimen in order to compare static and dynamic moduli at small strain.

3.1.1 Limitations and Improvement of the Triaxial Test

The degree to which the conventional triaxial test approximates idealized assumptions relative to homogeneity of stress and strain within the test specimen has been of long standing interest. Analytical and experimental studies of stress and strain distribution within test specimen have led to various suggestions for improvement. Internal and external displacement patterns have been studied using a variety of experimental techniques, whereas stress distribution characteristics have generally been inferred from displacement observations.

External measurement of axial deformations along segments of a traixial specimen suggest that the assumption of uniform axial strains is reasonable for triaxial compression (Roscoe etal, 1963). In addition, radial strains were found to be uniform over the height of the sample for small strains. Large deviations from uniformity were observed in triaxial extension tests at post peak strain levels. Re-examination of this result (Barden and Khyatt, 1966) showed that nonuniformities in large strain extension tests occur as a result of necking. This effect was significantly reduced through use of lubricated (also called free or frictionless) ends. A study of internal strain distribution that was made using embedded strain gages (Januskevicius and Vey, 1965) also showed uniform strain distributions for specimens with minimum end restraint. X-ray techniques were used by Kirkpatrick and Belshaw (1968) and Kirkpatrick and Younger (1971) to study the nature of internal displacement. Provided end restraint efects are negligible, radial displacements were shown to be proportional to radial position by monitoring the location of embedded lead shots. These results imply equality of radial and tangential strains in triaxial specimen.

Uniform deformations are best achieved in conventional triaxial specimen with a correct emphasis on necessary improvements. In general, the problem of nonuniform deformation would be less significant as opposed to obstacles to true soil deformation measurement in small strain considerations. In this sense, the real benefit of some previously adopted improvement measures, e.g. the use of free ends, would be open to question. Inherent limitations specific to the conventional triaxial test and suitable improvement alternatives that were implemented to promote a reliable measurement of small deformations in sand are discussed in the following.

3.1.1.1 Ram Friction

When the applied axial load is measured outside the cell, the actual load carried by the specimen is different than the registered load due to ram friction. Error due to ram fricton has been avoided by measuring the load internally within the cell (Barden and Khayatt, 1966; El-Sohby and Andrawes, 1972; Green, 1969). Continuous air bleed bushings can also virtually eliminate resistance due to ram friction (Chan, 1975). The magnitude and significance of ram friction would depend on ram and sample areas as well as equipment characteristics. The axial force was measured externally. By using a low ram to sample area ratio together with linear ball bushings and a lubricated O-ring seal, ram friction effects were made negligible.

3.1.1.2 Membrane Penetration

The cylindrical surface of triaxial specimen is covered by a rubber membrane. When stress paths of changing cell pressure are followed, measured volume changes are subject to error resulting from membrane penetration (Newland and Allely, 1959). Even though this effect has important implications as to interpretation of strains in drained tests, there appears to be a considerable ambiguity regarding correction procedures (Newland and Allely, 1959; Roscoe et al, 1963; Raju and Sadasivan, 1974; Wu and Chang, 1982). A critical review of current correction methods and development of more rational alternatives carried out in conjunction with this study have been reported previously (Vaid and Negussey, 1984). Experimental observations have shown that a sand skeleton rebounds isotropically upon hydrostatic unloading (El-Sohby and Andrawes, 1972). Hence it was possible to determine volume change due to membrane penetration as the difference between total and soil volume changes during isotropic unloading. For the sand and membrane used in this investigation, the membrane penetration curve shown in Figure 3.1 was used to correct measured volume changes under conditions of changing effective confining pressure.

3.1.1.3 End Restraint

Validity of assumed homogeneity of stress and strain within triaxial specimens have been observed to depend on conditions of end restraint. The influence of end restraint on strength has been shown to be minimal when a height to diameter ratio of 2 or larger is used (Taylor, 1948; Bishop and Green, 1965). Furthermore, the effect of end restraint on strain increment ratio does not appear to be severe (Barden and Khayatt, 1966; Rowe, 1971; Green, 1971). Provision of lubricated rubber interface between the soil and rigid end platens has been adopted to diminish end restraint (Rowe and Barden 1964, Barden and Khayatt, 1966) and thus enable uniform deformations at a reduced height to diameter ratio of one. This was found effective in aiding development of multiple and hence general failure in sand. However, frictionless ends were better approximated with use of a double rather than single membrane (Bishop and Green, 1965).

Use of free ends was attempted in this study, but initial results were not encouraging. Uniform deformation developed only along the lower half of the specimen. This phenomenon was also reported previously (Rowe and Barden, 1964; Green, 1969). A two stage sample forming process was found effective in improving the mode of deformation (Green, 1969). First, the top half of the specimen was

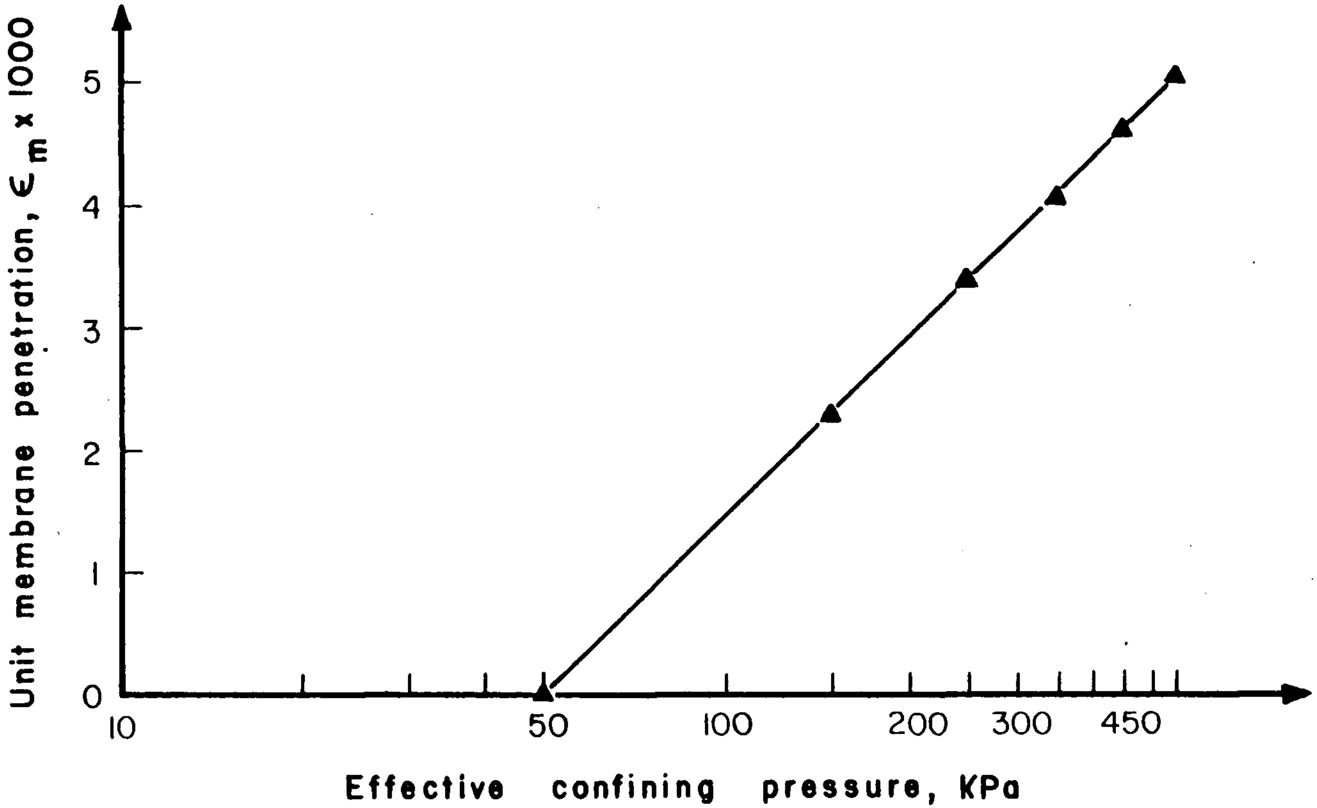

Fig. 3.1 Membrane Penetration Per Unit Surface Area with Changing Effective Confining Pressure

formed over a dummy block. The mold was then inverted and the block removed to complete sample forming. The method of sample forming adopted in this research precludes this solution. On the other hand closure of the top drain line was suggested to enhance uniform deformation (Rowe and Barden, 1964). This remedy was not found effective in this research and also by Green (1969). There appears to be no conclusive explanation for the phenomenon as well as the apparent remedies.

Review of previous studies strongly suggests that the end restraint error contribution to small strain response may not be serious. This view is supported by conventional triaxial compression test results of free and fixed ends reported by Rowe and Barden (1964) and a similar comparison by Barden and Khayatt (1966) for triaxial extension tests. Both studies suggest that the advantages of using free ends become apparent only for large strain conditions. The strain increment ratios are even much less affected (Barden and Khayatt, 1966; Rowe, 1971). Hydrostatic loading of samples with free ends was found to result in about 10 percent higher volumetric strains when compared to similar but fixed end conditions by El-Sohby and Andrawes (1972). The results were based on tests made on specimens that have a height to diameter ratio of one. Thus, the underestimate of volumetric strains in a conventional sample having a height to diameter ratio of two would be less than 5 percent. In addition, use of smooth polished metal platens with small diameter and centrally located porous stones, the techniques adopted in the study, would further reduce the margin of error. Considering the degree of scatter evident in the reported results of El-Sohby and Andrawes (1972); it appears that small strain response can be studied without resorting to the use of free ends. This not only simplified experimental procedure but was also desirable because the associated bedding errors were eliminated as will be described subsequently.

3.1.1.4 Bedding Error

Use of lubicated platens have been shown to contribute to serious bedding error in the measurement of axial deformations (Sarsby et al, 1980). For the material tested in this study, the contribution of bedding errors to axial deformation have been indicated to be comparable to membrane penetration in obscuring real volume change (Sarsby et al, 1982). Calibration and development of correction curves have therefore been advocated. Compressibilities in measuring equipment and bedding between elements of the apparatus were identified to be the major components of aggregate bedding error (Daramola and Vaughan, 1982). However, bedding error is not a function of sample height and its relative influence would diminish with use of larger sample heights. Up to 80 percent of measured axial deformation in samples with a height to diameter ratio of one may be due to bedding error in small strain observations (Sarsby et al, 1980). This estimate would be reduced to about 40 percent and would thus still remain significant for samples with a height to diameter ratio of 2. Details of equipment set up relevant to axial deformation measurement adopted in this study are shown in Figure 3.2. The top cap and the loading ram were permanently attached. Use of small diameter stones not only minimized end restraint but also virtually eliminated movement due to improper seating of porous stones on to end platens. The load cell was located above the LVDT bracket such that

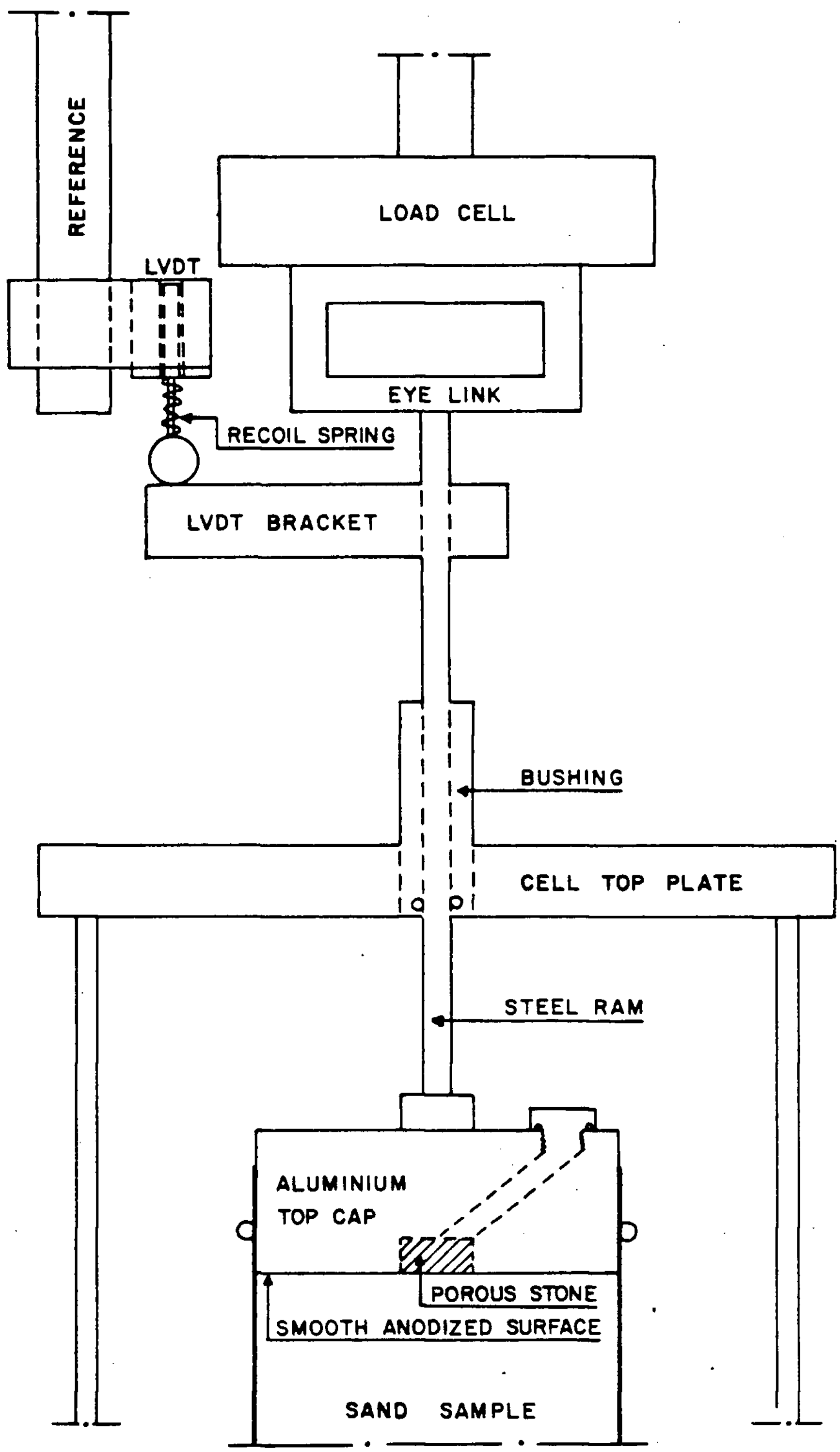

Fig. 3.2 Details of Axial Deformation Measurement

its compliance did not influence deformation measurement. Tilting of the top cap was restricted by the guide bushing.

Design improvements and overall test considerations were reviewed to optimize characterization of true soil behaviour. The influence of end restraint was minimized and lubricated platens were not considered necessary. This had the further advantages of virtually eliminating bedding errors as well as facilitating use of improved sample preparation techniques.

3.1.2 Stress Path Control

The choice of stress paths that can be followed in a conventional triaxial test are very restricted. Conventionally, the cell pressure is maintained constant. Compressional or extensional deviator stress is applied under either a stress or strain controlled condition. Isotropic loading can be effected by simply increasing the cell pressure. As well, constant shear paths can be followed by applying the desired deviator stress and manipulation of either cell or back pressure. Other stress paths would require simultaneous changes and adjustments in lateral and axial stress. Independent control of cell and deviator stresses would tend to result in uneven stress path that would be difficult to replicate precisely. A stress path analog was developed to facilitate simultaneous control of cell and deviator stress such that smooth and repeatable stress paths could be followed. Essential features and underlying principles of the system are presented below. Additional details including operation and performance have been described previously (Vaid and Negussey, 1983).

3.1.2.1 Description of the System

A schematic layout of the stress path device is shown in Figure 3.3. The loading system consists essentially of an adjustable ratio, reversing and volume booster pneumatic relays, three pressure regulators and a double acting loading piston. The signal pressure regulator R_3 controls the cell pressure P_3 which is also the input pressure to the pneumatic relays. The relays ultimately deliver the output pressure to the air piston, which applies the desired deviator load to the sample. The signal pressure regulator can be operated either manually or coupled to a variable speed motor if a constant rate of loading of the sample is desired.

The pneumatic relays transform the signal pressure P_3 to an output pressurure P_0 in the following manner:

$P_0 = SP_3$	Adjustable Ratio Relay	(3.1)
$P_0 = K - P_3$	Reversing Relay	(3.2)
$P_0 = K + P_3$	Volume Booster Relay	(3.3)

in which S and K are positive constants. If the reversing relay is used concurrent with the ratio relay, the output pressure obtained will be:

$$P_0 = S(K - P_3) \tag{3.4}$$

Since the output pressure is restricted to be positive; $K > P_3$.

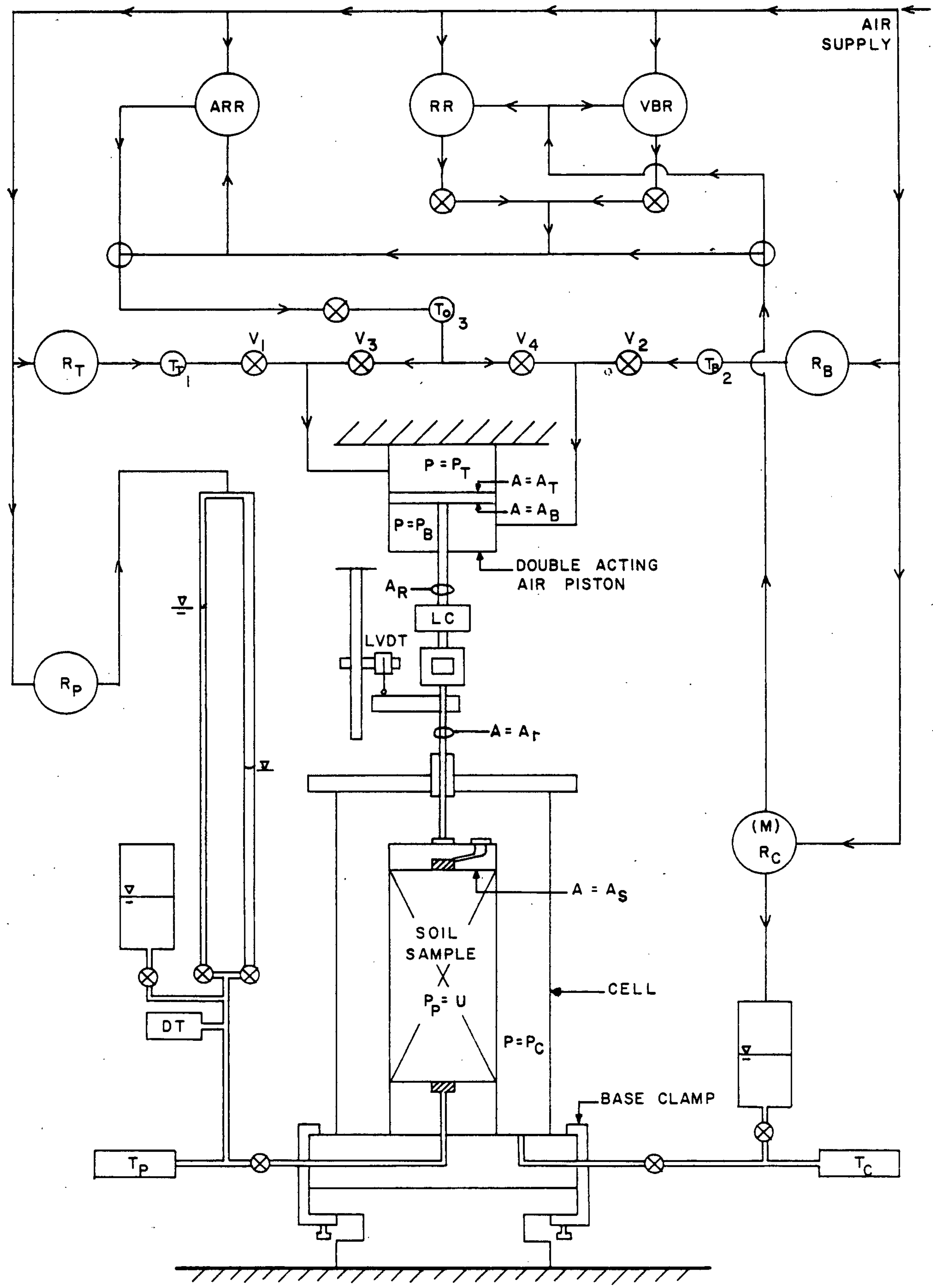

Fig. 3.3 Schematic of the Pneumatic Stress Path Analog System

LEGEND FOR FIGURE 3.3 SCHEMATIC OF STRESS ANALOG SYSTEM

SCRIPTS

A - AREA

ARR - ADJUSTABLE RATIO RELAY

LC - LOAD CELL

(M) - MOTORIZED OR MANUAL

P - PRESSURE

R - REGULATOR

RR - REVERSING RELAY

T - TRANSDUCER

V - VALVE

VBR - VOLUME BOOSTER RELAY

SUB-SCRIPTS

B - BOTTOM PISTON CHAMBER

C - CELL

O - OUTPUT

P - PORE OR BACK PRESSURE

r - RAM

R - ROD

S - SAMPLE

T - TOP PISTON CHAMBER

SYMBOLS

$\otimes$ - SHUT-OFF VALVE

$\ominus$ - THREE WAY VALVE

Similarly, use of the volume booster in place of the ratio relay results in

$$P_0 = S(K + P_3) \tag{3.5}$$

Both K and P_3 are positive and a restriction on their relative magnitudes is not necessary. For components used in this investigation, the ratio relay factor, S, can vary between 1/30 and 30. The K factors for the reversing and volume booster relays can be between 15 to 1000 KPa, with the upper range being usually limited by available supply line pressure.

3.1.2.2 UNDERLYING PRINCIPLES

For the triaxial test set up shown in Figure 3.3, let

A_1 = Upper chamber area of loading piston

A_2 = Lower chamber area of loading piston (this is less than A_1 by an amount equal to piston rod area)

A_s = Sample area

A_r = Sample loading rod area

P_1 = Pressure in the upper piston chamber

P_2 = Pressure in the lower piston chamber

P_3 = Cell pressure

u = Porewater pressure in the sample

Vertical equilibrium of the sample then requires

$$A_s\sigma'_v = P_1A_1 - P_2A_2 + P_3(A_s - A_r) - A_su \tag{3.6}$$

or

$$\sigma'_v = P_1(\frac{A_1}{A_s}) - P_2(\frac{A_2}{A_s}) + P_3(1 - \frac{A_r}{A_s}) - u \qquad (3.7)$$

also

$$\sigma'_h = P_3 - u \qquad (3.8)$$

In Equations (3.7) and (3.8), σ'_v and σ'_h are respectively the vertical and lateral effective stresses in the triaxial sample. These stresses would be expressed incrementally in the following form:

$$\Delta\sigma'_v = \Delta P_1(\frac{A_1}{A_s}) - \Delta P_2(\frac{A_2}{A_s}) + \Delta P_3(1 - \frac{A_r}{A_s}) - \Delta u \qquad (3.9)$$

$$\Delta\sigma'_h = \Delta P_3 - \Delta u \qquad (3.10)$$

Since the porewater pressure is constant in drained tests, $\Delta u = 0$ and $\Delta\sigma'_h = \Delta P_3$.

The incremental direction of a desired stress path would be given by:

$$\frac{\Delta\sigma'_v}{\Delta\sigma'_h} = \frac{\Delta P_1}{\Delta P_3}(\frac{A_1}{A_s}) - \frac{\Delta P_2}{\Delta P_3}(\frac{A_2}{A_s}) + (1 - \frac{A_r}{A_s}) \qquad (3.11)$$

By holding either of P_2 or P_1 constant, increments in the other can be expressed in terms of ΔP_3 as

$$\Delta P_1 = \Delta P_3 \left[\frac{A_s}{A_1}\left(\frac{\Delta\sigma'_v}{\Delta\sigma'_h}\right) + \frac{A_r}{A_s} - 1 \,)\right] \qquad (3.12)$$

when $\Delta P_2 = 0$; and

$$\Delta P_2 = \Delta P_3 \left[- \frac{A_s}{A_2} \left(\frac{\Delta\sigma'_v}{\Delta\sigma'_h} + \frac{A_r}{A_s} - 1 \right) \right] \tag{3.13}$$

when $\Delta P_1 = 0$.

The terms within the square brackets can be determined and would remain constant for a linear path. Given initial values of P_{1_o}, P_{2_o} and P_{3_o}; equations 3.12 and 3.13 can be converted to expressions identical to equations 3.4 or 3.5. Thus smooth stress paths can be followed by controlling only the cell pressure P_3 and choosing appropriate constants S and K on the pneumatic relays. It turns out that the ratio relay setting S is a function of only the stress direction whereas K for either the volume booster or reversing relays depends both on stress direction and stress state.

3.1.3 Measurement Devices

3.1.3.1 Load and Deformation Monitoring

Transducers were used to measure axial load and monitor pressures together with gauges for visual inspection. The cell and backpressure were monitored by separate transducers. Two additional pressure transducers were required for setting and monitoring the stress path analog. All pressure transducers were calibrated with reference to a precision dead weight gage tester. The load cell was calibrated against dead weight.

Axial deformations were measured with a sensitive transducer suitable for detection of small displacements. The transformer was mounted on to a fixed reference outside the influence of cell pressure variation (Figure 3.2 and 3). The core reacted against but was not attached to a stubby bracket that was rigidly clamped to the loading rod. A plexiglass polished ball was fitted to one end of the core. The other end was inserted into the transformer through a centering collar. Between the ball end and the base of the collar a soft recoil spring was placed. These arrangements and details as shown in Figure 3.2 were found necessary to minimize tilting and drag of the core against the transformer wall. The displacement transducer was calibrated against a micrometer and was also checked in parallel with a precision dial gauge. Displacements of the order of 1×10^{-3} mm can be detected by the transducer reliably.

Volume change was measured by monitoring the height of water column in a 4 mm bore grduated pipette. A standby 2 mm bore pipette was also available for more accurate volume change measurement. This pipette was used primarily in the testing of small 35.6 mm diameter samples for membrane penetration study to result in a comparable accuracy of volumetric strain measurement between sample sizes. A low range (35 KPa) differential pressure transducer was used to monitor volume change electronically by sensing the height of water column within the pipette. Volume changes of 0.01 cc could be detected in the 4 mm pipette, both visually and by the differential transducer.

3.1.3.2 Standard References and data Acquisition

All transducers were excited by a common power supply that was set at 6.00 volts. Supply pressure to the test frame was regulated to a maximum of 750 KPa and below line operating range. The laboratory represented a temperature controlled environment to within ± 1/4°C. These conditions remained standard for all tests.

The zero load output of the two transducers used with the stress path analogue was balanced to 1.000 mv. All other devices were read above zero load output without balancing. Pore and cell pressure transducers were referenced to a water level at sample mid-height. The differential pressure transducer reference was read with atmospheric common pressure and at zero water level in the volume change pipette. The suspended load cell output was taken as reference zero load. At the beginning and end of each test, zero references were read three times. An average of these readings was taken as the zero reference for a test. These initial and final reference readings were essentially identical for all tests reported.

Test data was acquired on a cassette tape. At the beginning of each test, initial dimensions and sample identification were entered on to the casette through a desk top computer. Data scanning was then initiated by manual or automatic triggering at prescribed time intervals. A total of ten channels were monitored in each scan. The first two carried time and predata information. Transducer readings were contained in the subsequent seven channels whereas the last channel monitored the excitation voltage. Each current and previous scans were displayed on the video monitor of the data acquisition system. This feature permitted ready comparison of successive readings and was useful for setting the stress path analog parameters. At the end of the test, the data acquired on cassette was transferred to disk for processing and duplicate storage.

3.2 Material Tested and Sample Size

3.2.1 Material Tested

A naturally occurring medium silica sand from Ottawa, Illinois, commonly known as Ottawa sand, was used in this study. Its mineral composition is primarily quartz with a specific gravity of 2.67 and a material friction angle of about 25°. Individual particles are rounded and the average particle size D_{50} is 0.4 mm. Reference maximum and minimum void ratios used are 0.82 and 0.50, respectively. All test samples were formed using a fixed oven dry weight of 640 gms. No detectable difference in gradation between a fresh batch and one subjected to several recycling could be observed, as shown in Figure 3.4. Similar conclusions were reached in studies at confining pressures of up to 2500 KPa by Vaid et al (1983). This is due to quartz being a relatively hard mineral, and individual sand particles are rounded. Both gradation curves conform to the limits specified by ASTM Designation C-109-69 for Ottawa sand and particle crushing was not detectable.

3.2.2 Sample Size

The relative significance of equipment related experimental error can be minimized by a proper choice of sample size. Aside from adopting a widely accepted height to diameter ratio of 2 to 1, there is often less emphasis on deliberate choice of sample size. A number of previous studies have been based on 38 mm diameter samples.

With reference to experimental limitations discussed previously, the influence of ram friction and error due to membrane penetration decrease with increasing sample diameter. End restraint effects

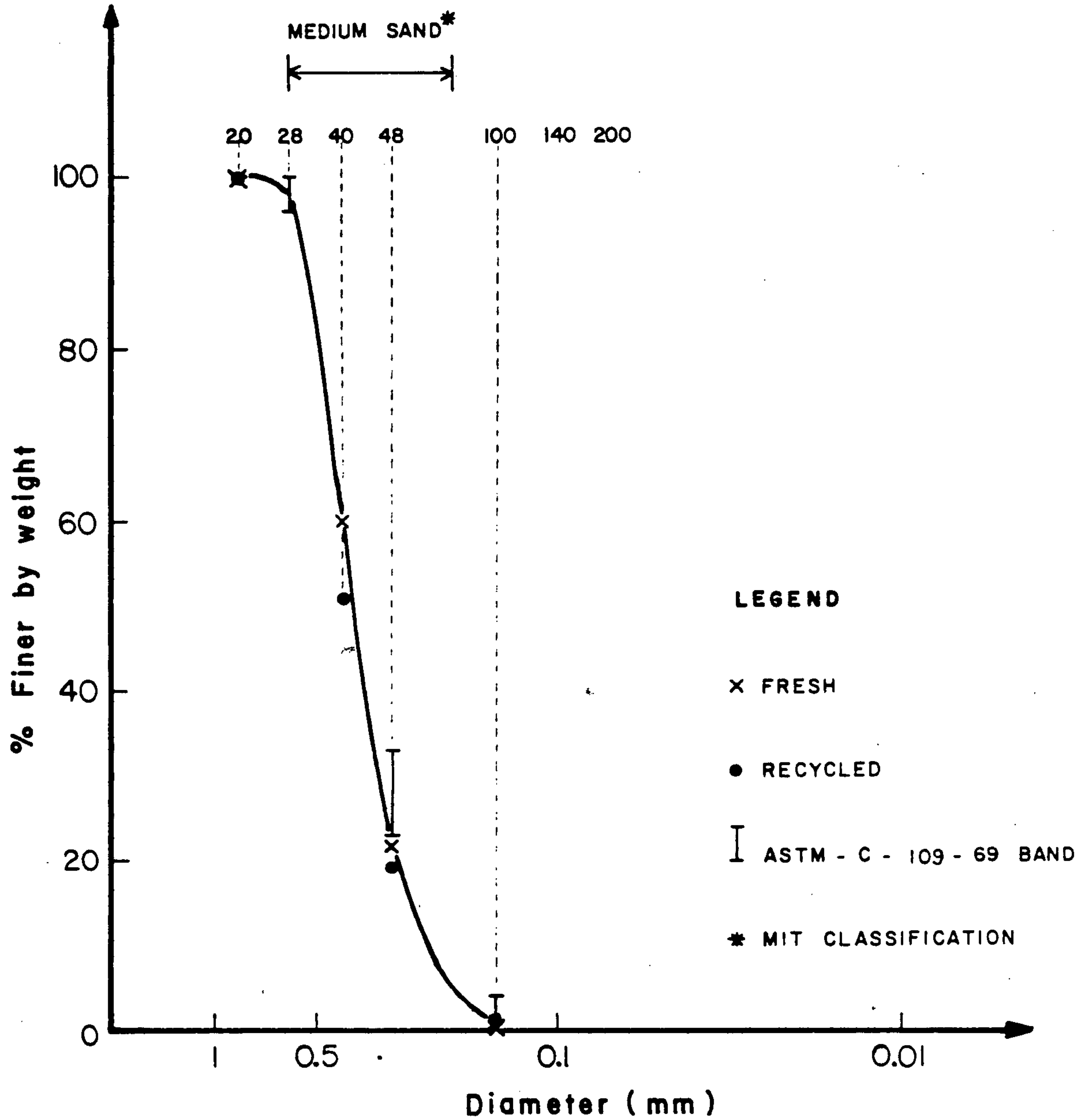

Fig.3.4 Grain Size Distribution Curve for Ottawa Sand

larger sample height. Disturbance to the sample during set up would be less severe for a larger diameter sample. Given the equipment capabilities discussed previously, a choice of sample size that would promote reliable detection of comparable axial and volumetric strain magnitudes was desired.

Taking into account the above considerations a 63.5 mm diameter sample with, an approximately, 2 to 1 height to diameter ratio was adopted. As will be described subsequently, the actual sample height varied depending on the relative density of interest. This is because the soil weight and diameter remained the same and density was controlled by change in height. Overall, this choice of sample size was found favourable in reducing the relative significance of equipment related test errors. It also permitted reliable detection of axial and volumetric strains at comparable levels and in the order of 1×10^{-5}.

3.3 Testing Procedure

3.3.1 Sample Preparation

At a given instant in time, a test sample is assumed to represent a point in stress space. The sample preparation technique must therefore promote development of homogeniety of density and structure within an individual sample. Experimental investigations invariably require testing of several samples. A high degree of sample reproduction capability is therefore essential for meaningful correspondence and repeatability of test results.

The stress-strain response of sand is sensitive to variations in sample preparation technique. Researchers have identified a number of factors to be significant in sample forming. Method of placement, height and rate of pouring have been suggested to be important (Kolbuszewski, 1948; Muira and Toki, 1982; Mulilis et al, 1975; Tatsuoka et al, 1982). The medium of deposition, whether air or water, affects structure and initial packing (Kolbuszewski, 1948 and 1948a). Direction of pouring has been shown to determine grain orientation and hence inherent anisotropy (Arthur and Menzies, 1972; Yamada and Ishihara, 1979; Oda, 1972). Placement water content and method of densification also control sand behaviour. There is a broad disagreement regarding the relative importance of some of these factors. This may in part be because evaluations have been based on empirical results and their degree of importance depends on the method of sample preparation. Of all current disagreements, however, the effect of height of drop is the most unclear and contradictory. Its influence on initial void ratio was found to be significant (Kolbuszewski, 1948 and 1948a; Tatsuoka et al, 1982; Ishihara and Towhata, 1983) to the extent that desired initial densities were controlled by height of pouring. On the other hand, results that have indicated a minor (Mululis et al, 1975) to negligible (Muira and Toki, 1982) influence of height of drop on initial density have also been reported.

This contentious issue was examined from theoretical and experimental considerations in a limited background study (Vaid and Negussey, 1984a). Terminal velocity of sand grains would be attained almost instantaneously and within negligible drop height when pluviation takes place in water. However, for pluviation through air, the influence of height of pouring on initial density was found to vary from significant to insignificant in the low range of drop heights.

Pluviation through water would thus be more effective in promoting homogeneity and repeatability of test samples and was therefore used in this study.

3.3.1.1 Adopted Method

The basic method of sample preparation adopted in this study has been in long use at UBC. Further refinements were introduced to enhance attainment of desired objectives of simplicity and precise replication of structure as well as density. Samples were formed with extreme care and diligence to ensure repeatability and consistency of test results. The adopted method may also be considered as an improved version of that suggested by Chaney and Mulilis (1978).

A fixed mass of oven dried sand was weighed in a dry flask. Water was added to near filling. The sand water mixture was then boiled for about 20 minutes. After cooling to room temperature, it was kept under vacuum until sample forming. Porous stones were also boiled in water and cooled to room temperature. De-aired water was used in all saturation and drainage lines.

Samples of 63.5 mm diameter were formed in rubber membrances that were stretched and folded over a split mold. Membranes having 60 mm diameter and 0.3 mm thickness were cut to 190 mm lengths. The membrane was sealed to the base of pedestal and folded over the former to an established level. It was stretched to the wall of the split mold by applying a small vacuum suction. The cavity thus formed was filled with de-aired water. The effective vacuum suction applied to the boiled sand was released. A special tapered rubber stopper with a glass tube nozzle was fitted to the flask. De-aired water was added untill overflow. By gentle overturning of the flask preventing flow, the nozzle tip was allowed to make shallow penetration of the water surface within the former. The flask was then fastened to a movable stand with a fixed clamp. Deposition of sand proceeded under gravitational influence and mutual displacement with water. All samples were formed by deposition from the top and center of mold. However, when the flask was near empty, the stand was moved laterally to produce a level surface.

The diameter of the mold, membrane thickness and dry weight of sand were constant. Thus, desired relative densities were obtained by controlling specimen heights. Prior to assembling the sample former, a target height was established. This was done by placing an aluminum dummy sample of known height between the bottom pedestal and top cap. A flat head nut was fitted temporarily to the load end of the loading rod which was permanently attached to the top cap. A reference reading was then taken on top of the loading rod using a dial gauge that was mounted on a movable stand. Knowing the height of the dummy sample, the dial target reading required for a sample of the desired height was calculated. Following deposition and levelling, the flask was removed from the stand and the top cap was put in place. The dial gauge was located on top of the loading rod. The specimen was then densified by high frequency low amplitude vibration induced along the top of cell base. This procedure was found effective in preventing tilting of the top cap and uneven settlement. Densification with top cap in place and thus effective confinement was found useful in promoting development of uniform densities within test samples (Vaid, 1981, 1983). Both top and bottom drainage lines were kept open and change in height was continually monitored during densification. On approaching the target height, densification was terminated. From several attempts, points of termination that would lead to a target height to cell assembly and desired initial relative density were determined.

At the appropriate termination reading to target setting, the membrane was pulled over the top cap and sealed with an O ring. Keeping the base drainage open, the top drainage line was plugged. A vacuum of 17 KPa was then applied to the sample along the base drainage line. Thus the sample was given effective confinement by virtue of the applied vacuum and the mold was dismantled. Height monitoring was subsequently terminated and the triaxial cell was assembled. The base drainage line was shut off to maintain confinement and the vacuum line was disconnected. The cell was filled with de-aired water and the sample preparation phase was completed.

3.3.2 Sample Set-up

After placing the triaxial cell within the loading frame, initial readings of all transducers were taken and the cell line was connected to the cell pressure system. A cell pressure of 20 KPa was applied and the confining vacuum was released. The sample drainage line was then connected to the volume change device, air free, and the loading ram connected to the loading piston. An intermediate scan of all transducers was taken. Volume change during sample connection was estimated by assuming isotropy from height difference between the intermediate and initial scans. With the sample maintained undrained, saturation of the specimen and membrane leakage were checked. The sample was then brought to an effective hydrostatic stress state of 50 KPa with a back pressure of 100 KPa. When desired to bring the stress state to a stress ratio, R, a deviator stress was applied under drained conditions, while maintaining the effective confining pressure constant. A reference reading of all transducers was made. This stress state was taken as the initial stress state for the test. All of the above steps were carried out with continued recording of associated deformations. Sample dimensions at the initial stress state were used in strain calculations. Procedures were carefully repeated to enhance sample reproduction and consistency of test results.

3.3.3 Repeatability of Test Results

Experimental observations and conclusions derived therefrom depend on consistency and repeatability of tests. Repeatability of otherwise consistent test results on sand depend on reproduction of relative density, replication of structure, measurement accuracy and exact duplication of test routine. Through procedures described previously, the weight of sand grains and initial sample dimensions can be controlled to enable reproduction of relative density to within one percent of the desired target. In order to replicate grain structure as closely as possible, the same sample forming technique was followed throughout. One interesting feature that was adopted in the testing routine was the repeated monitoring of deformations at constant effective stress and following application of a stress increment. Although time independence in the sense of sand compared to clay behaviour is acceptable when considering a long time frame, time dependent effects may not be ignored in a laboratory setting. Depending on stress level and stress paths, various amounts of time dependent deformation was observed to occur at constant effective stress and as a consequence of slip and load shedding. Only time independent readings were associated with corresponding stress increments. Appropriate measurement devices were selected, test equipment was modified and testing techniques were improved in order to enhance accuracy in the application of stress and measurement of resulting deformations. The repeatability of test results is an overall manifestation of the above tasks.

Some results from repeated testing of identical samples in hydrostatic compression are presented in Figure 3.5. Excellent repeatability may be noted in mean normal stress against both volumetric and axial strain plots. Differences in both axial and volumetric strain observations at equal mean normal stress show a slow rate of accumulation with strain magnitude. Individual test results are smooth and well defined and these differences have therefore little effect on description of incremental behaviour.

Response of two identical samples to constant mean normal stress shearing is shown in Figure 3.6. The comparison includes only shearing response and represents results after hydrostatic compression, as is customary. It may be noted that reproduction within the strain range of interest is exceptionally good.

Behaviour representing different densities and stress levels for constant mean normal stress and hydrostatic compression are shown in Figures 3.7 and 3.8, respectively. Clear and consistent relationships can be identified at small strain range. The results represent a reliable magnification of small strain phenomena as observed from data obtained by direct measurement of deformations.

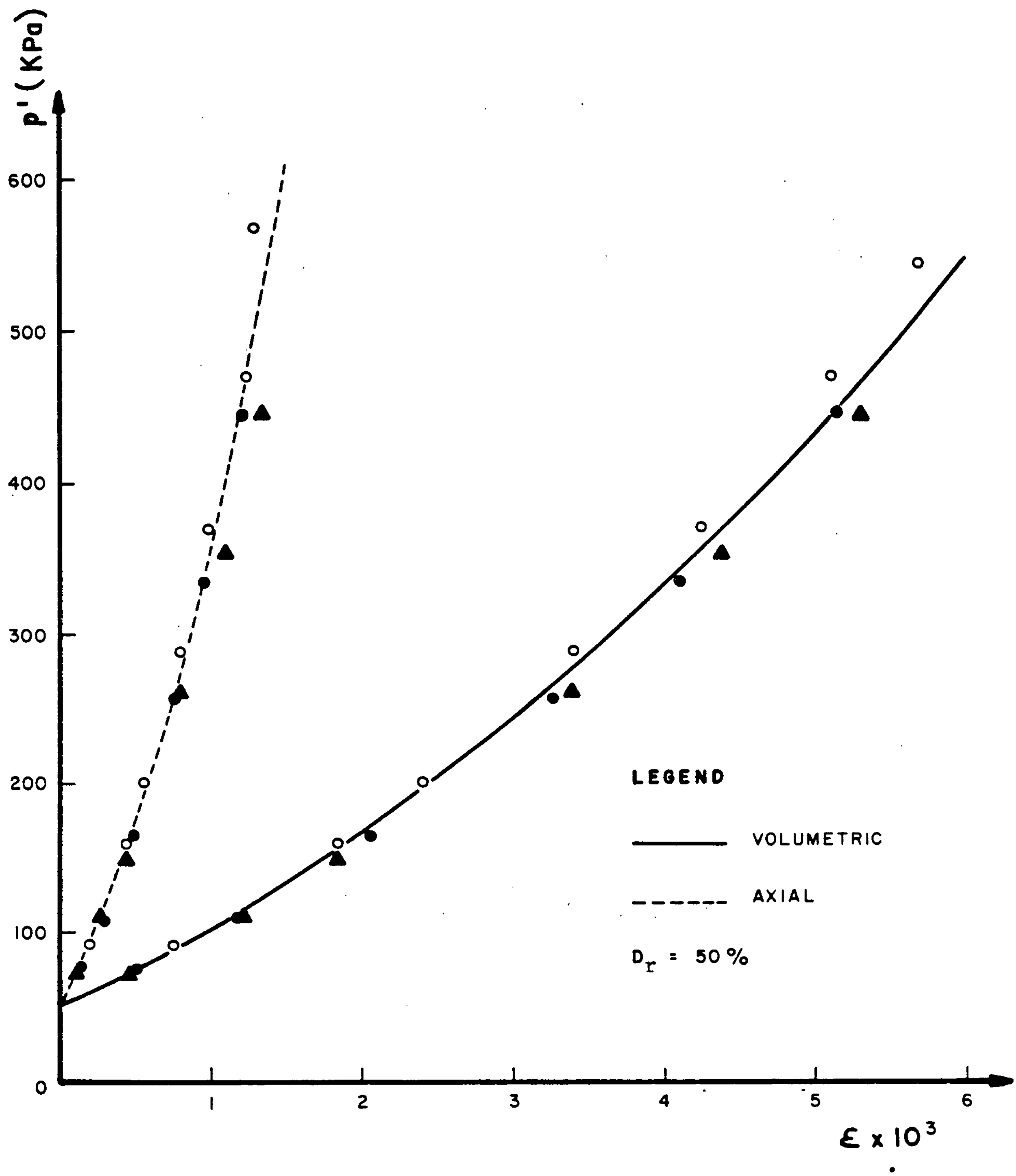

Fig. 3.5 Repeatability of Test Results in Hydrostatic Compression

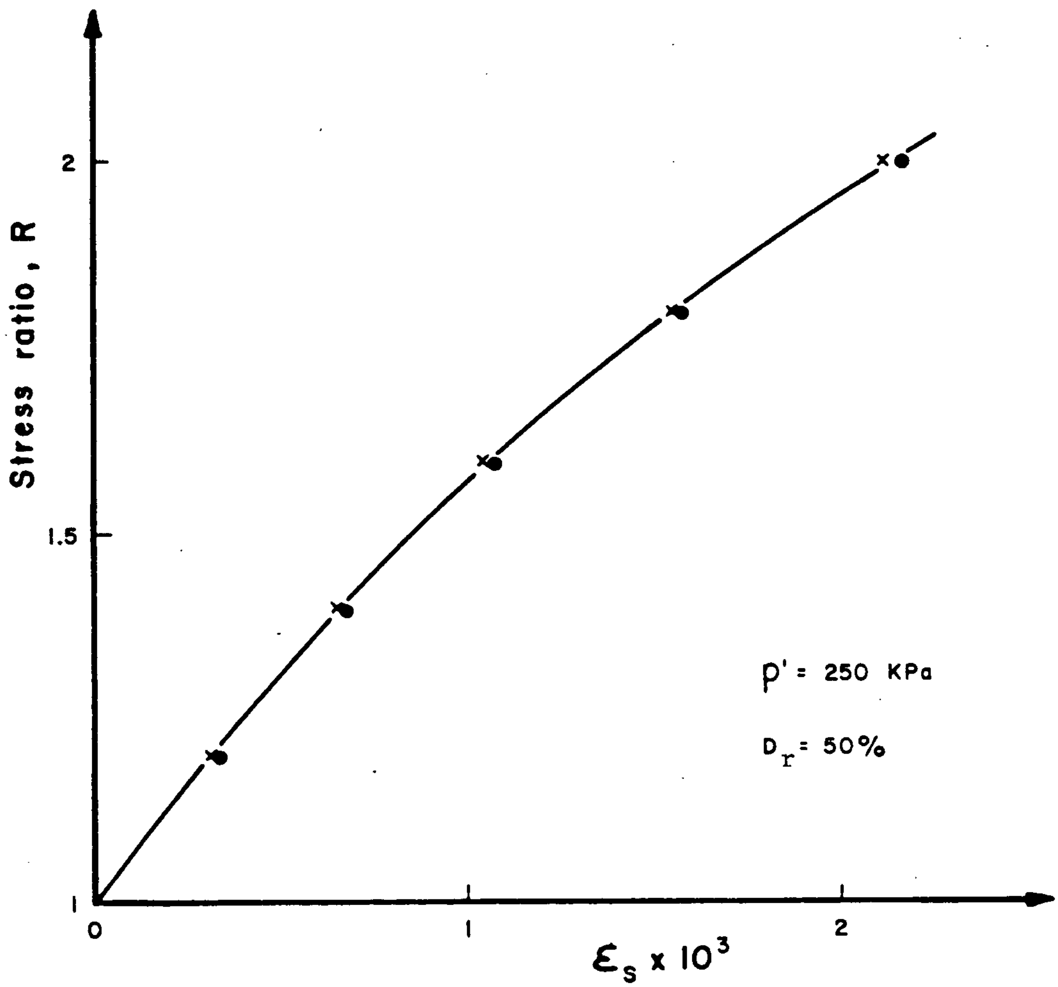

Fig. 3.6 Repeatability of Test Results in Shear Loading

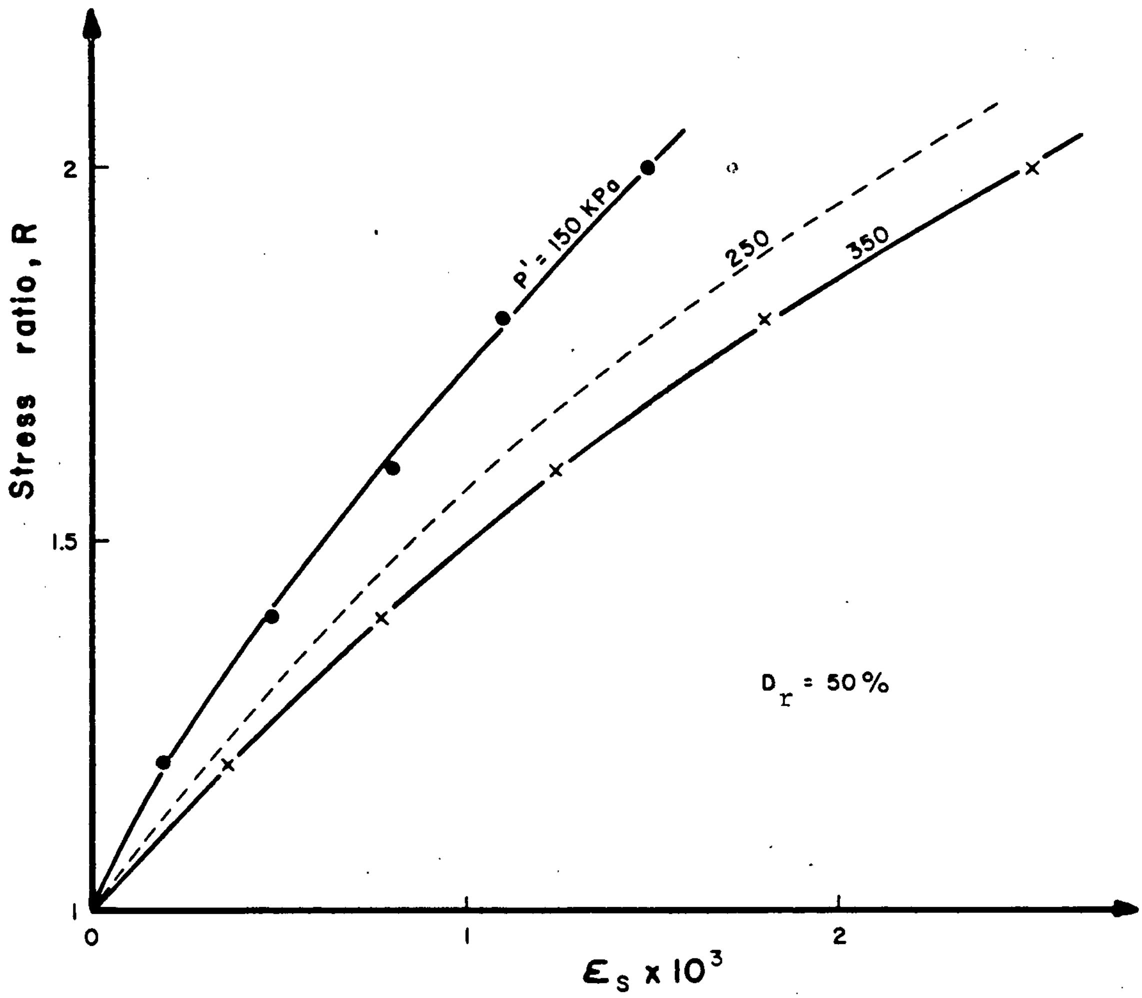

Fig. 3.7 Comparisons of Response to Shear at Three Levels of Mean Normal Stress

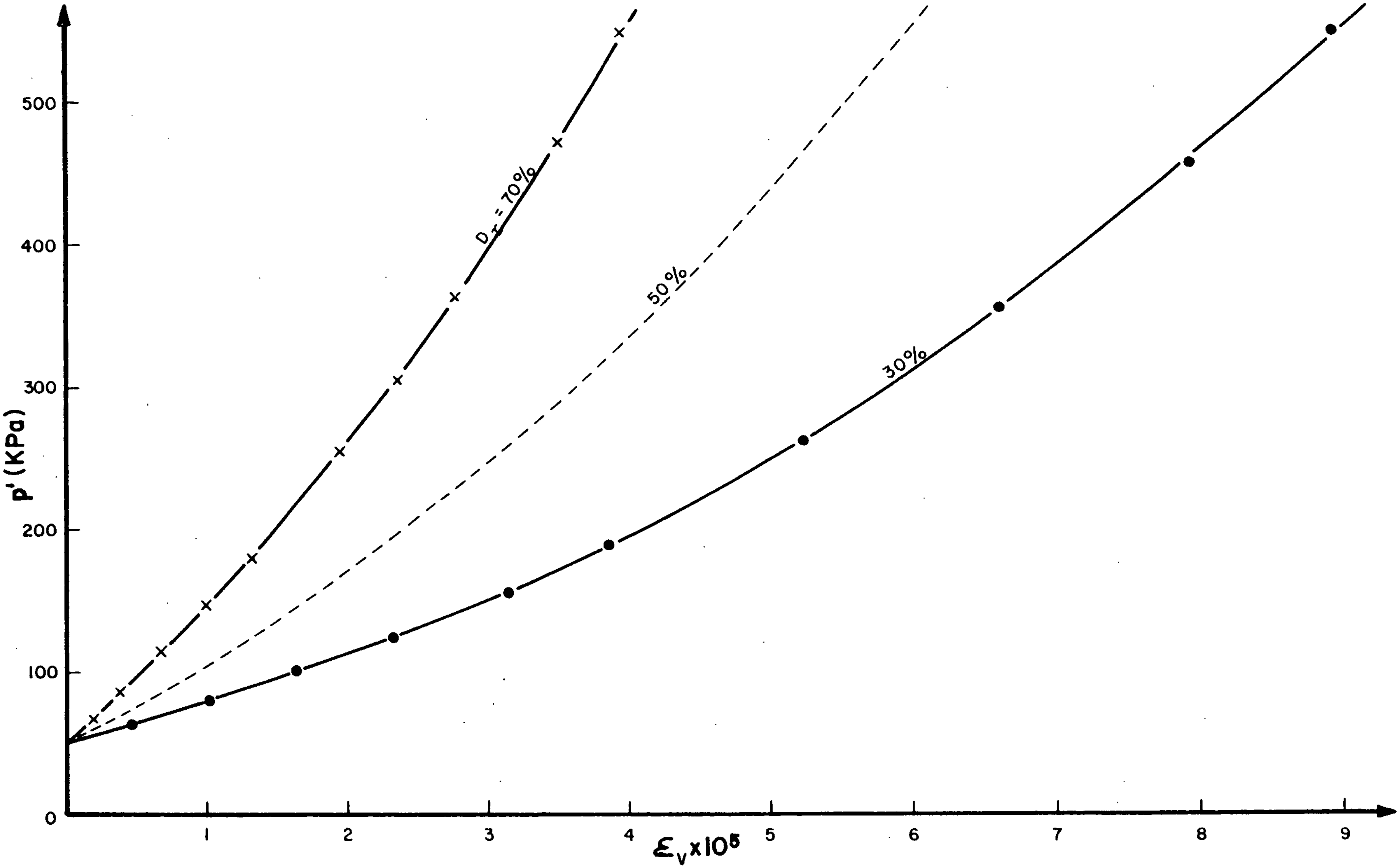

Fig. 3.8 The Influence of Relative Density on Strain Response to Hydrostatic Compression

CHAPTER IV - EXAMINATION OF PREVAILING FRAMEWORKS FOR DESCRIBING SMALL STRAIN RESPONSE

Previous experimental investigators have attempted to describe the stress strain response of sand within several frameworks such as incrementally elastic, elasto-plastic and particulate. For the most part, such frameworks have been derived from detailed study of behaviour either at very small strains, less than 1×10^{-4}; or with emphasis at large strain response, above 1×10^{-2}. Sometimes behaviour at these two extremes has been force connected, such as in attempts to specify dynamic moduli in terms of shear strength. Otherwise, each region has been treated separately neglecting the existence of the other. Such a simplification meets difficulty, however, when the range of interest is extended from either side to include the small strain range, 1×10^{-4} to 1×10^{-2}. A variety of carefully conducted tests on sand covering small strain response are presented in this chapter. The usefulness of widely accepted frameworks and similarity of behaviour to common but fundamental assumptions will be examined.

4.1 Incremental Elastic Representation

In a vast majority of current geotechnical analyses, sand at given void ratio is idealized as an incrementally linear elastic isotropic continuum. Appropriate moduli for incremental equations are prescribed, as state variables in stress strain space, using suitable analytic expressions that are derived from large strain data. The usefulness of this procedure for describing small strain moduli under uniaxial loading conditions as well as the influence of stress path on small strain moduli will be examined. All experimental results and conclusions therefrom are based on tests at a common relative density of 50 percent.

4.1.1 Moduli in Uniaxial Loading

Small strain test results from conventional triaxial compression tests at different levels of confining stress (σ_3') are shown in Figure 4.1. In incremental elastic approximations, such stress-strain results are most often simulated by hyperbolas. A hyperbola is described by an equation in which the dependent and independent variables are related by two parameters. The first parameter is the ultimate value of the dependent variable. In hyperbolic simulation this parameter is considered to be specified by the failure criteria appropriate for the confining stress in question. The second parameter in a hyperbolic equation is given by the initial slope, E_i, of the hyperbolic curve.

4.1.1.1 Initial Moduli, E_i

Initial slope and thus modulus (E_i) is a key parameter for a hyperbolic description. Initial moduli are determined from transformed plots, such as Figure 4.2(a) for the test at $\sigma_3' = 50$ kPa. It may be noted that the data points do not form a straight line fit. Thus, the stress-strain curve is not perfectly hyperbolic. For sand, such an imperfect fit is in general the rule rather than the exception.
As a result, initial moduli so determined are independent of small strain data. Neither the improved accuracy nor the availability of additional small strain results would lead to a better definition of E_i.

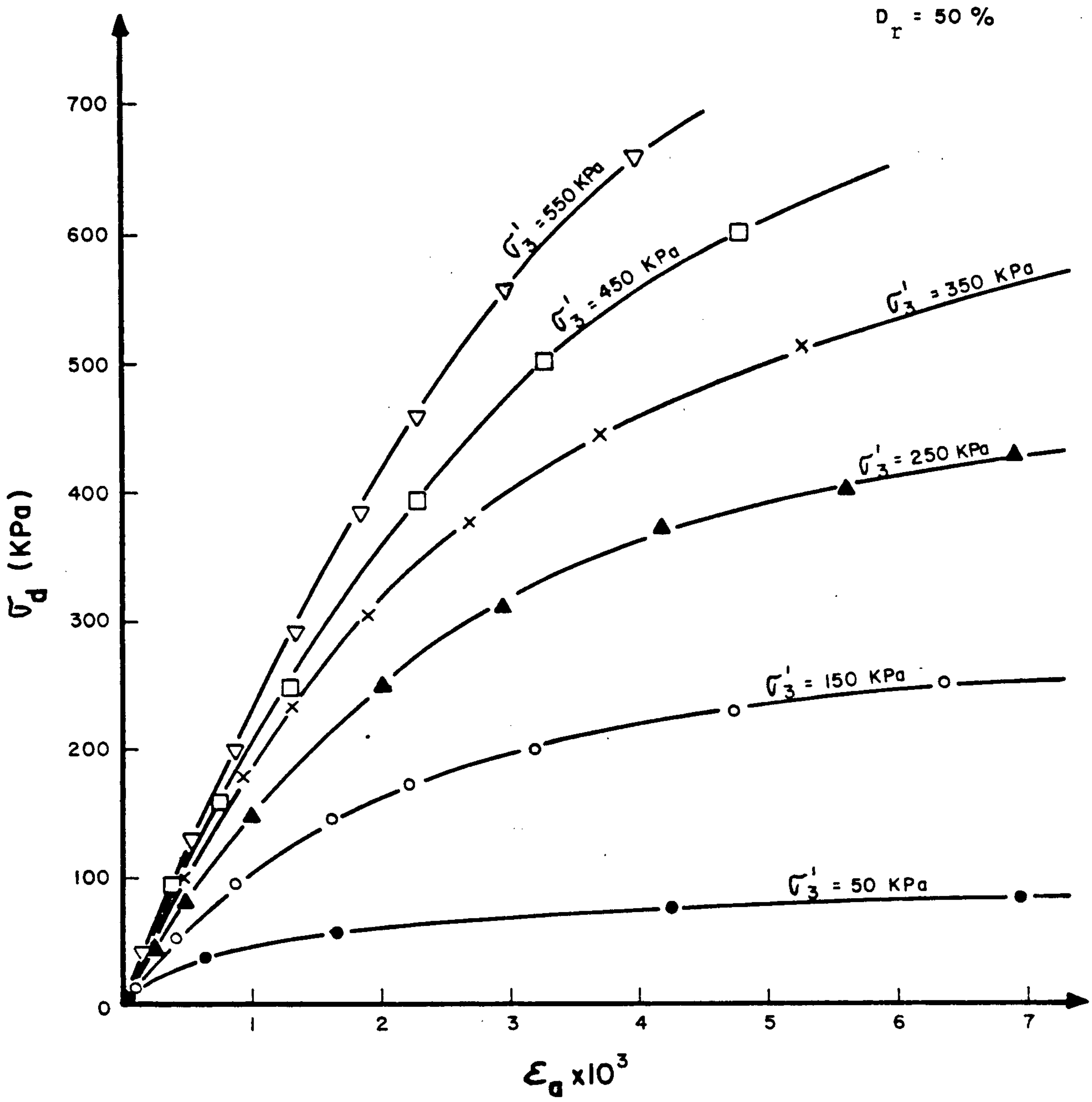

Fig. 4.1 Results of Conventional Triaxial Tests at Different Confining Pressures

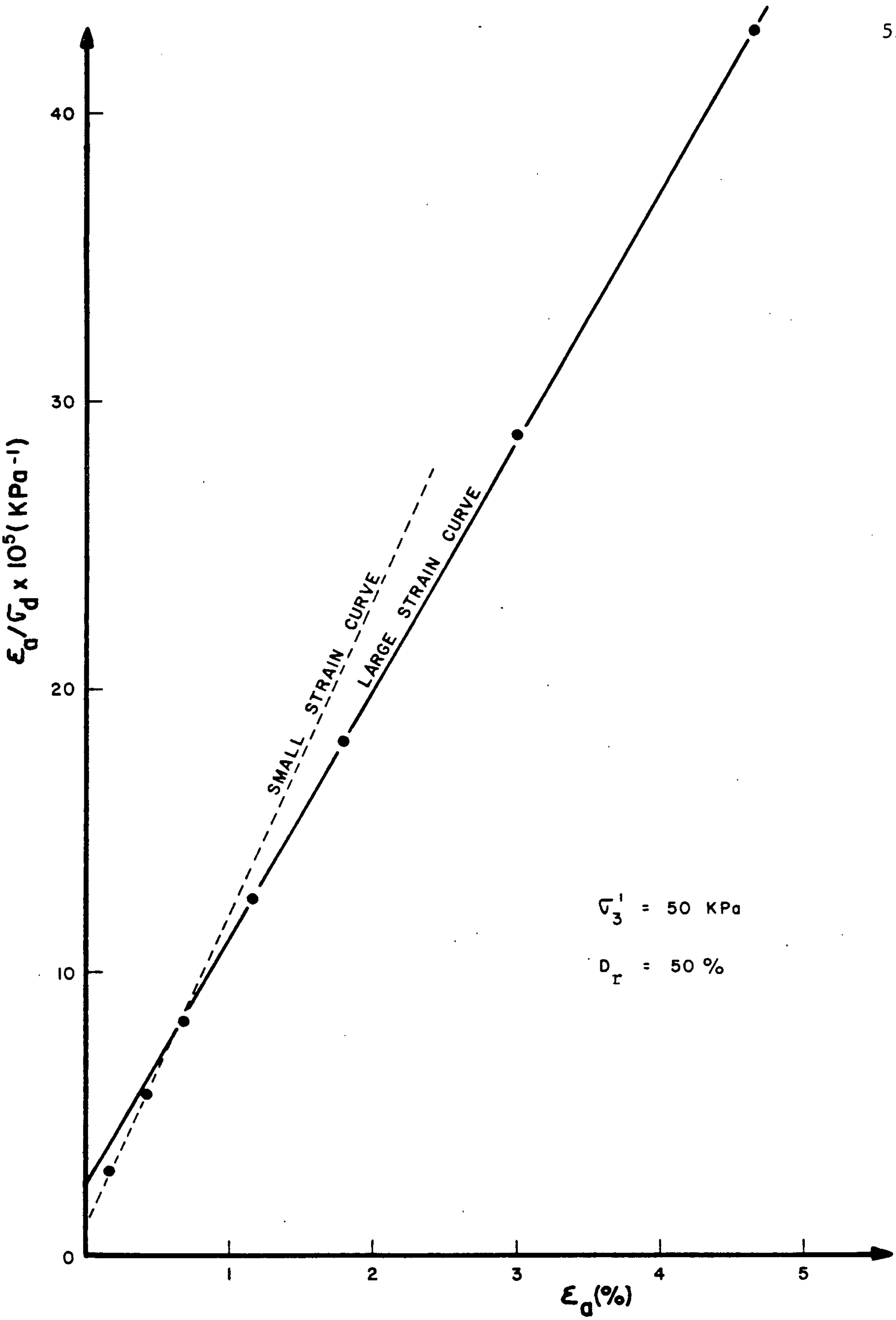

Fig. 4.2a Comparative Interpretation of a Triaxial Test Result on the Basis of Data at Small and Large Strain

On considering test results in Figure 4.1 in the region of small strain, 1×10^{-4} to 1×10^{-2} alone; a separate straight line fit and initial moduli can be noted, as shown in Figure 4.2(b). These results suggest that small strain response can also be approximated by a hyperbolic function which is separate from that for large strain. Use of two separate initial moduli and thus a dual hyperbolic fit to the data would appear to result in an improved stress-strain relationship. However, whereas the additional parameter has been prescribed by failure criteria in large strain considerations, the corresponding parameter can not be specified readily for small strain data. Hence a dual hyperbolic representation would appear to require an alternative assumption for the required second parameter. Such an alternative approach is considered later in Chapter VI.

4.1.1.2 Relationships Between E_i and E_{max}

There has been some uncertainty about the meaning of E_i and its relationship with E_{max}, as derived at extremely small strain (of the order of 1×10^{-6}) from resonant column tests. Before proceeding, however, it would be useful to restate that the E_i determined from large strain considerations is a fictitious modulus and has in general little to do with small strain response. In the following comparison of E_{max} to E_i; unless specified otherwise, a reference to E_i pertains to initial moduli determined from small, 1×10^{-4} to 1×10^{-2}, strain data alone as shown in Figure 4.2(b).

Changes in initial moduli, E_i, with confining pressure derived from Figure 4.2(b) are shown in Figure 4.3. Secant moduli obtained directly from Figure 4.2(b) and at strain levels of 1×10^{-4} and 10^{-3}

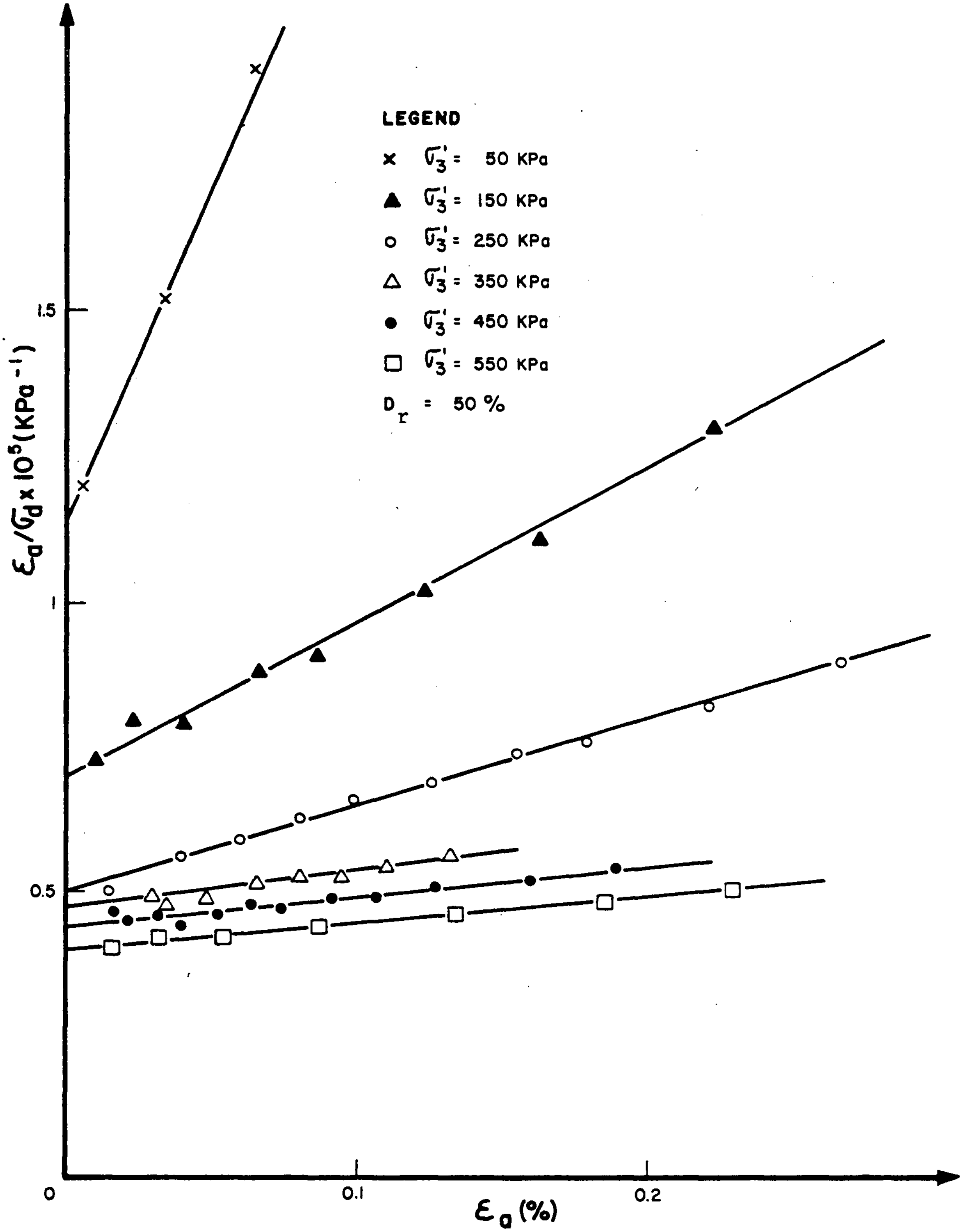

Fig. 4.2b Transformed Plot of Triaxial Test Results in the Small Strain Range

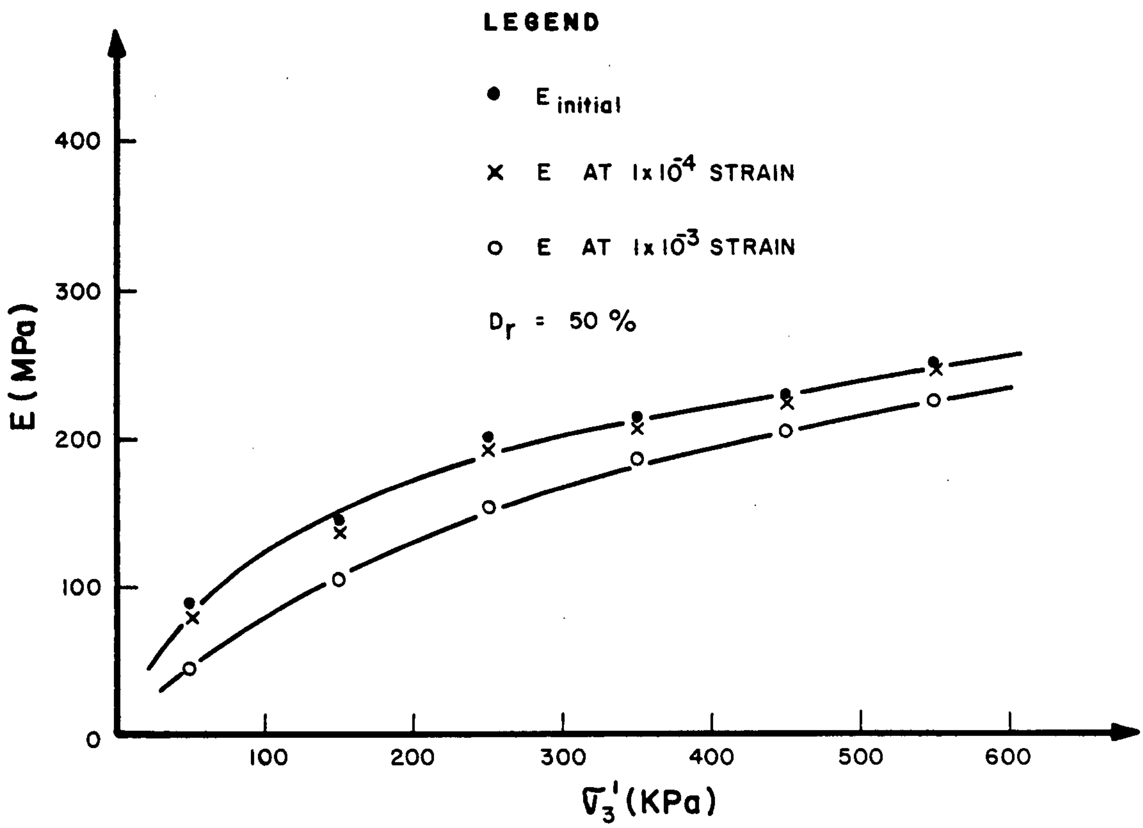

Fig. 4.3 Variation of Static Moduli with Strain Level and Confining Pressure

are also shown. Both E_i and secant moduli at comparable strain levels may be noted to increase with confining stress. There is however little difference between E_i and E at 1×10^{-4} strain.

In order to clarify questions regarding E_{max} and E_i, resonant column tests were conducted on triaxial specimen formed at the same relative density. Tests were made at corresponding confining pressures and axial strain levels of 1×10^{-6} to 10^{-4}. In order to allow ready comparison of secant Young's Moduli without recourse to estimation of Poisson's ratio or cross referencing of strain levels, only longitudinal excitations were applied. Thus overlap in initial void ratio, confining stress and strain level was maintained.

Relationships between secant modulus, confining stress and strain level as determined from the resonant column test results are shown in Figure 4.4. Secant moduli at comparable strain levels increase with confining stress. Furthermore, modulus degradation with strain appears to progress at a relatively slow but similar rate at all confining pressures for strain levels between 1×10^{-5} and 10^{-4}. Below a strain of 1×10^{-5} the rate of modulus degradation is observed to increase with confining pressure. However, presentation of the data in Figure 4.4. in semi-log form, Figure 4.5, shows that moduli can be considered relatively constant below 1×10^{-6} strain and as is commonly used this form of representation fascilitates determination of E_{max} . These observations are, in general, consistent with current understanding, as well as additional results by Lui (1984).

Values of E_{max} and E at 1×10^{-4} axial strain from resonant column tests have been plotted against confining stress in Figure 4.6. Relatively independent of confining stress, the ratio of E_{max} to E at

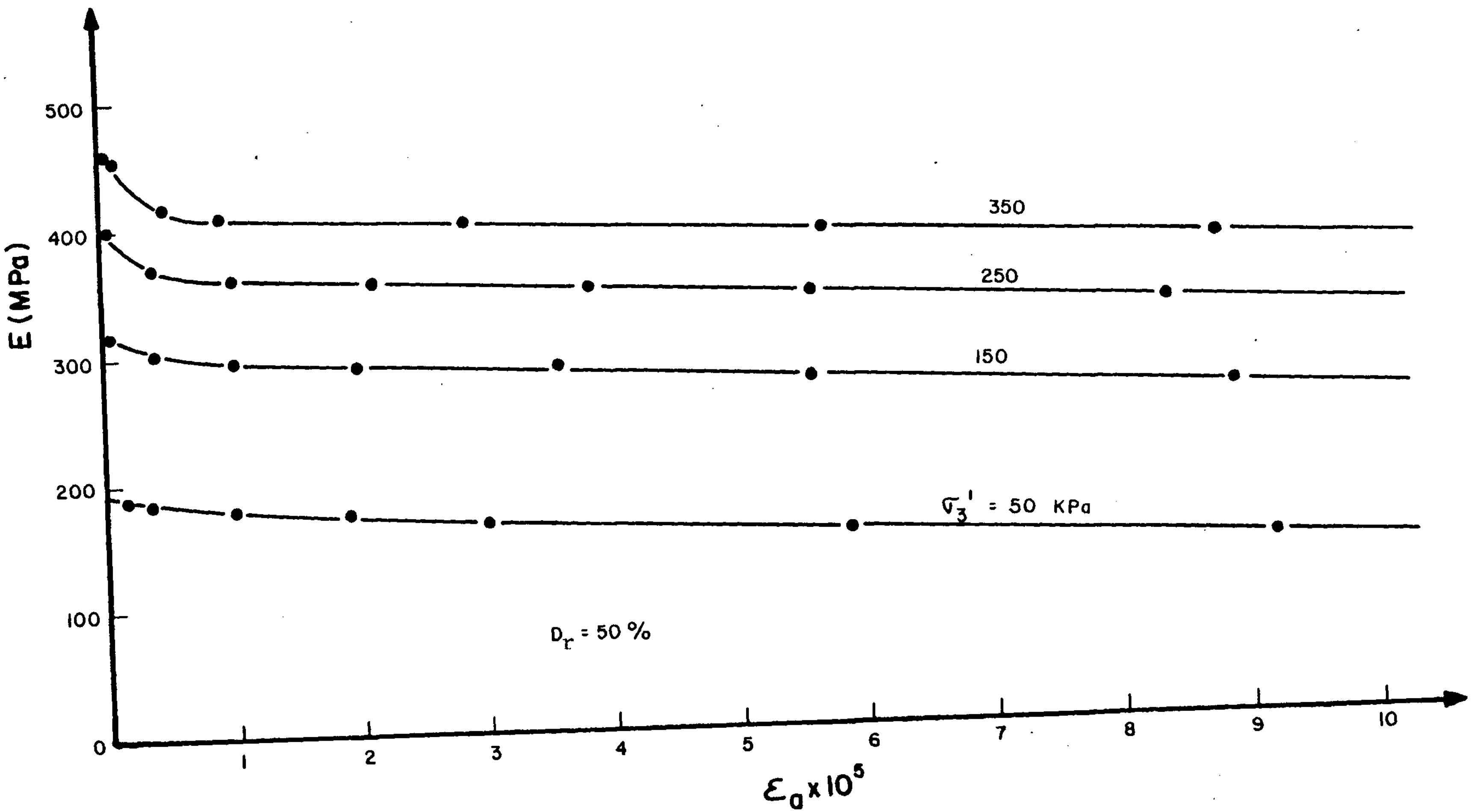

Fig. 4.4 Young's Moduli From Resonant Column Testing in Longitudinal Mode

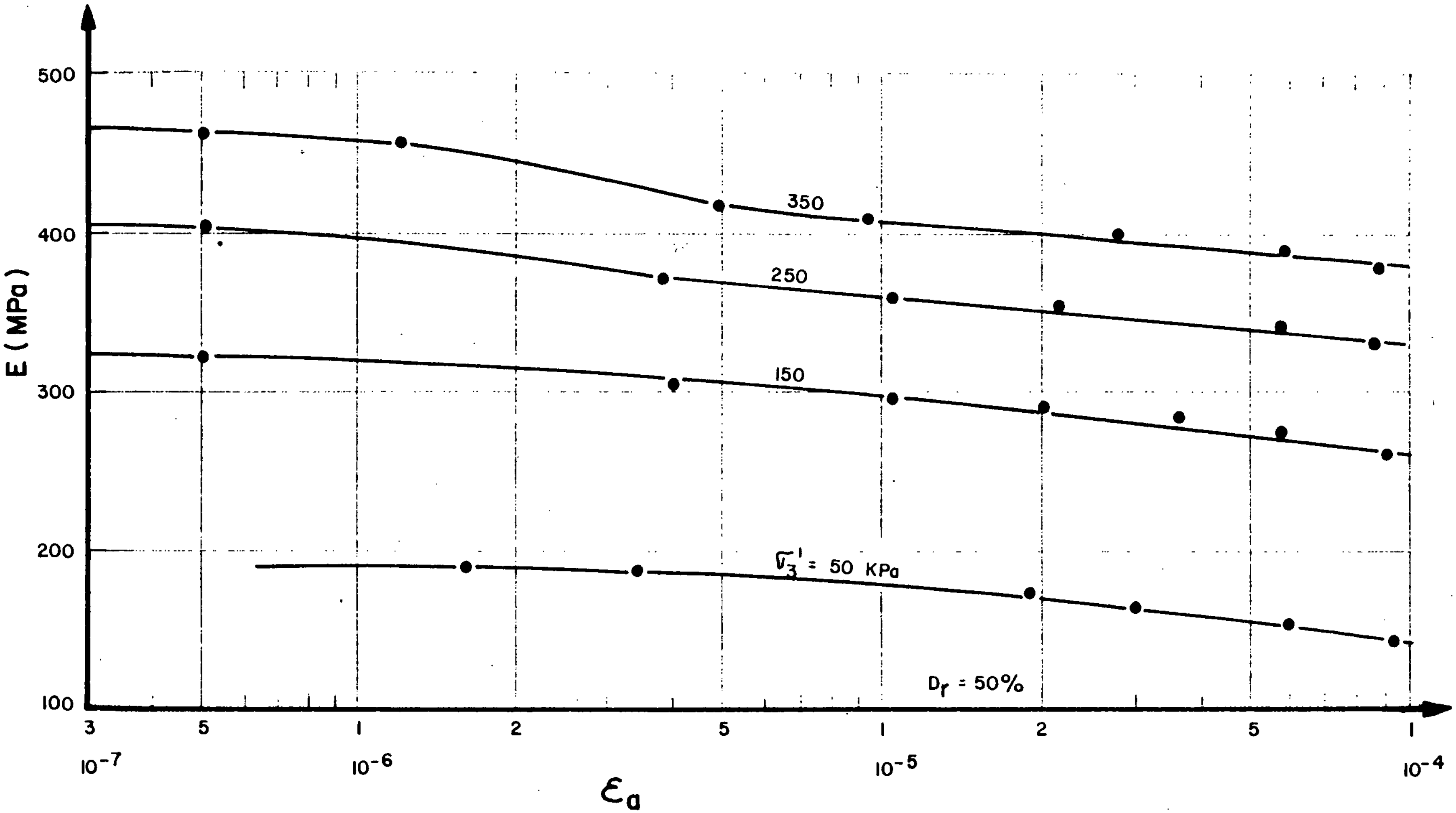

Fig. 4.5 Young's Moduli with Strain and Confining Stress Level as Determined from Resonant Column Tests

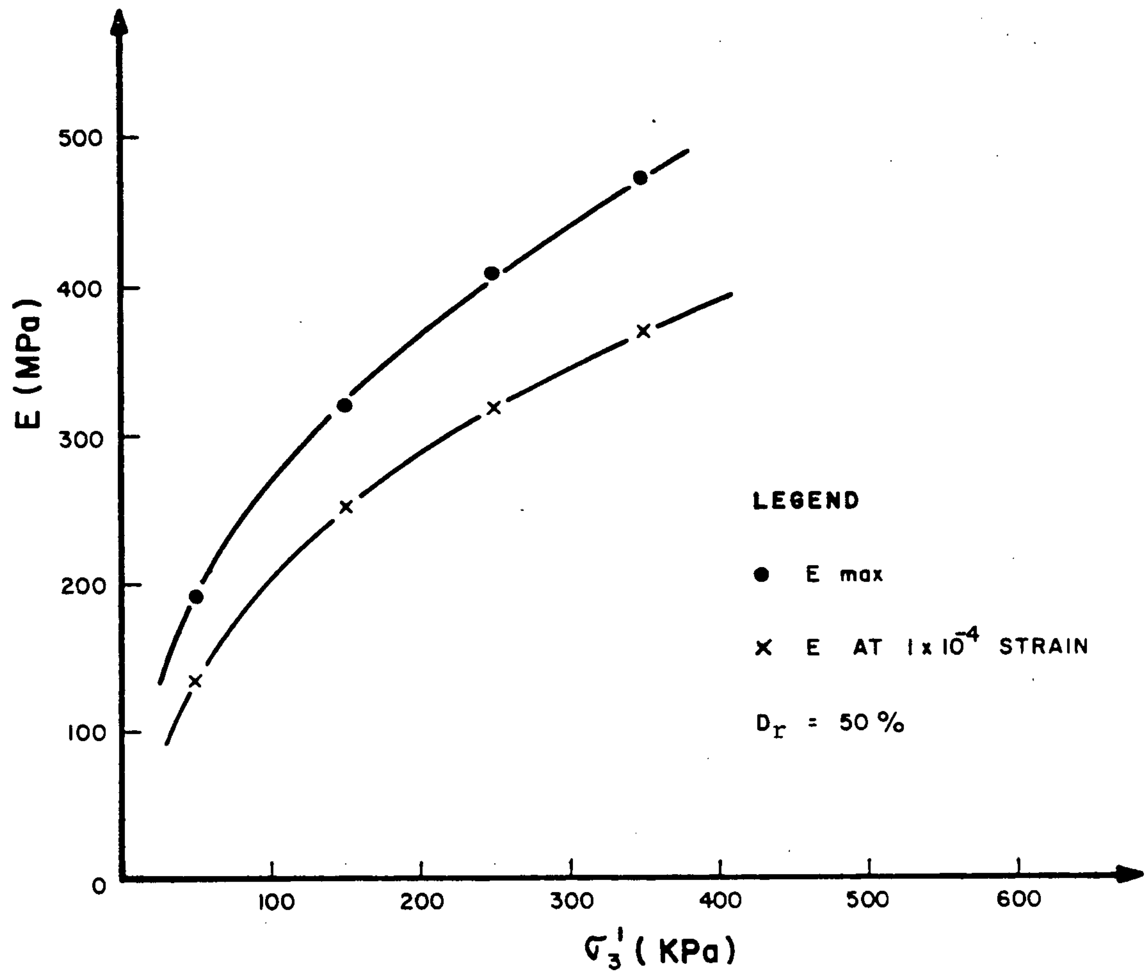

Fig. 4.6 Change of Dynamic Moduli with Strain Level and Confining Pressure

1×10^{-4} strain from resonant column tests is about 1.3. Whereas, the corresponding ratio of E_i to E at 1×10^{-4} strain from triaxial testing, Figure 4.3, is between 1.0 to 1.1. E_{max} and E_i as well as E at 1×10^{-4} from both resonant column and triaxial test results are comapred in Figure 4.7a and b. E_{max} can be observed to be grater than E_i by a factor of about 2.3 and at a strain level of 1×10^{-4} moduli from resonant column are higher than moduli from triaxial tests by a reduced factor of 1.6.

Both E_{max} and E_i are observed to increase nonlinearly with confining stress, Figure 4.7(a), and in approximately the same proportion to each other. The relationship of E_{max} and E_i with confining stress can also be viewed in log-log space as in Figure 4.8, wherein data points corresponding to resonant column and triaxial results can be observed to fit closely along approximately parallel straight lines. This implies that both E_{max} and E_i may be described by power functions of stress that have the same exponent but different coefficients. The exponents would be given by the slope of moduli and confining stress relationships in log-log space, as in Figure 4.8. For both results shown, the slope and thus power exponent is about 0.47. It may be of interest to note that this value is in the mid range of reported values for various sands and E_i from large strain considerations by Duncan et al (1980). It is also close to the exponent of 0.5 that is often used to relate moduli and confining stresses in very small strain cyclic loading considerations (Hardin and Drenevich, 1972; Seed and Idriss, 1970). Because their power exponent is the same, the ratio of E_{max} and E_i, once established, would remain unchanged at corresponding confining stresses. These observations may be of some interest and possible usefulness but do not provide a basis

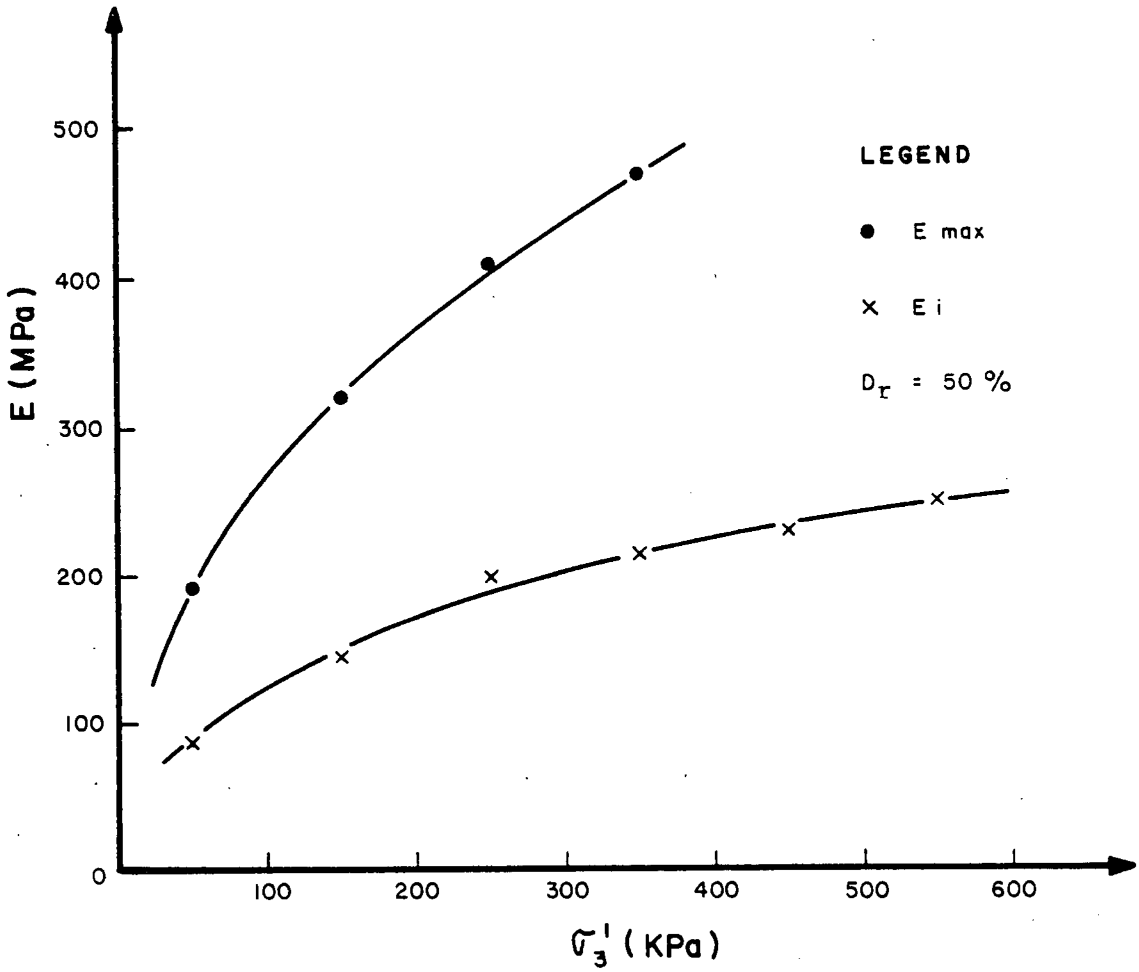

Fig. 4.7a Comparison of E_{max} and E_i as Determined from Resonant Column and Triaxial Tests

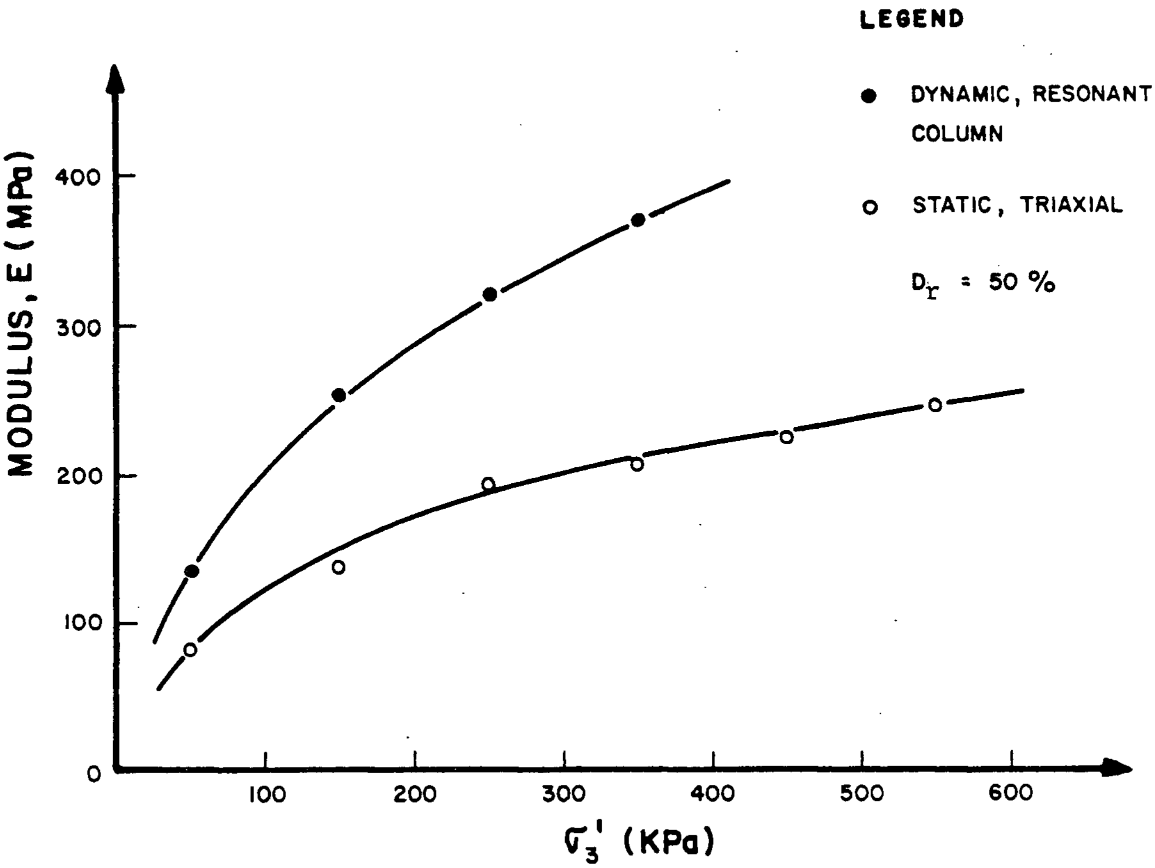

Fig. 4.7b Comparison of Dynamic and Static Moduli at 1×10^{-4} Axial Strain Level with Confining Pressure

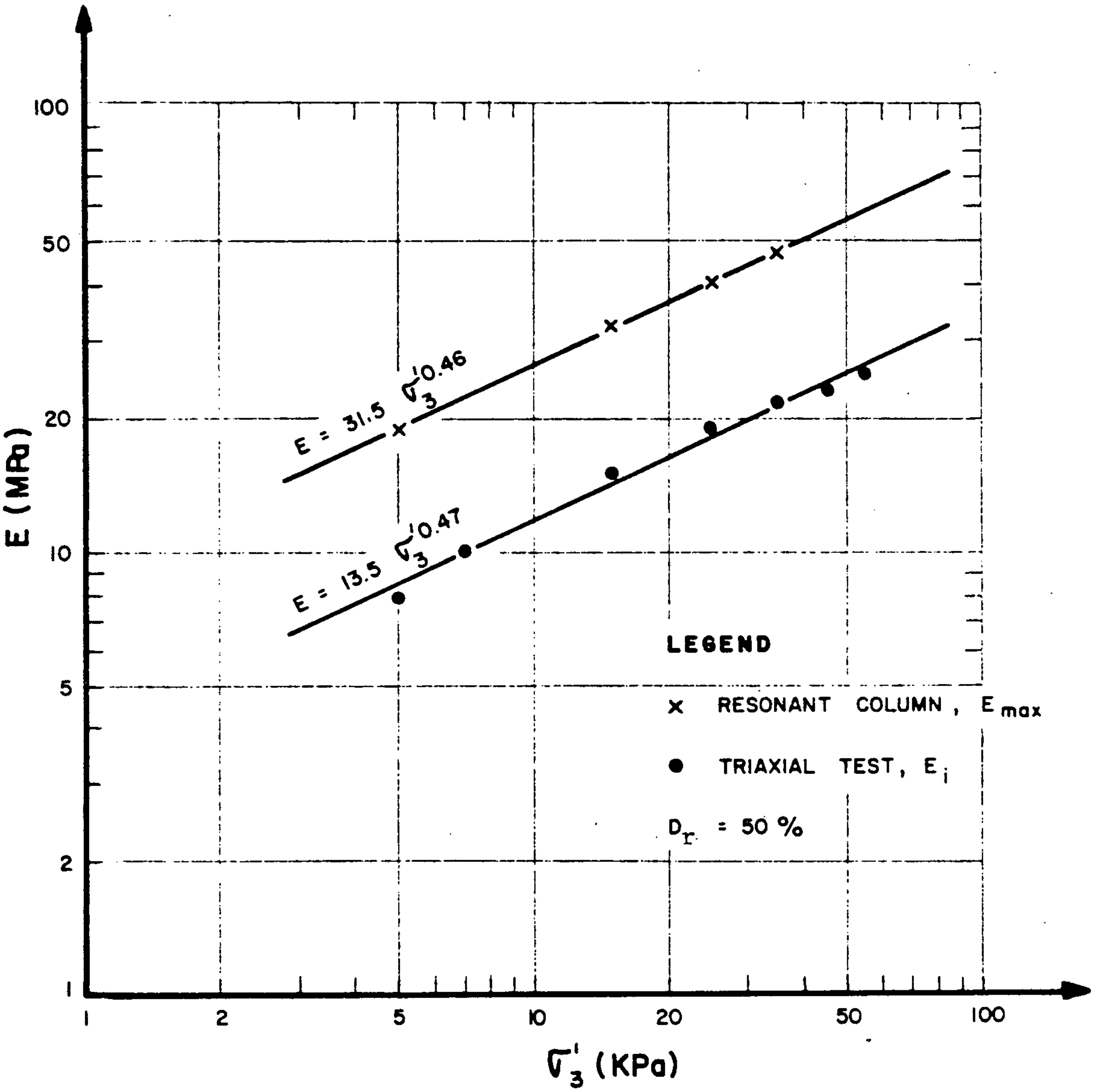

Fig. 4.8 Alternative Comparison of E_{max} and E_i at Different Confining Pressures

for interpreting discrepancies between E_{max} and E_i. Observations of static and dynamic moduli from higher strain levels might lead to further insight.

Because of limitations in direct measurement of small deformations, E_i was determined by extrapolation of secant moduli from strain levels above 1×10^{-5} to zero crossing. Observations of moduli at strain levels of 1×10^{-4} would appear to provide an alternative and more reliable perspective for examining relationships between E_{max} and E_i. It was previously noted that static and dynamic moduli at a strain level of 1×10^{-4} differ by a factor of about 1.6. The primary cause for this difference appears to be related to stress history. The resonant column sample was subjected to no less than a few thousand cycles of loading and unloading because resonant frequencies for the sand tested and in the range of confining pressures used were of the order of 250 Hz. Whereas, the triaxial sample was still within the first quarter of its first cycle of loading. Comparison is therefore being made of initial loading with reloading behaviour. The accumulated deformation during initial loading would contain a greater proportion of non recoverable deformation than would be the case for reloading. Hence static moduli at 1×10^{-4} strain would be less than corresponding dynamic moduli at the same strain level. If extrapolation of moduli to zero strain were to be made from moduli that were derived from strain levels at and in excess of 1×10^{-4}, the extrapolated moduli at zero strain from initial loadings would clearly be much less than those obtained from cyclic loading. This difference in intercept moduli is similar to the previously discussed difference in initial moduli for small and large strain considerations. This is because, as the strain amplitude approaches zero, cyclic loading history becomes of no consequence. Hence, the true zero strain intercept moduli for static and cyclic loading become one and the same; which means E_{max} should be equal to E_i. The modulus degradation of sand should therefore begin from E_{max} for both static as well as cyclic loading conditions. Therefore, E_i determined from small strain results must also be considered fictitious as was the E_i derived from large strain data. Their usefulness in prescribing moduli within various segments of strain response is analogous therefore to the conceptual use of apparent cohesion in specifying failure strength for granular materials over a range of confining pressures. As is the case for apparent cohesion, E_i should vary to enable improved correspondence between stress and strain.

From observations so far, three initial moduli that characterize broad behaviour classifications can be identified. The first would be the initial modulus determined by following conventional procedure and with emphasis on two data points corresponding to mobilization of 70 and 95 percent of shear strength (Duncan et al, 1980). As pointed out previously, this modulus is generally derived from large strain observation at near failure and steady state conditions. It would therefore be inclined to be associated with significant slip deformations. At the other end of the spectrum, E_{max} would represent an initial modulus for a response region wherein the proportion of recoverable strains would be more significant. Of course, the transformation from justified approximation at one extreme to the other is a gradual one. However, because this gradual transformation is difficult to track and actual deformations related to response near

E_{max} tend to be relatively very small, it has in the past been customary to utilize large strain representation throughout. This procedure has been found to invariably lead to overestimation of small strain response and has not been entirely satisfactory. Even for limited small strain results and considerations, the required use of failure parameters in conventional hyperbolic representation has been found objectionable. Alternative suggestions for distortion of the stress strain curve and forced fitting of data have been introduced by Hardin and Drenevich (1972). These additional steps were required to overcome basic inconsistencies in procedure and are a result of mixing small and large strain response.

It has been shown, Figure 4.2(b) that transitional initial moduli representing an approximate response region between 1 x 10^{-4} and 1 x 10^{-2} strain can be identified. Both recoverable and non-recoverable deformations would assume relative significance and this strain region is in general of greater relevance to many deformation problems. These initial moduli have further been shown to maintain a relatively fixed proportion to E_{max} values at corresponding confining pressure. However, adoption of these initial moduli within current procedure would require further development relative to specification of slopes in transformed plots, as noted previously.

4.1.1.3 Comparison of E_{max}, E_i, E_{iu} and E_{ir}

Conventional triaxial and resonant column tests were made at a common relative density of 50 percent in order to examine relationships between alternative initial Young's Moduli of E_{max}, E_i, E_{iu} and E_{ir}.

Test results from cyclic loading in conventional triaxial paths and from which E_i, E_{iu} and E_{ir} have been determined are shown in Figure 4.9. These results are presented with E_{max} and secant moduli at a strain of 1 x 10^{-4} that were obtained from resonant column tests as shown in Figure 4.10.

As argued previously, direct measurement of deformations cannot be considered suitable for reliable evaluation of moduli at well below the measurement accuracy of the testing apparatus. At the same time, for a given confining pressure and in the vicinity of zero strain; E_i, initial loading modulus; E_{iu}, initial unloading modulus; and E_{ir}, initial reloading modulus; must all converge to E_{max}. In reality and because of measurement limitations; E_i, E_{iu} and E_{ir}, shown in Figure 4.9 represent secant moduli at strain levels of about 1 x 10^{-4}. Moduli from resonant column testing are determined from a mean slope of a hysteresis loop and represent a secant modulus. Both $E_i$and E_{ir} as well as E at 1 x 10^{-4} strain from resonant column testing are significantly lower than E_{max} and thus reflect modulus degradation with strain, Figure 4.10. The extent of degradation is more severe for E_i as opposed to E_{ir}. While there is a relatively large difference between E_i and E_{ir} for first reloading, further stiffening on subsequent reloadings was small as E_{ir} appeared to increase very little. As may be noted, E_{ir} is slightly below E at 1 x 10^{-4} strain from resonant column results and this small difference would appear to be the effect of stiffening due to a large number of repeated loading and unloading. On the other hand, E_{iu} is approximately equal to E_{max} and there is

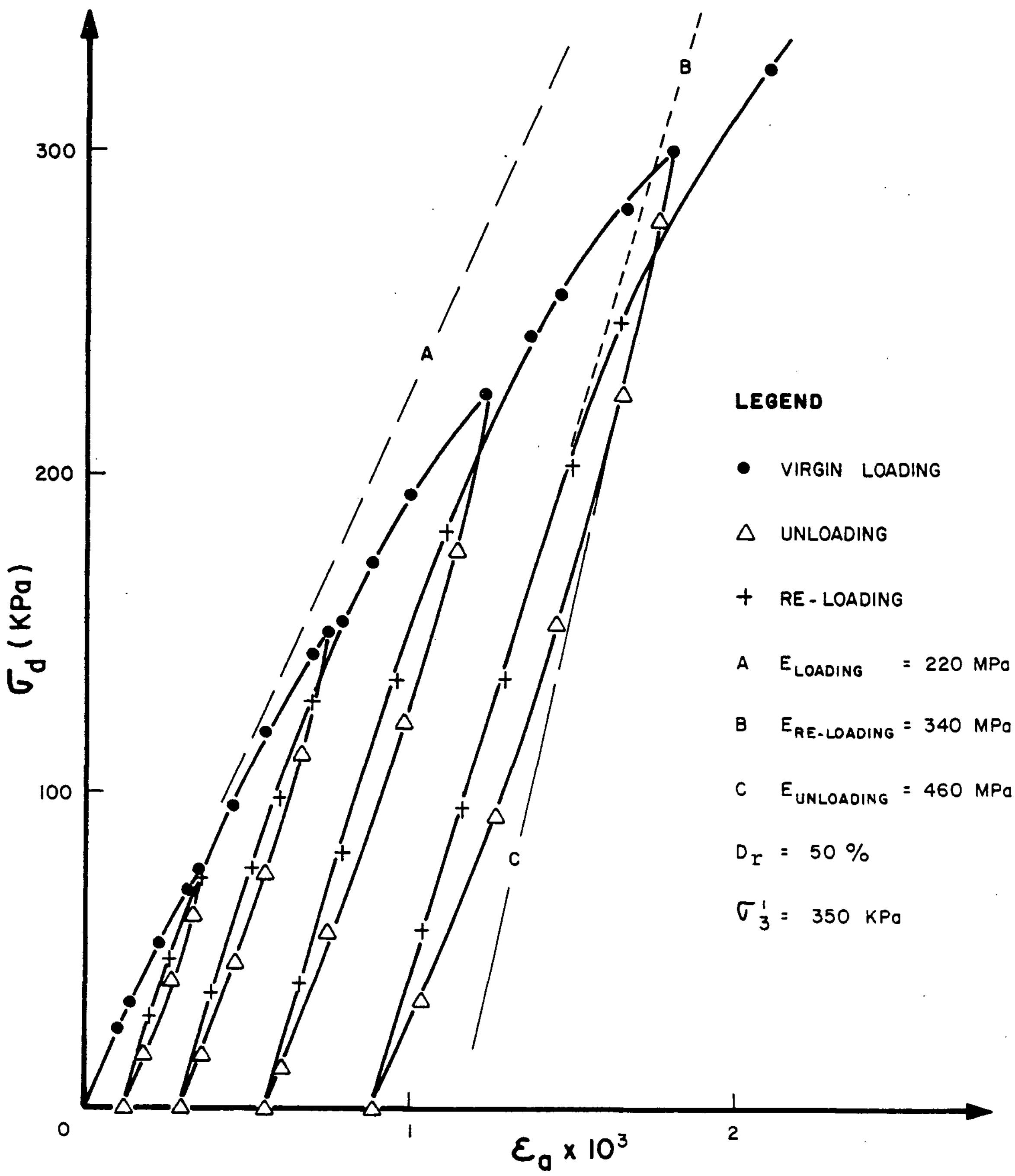

Fig. 4.9 Loading and Unloading Response in a Conventional Triaxial Path

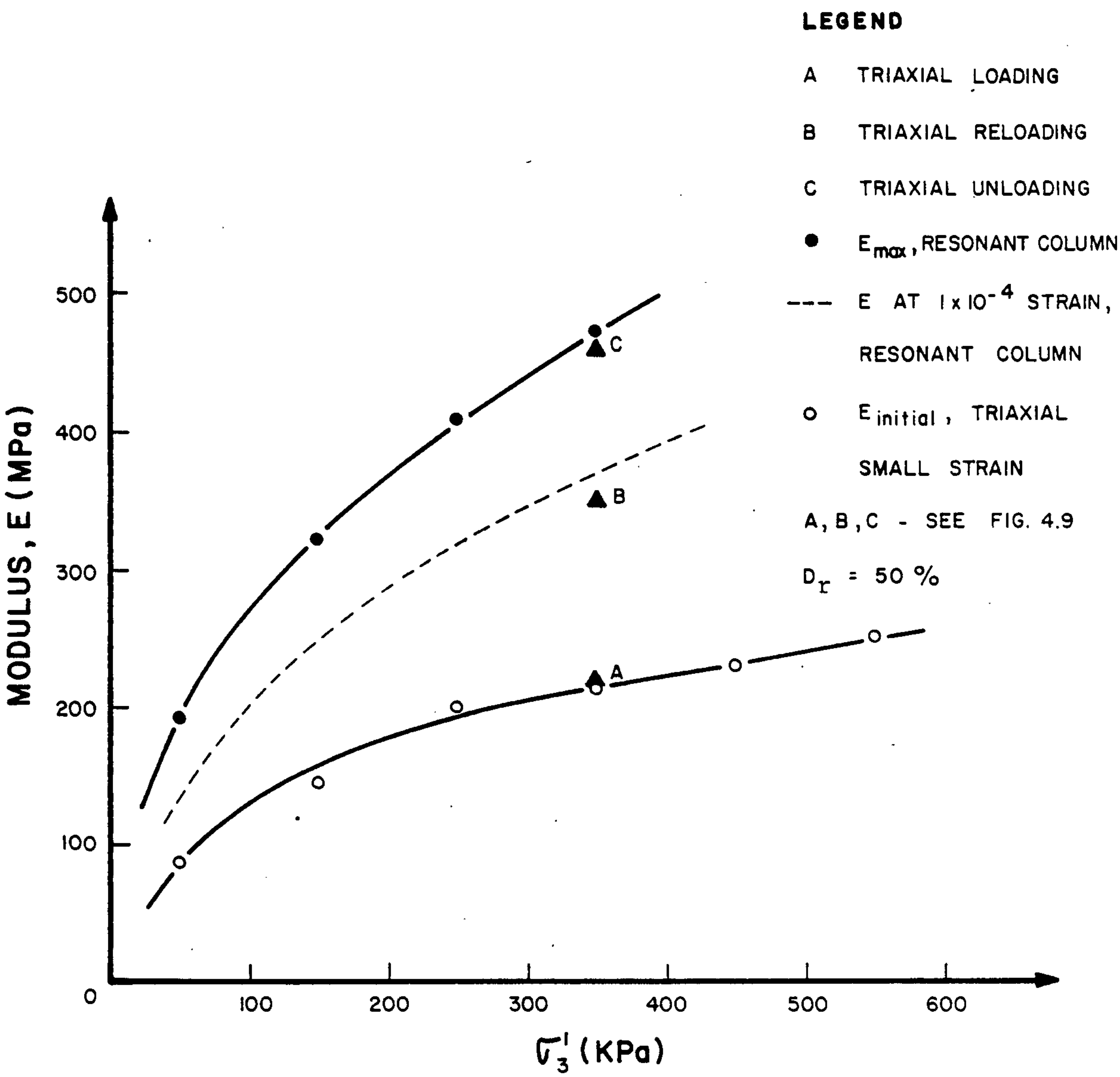

Fig. 4.10 A Comparison Between E_{max} and Various Initial Moduli, E_i

therefore very little modulus degradation with strain during unloading. For practical purposes, both E_{iu} and E_{ir} can be considered to be independent of deviator stress level and cycles of loading and unloading. This implies relatively unique values of E_i, E_{ir}, E_{iu} and E_{max} would be associated with each confining stress and void ratio. Furthermore, because E_{max} is approximately equal to E_{iu}, reliable estimates of E_{max} can be obtained from small strain static test results. It should be noted, however, that behaviour and relationships so far observed pertain to conventional triaxial tests and thus do not reflect the possible influence of stress paths.

4.1.2 The Influence of Stress Paths

The stress strain behaviour of sand has long been recognized to depend on stress paths. In many practical situations, stress paths may differ from conditions of uniaxial loading. Incremental approaches are usually employed in numerical analyses to simulate response to arbitrary stress paths assuming isotropy and moduli to be state variables. These incremental evaluations are made from hyperbolic representations of stress-strain data from uniaxial loading. One of the aims of the following experiments was to observe the general character of stress strain relationships from widely differing stress paths. Another was the evaluation of incremental moduli at common stress states that were reached by following different stress paths. These moduli are then compared to moduli determined from uniaxial tests in order to assess the relative influence of stress paths and establish overall trends.

4.1.2.1 Stress-Strain Relations in Different Paths

The stress path analog and small deformation measurement capability developed in this research enabled reliable observation of behaviour in a variety of stress paths. Some typical stress paths investigated are shown in Figure 4.11, in which the conventional triaxial path corresponds to label 2. All selected stress paths satisfy conditions of increasing or constant stress ratio, mean normal and shear stresses. There was no unloading in terms of any stress variable. As shown in Figure 4.12, these paths result in widely different stress-strain responses.

Failure and deformation of sand are strongly influenced by stages in overall shear to mean normal stress ratio. Relationships between deviator stress and axial strain resemble a hyperbola only in paths that ultimately lead to a failure stage. On the other hand, increases in deviator stress in paths having an obliquity well below failure (test #4 in Figure 4.12) lead to contraction. Moduli increase with strain level and a parabolic rather than hyperbolic approximation may be more suitable. Consequences of assuming moduli to be state variables are examined in the following section.

4.1.2.2 The Influence of Stress Paths on Incremental Moduli

Considering conventional triaxial test results, for a given magnitude of deviator stress different moduli may be specified depending on the confining stress level. Moduli are evaluated at

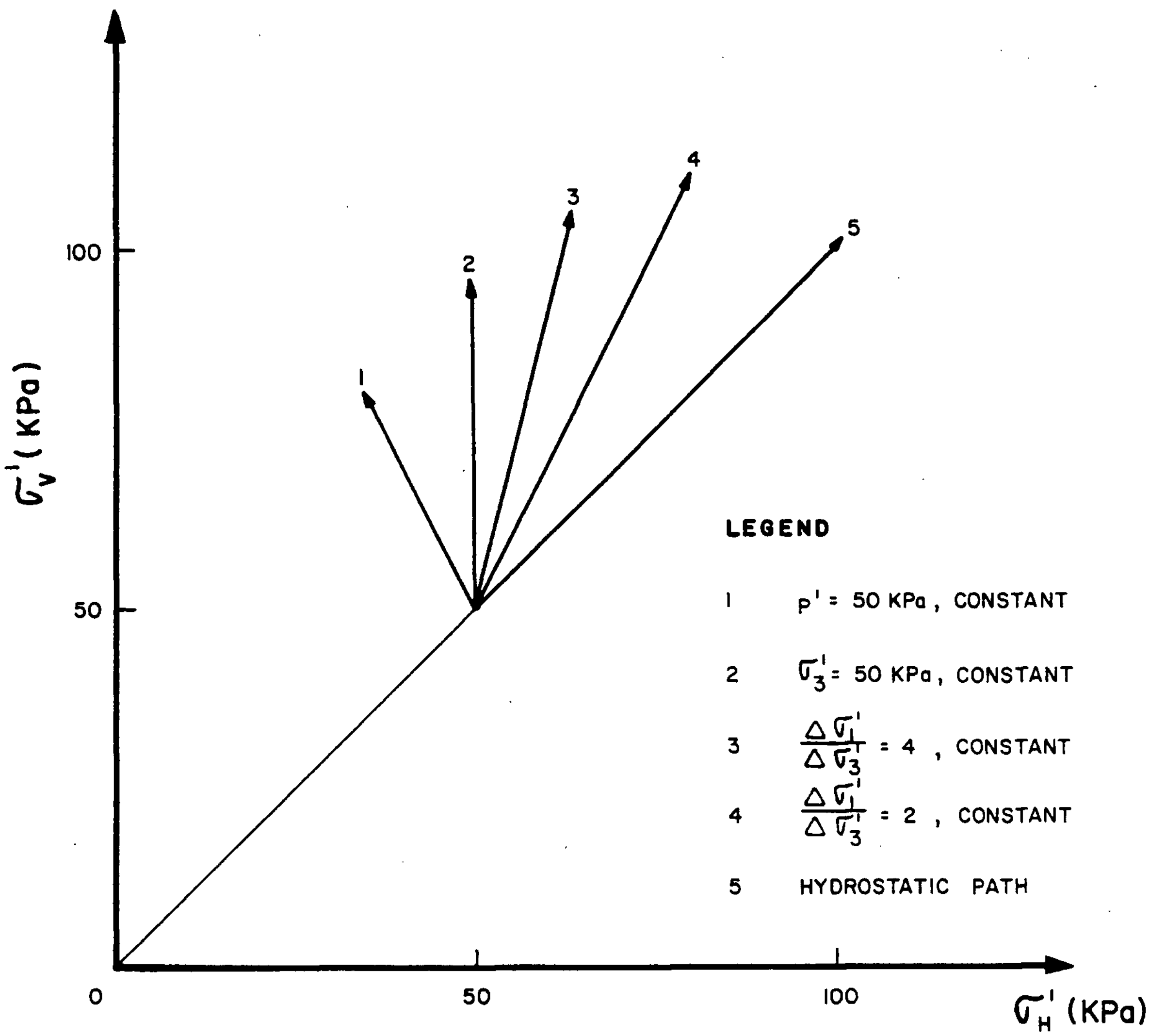

Fig. 4.11 Stress Paths Investigated

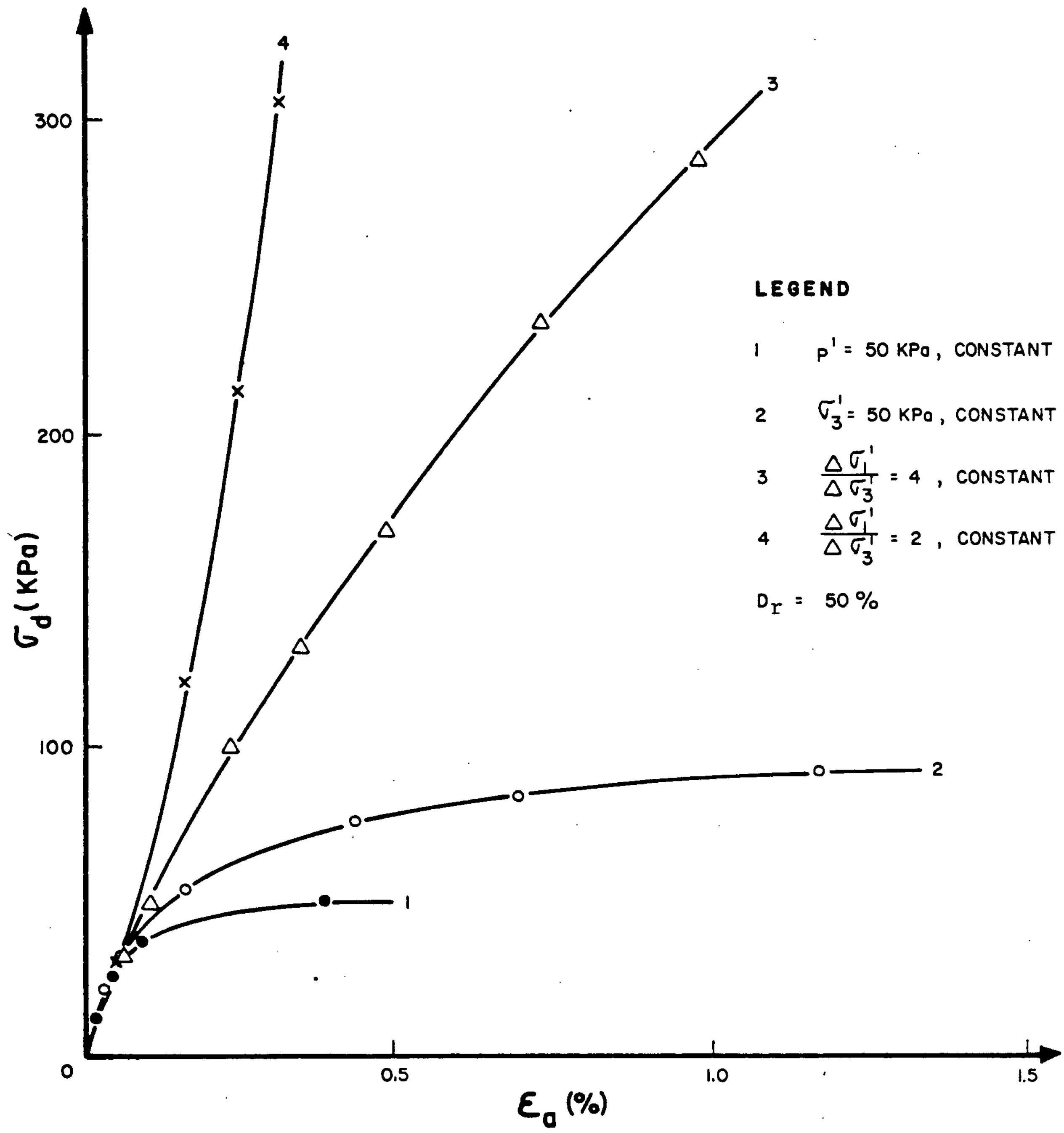

Fig. 4.12 Stress Strain Response From Tests Performed Along the Various Stress Paths

stress points, with the implicit assumption of path independence. To examine the influence of stress paths on moduli, tests were conducted to common stress states following paths shown in Figure 4.13. Stress points C, G and F were reached in two different ways by following either a constant confining or mean normal stress path. Point F was also reached following a path in which the incremental stress ratio was held to 4. Successive intersections between triaxial and a path with an incremental stress ratio of 2 are represented as points A, B, C, D and E.

These test results were used to evaluate and compare incremental moduli that have been determined along different stress paths at common stress point.

Corresponding plots of deviator stress against axial strain on which homologous stress points have been labelled are shown in Figures 4.14(a),(b) and (c). However, moduli at common stress states determined from deviator stress-axial strain space cannot be compared directly. Considering a simple linear elastic representation within a small neighbourhood of the individual stress states; the incremental expression for tangent modulus would be:

$$E_t = \frac{1}{\delta\varepsilon_a}(\delta\sigma'_a - 2\mu\delta\sigma'_r) \qquad (4.1)$$

or

$$E_t = \frac{\delta\sigma_d}{\delta\varepsilon_a} + \frac{\delta\sigma'_r}{\delta\varepsilon_a}(1 - 2\mu) \qquad (4.2)$$

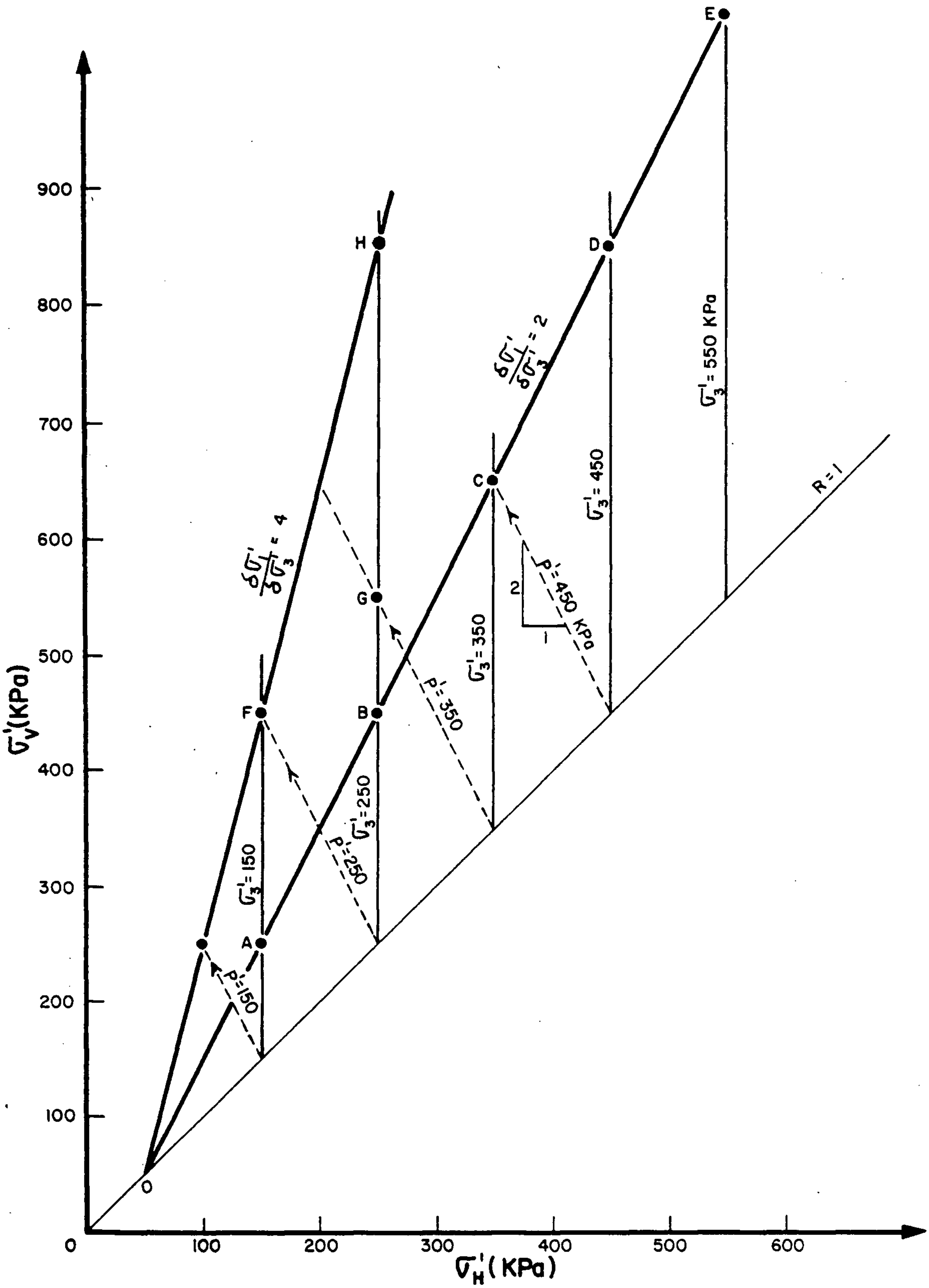

Fig. 4.13 Different Stress Paths and Common Points of Intersection

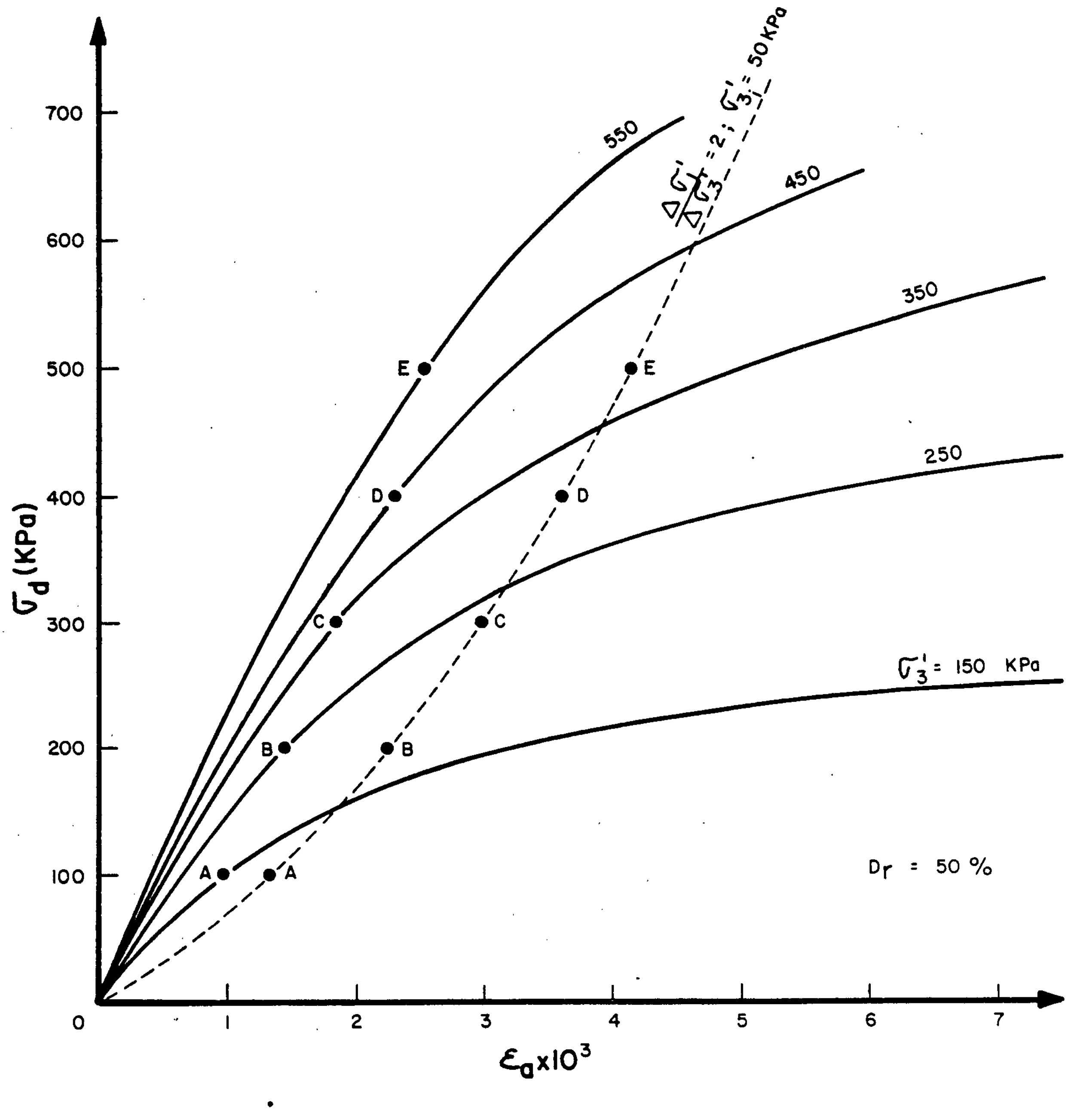

Fig. 4.14a Paths Dependence of Moduli Evaluated at Common Stress Points: Conventional Triaxial and $\frac{\delta\sigma_1'}{\delta\sigma_3'} = 2$ Paths

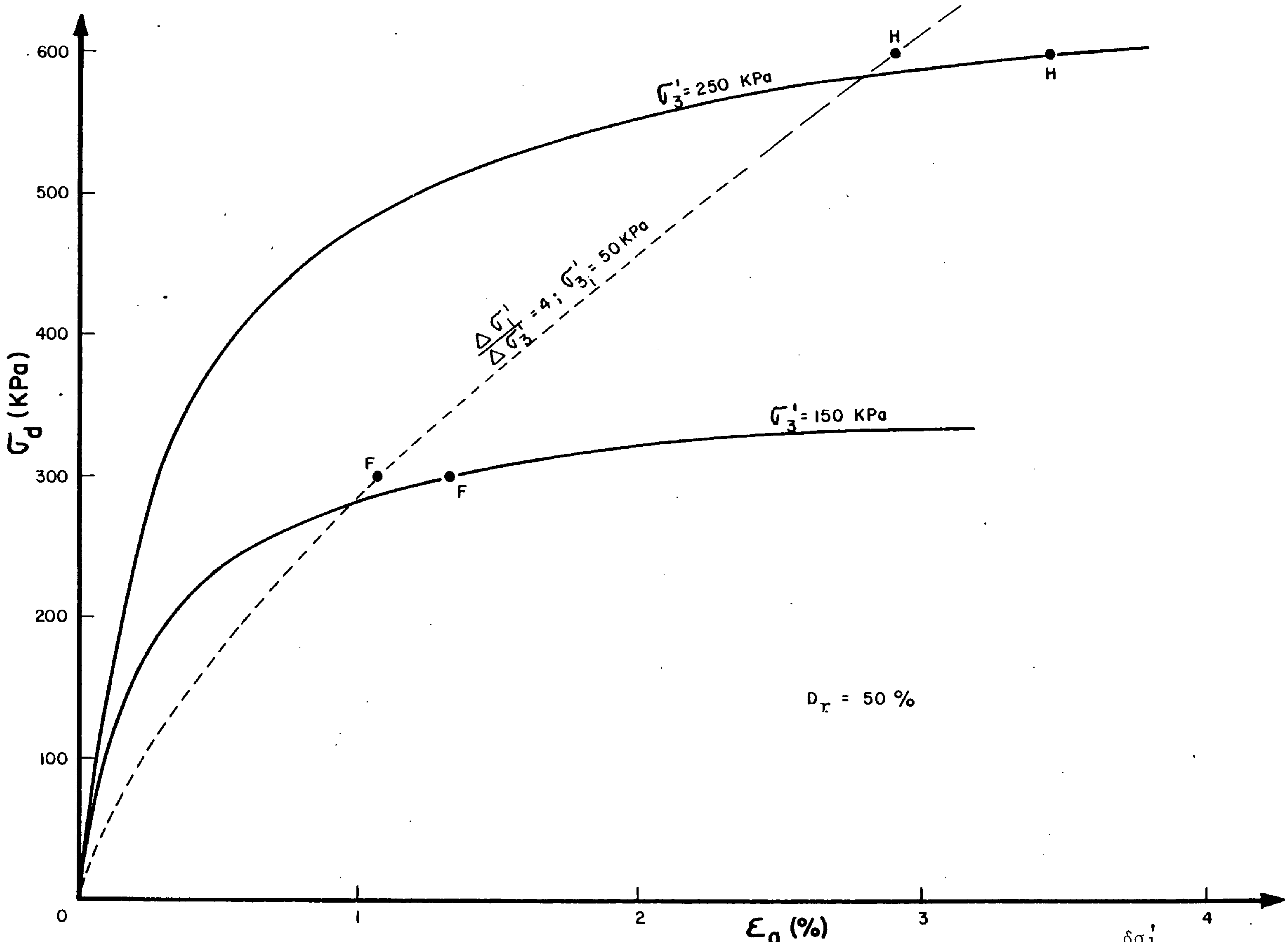

Fig. 4.14b Path Dependence of Moduli Evaluated at Common Stress Points: Triaxial and $\frac{\delta\sigma_1'}{\delta\sigma_3'}$ = 4 Paths

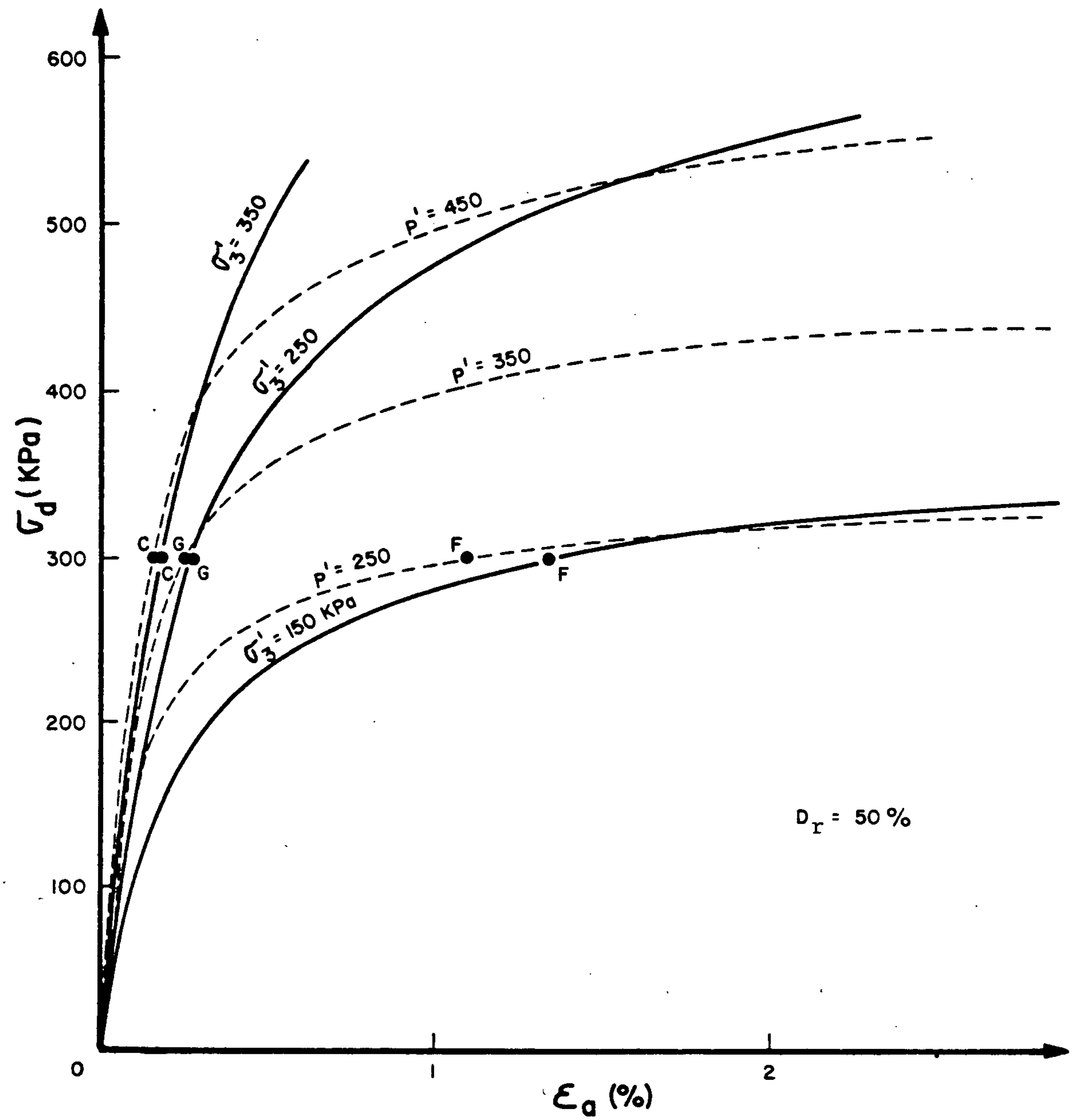

Fig. 4.14c Path Dependence of Moduli Evaluated at Common Stress Points: Triaxial and Constant Mean Normal Stress Paths

Moduli that would be determined from Figures 4.14a, b and c are then

$$E'_t = \frac{\delta\sigma_d}{\delta\varepsilon_a} \tag{4.3}$$

such that

$$E_t = E'_t + \frac{\delta\sigma'_r}{\delta\varepsilon_a}(1 - 2\mu) \tag{4.4}$$

for the special case of the conventional triaxial test, $\delta\sigma'_r = 0$ and $E_t = E'_t$. In other cases $E_t \neq E'_t$. For conditions wherein $\delta\sigma_d = 0$; $E'_t = 0$ and $E_t = \frac{\delta\sigma'_r}{\delta\varepsilon_a}(1 - 2\mu)$ which would lead to the familiar expression for tangent bulk modulus as:

$$B_t = \frac{E_t}{3(1 - 2\mu)}$$

Letting r represent the ratio of stress increments, as $r = \frac{\delta\sigma'_a}{\delta\sigma'_r}$; then E'_t would be expressed in terms of r, as

$$E'_t = \frac{\delta\sigma'_r}{\delta\varepsilon_a}(r - 1) \tag{4.5}$$

and

$$\frac{\delta\sigma'_r}{\delta\varepsilon_a} = \frac{E'_t}{r-1} \tag{4.6}$$

such that

$$E_t = E'_t \left(\frac{r-2\mu}{r-1}\right) \tag{4.7}$$

The parameter r defines the stress path under consideration. Thus, moduli at the same stress point but obtained from considering different stress paths and stress increment directions can therefore be compared through the use of Poisson's ratio, μ. Equivalent Poisson's ratios were found to lie generally between 0.2 and 0.4. The variation being a function of the combined effects of stress level and stress path and also reflects in part the imposition of the simplifying assumption of isotropy.

An average Poisson's ratio of 0.3 was used to determine corresponding moduli for different stress paths at the same stress states, σ'_3 and $\sigma_d = (\sigma'_1 - \sigma'_3)$. A comparison of results, as shown in Figure 4.15, demonstrates that moduli determined from uniaxial loading results differ from those derived from considering other stress paths. In general, moduli for paths oriented to the left of the conventional triaxial path (see Figure 4.11) would be overestimated. Consequently, predicted deformations for such paths would be lower than actual. With increasing strain level and on approaching failure states, the relative difference in moduli would diminish rapidly. However, at this stage, deformations would be intolerably large and concern would focus on

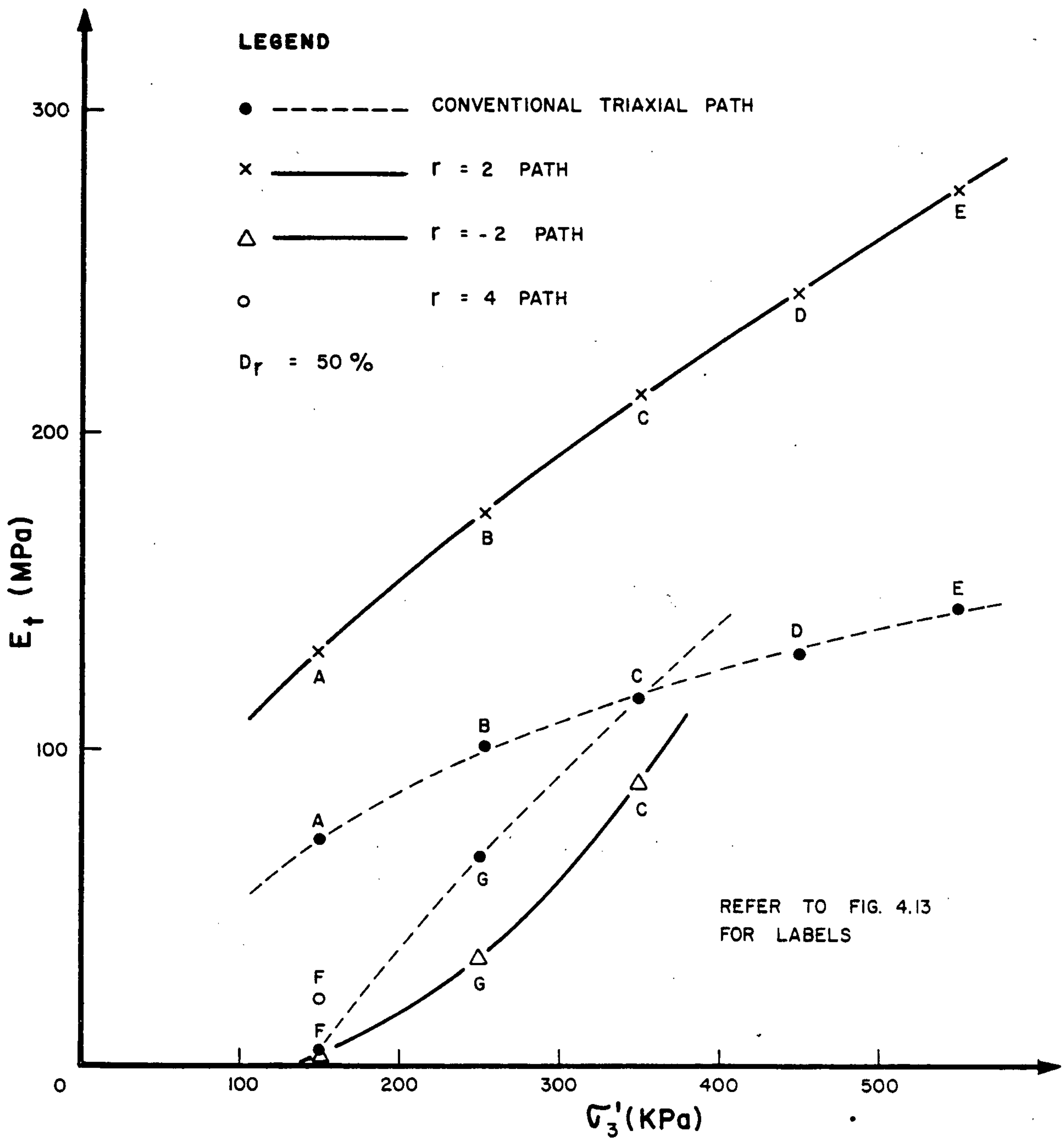

Fig. 4.15 Comparison of Moduli Evaluated at Common Stress Points Following Different Stress Paths

failure rather than deformation. For stress states at small stress ratio where deformation considerations are important, the two moduli may be seen to differ by a factor as large as 2. On the other hand, equivalent moduli estimated from paths oriented to the right of the triaxial path are seen to be underestimated, Figure 4.15. Predicted deformations for such paths would thus be higher than actual and there is a slight but consistent tendency for the relative difference in moduli to increase with confining stress. Overall, in a majority of practical situations wherein assessment of deformations is the primary objective, both shear and confining stresses tend to increase simultaneously over most regions. Thus, evaluation of moduli at discrete stress points assuming path independence would appear to lead towards exaggerated prediction of deformations in a majority of cases.

4.1.3 Additional Remarks

Experimental studies of moduli led to incremental techniques for interrelating confining and shear stresses with axial strain for stress conditions akin to the triaxial path (Duncan and Chang, 1970). Even under simpler stress conditions of axial symmetry or plane strain, at least one more strain component needs to be determined for complete correspondence between states of stress and strain. Poisson's ratios were found to vary with stress. Imposition of an average value enabled characterization of behaviour by a two parameter model, in which dilatancy could not be simulated. Stress dilatancy features were later incorporated through a third parameter for large stress ratio responses (Byrne and Eldridge, 1982). Such further refinement enhanced realistic reproduction of volumetric response.

Incremental elastic representations are currently used in a vast majority of geotechnical deformation problems. This is a consequence not only of their convenience and simplicity but also because their performance is often comparable to other constitutive models for sand, at least in the current state of development (NSF/NSERC Workshop, 1980). Even with further development of more reliable comprehensive models, site conditions are in many cases not defined well enough to justify added complexity. It has therefore been suggested that such incremental elastic procedures will remain relevant for drained deformation problems (Griffiths and Smith, 1983). In this regard, further improvements relative to small strain response and also stress path effects would appear to make them more effective as well as enhance their current wide appeal.

There are various disadvantages inherent in incremental linear elastic approaches. Procedures for evaluating required parameters tend to ignore small strain response. The need to tie together small strain parameters with failure criteria have been found limiting. Although idealized as being isotropic, sand is in general anisotropic. Thus rotation of principal axes of stress, which so often occurs in many real situations, would have influence on stress strain response but cannot be accounted for by this form of representation. The stress path dependence of moduli has been shown, using test results and thus the notion that required parameters remain state variables in stress does not hold. Comprehensive relationships that would overcome these various limitations are ultimately desired. These objectives have been pursued in the past from both a continuum as well as particulate considerations.

4.2 Particulate Considerations

Study of the gross deformation characteristics of sand has also been attempted from fundamental considerations at the particulate level. Because sand grains vary in size, are irregularly shaped and have random packing, developments have of necessity remained empirical. The most significant of contributions reported from this line of development has been the stress dilatancy theory of Rowe (1962). For large strain and along selected stress paths, the stress dilatancy theory has been verified experimentally. However, its relevance to small strain response and along arbitrary stress paths of increasing stress ratio still remains in doubt and will be examined in this section.

The stress dilatancy equation, $R = KD$, proposed by Rowe originates from considerations of sliding between two particles. Sliding along a contact plane would be initiated when the corresponding Mohr-Coulomb shear strength is exceeded. Rowe postulated that the orientation of the plane of sliding would be so as to minimize the ratio of incremental energy input to output along the principal directions of stress and strain. This same mechanism was then extended to describe the deformation of a random assembly of irregular particles in contact. The particles were considered to be rigid and deformations to be a result of non recoverable slip.

Reported agreement with experimental results has been a mainstay for the stress dilatancy theory. The bulk of supporting experimental evidence has come from conventional triaxial tests. With improved test procedures and test equipment, the stress dilatancy equation has been shown to describe sand behaviour for conditions of increasing stress ratio starting from a hydrostatic state to peak and ultimate state (Barden and Khayatt, 1966). Confirmations were considered most favourable for dense states and upon reloading for loose conditions. Additional agreement with stress dilatancy was reported from plane strain and simple shear test results (Barden et al, 1969a; Cole, 1967). These further verifications together with previous confirmations have led to the view that stress dilatancy is path independent. In all reported experimental verifications, regardless of stress path and stress ratio level, consideration has always been based on total strains. It has been presumed that even upon reloading, sliding deformation predominates over elastic deformation of grains.

The focus of experimental study in this section has two parts. The first deals with a closer examination of stress dilatancy at small stress ratio and hence small strains in conventional triaxial paths. This issue has been raised recently by Nova and Wood (1979) and Nova (1982) and reservations relative to the form of the stress dilatancy relationship at small stress ratio have been expressed on the bases of conceptual arguments. The second objective is to examine the stress path independence of the stress dilatancy equation at small strain. As in all previous investigations, total strains will be used throughout and no attempt will be made to separate sliding and non sliding deformation components.

4.2.1 Stress Dilatancy in Conventional Triaxial Paths

4.2.1.1 The Influence of Stress Level

A plot of volumetric strain against axial strain from the results of a series of conventional triaxial tests at the same relative density of 50 percent but different levels of confining stress are presented in Figure 4.16. Incremental strain ratios were obtained as tangent slopes in Figure 4.16 from which dilatancy, $D = (1 - \frac{\delta\varepsilon_v}{\delta\varepsilon_a})$, was determined. Test data in Figure 4.16 show that at low strain levels, D is constant and appears to be relatively independent of confining pressure. Thus in the stress ratio dilatancy plot, Figure 4.17, resulting curves would have a common initial vertical segment. This implies a strain increment ratio characteristic to the stress path rather than the stress state would prevail at small strain. With increasing strain levels, the stress dilatancy curves transition to a slope parallel to but not coincident with K_μ, which corresponds to the interparticle friction angle ϕ_μ. Figure 4.17 also shows that the onset of increasing dilatancy, D, is delayed with increasing confining pressure and that the spacing between subsequent parallel lines and the actual K_μ line increases slightly. There is thus a discernable but slight dependence on confining stress in the relationship betwen R and D beyond the small stress ratio response region.

It is generally recognized that at a given void ratio dilation becomes suppressed with increasing confining stress. Therefore, at least in a qualitative sense, increasing density and confining stress have compensating effects. The influence of density has been recognized in stress dilatancy expressions by extreme settings relative to K_{cv} and K_μ. However, the possible existence of order on the basis of confining stress and within these extreme limits of the stress dilatancy expression has never been suggested neither as an assumption or a hypotheses nor has it been identified experimentally. The stress dilatancy theory in all its stages of development has remained entirely

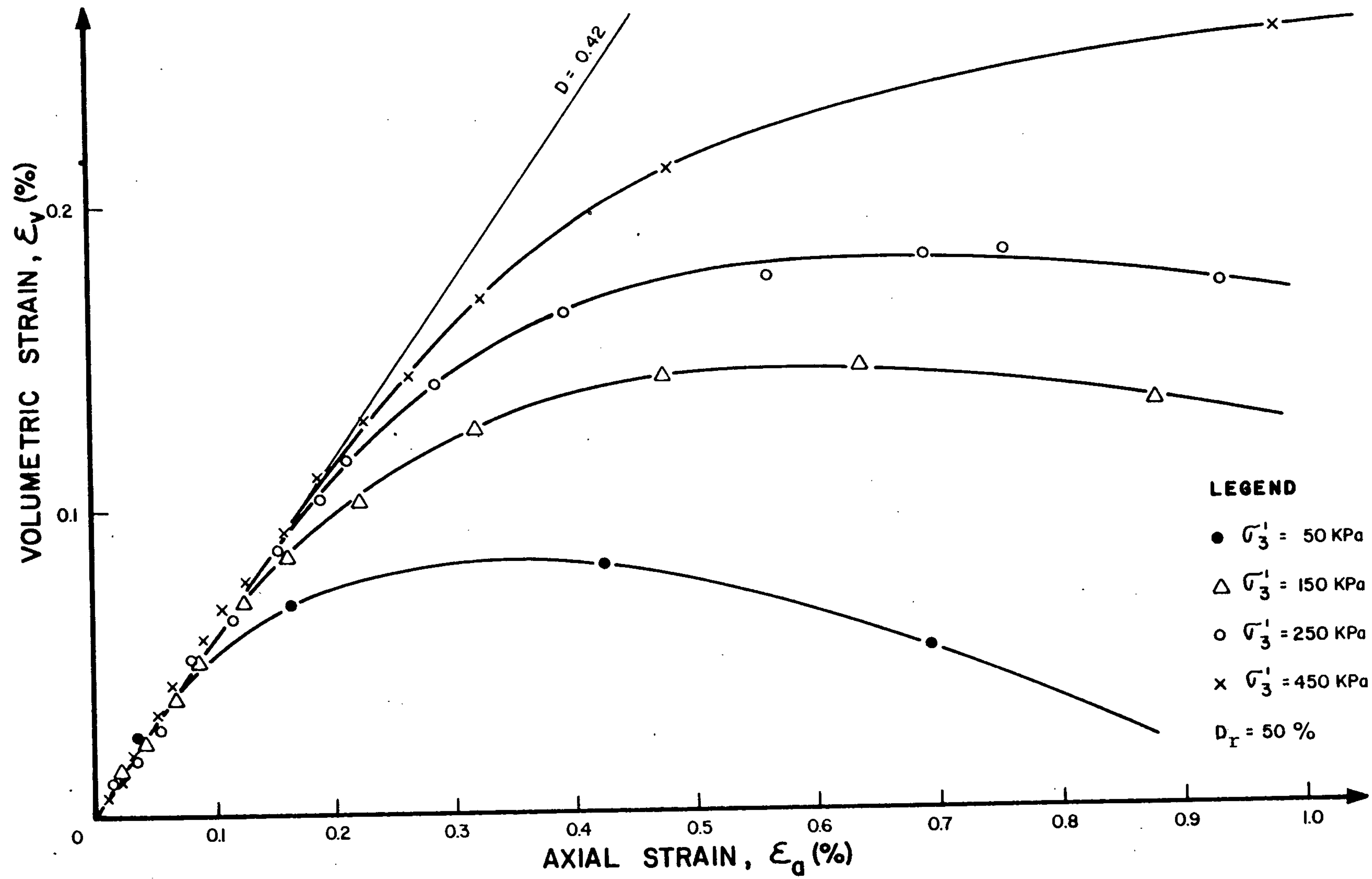

Fig. 4.16 Strain Paths for Conventional Traixial Stress Paths

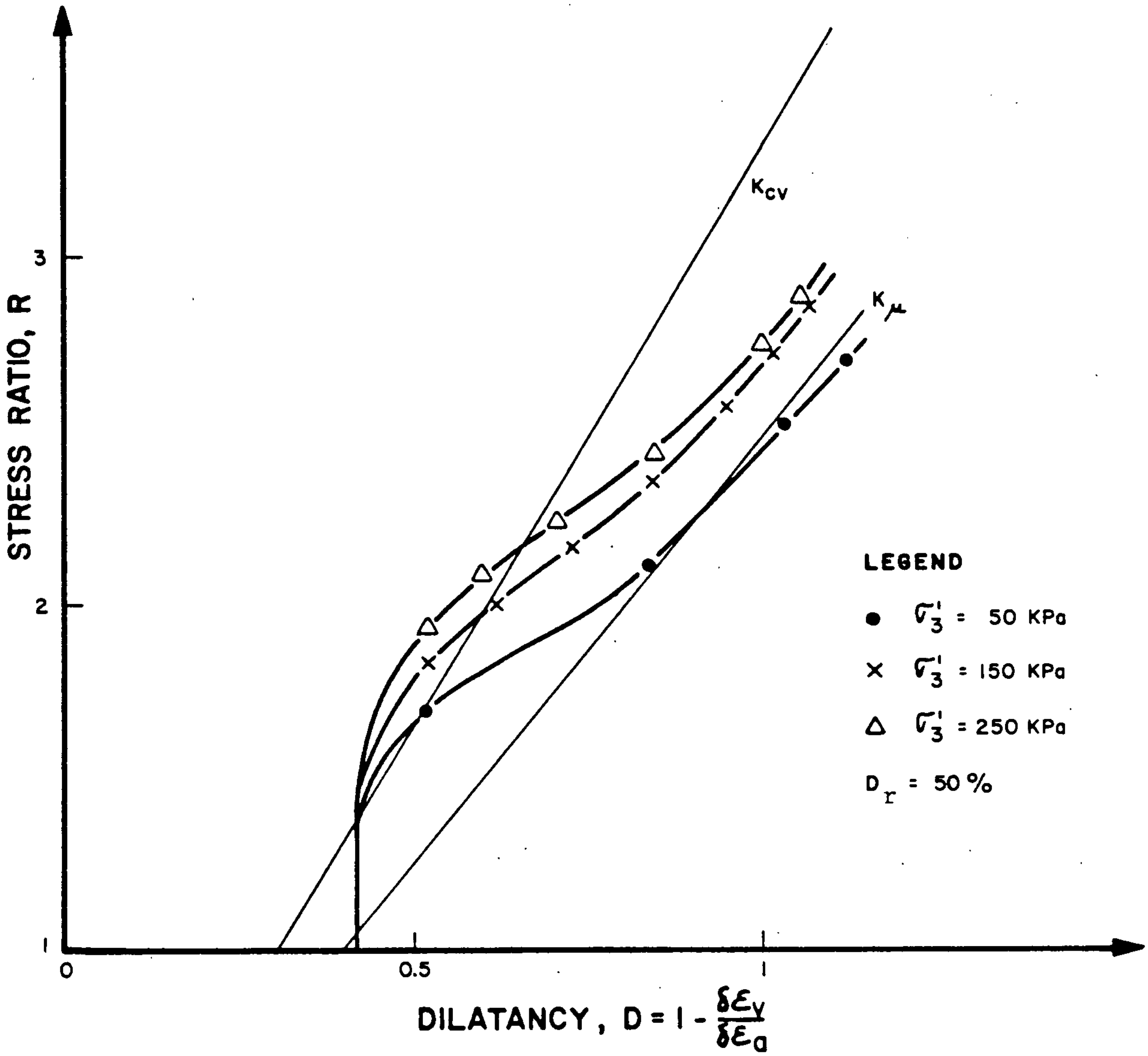

Fig. 4.17 Stress Dilatancy Plot of Conventional Triaxial Test Results

oblivious to the possible influence of confining stress.

At a given density, better agreement, in the sense of approaching K_{μ}, with the stress dilatancy equation was previously reported for conditions of reloading as opposed to initial loading (Barden and Khayatt, 1966). This opinion is, however, not supported by the small strain reloading test tesults shown in Figure 4.18. Again as for virgin loading, dilatancy in the small stress ratio region is constant and very close to the value for initial loading. Thus in the stress dilatancy plot, Figure 4.19, the initial vertical and transition segments are still in evidence. Although strain increment magnitudes associated with loading exceed those during reloading, both share a common strain increment ratio. This implies that strain increment directions are unchanged and thus the stress dilatancy expression would not vary.

4.2.1.2 <u>The Influence of Density</u>

A common initial strain path was also followed in loose sand as illustrated by test results at a relative density of 30 percent and at two confining stresses, Figure 4.20. In a stress dilatancy plot, Figure 4.21, this again corresponds to an initial near vertical segment. However, this stress dilatancy relationship initiates to the left of that for medium dense sand, and with increasing strain transitions towards parallel alignment to K_{μ} and K_{cv} at low and high confining stresses, respectively. Thus, the influence of confining stress in a stress dilatancy plot is similar but more significant for loose as opposed to medium dense sand. Therefore, comparison of loose and dense behaviour in stress dilatancy terms appears to require qualification with respect to level of confining stress. The

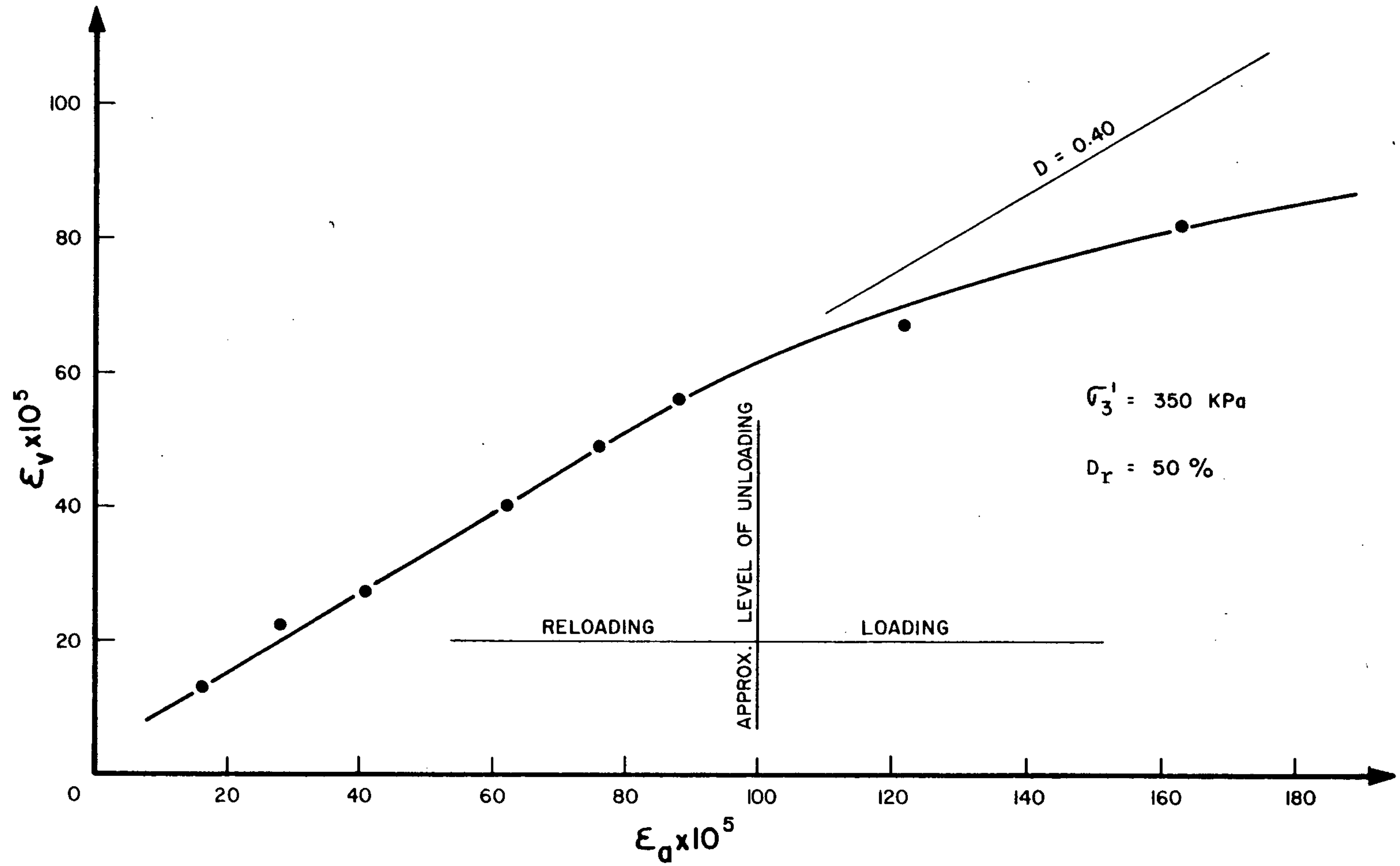

Fig. 4.18 Strain Paths for Conventional Triaxial Stress Paths in Reloading

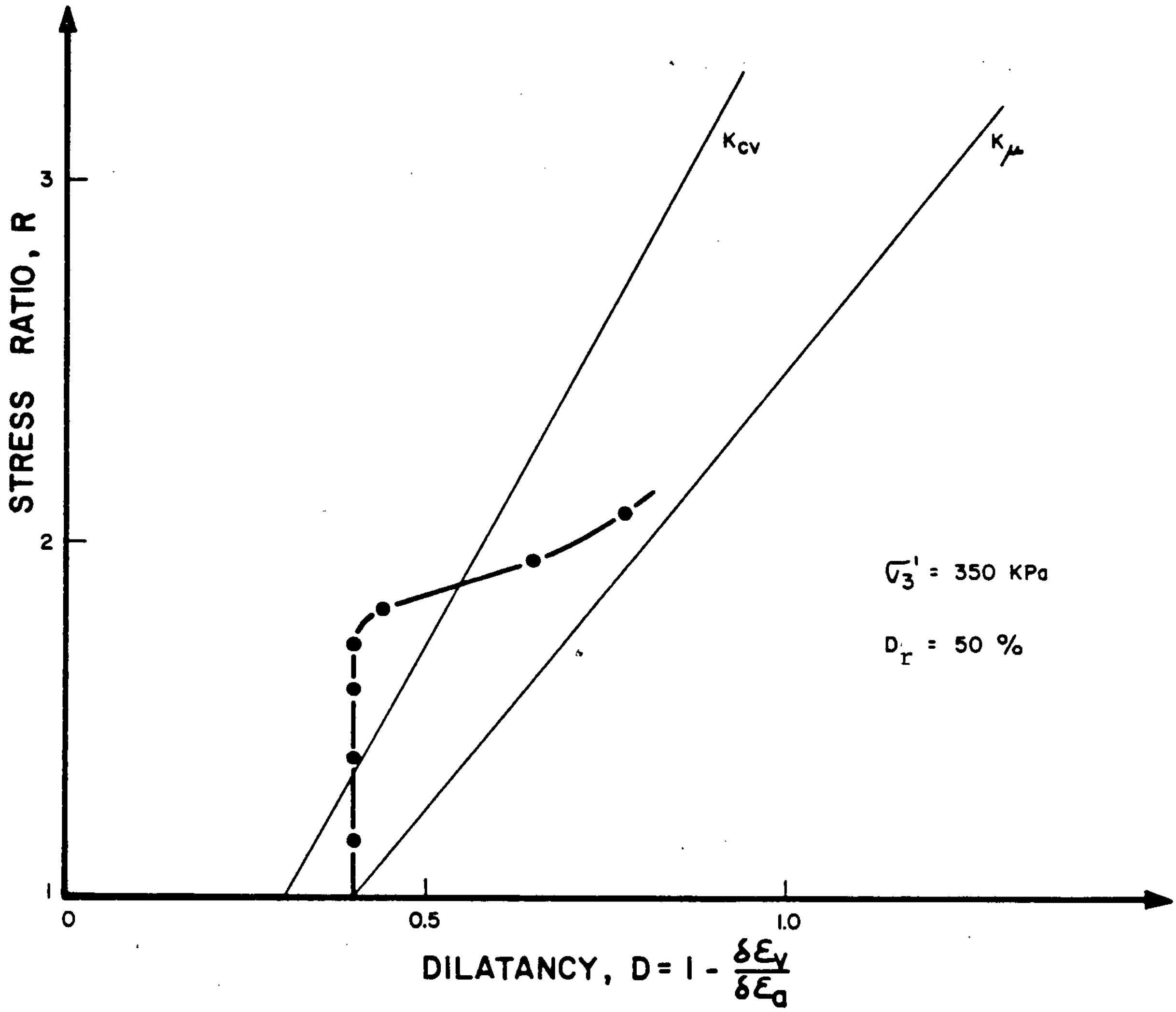

Fig. 4.19 Stress Dilatancy Plot of Conventional Triaxial Test Results During Reloading

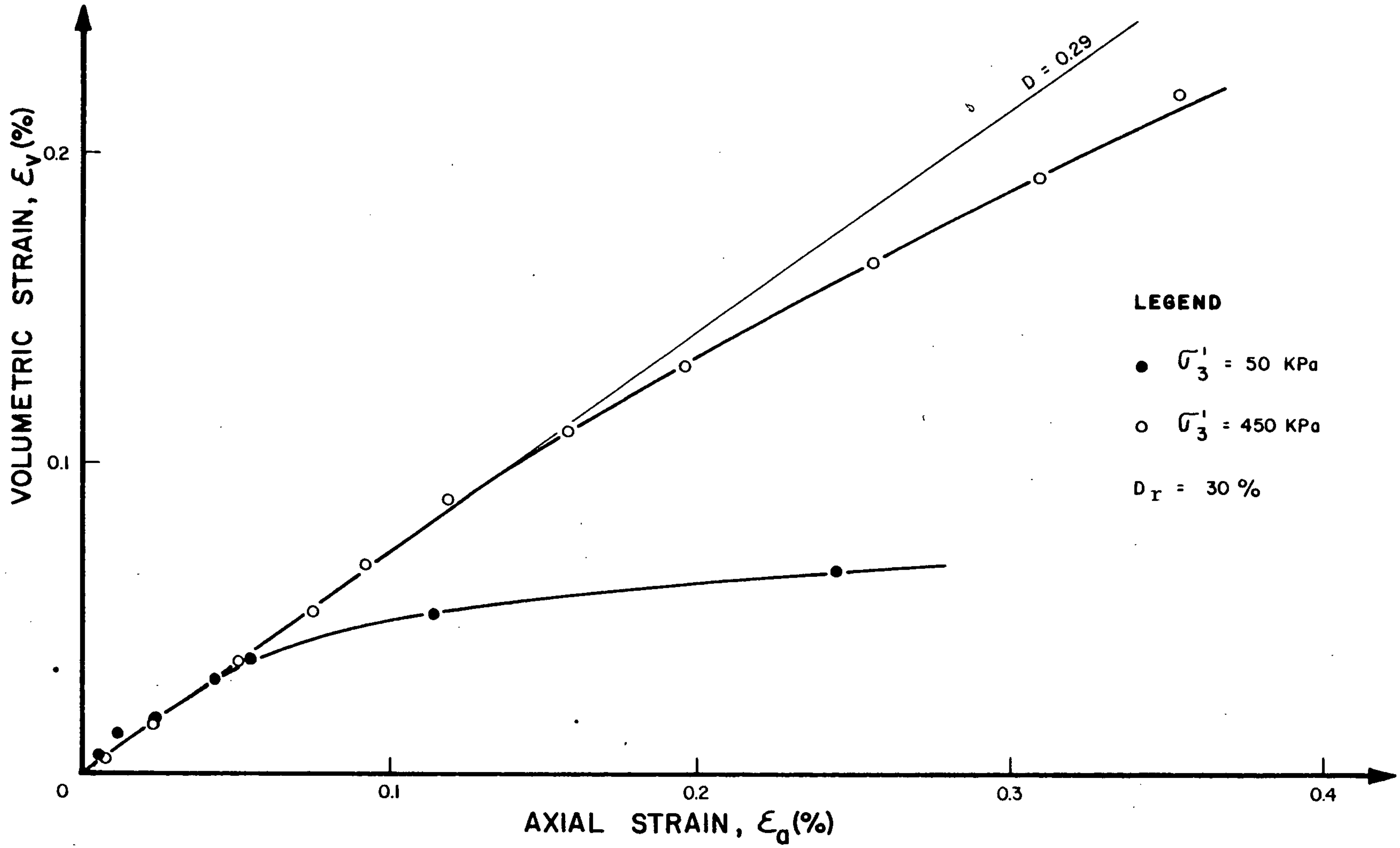

Fig. 4.20 Strain Paths for Conventional Triaxial Tests on Loose Sand

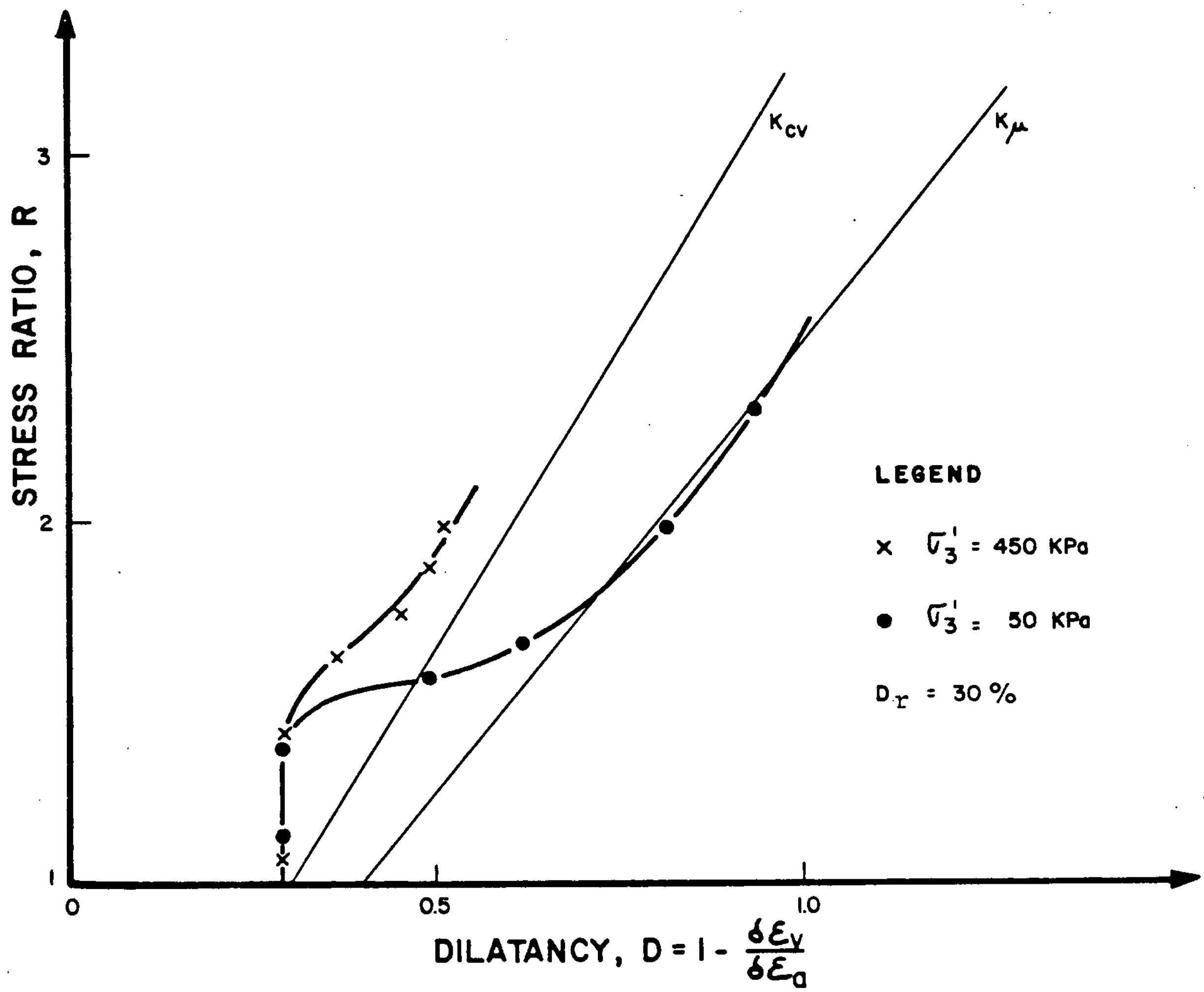

Fig. 4.21 Stress Dilatancy Plot of Conventional Triaxial Test Results on Loose Sand

approximately constant initial dilatancy factors increase with relative density. For dense states, relationships would originate below the K_μ line, whereas for loose conditions stress dilatancy curves initiate above K_{cv}. If the confining stress is high, the relationship tends to be parallel to K_{cv} and for a lower confining stress the alignment approaches K_μ. Hence, with increasing strain level, apparent agreement with stress dilatancy would depend not only on density but also on confining stress level.

4.2.2 Stress Dilatancy in Different Stress Paths

The preceding experimental results at small stress ratio and in conventional triaxial paths indicated that the stress dilatancy relationship did not continue as a straight line to a state of hydrostatic compression. Constant total strain directions that were independent of confining stress but dependent on density were observed for low stress ratio states. The hypothesis and subsequent experimental verifications advanced to justify the validity of the stress dilatancy equation for all states of increasing stress ratio starting from a state of R = 1 could not be supported. Further consideration of diverse stress paths in which the requirement of monotonically increasing stress ratio, as stipulated by stress dilatancy, are satisfied have been pursued to provide additional clarification.

Results from constant mean normal stress, constant incremental stress ratio as well as conventional triaxial paths, all at an initial relative density of 50 percent, have been plotted in terms of volumetric against axial strain to determine D for corresponding stress ratios, as in Figures 4.22a, b and c. It may be noted in Figure 4.22a that constant incremental stress ratio paths of 2 maintain a constant dilatancy factor of -0.5. The dilatancy term, D, would be zero for one dimensional deformation. A negative value of D implies both axial and radial strain increments are positive. Hence energy is input in both principal directions whether or not total or nonrecovered strains are considered. For an incremental stress ratio path of 4, the initial dilatancy factor is 0.37 (Figure 4.22b); whereas constant mean normal stress paths are initially associated with a dilatancy of 0.83 (Figure 4.22c). Conventional triaxial paths which were considered in the previous section maintain a dilatancy factor of about 0.42. These observations have been combined in a stress dilatancy plot, Figure 4.23, which shows that a unique initial dilatancy factor is implied for each stress path orientation. Paths of higher $\delta q/\delta p'$ may be observed to be associated with larger values of initial dilatancy.

The hypothesis that stress dilatancy is valid in all paths of increasing stress ratio, from hydrostatic to failure state does not appear to be supported by experimental evidence presented. Previous verifications of stress dilatancy were based on test results from conventional triaxial, simple shear and plane strain tests. Of these, however, a hydrostatic stress state is accessible only to the conventional triaxial test. Both plane strain and simple shear tests initiate from a state of one dimensional (K_o) compression. Stress ratios corresponding to K_o states are generally in excess of 2. Hence validity of stress dilatancy below a stress ratio of 2 could only be assesed on the basis of conventional triaxial test data. It may be noted (Figure 4.23) that the initial dilatancy factor for conventional

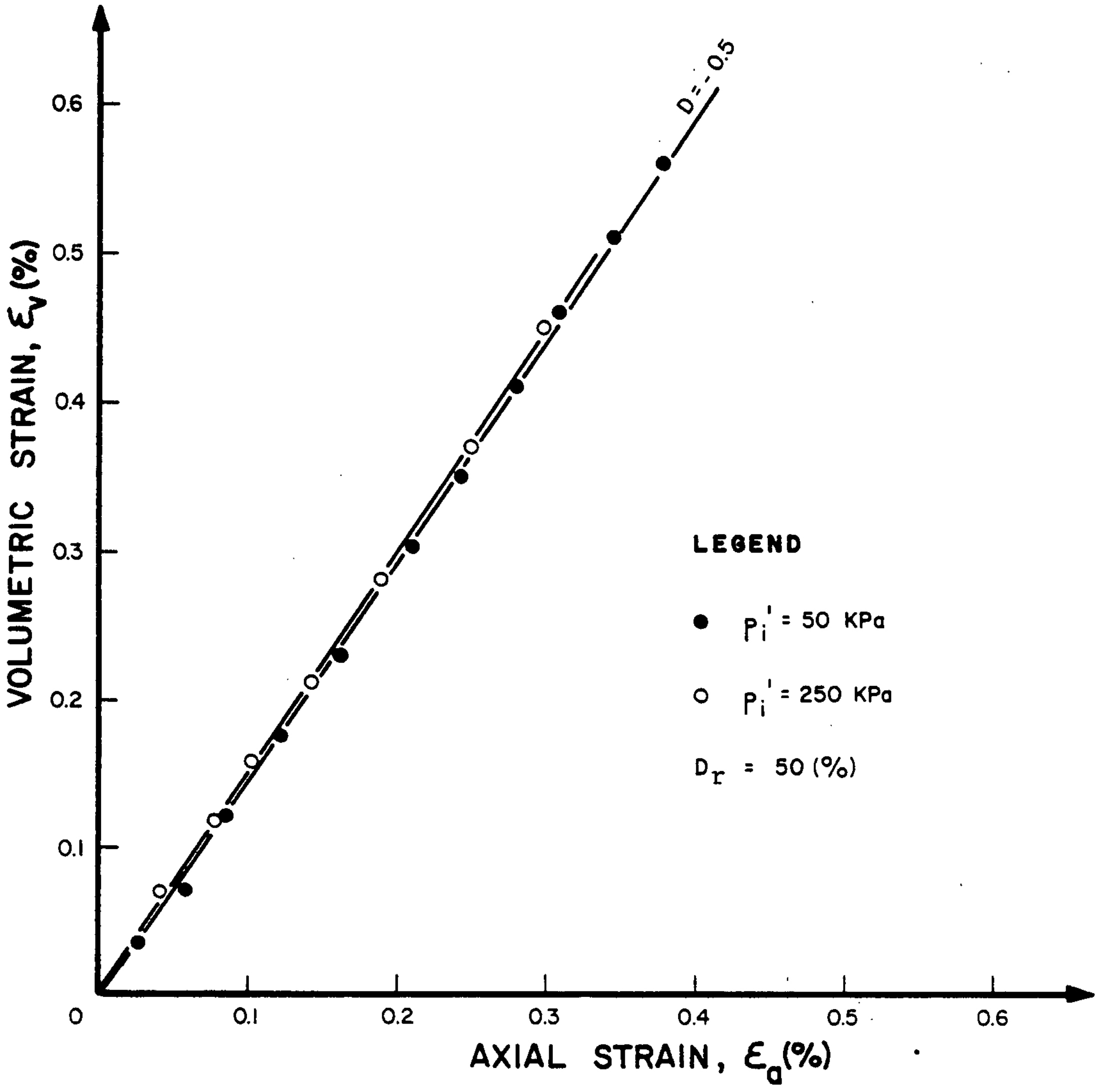

Fig. 4.22a Strain Paths for Stress Paths of Incremental Stress Ratio of 2

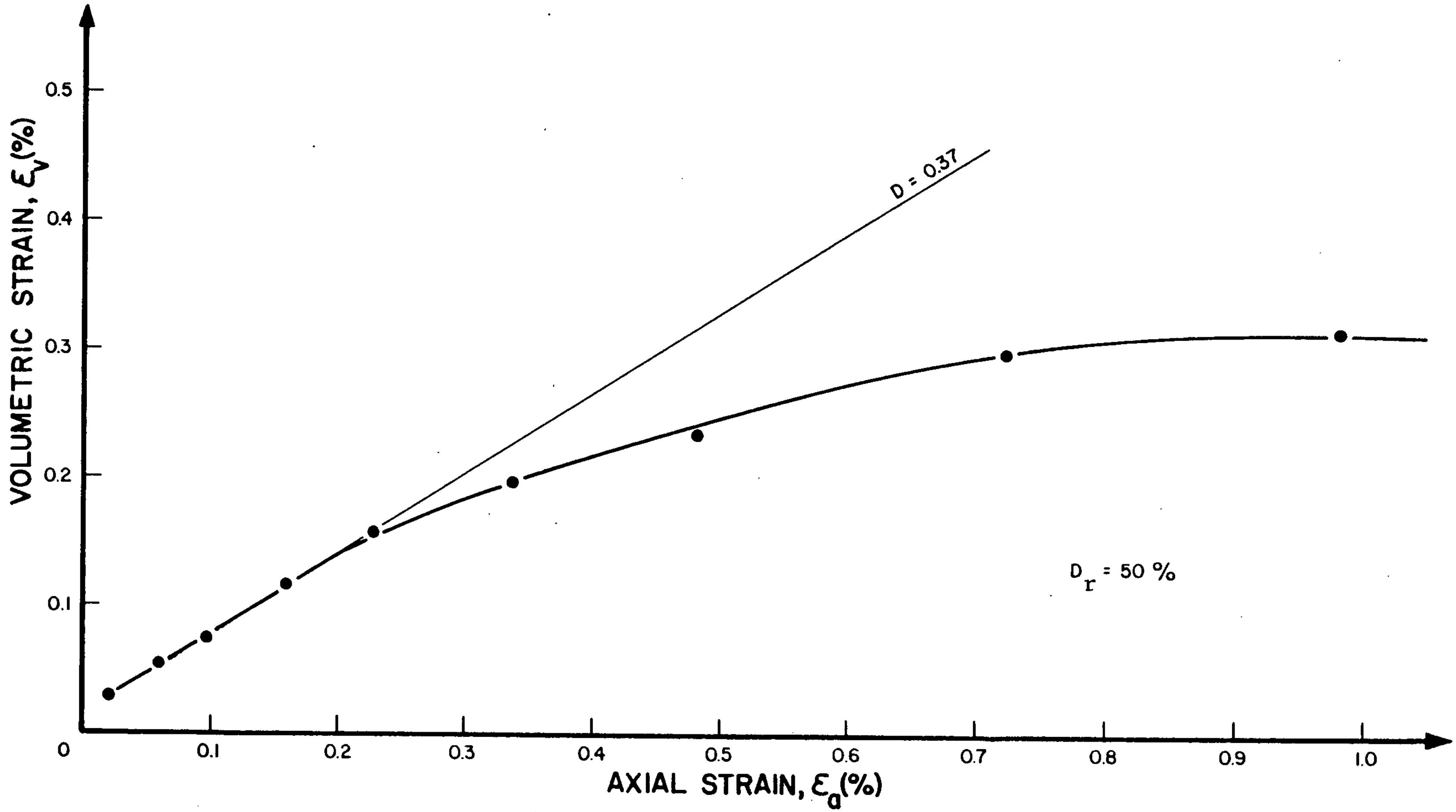

Fig. 4.22b Strain Paths for an Incremental Stress Ratio of 4 Paths

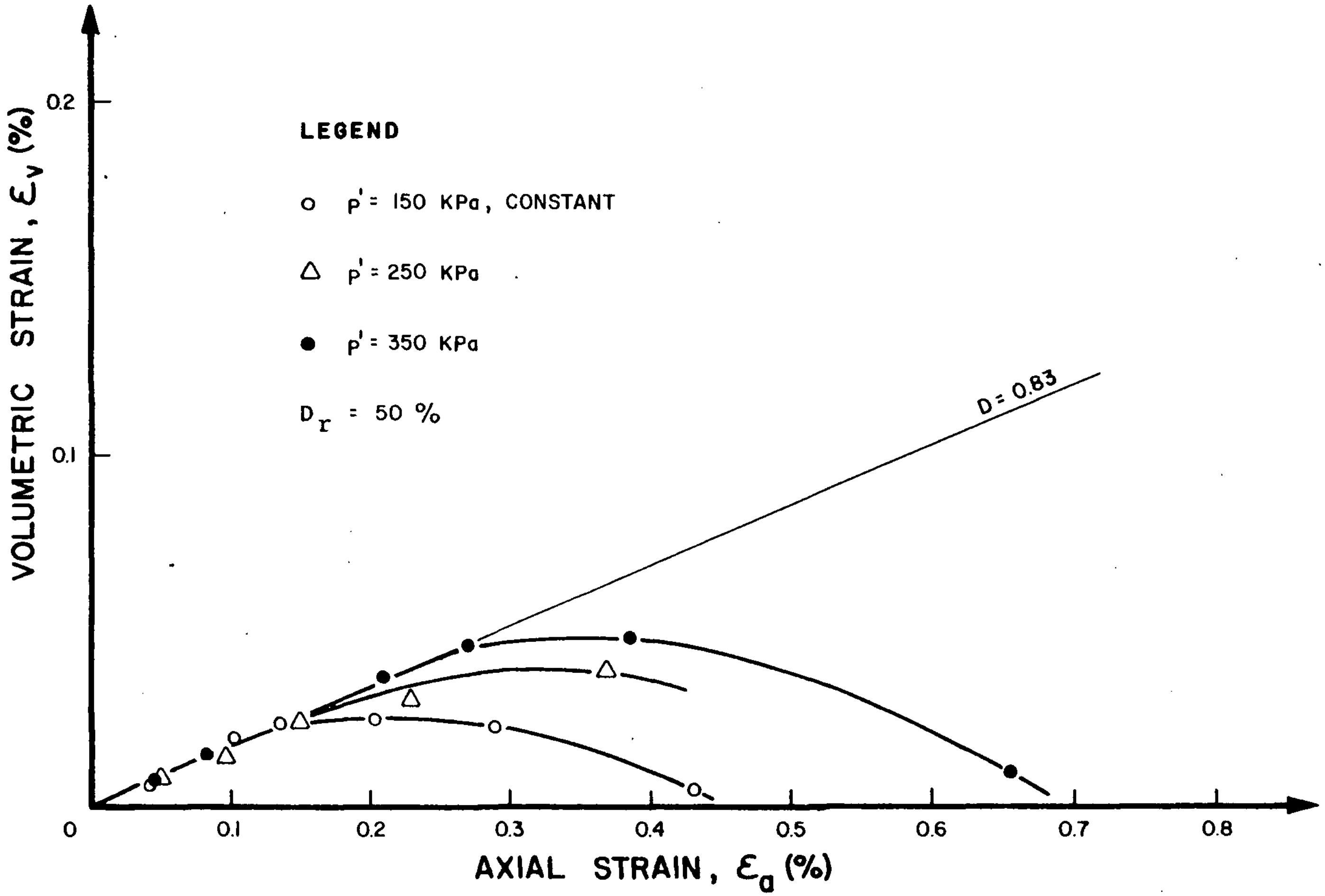

Fig. 4.22c Strain Paths for Constant Mean Normal Stress Paths

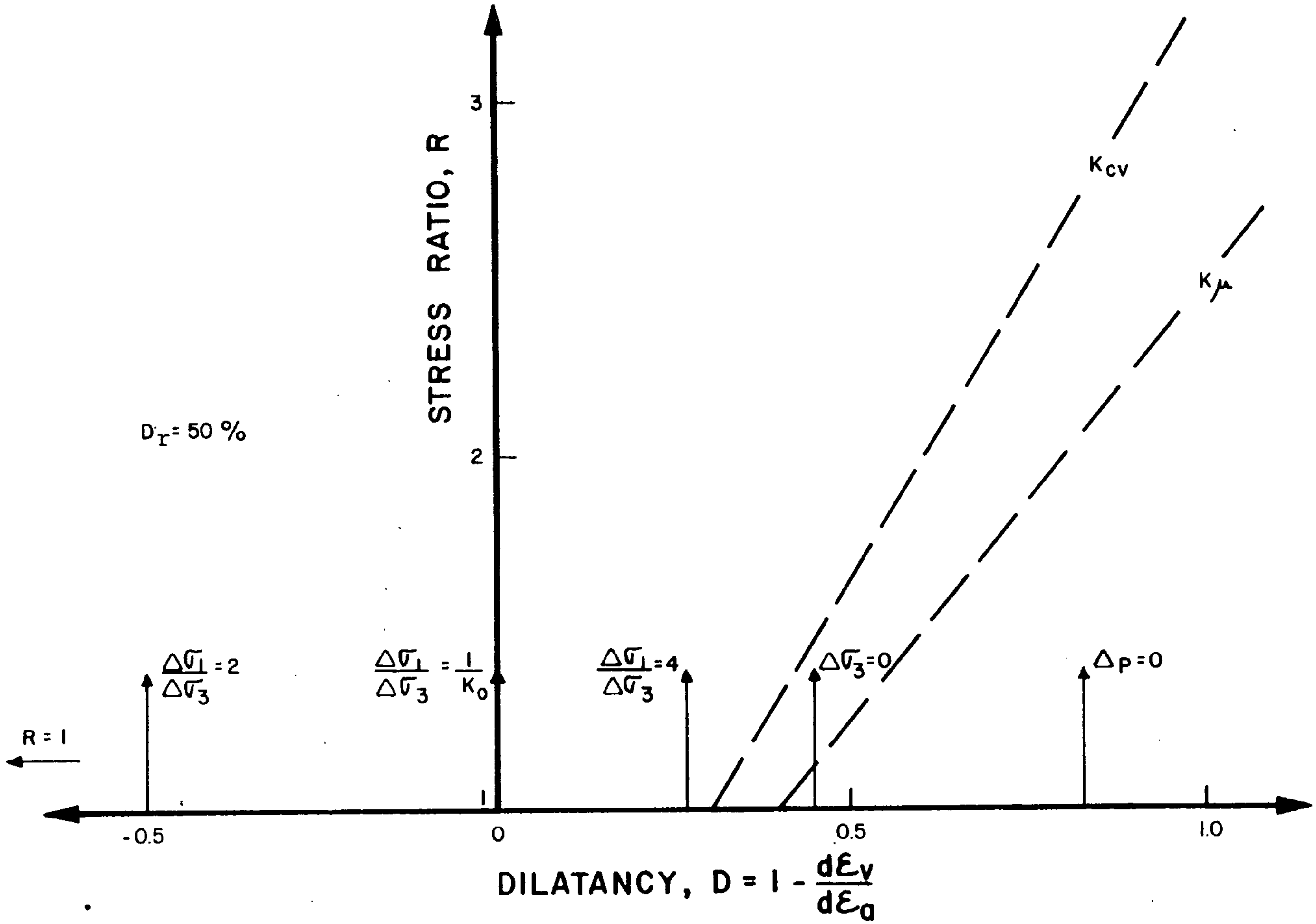

Fig. 4.23 Relative Location of Different Stress Paths on a Stress Dilatancy Plot

triaxial paths is located within close proximity of the upper and lower K_{cv} and K_{μ} bounds specified by stress dilatancy. This coincidence in conjunction with experimental limitations and uncorrected errors may have encouraged unjustifiable extrapolation of experimental evidence in previous studies in support of stress dilatancy.

4.2.3 Further Remarks

Experimental results presented above indicate that the stress dilatancy equation would not describe sand behaviour at small strain. An assembly of particles subjected to external load would deform simultaneously in rolling and sliding between grains as well as a consequence of elastic compression of the constituent grains. Elastic compression and rolling would have directional dependence on the causative stress. Whereas, slip deformation would require attainment of a threshold stress state. Sliding within an assembly of particles is considered to occur between clusters rather than individual grains (Horne, 1965). The size of sliding groups has been postulated to increase with density. In a medium and dense assembly, elastic deformation and rolling at unstable contacts would occur at small stress ratio. However, gross sliding would appear to be restrained until a large number of contacts reach limiting equilibrium states simultaneously. At which time, the predominant mode of deformation becomes sliding. This view emanates from consideration of an assembly of rigid particles in regular packing wherein no deformation would occur as R is increased from initial value of one until peak (Rowe, 1962). Simultaneous sliding would be initiated at all contacts upon attainment of peak stress ratio. Rowe's contention that stress dilatancy would be applicable at all stages of R was questioned on the basis of this idealized framework (Roscoe and Schofield, 1964). In the case of sand, with decreasing density, a larger number of unstable contacts would exist and sliding groups tend to be smaller. There would be more freedom for rotation and rearrangement and sliding would be more localized. Since sliding would not occur at a large number of contacts simultaneously, the overall stress ratio at which deformation due to sliding becomes prominent would be lowered. Even at small stress ratio, therefore, both rolling and sliding become significant. Thus description of behaviour relative to a mechanism of sliding alone would be inadequate. In this respect, previous observations relative to improved agreement with stress dilatancy upon reloading may be interpreted to be a consequence of reducing the relative significance of rolling and formation of larger clusters. However, predominance of sliding and development of larger clusters would in turn imply a larger magnitude of threshold stress ratio and thus less agreement with stress dilatancy. The linkage between cause and effect is not straightforward and agreement or disagreement of experimental results with the stress dilatancy theory would appear to require cautious interpretation.

At small stress ratio states, experimental results do not support previously reported straight line forms of the stress dilatancy relationship. In large measure, such disagreements with previous results stem from uncertainty in small deformation measurement, inadequate control of stress paths and unaccounted test errors. Improvements such as use of lubricated platten introduce bedding errors which, if uncorrected, diminish the dilatancy term. This in turn encourages false alignment of results along a straight line.

4.3 Strain Separation for Elasto Plastic Representation

Idealizations of sand behaviour as either entirely elastic or neglect of elastic strains and consideration of slip components only have not been entirely satisfactory. There has therefore been interest in modelling sand as an elasto-plastic material. Fundamentally, the elasto-plastic form of representation involves the separation, independent analysis and re-assembly of elastic and plastic strain components.

For an elastic-plastic material, the direction of the nonrecovered vector is a function of stress state and not the direction of the stress increment vector. Pooroosharb et al (1966) presented experimental results that show geometrically similar plastic potential surfaces, closing on the hydrostatic axis and failure line. Their work has been a basis for many subsequent model developments. However, in spite of its claimed generality to small stress ratio response, it has never been pointed out that actual verification for a plastic approximation of nonrecovered response was demonstrated only at a point close to incipient failure and where elastic strains are negligible. In view of its important implications, it would appear to be of fundamental interest to know as to whether the uniqueness of strain directions to stress state hold or fail in regions of small stress ratio. The following experiments are directed towards examination of this phenomenon.

Results of loading to and unloading from increasing magnitudes of hydrostatic compression have been plotted in strain space as shown in Figure 4.24. An approximately linear strain path may be noted for accumulated residual strain. Such residual strains are generally considered to be associated with nonrecovered deformations. A linear

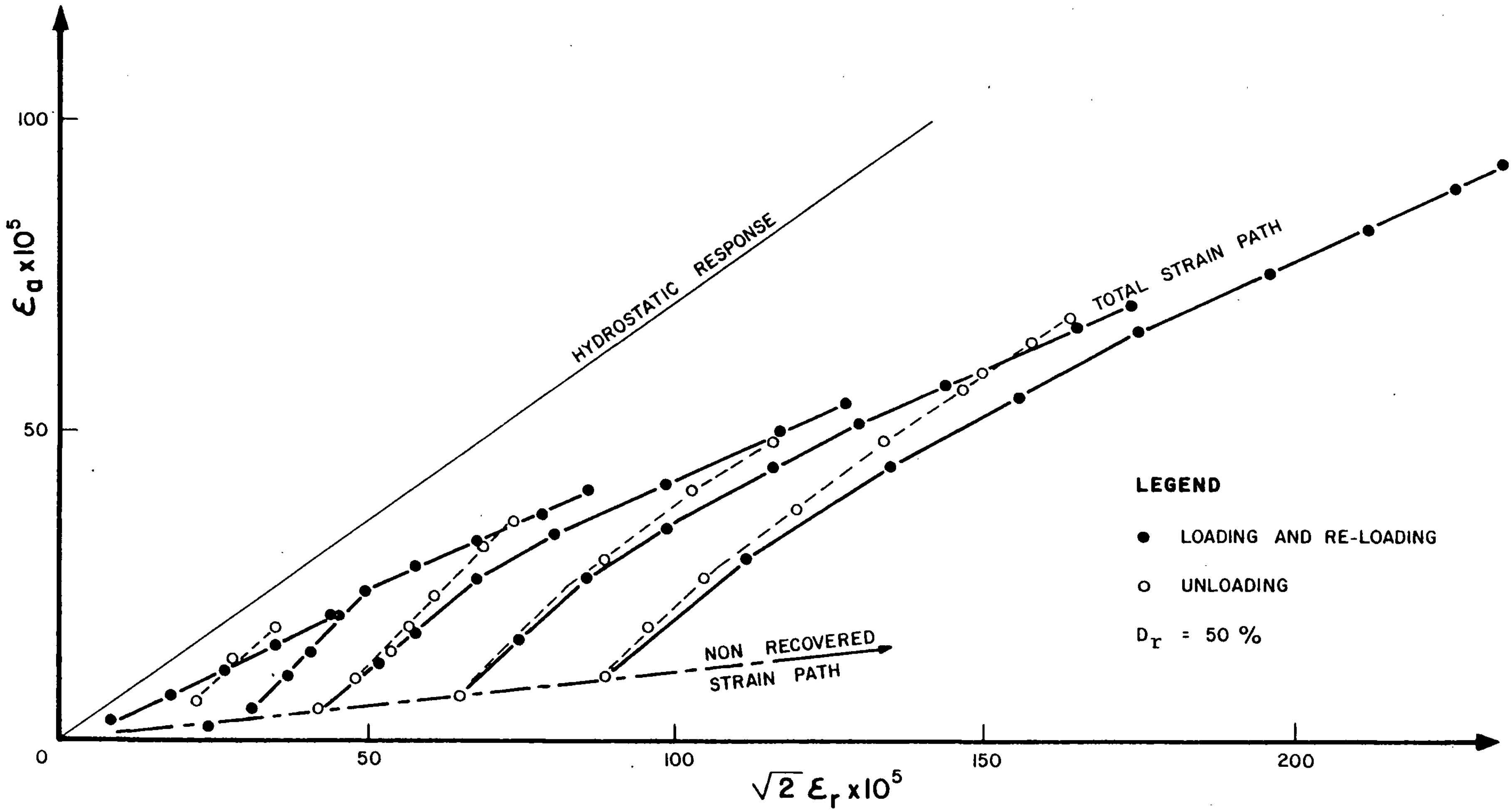

Fig. 4.24 Strain Paths for Conditions of Hydrostatic Loadings and Unloadings

strain path response for total, recovered and nonrecovered strains was noted by Rowe (1971) for constant stress ratio paths, including hydrostatic paths. A unique direction of non recovered strains for a hydrostatic stress states implies relative independence of strain directions on mean normal stress. Hence plastic potentials when closing on the hydrostatic axis must maintain normality to this strain direction as would be implied by the postulted geometric similarity of strain potentials.

Figure 4.25 presents results in strain space for loading and unloading to increasing levels of deviator stress along a conventional triaxial path and from a state of hydrostatic compression. For stress ratios maintained below 1.5, a distinct nonrecovered strain increment direction may be noted. If indeed nonrecovered deformations of sand were to be considered plastic, coincidence of nonrecovered strain paths at a stress point would be required. However, considering a hydrostatic stress state 0, Figure 4.26, from which hydrostatic and conventional triaxial stress increments are applied, two distinctly different non recovered strain directions result. This would imply occurrence of intersecting non recovered strain potentials at a stress point and that nonrecovered strains do not satisfy requirements of classical plasticity at low stress ratio states. Experimental observations advanced by Poorooshasb et al (1966) in support of a plastic classification of nonrecovered deformations in sand are not comprehensive and only apply to near failure stress states and at large strain.

Slip components of deformation are often considered to imply plastic strain. However, the occurrence of reverse slip on unloading

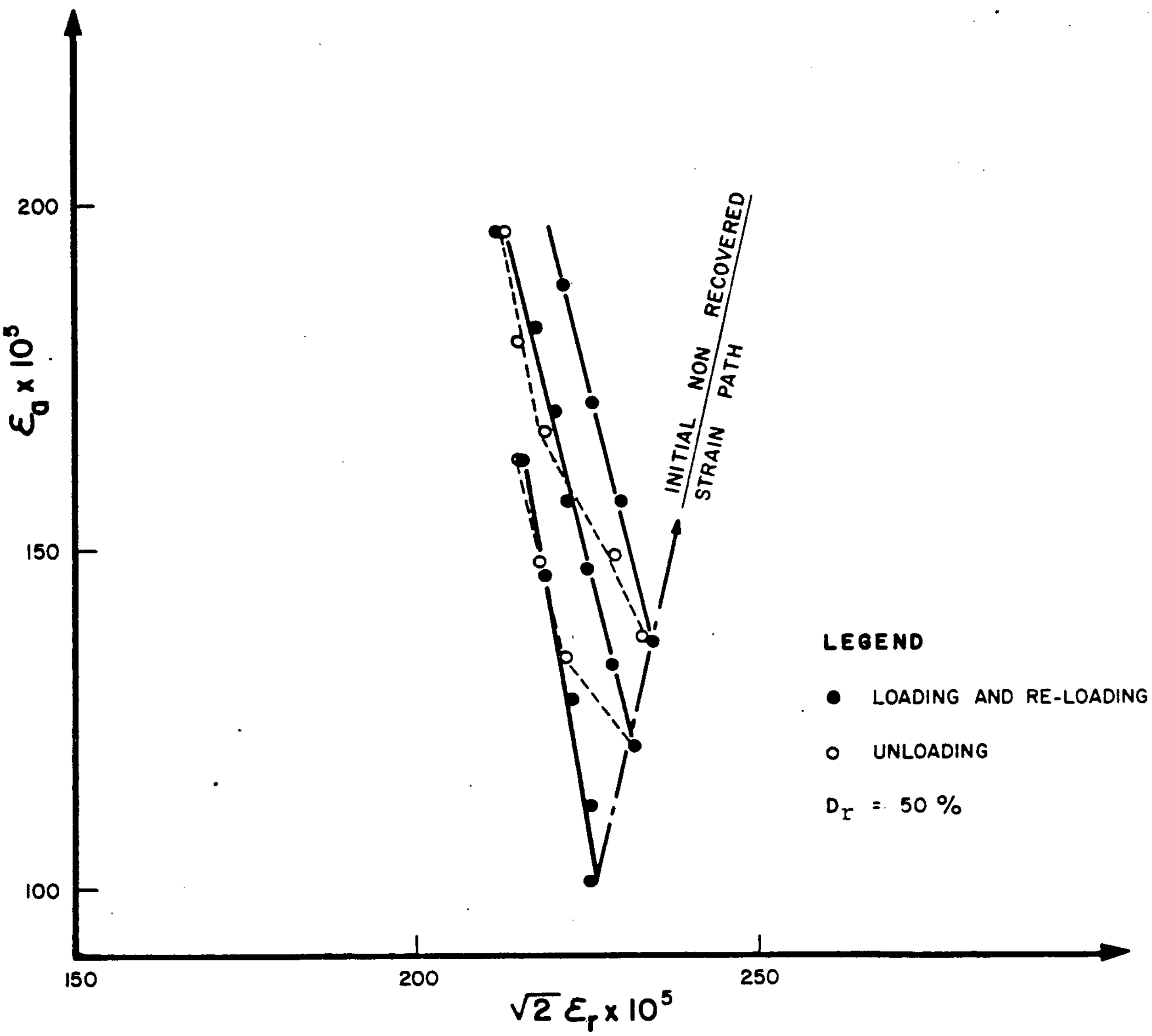

Fig. 4.25 Strain Paths for Conventional Triaxial Loadings and Unloadings

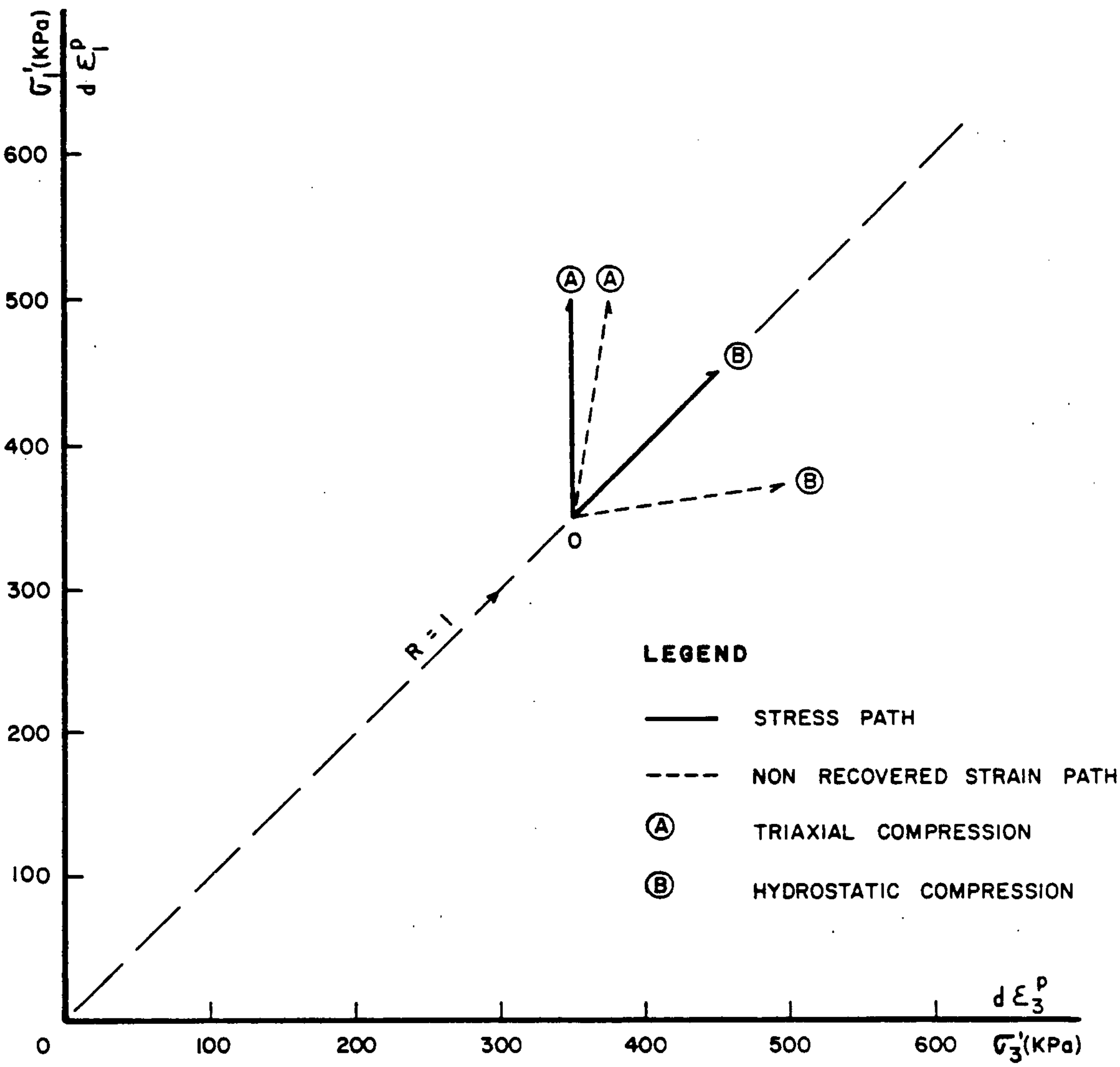

Fig. 4.26 Comparison of Stress and Non-Recovered Strain Direction at the Same Stress Point

cannot be denied and rolling as well as slip would contribute to nonrecovered deformations in sand. As discussed in Section 4.2.3, elastic deformation of grains and rolling would maintain directional dependence on the causative stress, whereas, sliding would depend on limit equilibrium considerations and attainment of threshold stress ratio levels.

As pointed out previously, Holubec's (1968) attempted verification of the elastic character of recovered strains was shown to be unsatisfactory (Merkele and Merkele, 1969; Coon and Evans, 1969) in that incremental equations were not complete and their integrals were path dependent. The finding herein constitutes experimental evidence in support of the corollary argument that nonrecovered strains are not plastic in character. At extremely small strains as encountered in the lower limit of strains in resonant column testing, sand can realistically be idealized as elastic without need of elastic-plastic separation. However, at large strains, experimental results from both continuum (Poorooshasb et al, 1966; Lade and Duncan, 1976) as well as stress dilatancy considerations (Rowe, 1962; Barden and Khayatt, 1966) have shown that association of strain increment ratios to stress states would be reasonably justified and hence plastic characterization. Indeed this latter opinion holds true regardless of considering total or nonrecovered strains. This would thus imply that at these stress states recovered strains are sufficiently small compared to slip strains and neither their inclusion nor omission has much significance. In this sense, the work of Rowe and Poorooshasb et al are complementary even though they have different beginnings.

Both recovered and nonrecovered strains assume relative significance in the strain range of 1×10^{-4} to 1×10^{-2}. Hence strain separation would be necessary to justify an elasto-plastic treatment. There are undoubtedly tremendous incentives to prefering an elasto-plastic framework for stress-strain relationships. However, unless and until successful separation can be demonstrated, progress in this direction will remain difficult. It would be fair to conclude that such evidence does not exist, not from a lack of need or interest but perhaps because it is virtually impossible to achieve, as has been suggested by Zytynski, Randolph, Nova and Wroth (1978).

4.4 Concepts Based on Normalized Work

On the basis of experimental observations and inspiration from earlier work by Roscoe and Burland (1968); Moroto (1976) poroposed a new parameter for describing the shear deformation behaviour of sand.

Expressing incremental work per unit volume done in shear, for example in a constant p' path, as

$$\delta W_s = p' \, \delta\varepsilon_v + q \, \delta\varepsilon_s \tag{4.8}$$

and normalized by p'

$$\frac{\delta W_s}{p'} = \delta\varepsilon_v + \eta \, \delta\varepsilon_s \tag{4.9}$$

Moroto suggested that

$$W_s = \int_a^b \frac{dw_s}{p'} \qquad (4.10)$$

represents a new state parameter and thus independent of stress paths. This concept has been central to some soil models proposed recently (Tobita and Yanagisawa, 1980; Varadarajan et al, 1983; Ghaboussi and Momen 1984, 1982). Through further examination of experimental results (Momen and Ghaboussi, 1982) the slope,

$$S = \frac{dW_s}{p'd\varepsilon_s} \qquad (4.11)$$

has been indicated to be a material function dependent only on the physical characteristics of the sand particles. S has been found to be independent of relative density as well as mean pressure p'. It has further been postulated that normalized plastic work functions for different stress paths would be related by functions of the Lode angle for stess path.

If indeed these suggestions hold true, discovery of this new parameter for sand would be a major achievement. The following consideration is intended to re-examine the possible usefulness of this concept.

It would be convenient to begin by expressing Equation 4.11 in the following equivalent form

$$S = \frac{d\varepsilon_v}{d\varepsilon_s} + \eta \qquad (4.12)$$

As the sand approaches a critical state at ϕ_{cv} and thus large shear strain; volume change would cease and Equation 4.12 would simplify to

$$S = \eta_{cv} \qquad (4.13)$$

In stress dilatancy terminology the equivalent expression can be shown to be;

$$S = \frac{3(K_{cv}-1)}{(K_{cv}+2)} \qquad (4.14)$$

and this relationship would be valid relatively independent of density and mean normal stress. Both normalized work and shear strain would continue to accumulate indefinitely at this constant rate. Clearly, in this context, S constitutes a material parameter. It may further be of interest to note that Equation 4.14 can be shown to describe reported results in support of this parameter, S, without exception. What needs to be examined experimentally therefore is the independence of S from density and mean normal stress level, p'; at small strain response regions.

Small strain experimental results from constant mean normal stress paths at a relative density of 50 percent are presented in the form of normalized work, W_s, against shear strain, as shown in Figure 4.27. It may be noted that the relationship does not form a unique curve and S

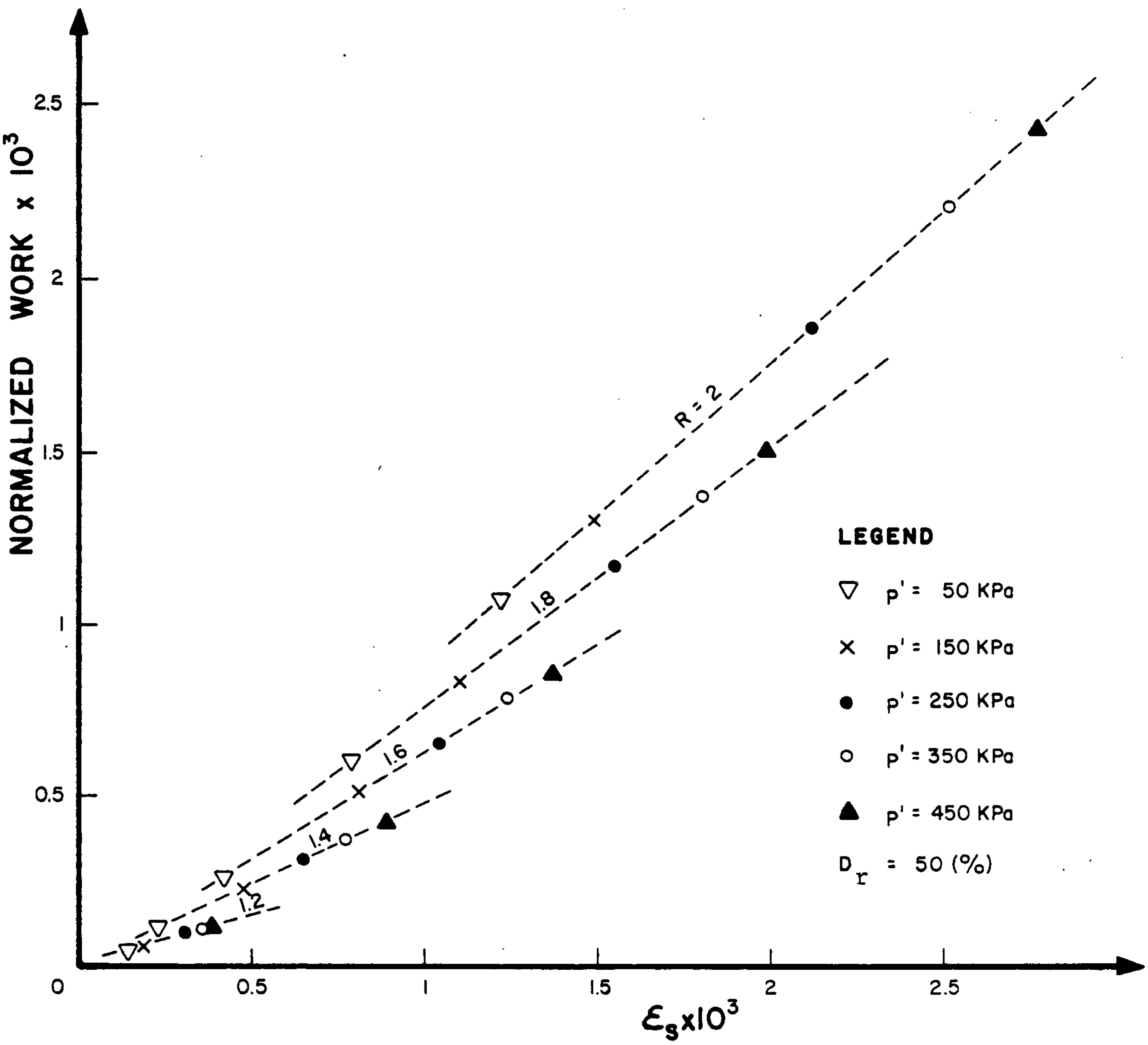

Fig. 4.27 The Influence of Mean Normal Stress on Normalized Work

is shown to depend on mean normal stress. Furthermore, each constant p' curve is non linear and S would not therefore be constant. Hence, S at small stress ratio does not represent a material parameter. However, a closer examination of Figure 4.27 suggests that constant stress ratio states but at different levels of p' form straight lines through the origin. Since initial dilatancy has been noted to remain relatively constant and independent of p', Section 4.2.2, S may therefore be specified as a function of η for corresponding stress paths, as implied by Equation 4.12. A means of determining strain increment ratios for various stress paths will be presented in Chapter VI.

Normalized work against shear strain for constant mean normal stress paths of 450 KPa but at relative densities of 30, 50 and 70 percent are presented in Figure 4.28. It may be noted that states corresponding to the same density, data points not connected, maintain separate and non-linear relationships. Hence, S would not remain unique and constant. Common stress states but at different relative densities fall along a straight line.

Overall, these experimental results demonstrate that the normalized work and shear strain relationship, at small stress ratio, is not unique and constant. It has been shown to be dependent on mean normal stress and relative density and would not be a material parameter as suggested. However, common stress ratio states along both different mean normal stress as well as density states trace linear relationships. This semblance of order has not been recognized previously. Alternative prescription of S in small stress ratio regions will be attempted with additional observations reported in

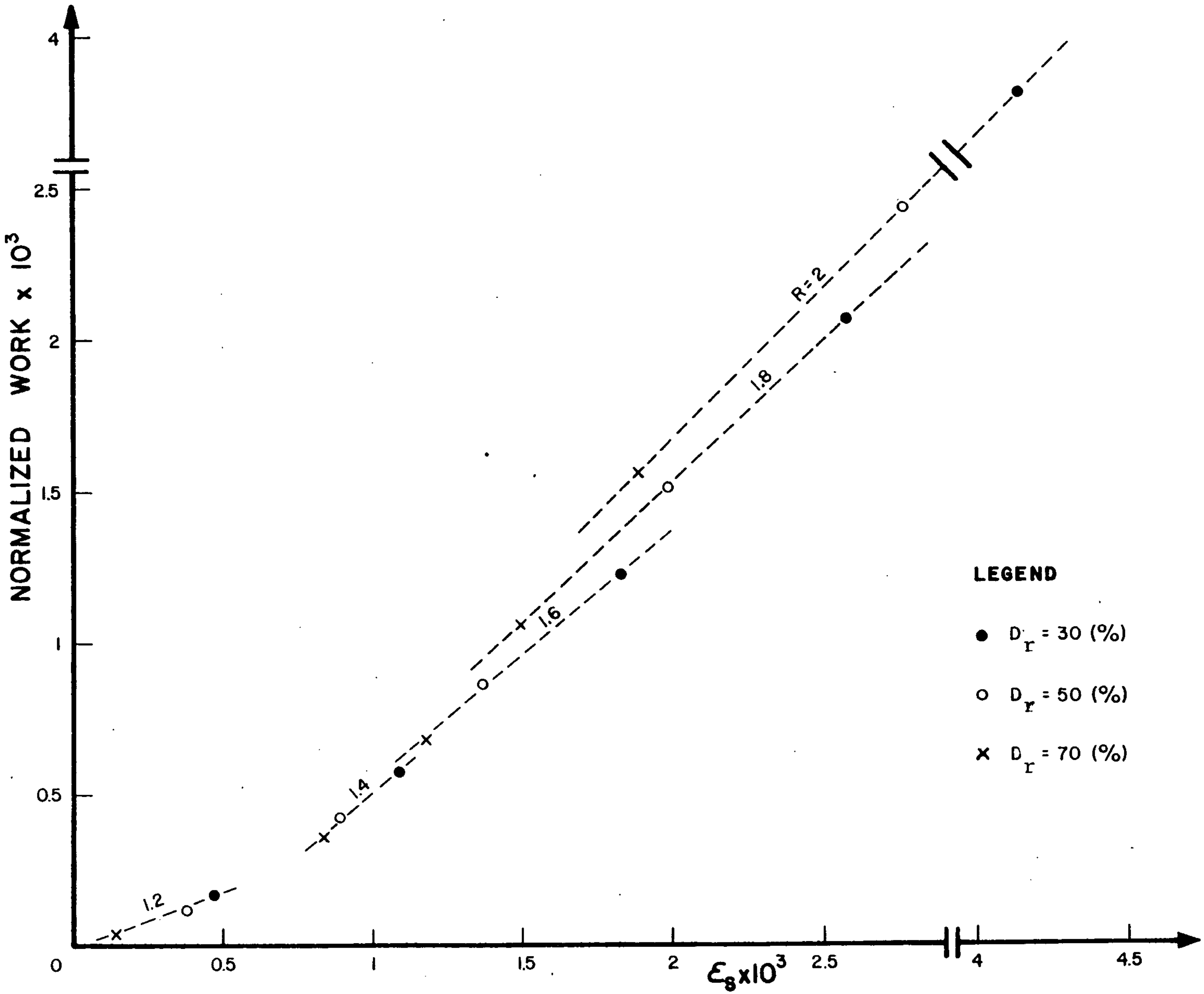

Fig. 4.28 The Influence of Relative Density on Normalized Work

Chapter VI. However, in terms of its meaning at large strain regions, the normalized work concept does not appear to embody new fundamental advantages for elasto-plastic representation.

4.5 Concluding Remarks

In the preceeding experimental investigations, the stress-strain behaviour of sand at small strain has been shown not to be an extrapolation of either large or very small strain response. Generally, elastic approximations of sand behaviour have been used in the very small strain range. Considerating slip modes of deformation to be significant, some common ground has also been indicated to exist between plasticity and the large strain response of sand. Resemblences to elastic and plastic behaviour have been demonstrated in regions where either elastic deformation of grains or slip between sand particles predominate overall deformation, respectively. In the extreme cases wherein one component of deformation becomes predominant, neither the inclusion nor omission of the other component makes a significant difference. All strains are considered to be elastic in resonant column considerations. On the other hand, conclusions that were reached regarding the association of plastic strain increment directions and stress state by Poorooshar b et al (1966) were previously established by Rowe (1962) assuming slip strains to be approximated by total strains.

The mechanisms of sand deformation at small strain levels is much more involved and complicated. Behaviour that has so far been demonstrated to apply for large strain conditions does not extrapolate to small strain response even when prevailing strains are presumed separated. Concepts like normalized work do not hold at small strain and assumed nonrecovered deformations maintain directional dependence on the causative stress increment. Yet, large strain observations are usually assumed to be relevant for small strain considerations and in situations wherein an assessment of nonrecovered deformations and associated pore pressure responses are desired.

In small strain response, both elastic deformation of grains and slip between particles assume relative significance. Neither can be regarded negligible and separation has been easier to assume than verify experimentally. At the same time, the existence of rolling at unstable contacts has also been recognized to be an alternative mode of deformation (Horne, 1965), even though its contribution is not explicitly recognized in any form of representation. Overall, as suggested by Zytynski et al (1978), there would appear to be no region or direction of loading or unloading along which isolation of response would be possible.

In what follows, the small strain response of sand will be investigated without assuming separation of strains and thus considering total strains. Stress-strain relationships will be examined in strain and mixed stress-strain spaces. Important stress parameters of stress ratio, shear and mean normal stresses will be varied systematically so as to allow isolated study of effects. The behaviour of sand under proportional loading is examined in the following chapter.

CHAPTER V - BEHAVIOUR OF SAND IN PROPORTIONAL LOADING

Proportional loading paths have been of fundamental interest in the study of stress-strain behaviour of sand. Stress components increase proportional to each other and thus the overall obliquity of applied stresses would remain fixed. Failure in a frictional material such as sand is characterized by relatively constant, thus limiting, stress ratio states. Whereas in other materials, failure is specified by shear stress level and constant stress ratio loading would eventually lead to creep and fracture. Below a threshold obliquity of applied external loads, proportional loading in sand induces stiffening and consolidation. With the overall stress ratio remaining well below that corresponding to the material sliding friction angle, no tendency for major interparticle slip would exist. The associated internal change of geometry would likely result in net contraction and corresponding strains would be small.

The response of sand to proportional loading will be examined in the first part of this chapter. All of the observations are based on tests performed at a relative density of 50 percent. As opposed to customary procedure, behaviour will be investigated in strain rather than stress space. In the second part of this chapter, test results at 30 and 70 percent relative densities will be reviewed. The influence of density on stress strain response will be assessed. Possibilities for quantitative relationships within and across relative densities will be investigated.

5.1 Behaviour at One Relative Density

5.1.1 Experimental Observations

Results of several constant R path tests on specimens of Ottawa sand at a relative density of 50 percent are shown in Figure 5.1. Stress ratio, R, is expressed as the ratio of axial, σ_a', to radial stress σ_r'. Tests that have R>1 are in states of compressional deviatoric stress ($\sigma_a' > \sigma_r'$). The test for which R=1 corresponds to hydrostatic loading ($\sigma_a' = \sigma_r'$) and stress paths with R<1 are in extensional deviatoric stress state ($\sigma_a' < \sigma_r'$). Overall stress ratios in the tests range between 0.82 and 2.

The results have been presented in the 'triaxial' strain plane (ε_a, $\sqrt{2}\varepsilon_r$). It may be noted that constant R stress paths result in linear strain paths in strain space. Such linear strain paths during constant R loading have also been observed by others (Barden et al 1969; El-Sohby 1969; 1972; Rowe 1971). Since the strain paths are linear, it follows that the incremental strain ratios must be constant and equal to the total strain ratios for a given stress path. All of the strain paths have positive slopes and are contained within the first quadrant of strain space. Thus both axial and radial strain increments are contractant, regardless of compressional or extensional mode of loading. The ratio of incremental energy input in each of the principal axes of stress is therefore also positive and constant.

Along the positive axial strain axis, radial strains are zero. This strain path of zero lateral deformation is associated with a stress path that is commonly known as the K_0 path. Axial strains are zero along the positive radial strain axis. A strain path oriented at

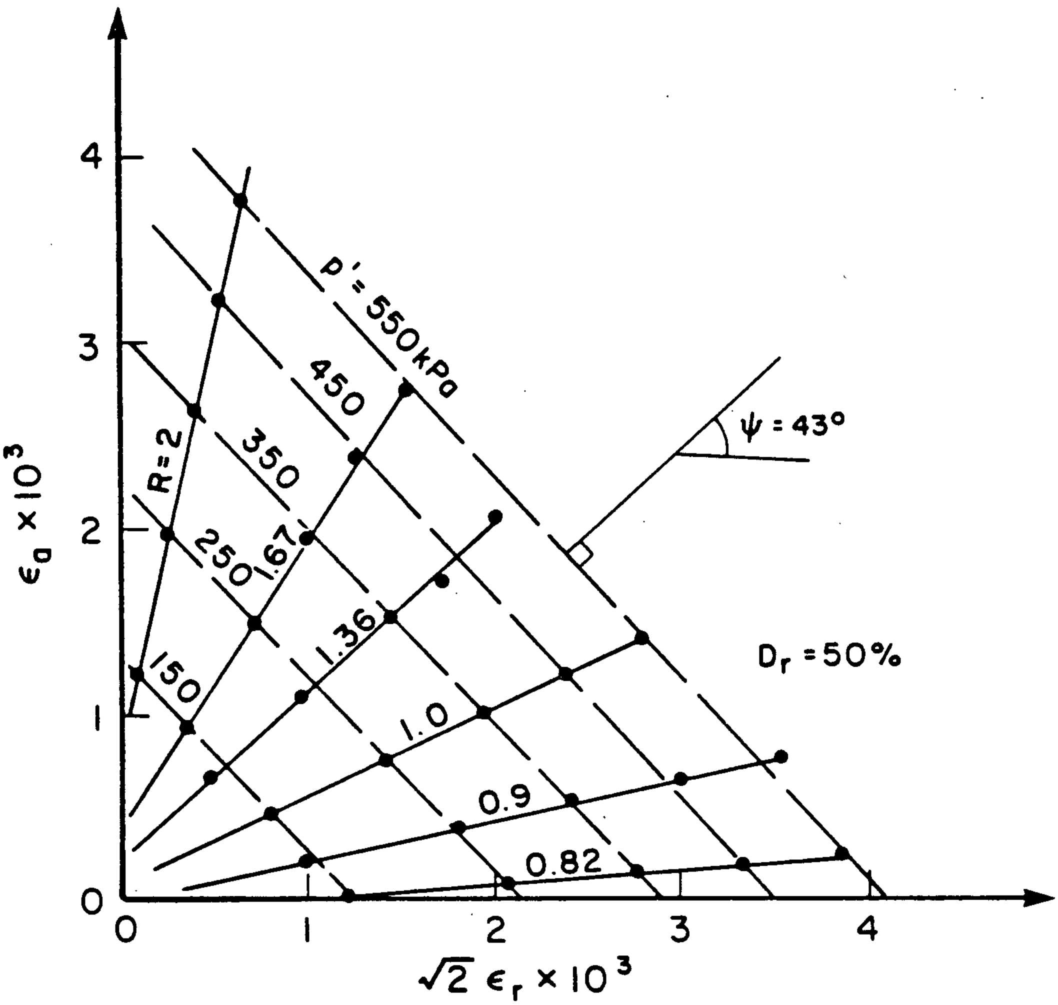

Fig. 5.1 Strain Paths for Proportional Loading and p' Equipotentials

an angle of 35 degrees to horizontal represents a path of equal axial and radial strain increments. In Fig. 5.1 the observed strain path for hydrostatic compression does not coincide with this 35 degree line. Deformation under hydrostatic loading is such that the radial strains are greater than axial strains. The specimen thus possesses an inherent anisotropy, as has been observed previously (Arthur and Menzies, 1972; El-Sohby and Andraws, 1972; Oda 1972; Yamada and Ishihara 1979). The linearity of strain paths also implies that anisotropy is fixed by R and is not altered by increasing hydrostatic stress (Rowe 1962).

Strain increment ratio, defined as the ratio of axial to $\sqrt{2}$x radial strain increment, $\varepsilon_a/\sqrt{2}\ \varepsilon_r$, would be zero for horizontal strain paths. Whereas, the ratio would tend to infinity for paths approaching vertical. If these same ratios were expressed as tangent inverses, the ensuing angle, θ, will range from 0 to 90 degrees. Such angles of strain increment ratios in triaxial strain space of Figure 5.1 are plotted against corresponding stress ratios in Figure 5.2. A linear relationship may be noted which is valid in regions of both compression and extension. Continuity of the relationship across compression and extension is maintained by expressing extensional stress ratios as negative inverse of those in compression. In triaxial tests, the principal stress axes are fixed. Because of axial symmetry, $\sigma_2' = \sigma_3'$ in compression and $\sigma_1' = \sigma_2'$ in extension. Thus, the $(\sigma_1', \sqrt{2}\ \sigma_3')$ stress plane will contain compression states when $\sigma_1' = \sigma_a'$ and $\sigma_3' = \sigma_r'$. If R is defined as σ_a'/σ_r', then proportional loading paths in compression would be described by $\frac{R}{\sqrt{2}}$. On the other hand extension states will

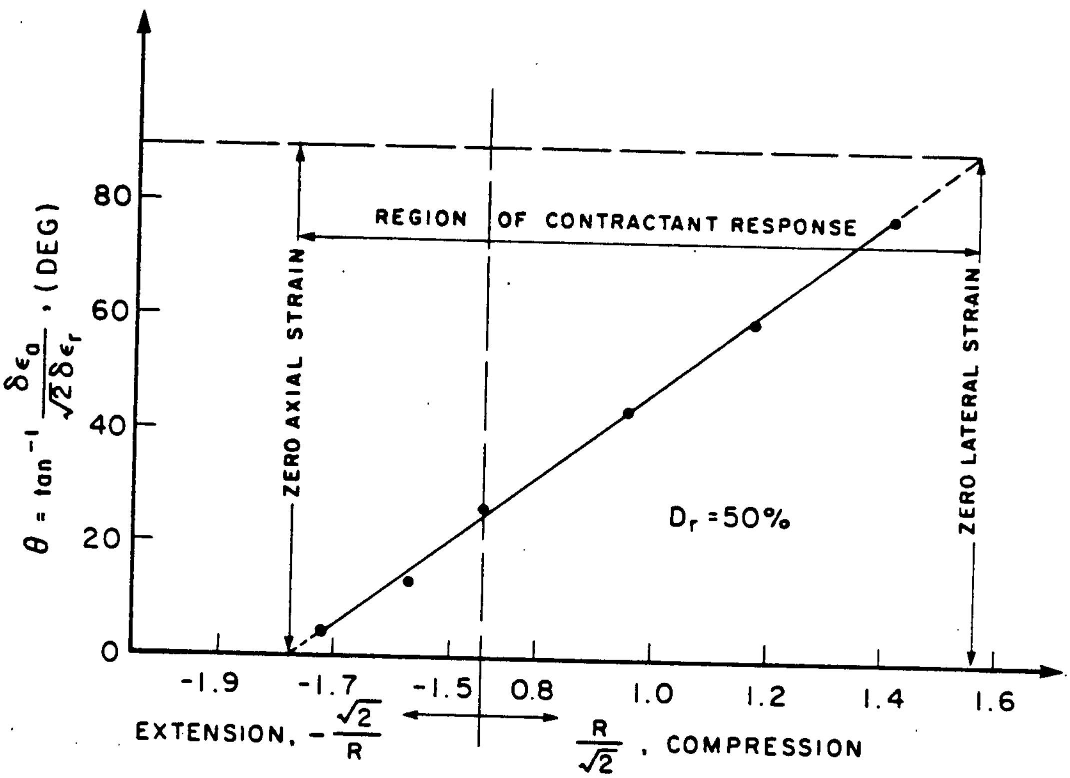

Fig. 5.2 Relationship Between Strain Increment Ratio and Stress Ratio

remain in the plane of ($\sqrt{2}\ \sigma_1'$, σ_3') for which $\sigma_1' = \sigma_r'$ and $\sigma_3' = \sigma_a'$. Hence proportional loading paths would be represented by $\sqrt{2}\ \frac{\sigma_r}{\sigma_a} = \frac{\sqrt{2}}{R}$. The two planes intersect along the space diagonal so that R = 1 is common to both. Similar representation of stress ratio was adopted in the study of metal behaviour under proportional loading (Mehan, 1961). Because stress states lie in separate planes that intersect along R = 1; separate expressions must be used in the extension and compression sides. But, since the slope is the same and R = 1 is common to both compression and extension, either of the relationships can be derived from the other. Thus, from Figure 5.2 strain increment ratios for compressional paths may be expressed by

$$\frac{\delta\varepsilon_a}{\sqrt{2}\delta\varepsilon_r} = \tan\left[a + b\left(\frac{R}{\sqrt{2}}\right)\right] \tag{5.1}$$

and for extensional paths

$$\frac{\delta\varepsilon_a}{\sqrt{2}\delta\varepsilon_r} = \tan\left[c + b\left(\frac{-\sqrt{2}}{R}\right)\right] \tag{5.2}$$

For the result on Ottawa sand shown in Figure 5.2;

$$a = -28, \quad b = 75 \quad \text{and} \quad c = 134$$

Since for R = 1 Equations 5.1 and 5.2 should yield identical values of strain ratio, $(a + b/\sqrt{2}) = (c - \sqrt{2}b)$, which means that only two of the three constants a, b and c are independent.

In Figure 5.1, if points representing equal mean normal effective stress p' along the linear strain paths are connected, the resulting loci are straight lines. Such straight line loci may be seen to be parallel for different values of p'. These straight lines will be referred to subsequently as equipotentials of p'. The gradient of equipotentials of p', i.e. the strain path which is normal to the direction of equipotentials of p', has a slope $\psi = 43°$ for the sand tested. From Figure 5.2 it may be seen that such a strain path will result from a stress path with R = 1.30.

5.1.2 Proportional Stress-Strain Relationships

The deformation behaviour so far observed can be structured to form a simple proportional loading stress-strain relationship that is valid for constant R paths in the first quadrant of strain space i.e. consolidation paths. The foundations of this relationship lie in the observed linearity and parallel orientation of equipotentials of effective mean normal stress and the linear relationship between stress ratio and θ. Thus, strains along a desired R path could be predicted using stress-strain relations for a known path.

Essential features of Figure 5.1 are represented in a simplified form in Figure 5.3. θ_i and θ are tangent inverses of strain increment ratios along the given and arbitrary R paths, respectively, whereas ψ is associated with strain increment ratios along a strain path coincident with the gradient of p'. Consider the given and arbitrary R paths at points of identical mean normal stress p' and subjected to

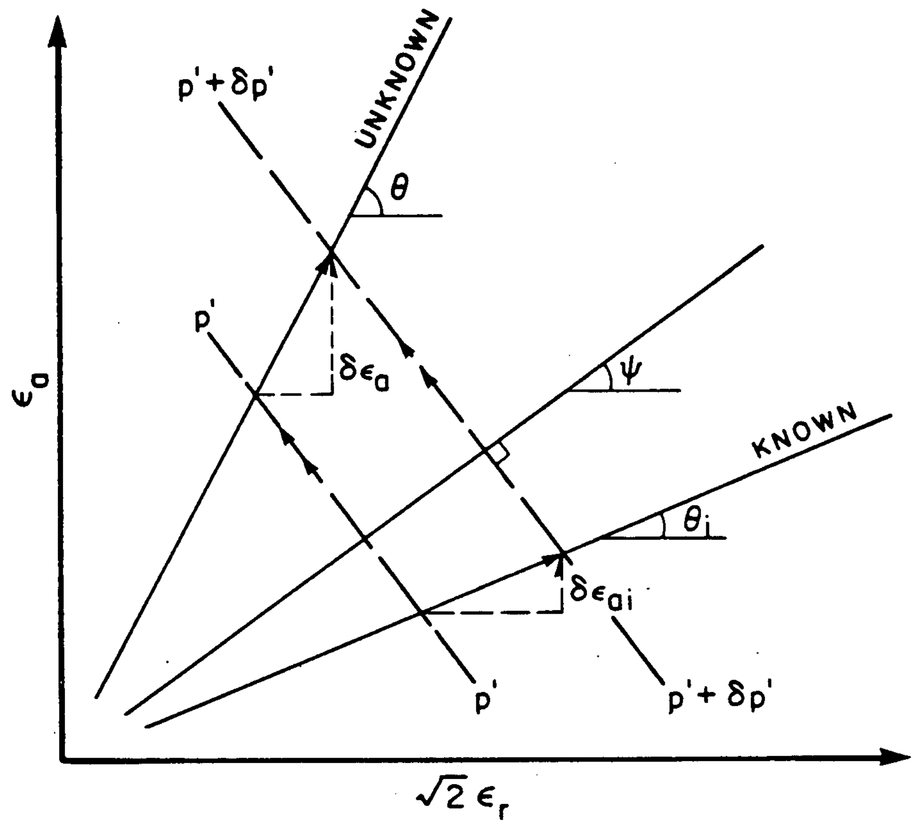

Fig. 5.3 Geometric Features of Strain Paths and p' Equipotentials

equal increments of mean normal stress, $\delta p'$. Let the resulting axial strain increments for the given stress paths be $\delta\varepsilon_{a_i}$. Then, from geometrical considerations, the corresponding strain increments, $\delta\varepsilon_a$, along the desired R paths may be shown to be

$$\delta\varepsilon_a = \frac{\sin\theta}{\sin\theta_i} \cdot \frac{\cos(\theta_i-\psi)}{\cos(\theta-\psi)} \cdot \delta\varepsilon_{a_i} \tag{5.3}$$

Since the volumetric strain increment

$$\delta\varepsilon_v = \delta\varepsilon_a + 2\delta\varepsilon_r \tag{5.4}$$

and noting that

$$\frac{\delta\varepsilon_a}{\sqrt{2}\delta\varepsilon_r} = \tan\theta \tag{5.5}$$

the volumetric strain increments in the desired R paths become

$$\delta\varepsilon_v = (1 + \frac{\sqrt{2}}{\tan\theta})\ \delta\varepsilon_a \tag{5.6}$$

Equations 5.3 and 5.6 together with the relationship in Equations 5.1 and 5.2 have been used to develop the stress-strain predictions shown in Figure 5.4. The known data base for these prediction constitutes the results of hydrostatic compression (R=1) test. Stress-strain predictions for both compressional and extensional constant R paths have been made and compared with observed stress-strain results. Even though the strains are very small,

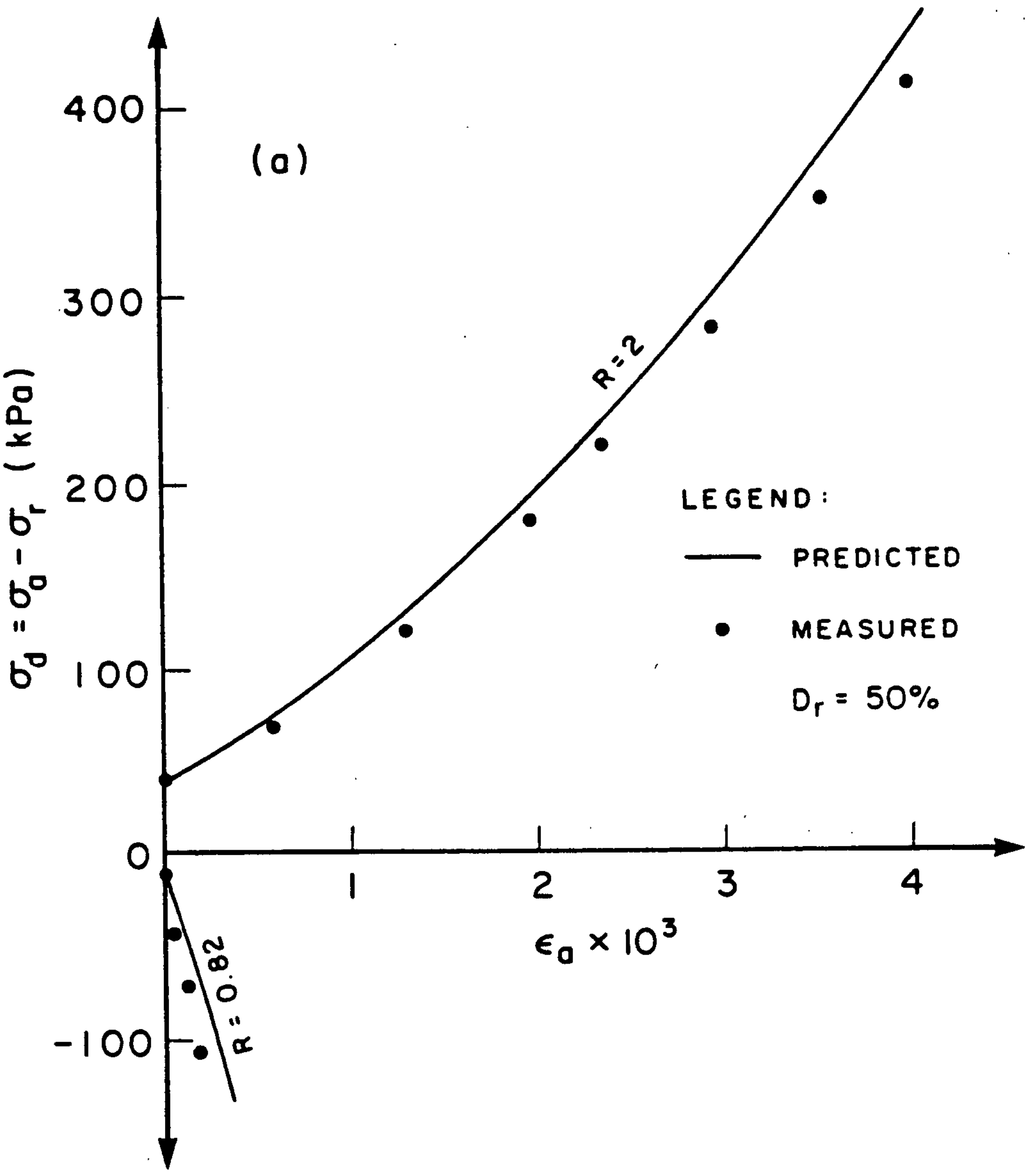

Fig. 5.4a Comparison of Measured and Predicted Axial Strain in Proportional Loading Paths

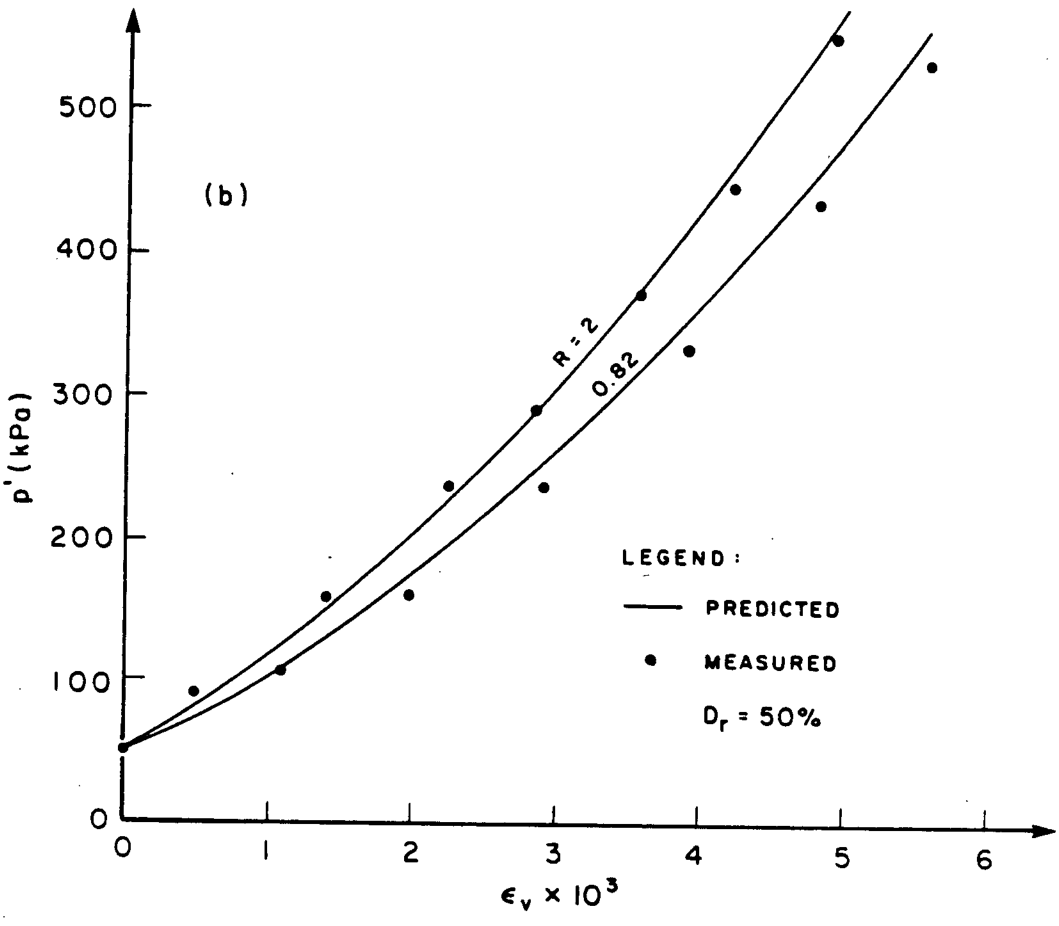

Fig. 5.4b Comparison of Measured and Predicted Volumetric Strain in Proportional Loading Paths

excellent agreement may be noted between the observed and predicted stress-strain response for both compressional and extensional modes.

The proportional loading stress-strain behaviour of sand at one relative density is therefore completely specified if results of two tests at different R values are known. One of such tests can be the simple hydrostatic compression test (R=1). The second test could be carried out at any other value of R, compressional or extensional. The results of these two tests will enable determination of all constants, namely a, b, c and ψ needed for a complete specification of proportional loading behaviour. The stress-strain results of any one of the two tests can serve as the reference data base for strain predictions under any R path loading.

The relationship expressed by Equation 5.3 has been derived from experimental results. This relationship has an important implication regarding the ratio of energy density increment (incremental energy input per unit volume) between any two constant R paths. The increment in energy density δQ resulting from an increment in stress is

$$\delta Q = \sigma_a' . \delta\varepsilon_a + 2\sigma_r' . \delta\varepsilon_r \qquad (5.7)$$

If the stress increment is along a constant R path for which $\sigma_a'/\sigma_r' = R$, $\sigma_r' = 3p'/(R+2)$, and $2\varepsilon_r/\varepsilon_a = \sqrt{2}/\tan\theta$, Equation 5.7 can be written as

$$\delta Q_R = \left[\frac{3}{R+2}\left(R + \frac{\sqrt{2}}{\tan\theta}\right)\right] p' \ \delta\varepsilon_a \qquad (5.8)$$

in which the subscript on Q refers to stress increment along a constant R path. For a given R path, since $\tan\theta$ is constant, the expression in square brackets in Equation 5.8 is a constant along the entire stress path. The energy, density increment ratio of any two stress paths at identical values of p' would thus be a constant multiple of the ratio of their axial strain increments. This ratio of axial strain increments may be seen to be a function of θ values associated with the two stress paths and the angle ψ (Equation 5.3). Since both θ values are fixed for the specified stress paths and ψ is constant, the ratio of the axial strain increments is constant along the entire stress paths. Hence the energy density increment ratio of the two R paths with identical mean normal stress histories is also constant.

The ratios of energy density increment at various R values to the energy density increment at reference hydrostatic stress ratio R = 1 are shown in Figure 5.5. It may be seen that for each R, this ratio is essentially constant, regardless of the level of p'. Furthermore, the magnitude of this ratio is a minimum for R~1.30, which corresponds to the stress ratio yielding the ψ strain path coincident with the gradient of equipotentials of p' in the strain space. The implication of the association of minimum energy density increment with strain vector in the ψ direction is not immediately clear at this time.

5.2 Extensions to Other Relative Densities

The previous observations and stress-strain predictions under proportional loading were based on results obtained from tests on specimens at a relative density of 50 percent. Additional tests were made to investigate possible extensions to behaviour at other relative densities. Two series of tests, one each on loose and dense specimens

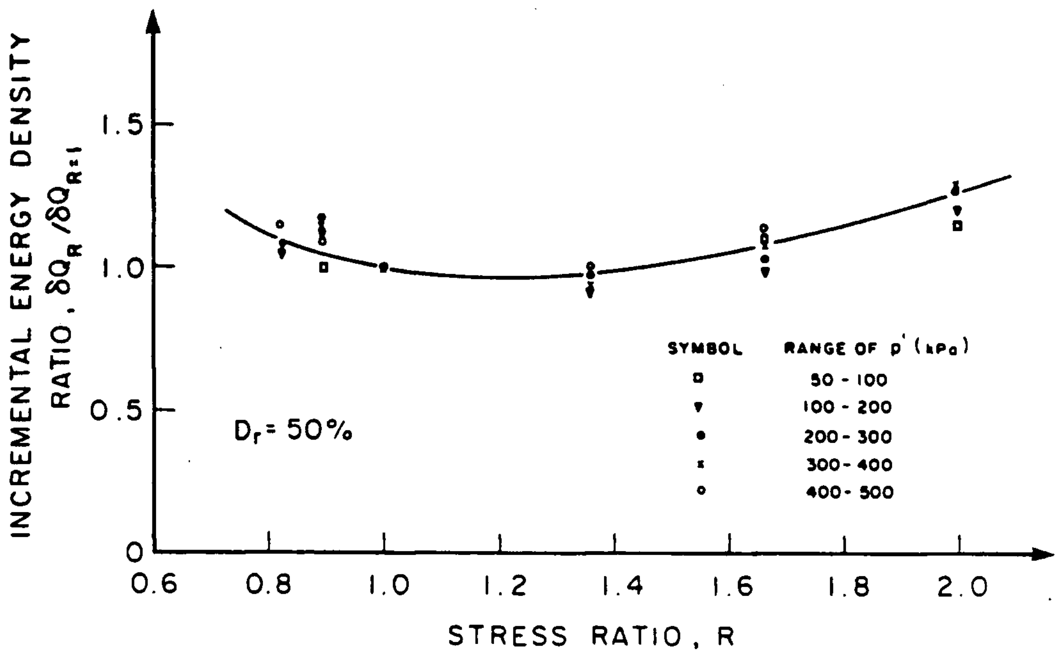

Fig. 5.5 Variation of Incremental Energy Density Ratio with Stress Ratio

at relative densities of 30 and 70 percent, were carried out.

5.2.1 Experimental Observations

Test results on loose and dense specimens in the form of Figure 5.1 are presented in Figure 5.6. Once again constant R stress paths may be seen to result in linear strain paths for both relative densities. Also equipotentials of mean normal stress seem linear and parallel with essentially the same orientation for all relative densities. This implies that ψ is independent of relative density. As would be expected, for equal stress states the magnitude of contractant strain response decreased markedly with increase in relative density.

Results of tests on specimen of different relative densities but at equal stress ratios are presented in Figure 5.7. Under hydrostatic loading at R = 1 the slope θ of the strain path for the dense sample is ~35 degrees, which implies isotropic behaviour. With decreasing relative density, inherent anisotropy increases progressively, as indicated by the slope of strain path which deviates more and more below 35°. It may also be noted that equipotentials of mean normal stress connecting strain paths of equal R but different relative densities are linear and parallel. The gradient of these p' equipotentials, however, is not constant but depends upon the value of R.

Relationships between stress ratio, R, and strain increment ratios at different relative densities are shown in Figure 5.8. As observed previously for a relative density of 50%, linear relationships between stress ratio and θ, the tangent inverse of the strain increment ratio, may also be noted for other relative densities. The slope of

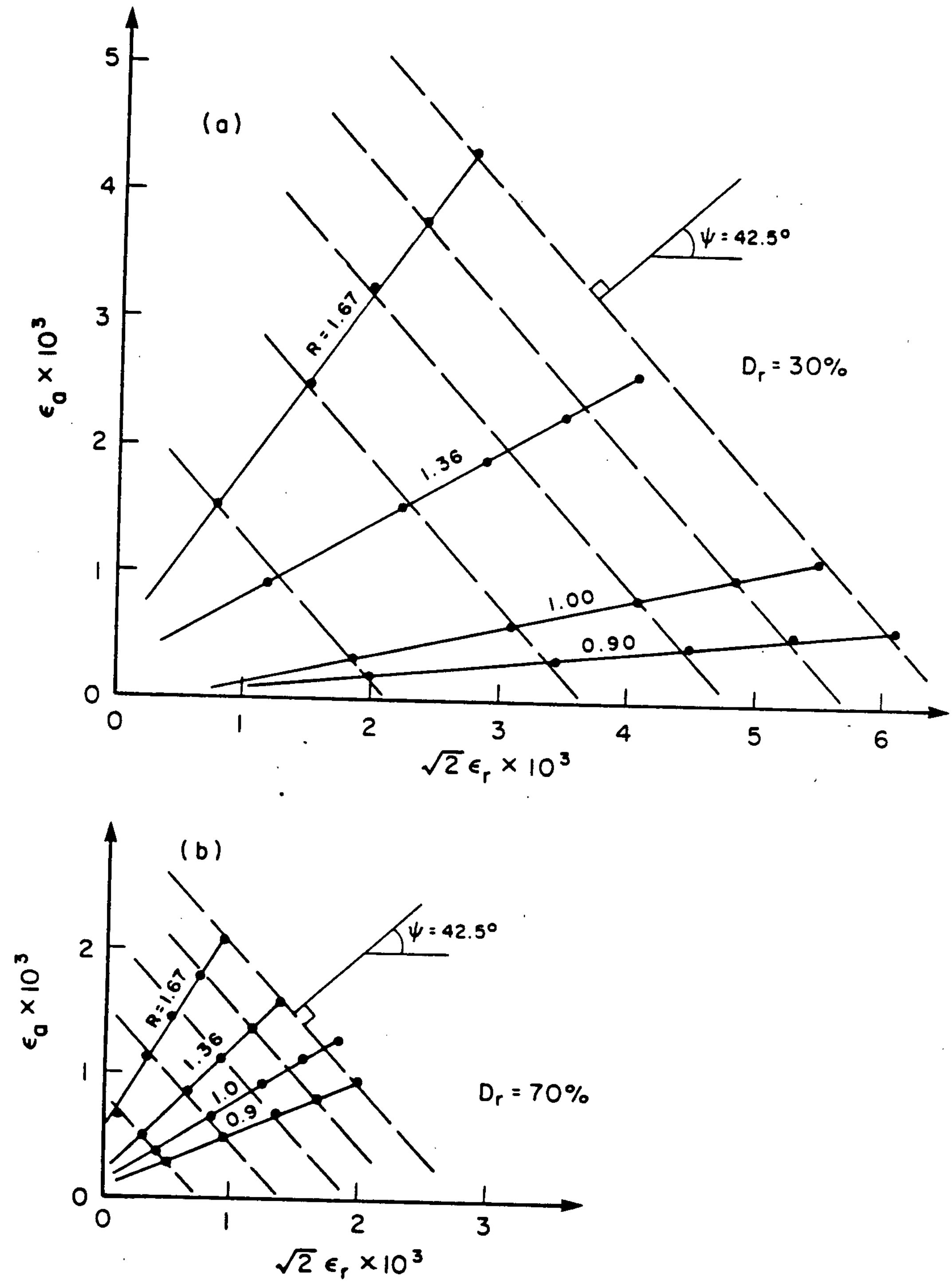

Fig.5.6 a & b Strain Paths for Proportional Loading and p'Equipotentials:
a) D_r = 30% and b) D_r = 70%

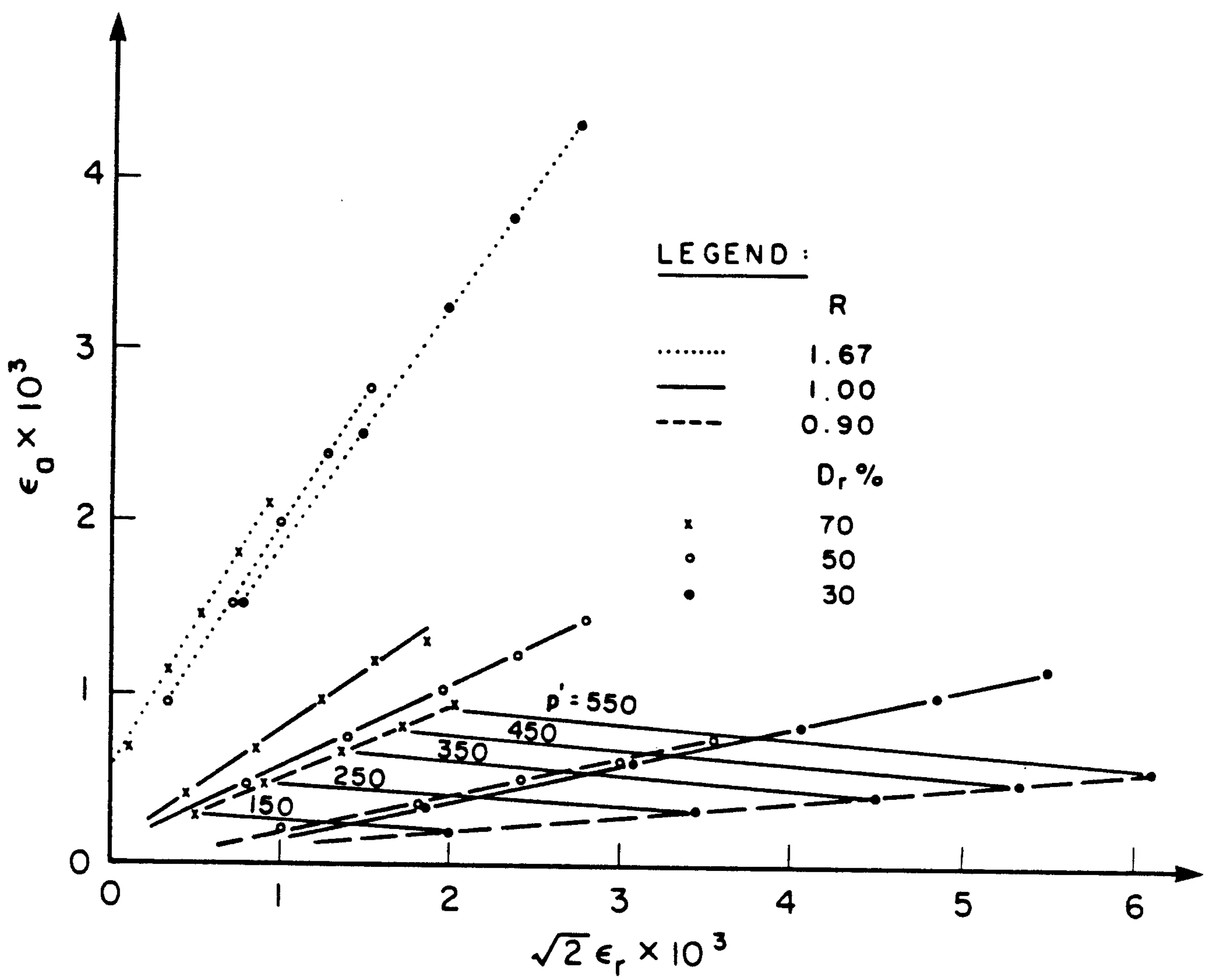

Fig. 5.7 The Influence of Density on Strain Paths from Proportional Loading

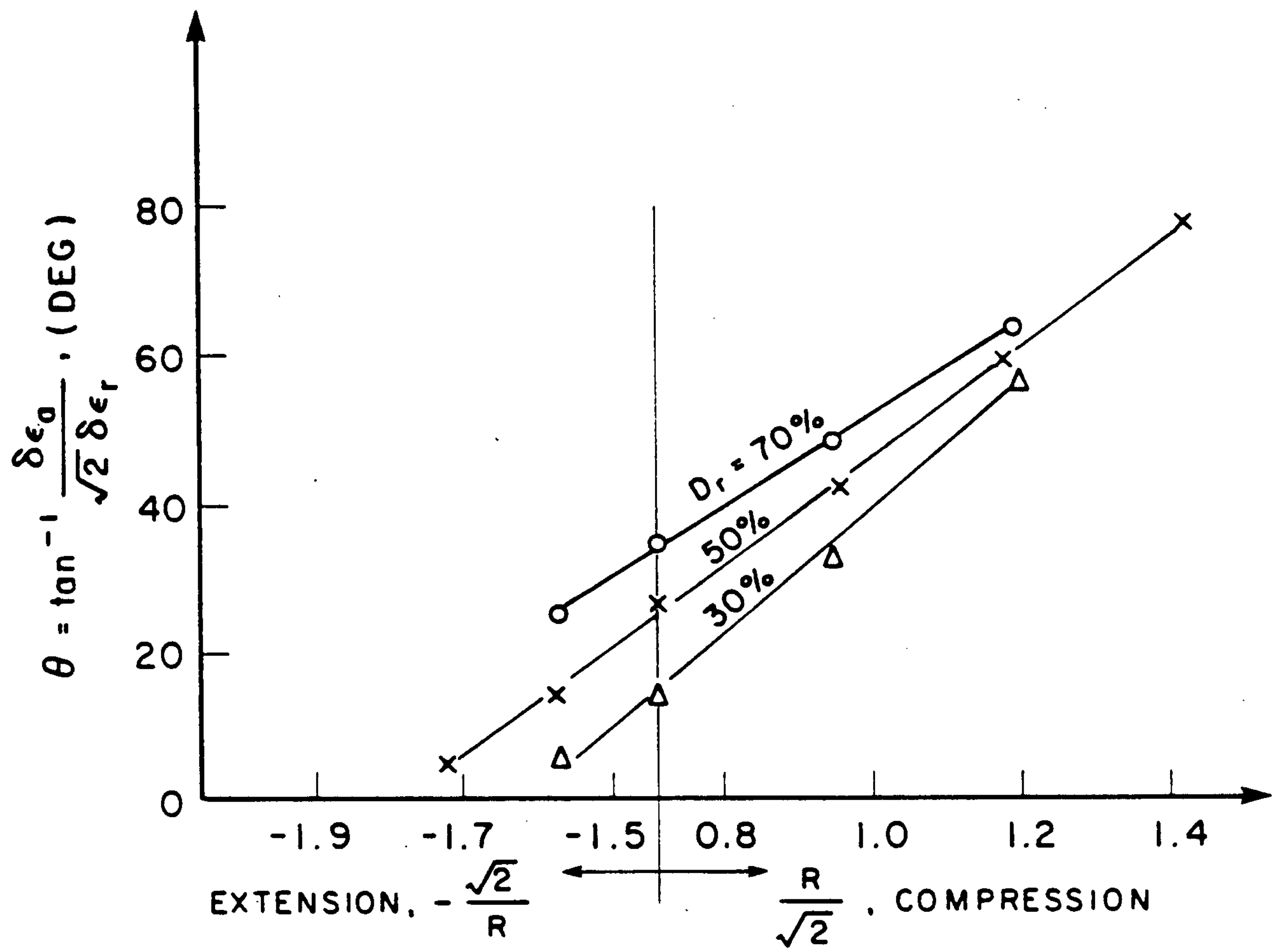

Fig. 5.8 Relationships Between Strain Increment Ratio and Stress Ratio at Different Relative Densities

these relationships, however, decrease as the relative density increases. Existence of increasing inherent anisotropy with decreasing relative density is again indicated by the data points (deviation of θ from 35°) corresponding to the hydrostatic, R = 1 loading.

The relationships between θ and relative density at several constant values of R are shown in Figure 5.9. It may be noted that linear relationships exist between θ and relative density at each value of R. The slope of these straight lines decrease progressively with increasing R.

The linear relationships observed in Figures 5.8 and 5.9 when combined, result in a plane surface in three dimensions with % relative density D_r, stress ratio, R, and θ as coordinates. The equation of this plane, which describes completely the contractant proportional loading behaviour of Ottawa sand is, for compression

$$D_r + A\left(\frac{R}{\sqrt{2}}\right) + B\theta + C = 0 \qquad (5.9)$$

and for extension

$$D_r + A\left(\frac{-\sqrt{2}}{R}\right) + B\theta + D = 0 \qquad (5.10)$$

in which A,B,C,D are constants. Since R = 1 is common to both compression and extension, this requires $(A/\sqrt{2}+C) = (-\sqrt{2}A+D)$, and thus there are only three independent constants. For Ottawa sand the values of the constants are;

A = 189, B = -2.6, C = -115 and D = 287.

The plane surface represented by Equations 5.9 and 5.10 for this sand is shown in Figure 5.10. This plane surface can be completely

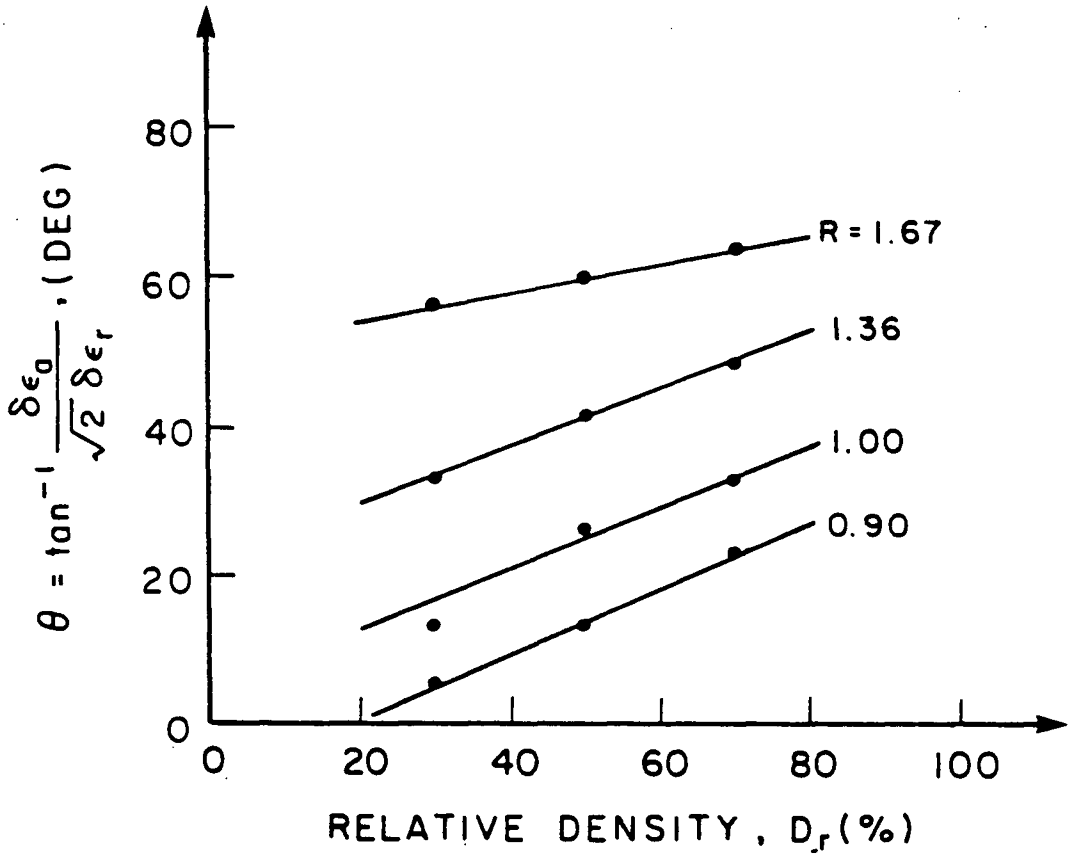

Fig. 5.9 Relationships Between Strain Increment Ratio and Relative Density for Different Stress Ratios

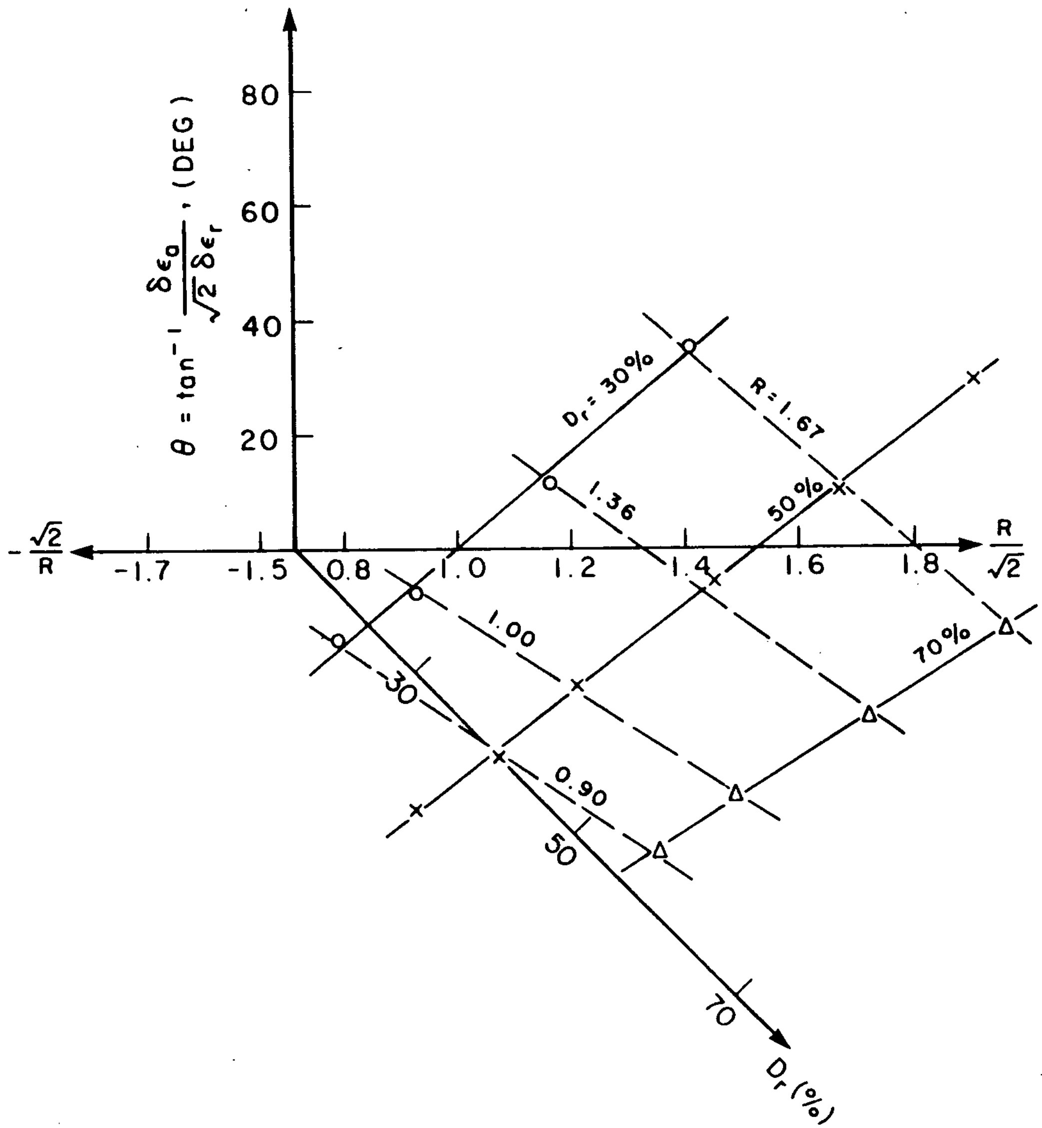

Fig. 5.10 Contractant Constant R State Surface for Ottawa Sand

determined by performing only three proportional loading tests on the sand. The magnitude of strain increment ratio under proportional loading can therefore be completely specified under any R and D_r, once the plane surface in Figure 5.10 for the sand has been established.

A relationship of strain increment ratio to stress ratio R is also implied by the stress-dilatancy theory. The stress-dilatancy theory, however, neither enables precise numeric prediction of strain increment ratio, nor takes explicit account of the relative density as a state variable. Furthermore, as pointed out earlier, stress-dilatancy theory cannot, in principle, describe contractant deformation response of sand, which is the subject of the present investigations.

The ability to predict strain increment ratio alone for any R value does not, however, enable determination of individual strain components. Determination of individual strain components will now be attempted by establishing energy density increment relationships across relative densities, similar to those discussed earlier at one relative density.

From examination of test results at a relative density of 50%, it has been shown that the ratio of axial strain increments of two R paths are constant, provided the mean normal stress histories are identical. The implication of that result was demonstrated to require the ratio of energy density increments to be constant all along the two stress paths (Figure 5.6). A similar behaviour with regard to constancy of energy density increment ratio may be seen in Figure 5.11 for relative densities of 30 and 70%. It would now be of interest to examine possible energy density increment ratio relationships between

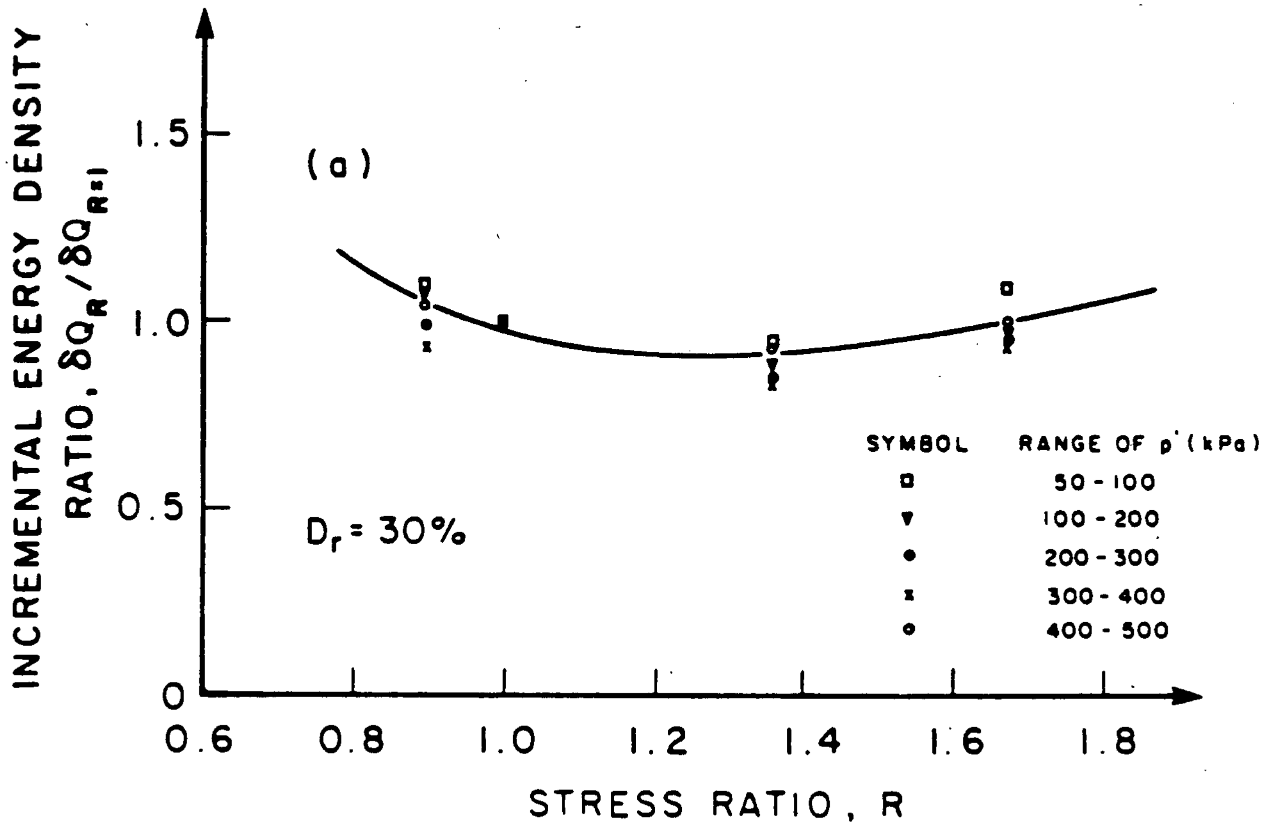

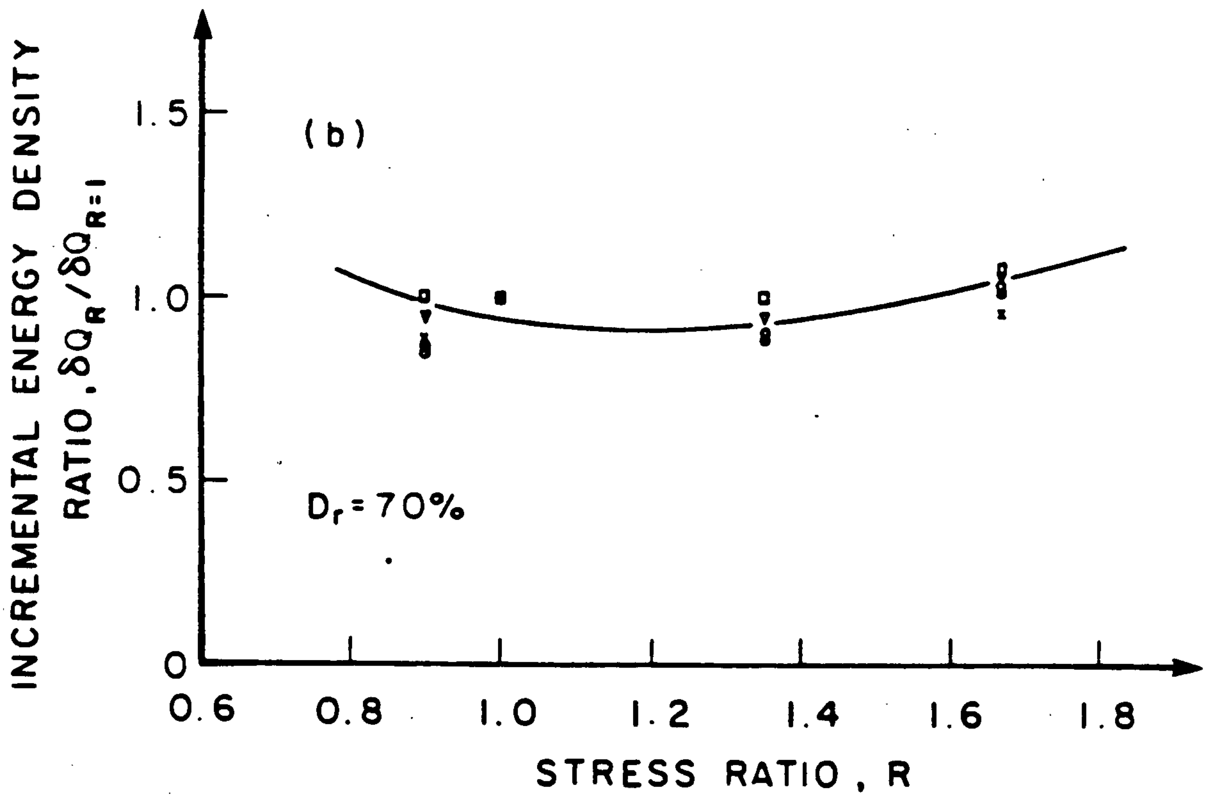

5.11 Variation of Incremental Energy Density Ratio with Stress Ratio: a) $D_r = 30\%$ and b) $D_r = 70\%$

specimen having identical stress histories (p' and R) but different relative densities. Such energy density increment ratios are shown plotted against stress ratio R in Figure 5.12. At each relative density, the energy density increment ratio shown is the ratio with respect to the energy density increment for $D_r = 50\%$. The results suggest that for any value of R the energy density increment ratio of two specimen having identical stress histories but different relative densities remain reasonably constant. Furthermore the magnitude of this ratio is essentially the same regardless of the identical R value for which the energy density increments are considered. Average lines have been drawn in Figure 5.12 through data points for each energy increment ratio considered, in order to determine the constant values of these ratios.

Values of the constant energy density ratios in Figure 5.12 are now plotted against the inverse ratio of the corresponding relative densities in Figure 5.13. A linear relationship with a slope equal to unity is obtained. Thus

$$\frac{\delta Q_1}{\delta Q_2} = \frac{D_{r2}}{D_{r1}} \tag{5.11}$$

in which subscripts on Q and D_r associate corresponding energy and relative density states D_{r1} and D_{r2}. Equation 5.11 may be stated as follows:

Given two specimen at relative densities D_{r1} and D_{r2} proportionally loaded under identical R to mean effective stress p'; if identical stress increments $\delta p'$ were to be applied to each specimen, energy

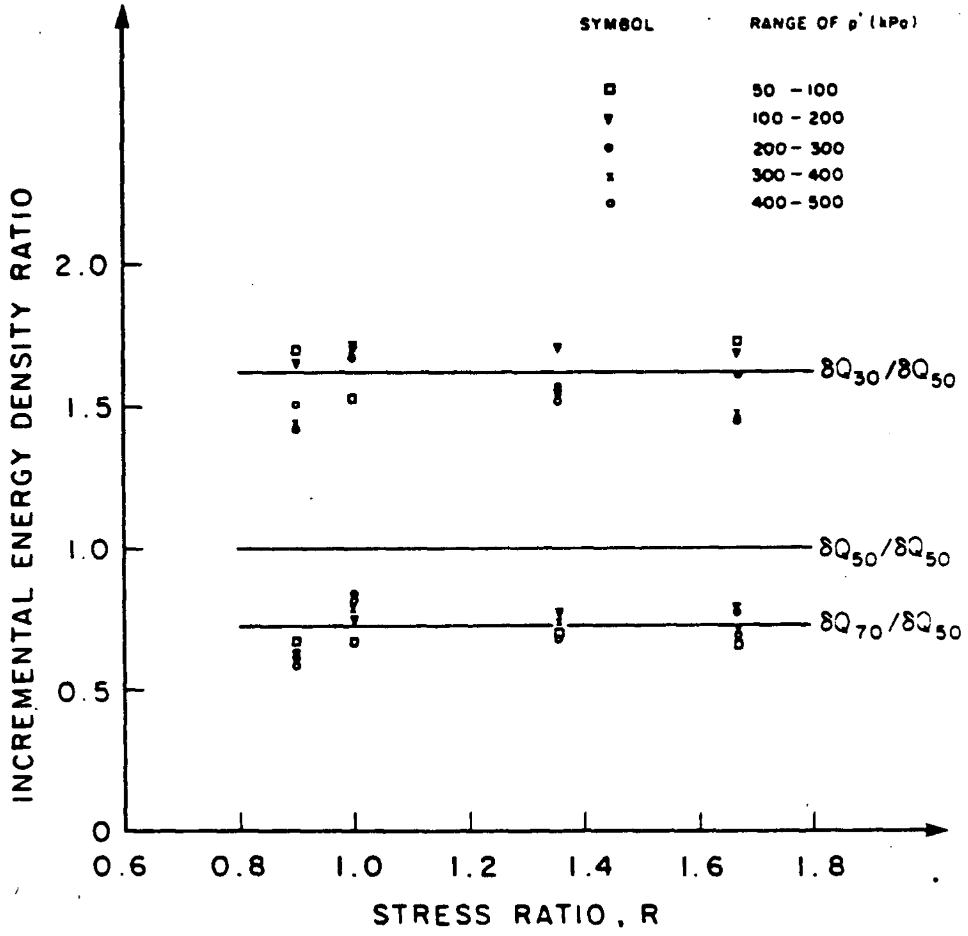

Fig. 5.12 Relationships Between Incremental Energy Density Ratio with Stress Ratio

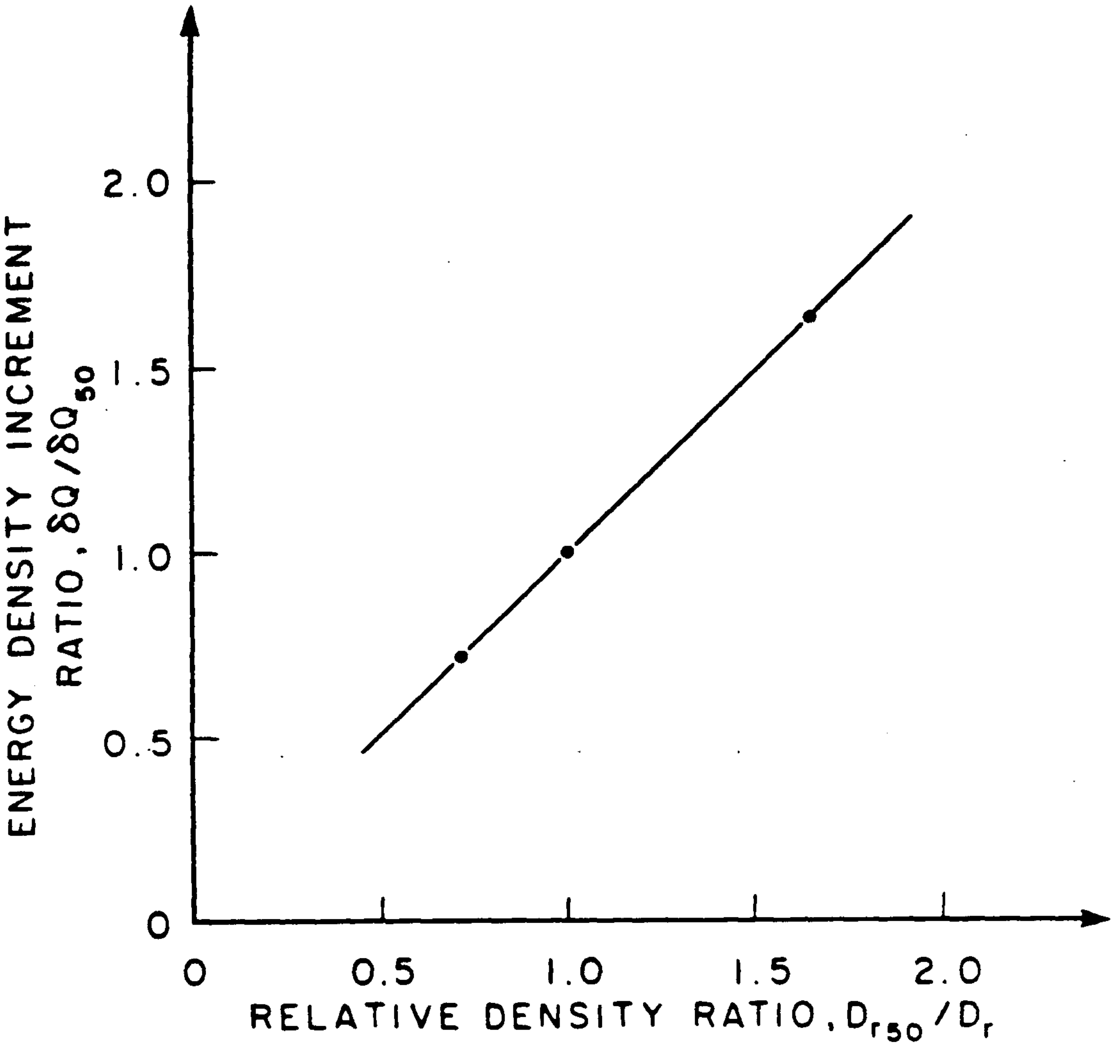

5.13 Relationships Between Ratios of Energy Density Increment and Relative Density

density increments of δQ_1 and δQ_2 would take place. The ratio of these energy density increments is equal to the inverse ratio of their relative densities, regardless of the magnitude of the identical R value under which proportional loading occurred. Using Equation 5.8, the energy density increment ratio may be written in terms of strain increments as

$$\frac{\delta Q_1}{\delta Q_2} = \frac{\delta\varepsilon_{a1}\left(R + \frac{\sqrt{2}}{\tan\theta_1}\right)}{\delta\varepsilon_{a2}\left(R + \frac{\sqrt{2}}{\tan\theta_2}\right)} \tag{5.12}$$

and from Eq. 5.11

$$\frac{D_{r2}}{D_{r1}} = \frac{\delta\varepsilon_{a1}\left(R + \frac{\sqrt{2}}{\tan\theta_1}\right)}{\delta\varepsilon_{a2}\left(R + \frac{\sqrt{2}}{\tan\theta_2}\right)} \tag{5.13}$$

in which $(\delta\varepsilon_{a1}, \theta_1)$ and $(\delta\varepsilon_{a2}, \theta_2)$ are associated with relative densities, D_{r1} and D_{r2} respectively and the stress ratio R.

5.2.2. Proportional Stress-Strain Relationships

Equation 5.13 enables prediction of axial strain increments at any desired relative density from a known stress-strain relationship at another relative density, provided the stress histories (p', R) of two samples are identical. Earlier, Equation 5.3 was shown to enable predictions of axial strain increments under any stress ratio from a known stress-strain relationship at another stress ratio, provided the two samples have identical relative densities. It is thus possible to predict axial strain increments under any relative density D_r and stress ratio R by a simple superposition of the identical relative density process (Equation 5.3) and identical stress history process (Equation 5.13).

Considering the identical relative density process, the axial strain increment $\delta\varepsilon_a'$ under R at D_{ri} is given by (Equation 5.3)

$$\delta\varepsilon_a' = \frac{\sin\theta'}{\sin\theta_i}\,\frac{\cos(\theta_i-\psi)}{\cos(\theta'-\psi)}\cdot\delta\varepsilon_{ai} \qquad (5.14)$$

in which $\delta\varepsilon_{ai}$ is the known axial strain increment at D_{ri} and R_i and θ_i and θ' are associated with strain increment ratios at relative density D_{ri} under R_i and R respectively. Both θ_i and θ' can be evaluated for their respective stress ratio and relative densities from Equations 5.9 or 5.10. Now following next a constant stress history process, the desired axial strain increments at D_r and R are related to $\delta\varepsilon_a'$ by (Equation 5.13).

$$\delta\varepsilon_a = \frac{D_{ri}}{D_r}\;\frac{R+\dfrac{\sqrt{2}}{\tan\theta'}}{R+\dfrac{\sqrt{2}}{\tan\theta}}\cdot\delta\varepsilon_a' \qquad (5.15)$$

in which θ is associated with strain increment ratio at D_r under R. Substituting for $\delta\varepsilon_a'$ from Equation 5.14 into Equation 5.15 we get

$$\delta\varepsilon_a = \left[\frac{D_{r_i}}{D_r}\right] \cdot \left[\frac{(R + \frac{\sqrt{2}}{\tan\theta'})}{(R + \frac{\sqrt{2}}{\tan\theta})}\right] \cdot \left[\frac{\sin\theta'}{\sin\theta_i} \cdot \frac{\cos(\theta_i - \psi)}{\cos(\theta' - \psi)}\right] \cdot \delta\varepsilon_{ai} \qquad (5.16)$$

Since strain increment ratio $\delta\varepsilon_a/\delta\varepsilon_r$ ($=\sqrt{2}\tan\theta$) is uniquely prescribed in the plane surface by Equation 5.9 and 5.10 once R and D_r are specified, the radial strain increment $\delta\varepsilon_r$ (or volumetric strain increment $\delta\varepsilon_v$) can be readily calculated. Hence a complete stress-strain response under any R at D_r can be predicted from a known response under a known R_i and D_{ri}. In Equation 5.16 the three terms in the square brackets may be considered to reflect respectively the influences of (1) relative density, (2) variation in anisotropy due to changes in relative density and (3) the effect of stress path.

Equation 5.16 has been used to develop stress-strain predictions for specimen at 30, 50 and 70 percent relative densities (Figure 5.14, 5.15 , 5.16). Predictions are made for proportional loading under hydrostatic as well as in compressional and extensional modes and compared with the measured response. The known data base for these predictions consists of hydrostatic loading (R = 1) at a relative density of 50 percent. It may be seen that excellent agreement exists between predicted and observed response in each case. The agreement between predicted and measured axial strain response for loose sand in extensional loading (Figure 5.15a) may not be viewed as satisfactory. However, considering the extremely small magnitude of strains, the agreement can be regarded rather good.

It may be pointed out, that the stress-strain relationship proposed does not require any appeal to material isotropy, which is generally needed in most constitutive models. The effect of inherent

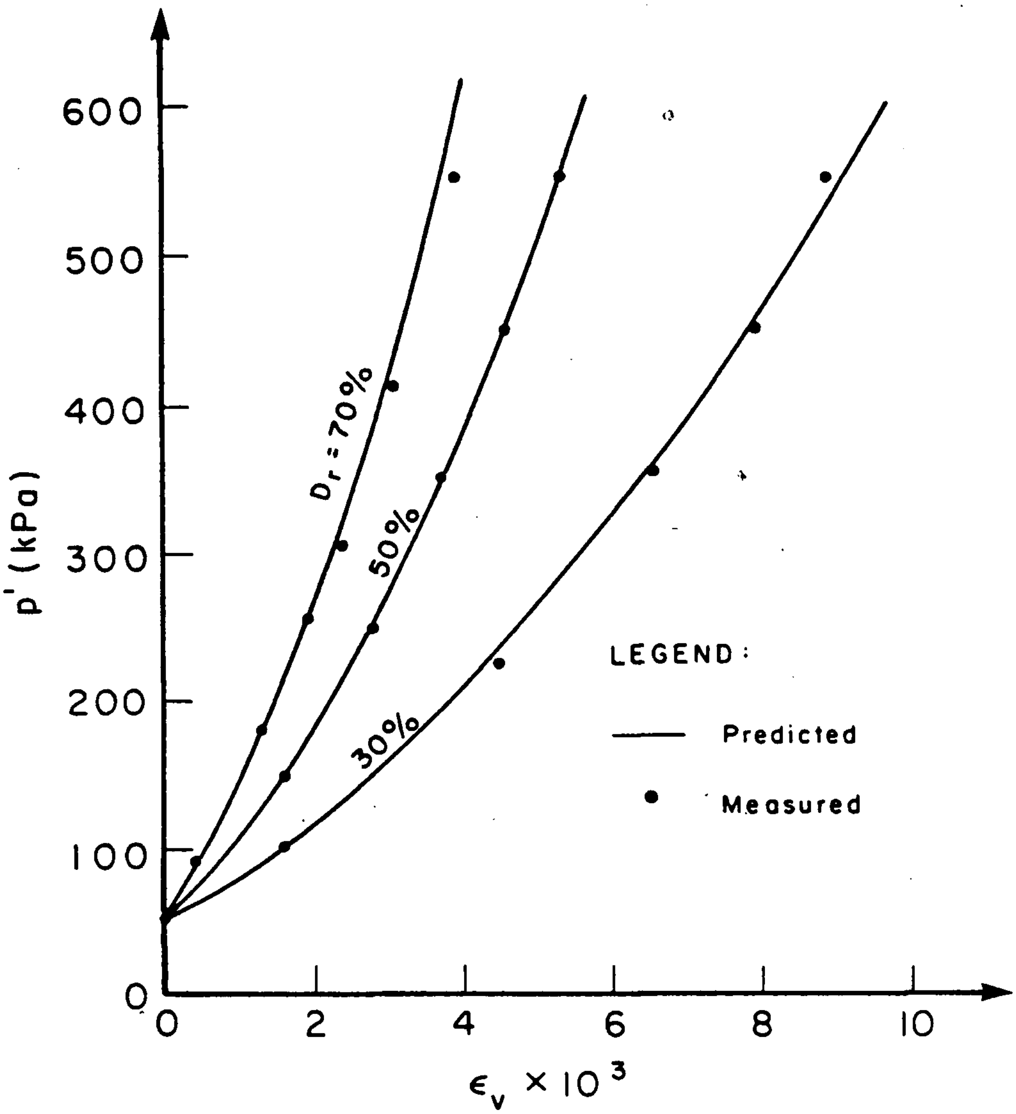

Fig. 5.14 Comparison of Measured and Predicted Volumetric Strains for Hydrostatic Loading at Various Relative Densities

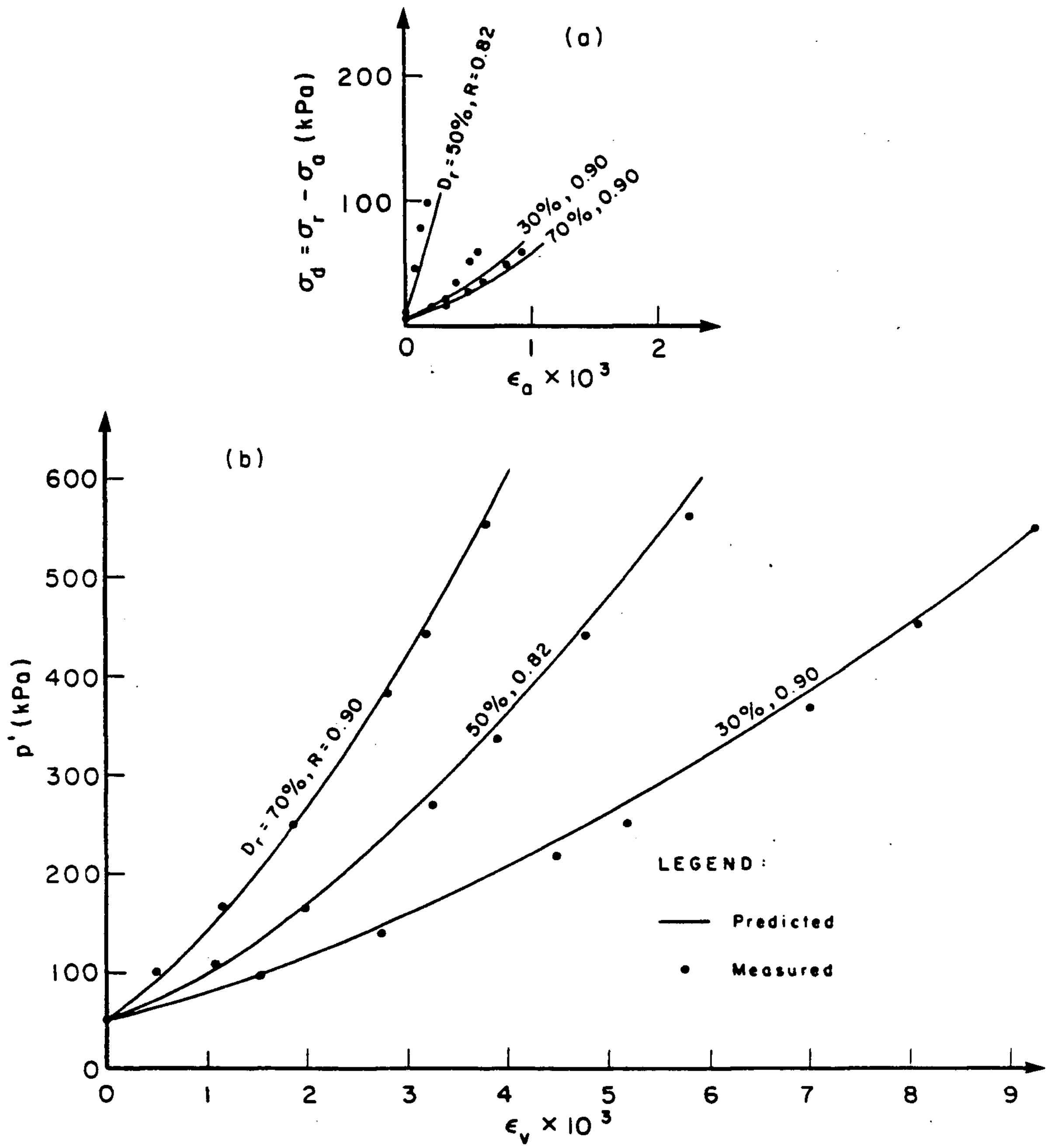

Fig. 5.15 a) & b) Comparison of Measured and Predicted Strains for Proportional Loading in Extension Mode and at Various Relative Densities: a) Axial Strain and b) Volumetric Strain

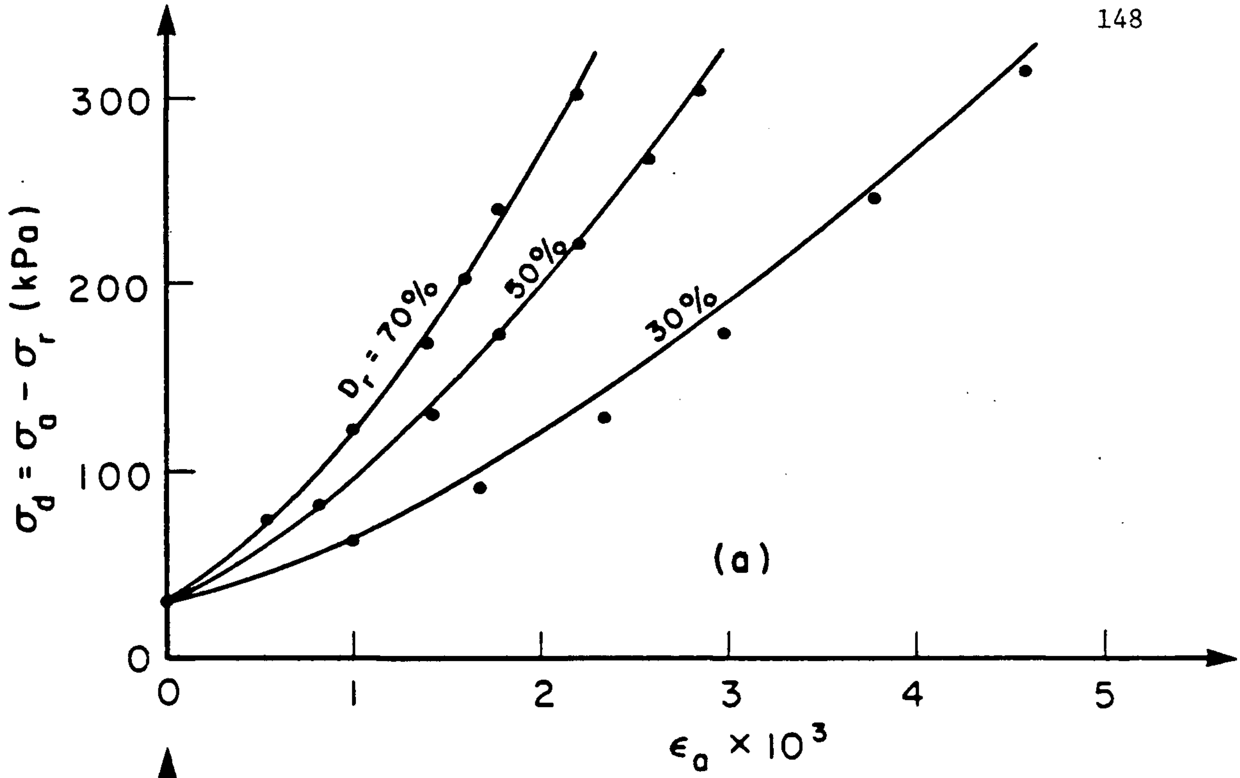

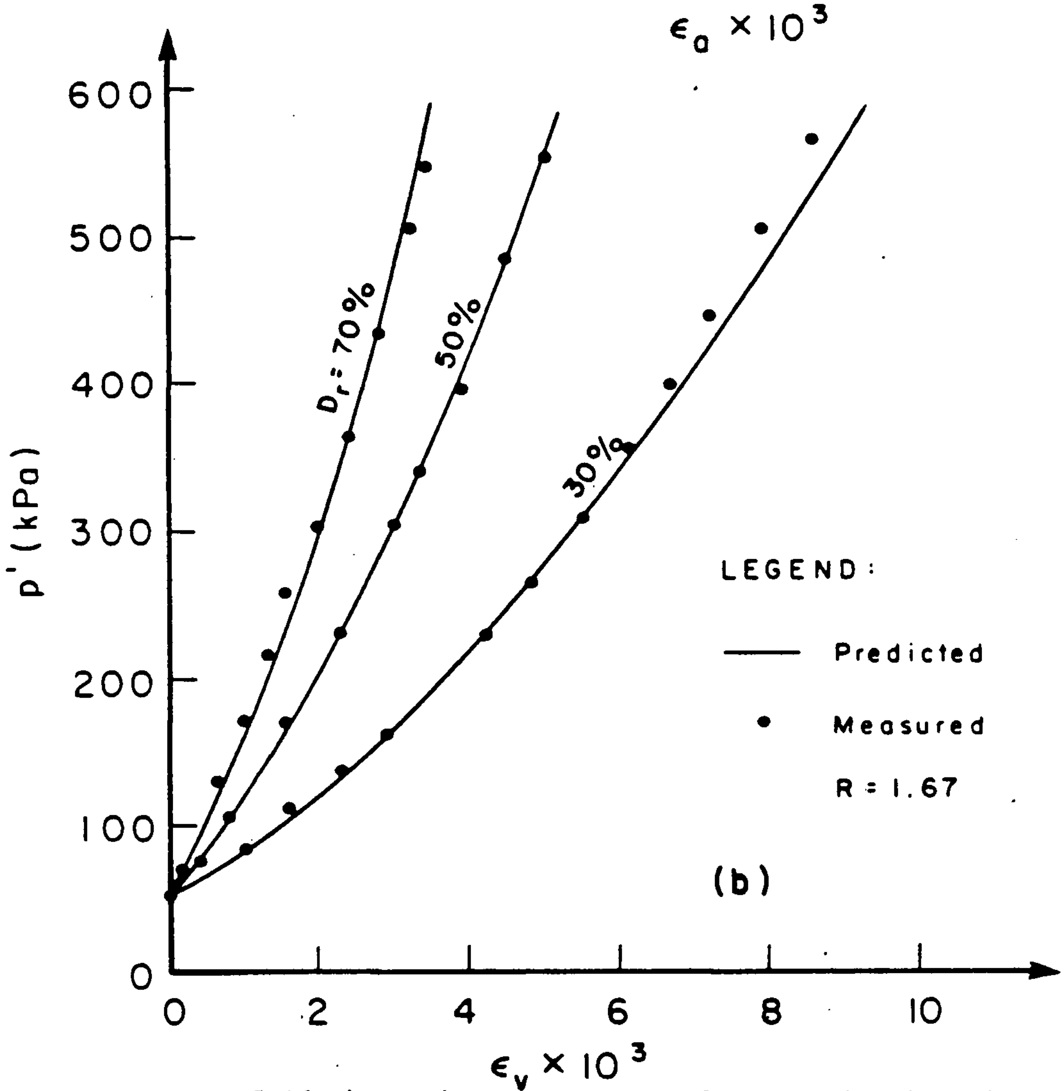

Fig. 5.16 a) & b) Comparison of Measured and Predicted Strains for Proportional Loading in Compression Mode at Various Relative Densities:
a) Axial Strain and b) Volumetric Strain

anisotropy in sand, which is considered to be associated with the one dimensional sedimentation process, is inherently contained within the proposed relationships. Furthermore, unlike most other material models, the proposed model takes account of relative density in the form of an independent state variable, enabling stress-strain predictions from one relative density state to another.

5.2.3 Required Parameters

In all, four parameters A, B, C (or D) and angle ψ are required for the overall relationship. Constants A, B and C (or D) determine the unique plane surface from which strain increment ratio (or θ) for any desired R and D_r can be determined. In addition, angle ψ is needed for evaluating axial strain increments for the desired R and D_r (Equation 5.16). All four constants can be determined from three triaxial tests. Two of these constant R tests must be at the same relative density in order to determine parameter ψ. The third test must be at another value of relative density. For simplicity two tests at different relative densities can be the conventional hydrostatic compression tests (R = 1). The three tests together thus provide three points required in R, D_r and θ space for defining the equation of the plane surface (Equation 5.9 or 5.10). The results of any one of the three tests can be used as the reference data base for prediction of stress strain behaviour under any R path at any D_r.

CHAPTER VI - NON-PROPORTIONAL STRESS PATHS

Experimental study of small strain behaviour of sand in proportional loading paths in Chapter 5 suggested a consistent pattern of response. The test results led to a framework capable of predicting deformations due to contractant proportional loading across relative densities and stress ratio. In this chapter small strain response is investigated in non-proportional stress paths in which the overall stress ratio does not remain fixed. Stress ratio can vary along a path with changes in either or both shear and mean normal stress. In the first part of this chapter, non-proportional total loading response, wherein none of stress ratio, mean normal stress or shear stress decrease, is examined. The influence of increasing or decreasing stress ratio, R, under alternate conditions of constant shear and constant mean normal stress, with stress reversal, on small deformation response is investigated in the second part.

6.1 Total Loading Paths

States of mean normal stress, shear stress and stress ratio are important in the specification of stress state for sand. These three stress parameters are of course not independent as specification of any two would determine the third. However, a change in state, in the sense of loading and unloading, cannot be prescribed without ambiguity in situations wherein anyone of these parameters is decreasing. In order to facilitate systematic study, only total loading paths in which none of the three stress parameters decrease will be considered in the following. On the compression side these stress paths cover a range from compression along the hydrostatic axis to a constant mean normal stress paths, all originating from a state of hydrostatic compression. The general objective is to examine relationships between parallel stress paths and possible association of stress and strain directions.

6.1.1 Parallel Loading Paths

Experimental investigations in Chapter 4 have shown that different stress paths from a common consolidation state result in corresponding different strain paths. The effect of consolidation stress level and density on strain paths is now examined from observation of test results derived from parallel stress paths originating from different consolidation states. Widely used incremental linear elastic approaches only require representation of parallel conventional triaxial results in analytic form and at only one density. The sub-class of parallel stress paths considered herein cover a broad range of stress paths including the conventional triaxial path. Alternatives for improvement of current incremental elastic procedures are considered on the basis of experimental observations at small strain.

6.1.1.1 Effect of Consolidation Stress on Strain Paths

Strain response in a series of conventional triaxial stress paths initiating from various hydrostatic consolidation stress levels is shown in Figure 6.1.a. It may be noted that all strain paths maintain a common initial orientation regardless of the level of initial consolidation stress. The initial slope of this strain path is -4.4. A slope of -2 represents zero volumetric strain. Hence incremental

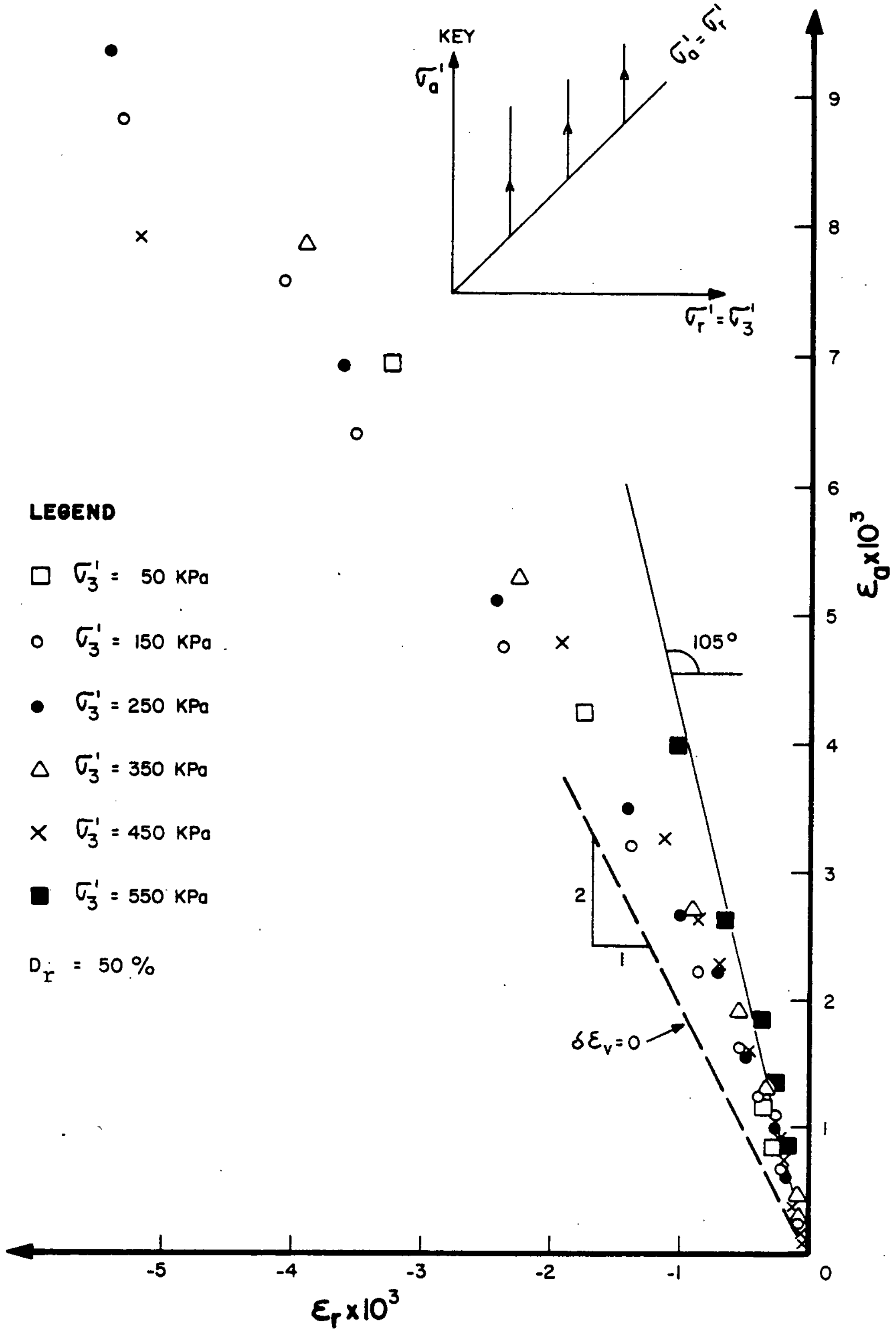

Fig. 6.1a Strain Paths for Conventional Triaxial Stress Paths from Different Consolidation States

volumetric strains for these stress paths are contractant. For each level of confining stress, non linearity of strain paths and dilatant tendencies did not commence until strain levels corresponding to stress ratios in excess of about 2 were reached.

Strain response in constant mean normal stress paths also resulted in a common and initially linear strain path which is independent of consolidation stress level, Figure 6.1.b. This common strain path is oriented at a slope of -2.4. Thus the contraction rate was smaller for constant p' paths than for the corresponding conventional triaxial paths. Clearly, the increase in mean normal stress that is associated with conventional triaxial paths contributes to contraction in addition to that resulting from shearing. It may be noted that even though both conventional triaxial and constant mean normal stress paths lead to initial strain paths that result in net volumetric contraction, radial strain increments remain expansive.

A linear strain path and expansive radial strain may also be observed for a stress path which followed an incremental stress ratio, $(\delta\sigma_1'/\delta\sigma_3')$, of 4 and from an initial confining stress $\sigma_3' = 50$ kPa, as shown in Figure 6.1.c. However, the contraction rate in this stress path, slope = - 5.2, is greater than for the conventional triaxial path because of its larger rate of mean normal stress increase with shear.

Stress paths in which the incremental stress ratio was held to 2 were also followed from different levels of hydrostatic compression. Once again, the strain path in each test, Figure 6.1.d, follows the same direction which is independent of the initial level of consolidation pressure. In these strain paths, both axial and radial strain components are, however, contractant and the strain paths have a positive slope of about 4.5. Between these stress paths and that

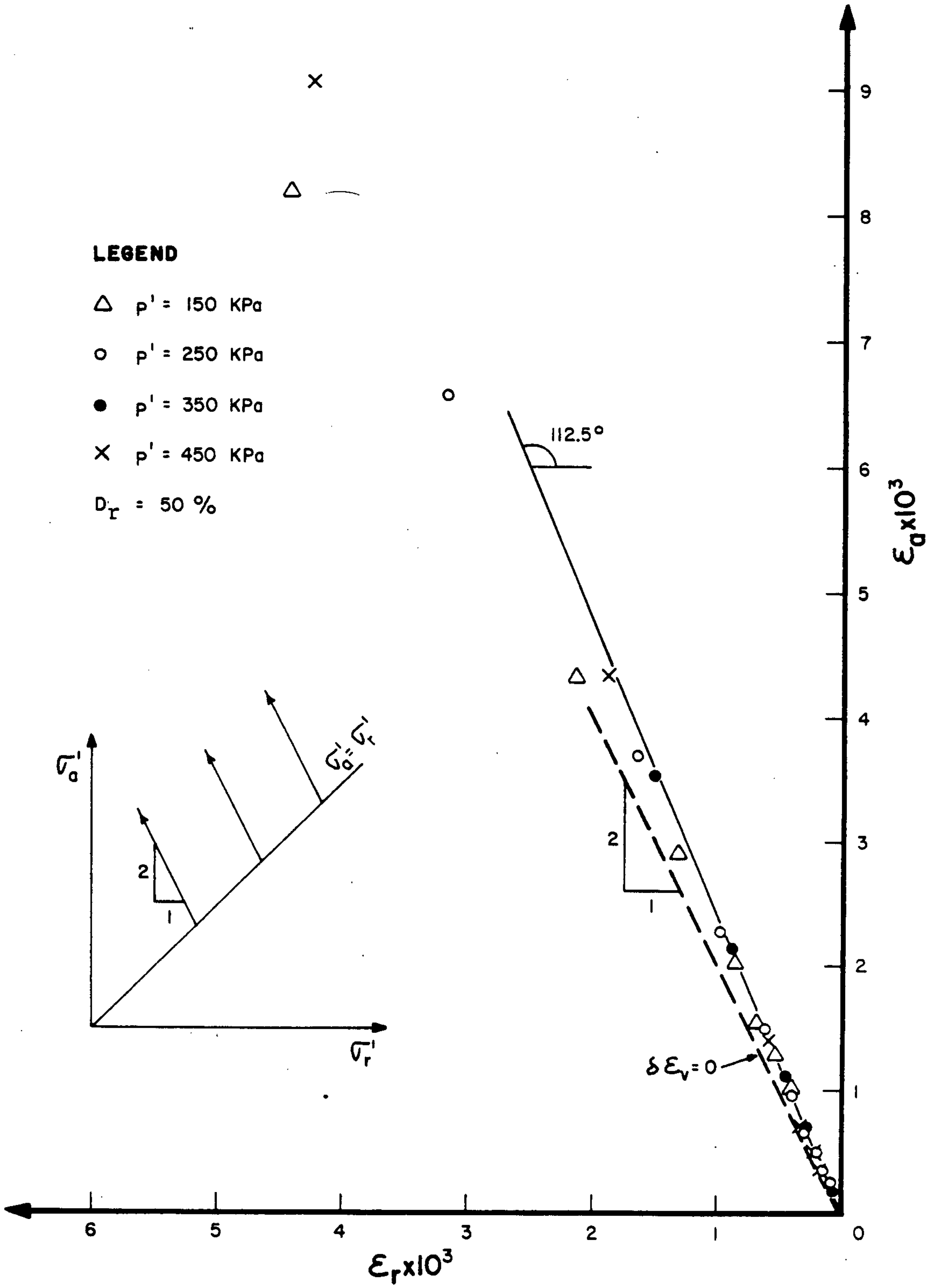

Fig. 6.1b Strain Paths for Constant Mean Normal Stress Paths from Different Consolidation States

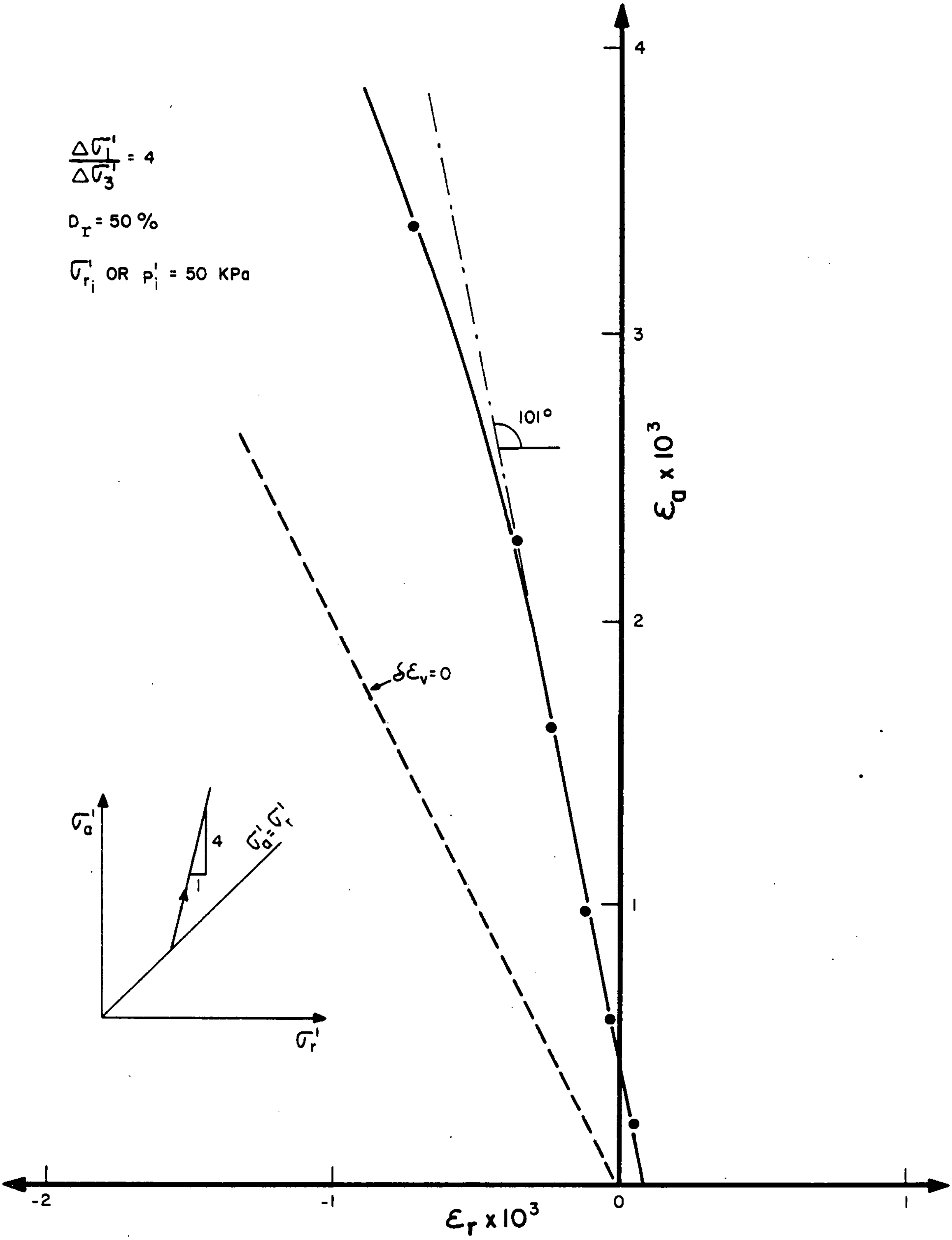

Fig. 6.1c Strain Path for a Stress Path of Constant Incremental Stress Ratio of 4

corresponding to a stress increment ratio of 4, there would exist an equivalent K_o path for which lateral strain increments would be zero.

In general, contractant volumetric strain in sand can result from independent increases in shear as well as mean normal stress. Even though these two effects cannot be isolated when they occur simultaneously; the trend in strain paths observed in Figures 6.1a, b, c and d suggests an increasing rate of volume change with stress paths of decreasing incremental stress ratio. This implies an increasing tendency for volume contraction as the stress paths progressively deviate from a constant p' direction towards a hydrostatic stress direction.

At moderate stress levels, hydrostatic compression alone is not effective in bringing about a major change in the density and structure of sand (Youd, 1972). Thus, the sense of inherent anisotropy would not be altered by hydrostatic compression. This view is consistent with the experimental results presented in Figures 6.1a, b, c and d which show that parallel stress paths that originate from different hydrostatic compression states share a common strain path. However, as shown in Figure 4.1; the stress-strain response stiffens with increasing compression stress levels. A unique linear strain path thus implies that stiffening as a consequence of compression occurs to the same degree in both principal strain directions.

The strain path corresponding to a proportional loading of R = 2, is also shown in Figure 6.1.d. It may be noted that this strain path is very close to the unique path associated with the constant incremental stress ratio path of 2. A sand specimen cannot exist in a

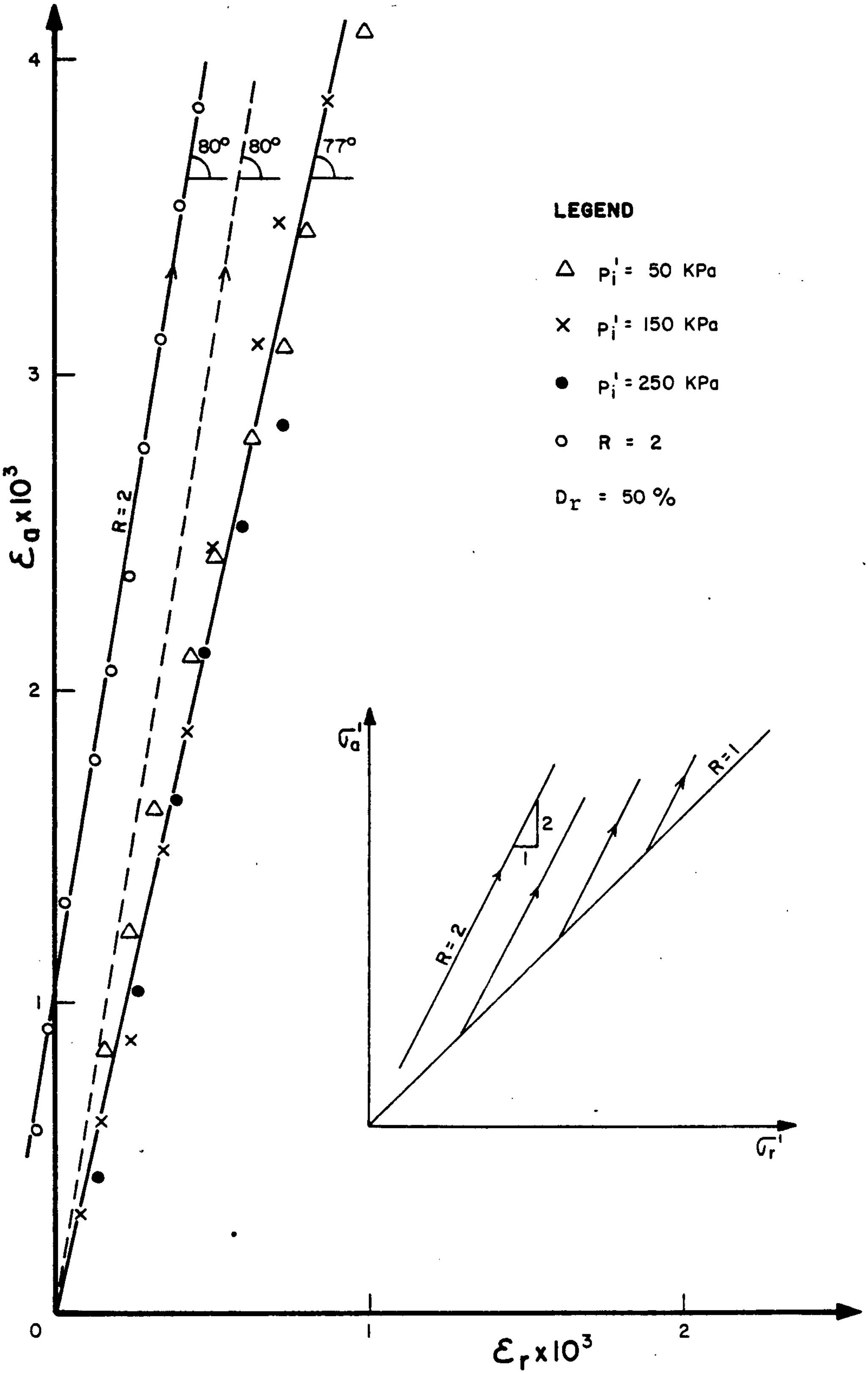

Fig. 6.1d Strain Paths for Stress Paths of Constant Incremental Stress Ratio of 2

stress free state. It is therefore not possible to initiate proportional loading from zero confining stress. This physical limitation and the necessary experimental approximation to proportional loading may explain the small difference between these strain paths. The results in Figure 6.1.d thus show an equivalence between proportional loading paths and incremental stress ratio paths in that both result in the same strain path. Consequently, since proportional loading does not conform to stress dilatancy Rowe (1971), constant incremental stress ratio paths, at small levels of overall stress ratio would also not conform to stress dilatancy, even though such stress paths are associated with increasing stress ratios, as required by stress dilatancy.

6.1.1.2 Effect of Density on Strain Paths

The association of linear stress and strain paths was also explored for other relative densities. Test results for various parallel stress paths and different densities are shown in Figure 6.2.a,b,c,d. It may be observed that for a given type of parallel stress paths, separate strain paths are followed for each density. The separation between strain paths corresponding to identical stress paths but at different densities may be noted to increase as stress path orientations tend towards hydrostatic compression. Thus the influence of density on strain paths appears to vary with stress path direction. However, such a correspondence between stress and strain paths can be shown to be a reflection of material anisotropy by comparing the response of an isotropic and cross isotropic materials subjected to hydrostatic and constant p' stress increments.

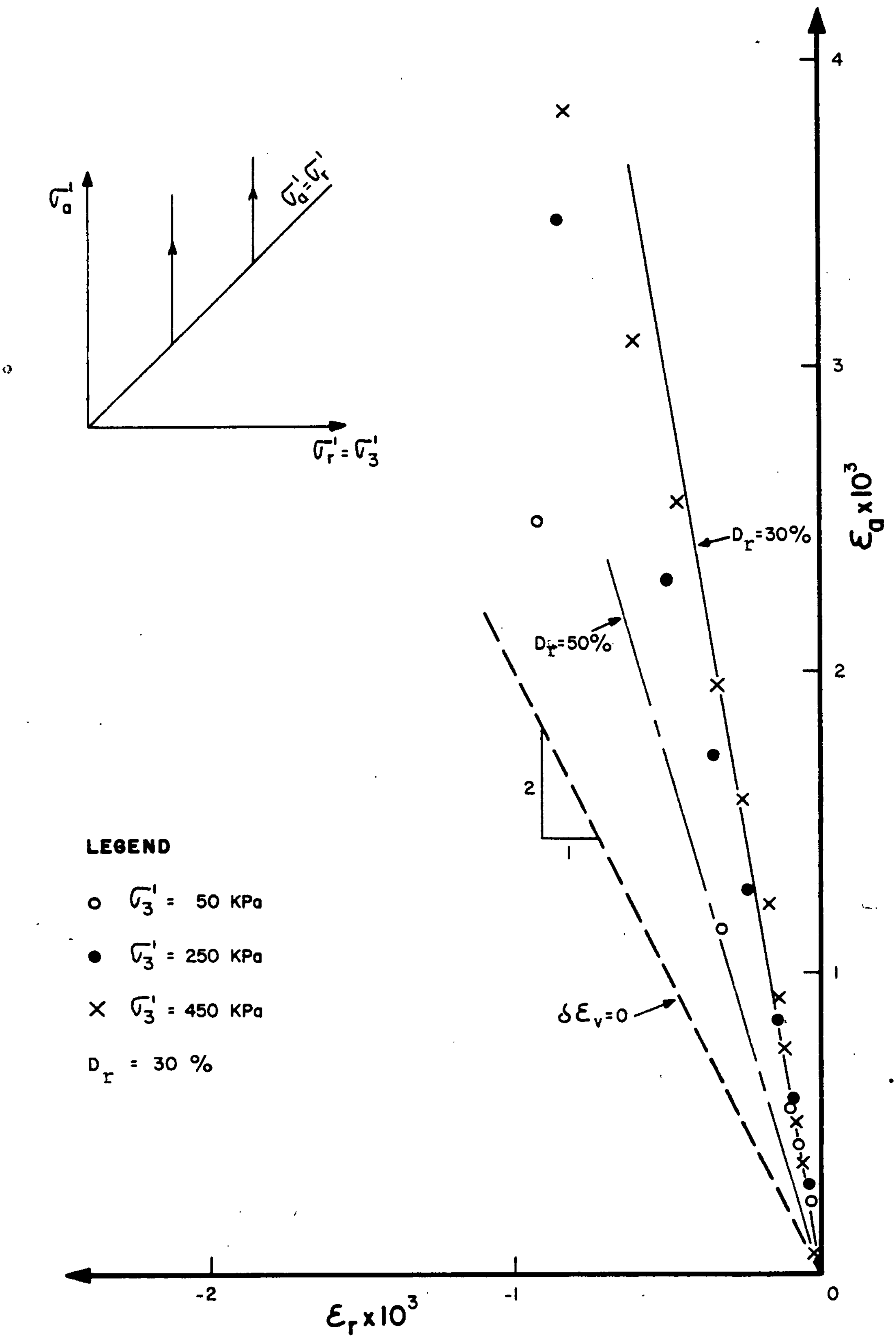

Fig. 6.2a The Influence of Relative Density on Initial Strain Paths for Conventional Triaxial Compression

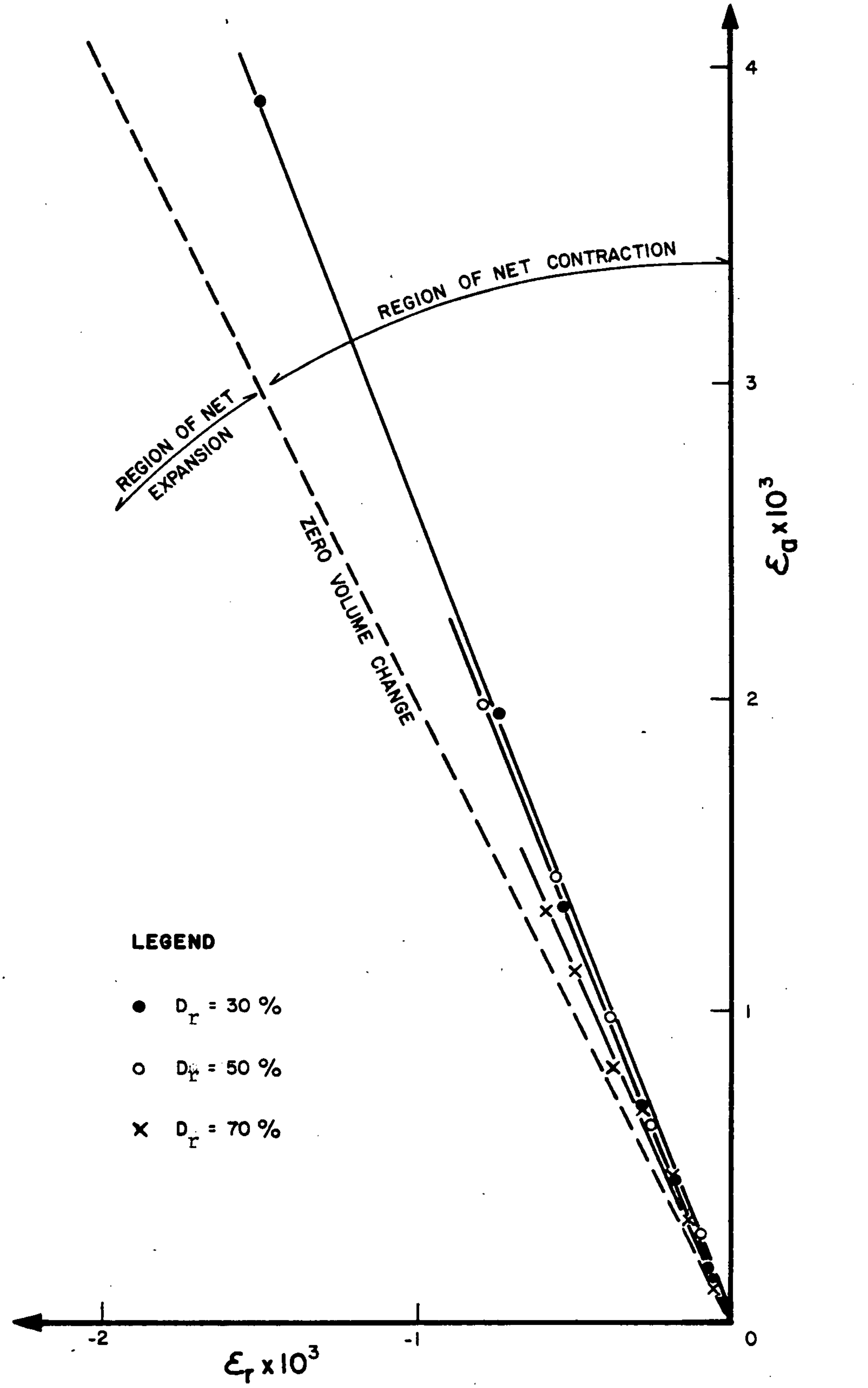

Fig. 6.2b Strain Paths for p' = 450 kPa Tests at Different Relative Densities

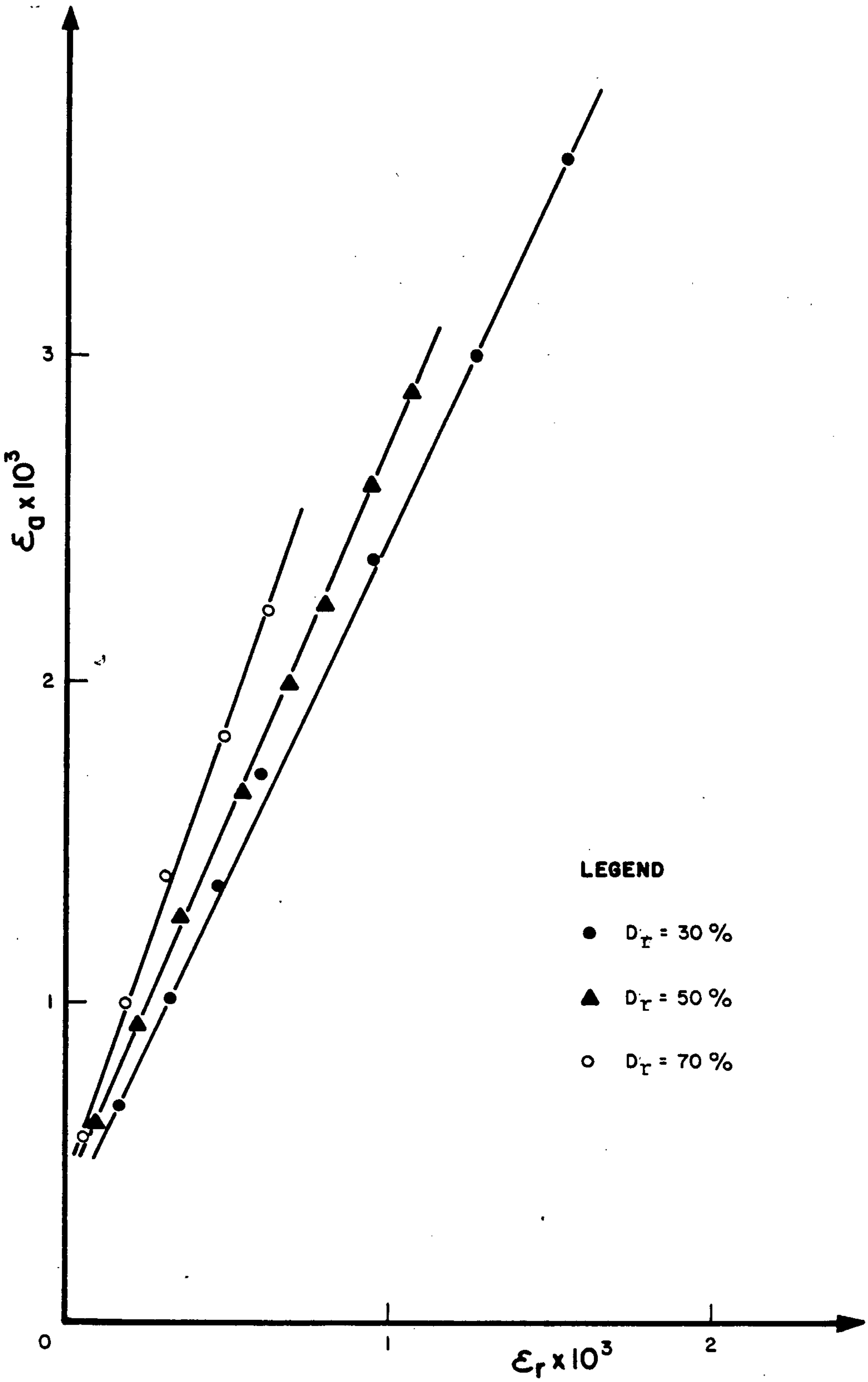

Fig. 6.2c Strain Paths for R = 1.67 Stress Paths at Different Relative Densities

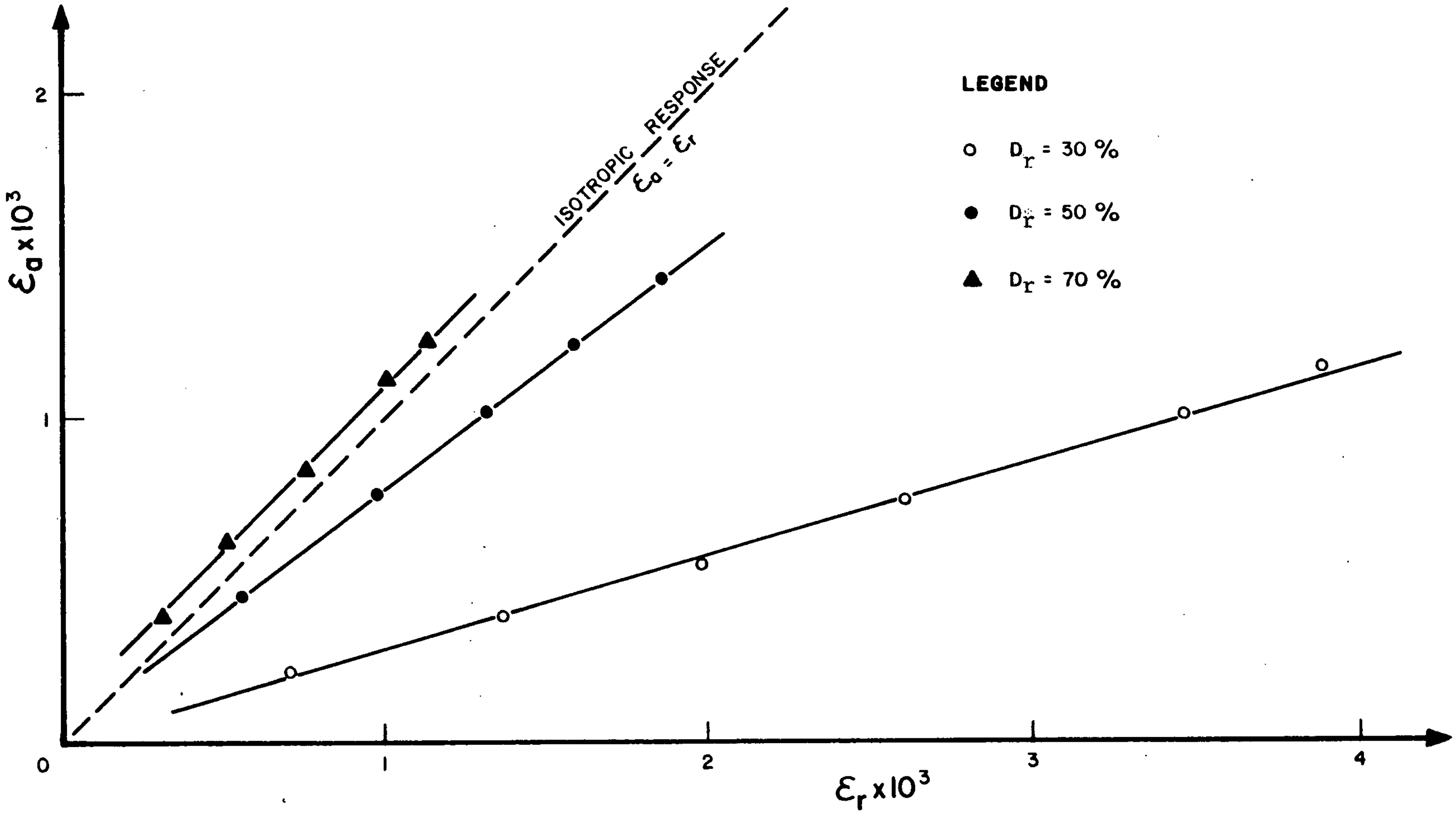

Fig. 6.2d Strain Paths for Hydrostatic Compression at Different Relative Densities

As noted in section 5.2.1 and also shown by the results for hydrostatic compression in Figure 6.2.d, sand specimens formed by pluviation turn progressively from being anisotropic to isotropic with increasing initial density. Hence the observed variation of strain paths with density appears to be mainly a consequence of different anisotropies. Clearly, if an isotropic loose sand were to be formed, its strain path during hydrostatic compression would coincide with that for dense sand. However, attempts to form loose isotropic samples by alternative procedures were not found successful. It therefore may be necessary to consider changing anisotropy and initial density to be concurrent phenomena; if so, the observed difference in strain paths may be justifiably linked to changes in density.

Figure 4.17 and 4.21 show that strain paths that have an initial negative slope transition from a constant to changing dilatancy. This change over occurs at a higher stress ratio with increasing density. Thus, the threshold stress ratio at which the linearity of strain paths terminate increases with density. As discussed previously, deformation in loose sand takes place in smaller clusters than would be in denser states (Horne, 1965). Hence, a limiting equlibrium state would need to be achieved at a relatively few contacts to induce significant sliding in loose sand and the overall stress ratio at which strain paths become non linear would therefore be lowered accordingly.

6.1.1.3 Stress Ratio Equipotentials

At low levels of stress ratio, strain paths have been shown to be associated with stress paths and independent of stress ratio. Hence parallel stress paths at different confining stresses will yield parallel strain paths. A family of such strain paths originating from a hydrostatic stress state and for conventional triaxial tests at a relative density of 50 percent are shown in Figure 6.3.a. Points representing equal stress ratio states along the strain paths are found to lie on straight lines when connected. These lines will be referred to as stress ratio equipotentials. A progresssive increase in the slope of stress ratio equipotentials with stress ratio level and convergence toward an approximate common origin may be inferred. This linearity and convergence to a common point implies $\frac{\delta\varepsilon_{aa}}{\delta\varepsilon_{ab}}$ = const along two parallel stress paths a and b for a change δR applied at stress ratio state R. Similar stress ratio equipotentials may be observed for deformation response under constant mean normal stress and constant incremental stress ratio, $\frac{\delta\sigma_1'}{\delta\sigma_3'} = 2$, paths as shown in Figure 6.3.b and 6.3.c, respectively. Corresponding stress ratio equipotential in different paths do not, however, maintain the same orientation. These experimental observations of behaviour regarding deformations under parallel stress paths can be linked within a coherent framework.

Consider a sand specimen at a stress state (σ_a', σ_r') subjected to an increment of stress ($\delta\sigma_a'$, $\delta\sigma_r'$) along a nonproportional loading path such that the incremental stress ratio $\delta\sigma_a'/\delta\sigma_r' = r$ is constant. This stress increment would induce a corresponding strain increment ($\delta\varepsilon_a$, $\delta\varepsilon_r$). The resulting energy increment per unit volume would be expressed by Equation 5.7 as

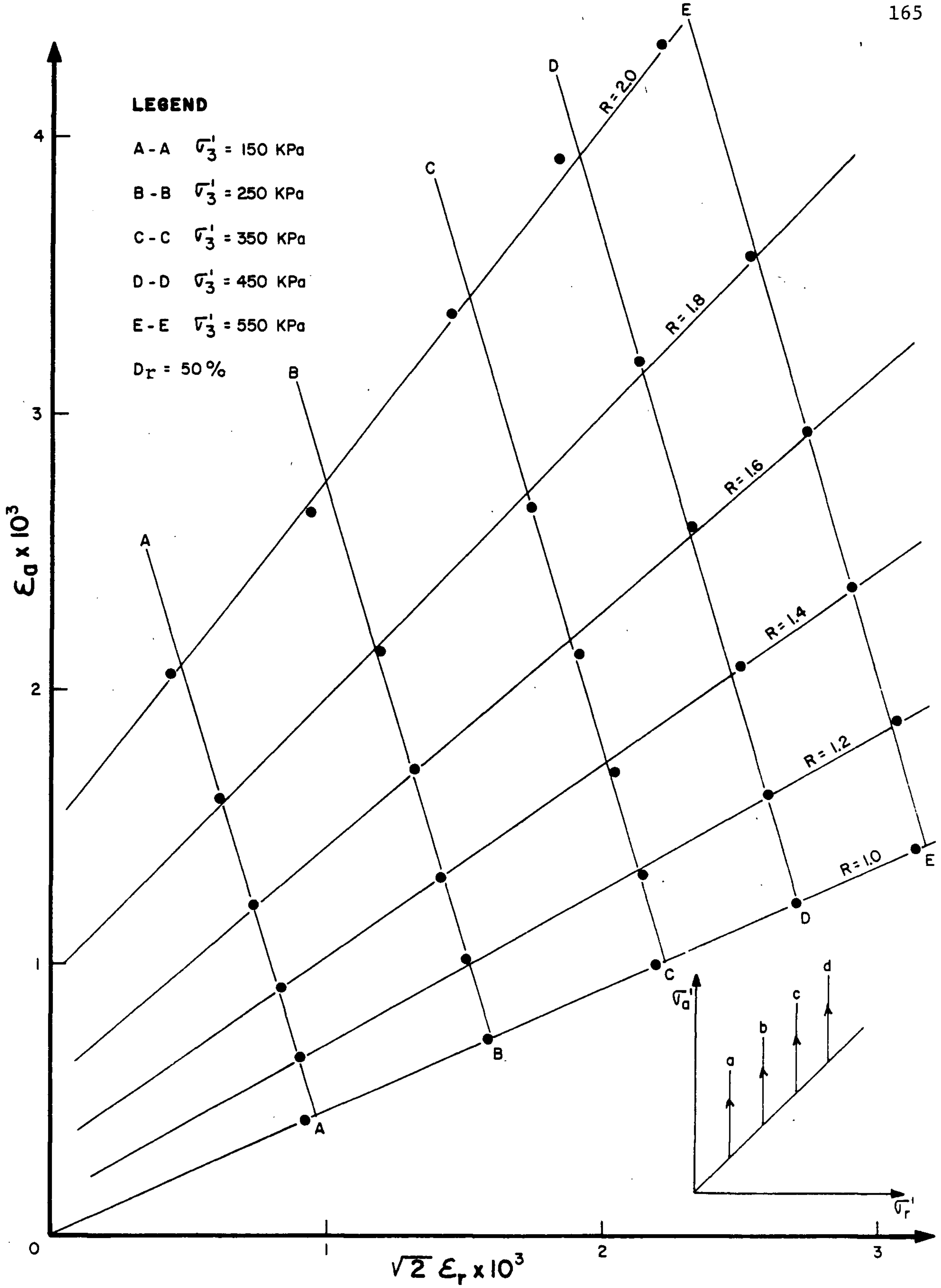

Fig. 6.3a Conventional Triaxial Strain Paths and Stress Ratio Potentials in Strain Space

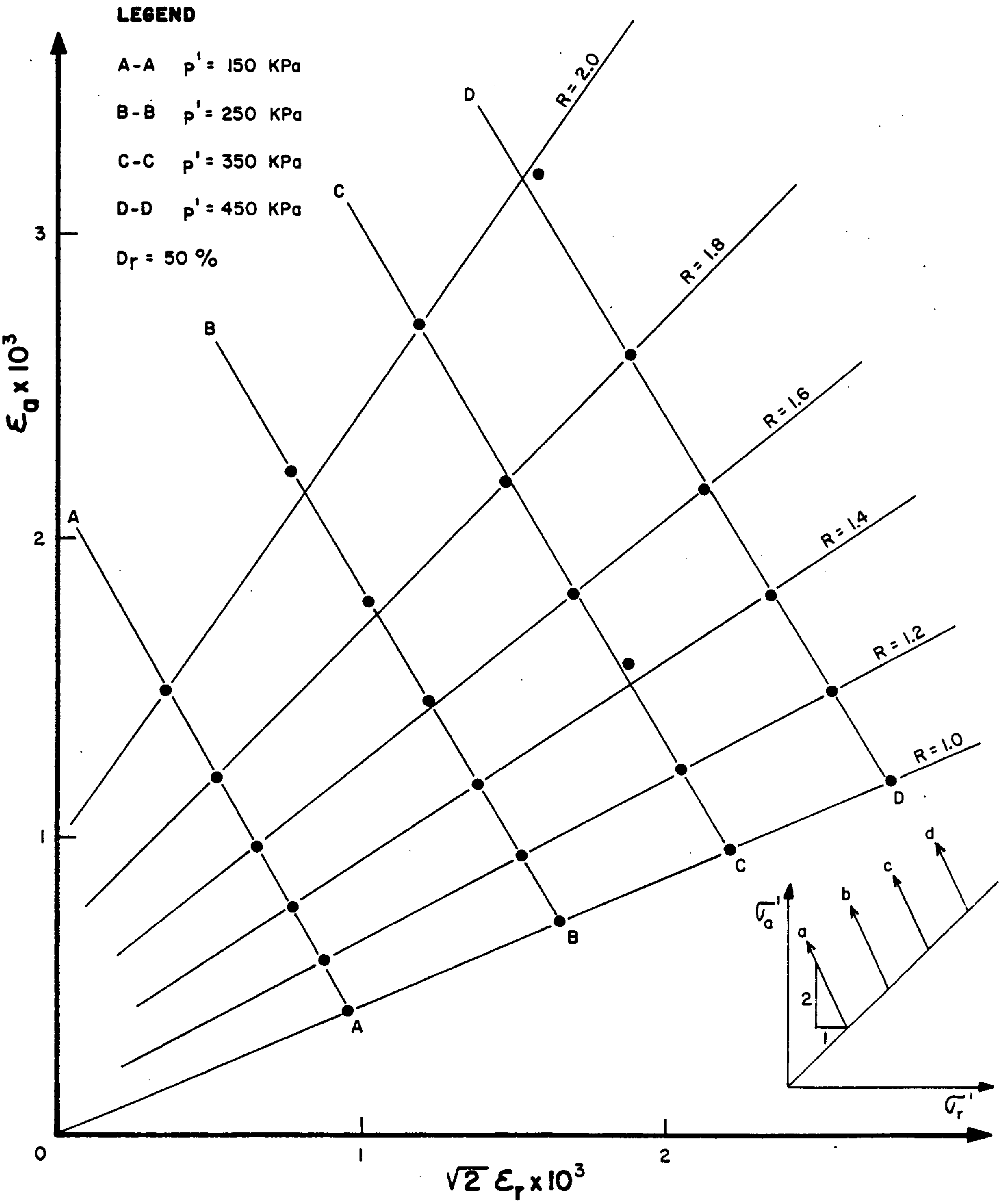

Fig. 6.3b Stress Ratio Potentials in Strain Space for Constant Mean Normal Stress Paths

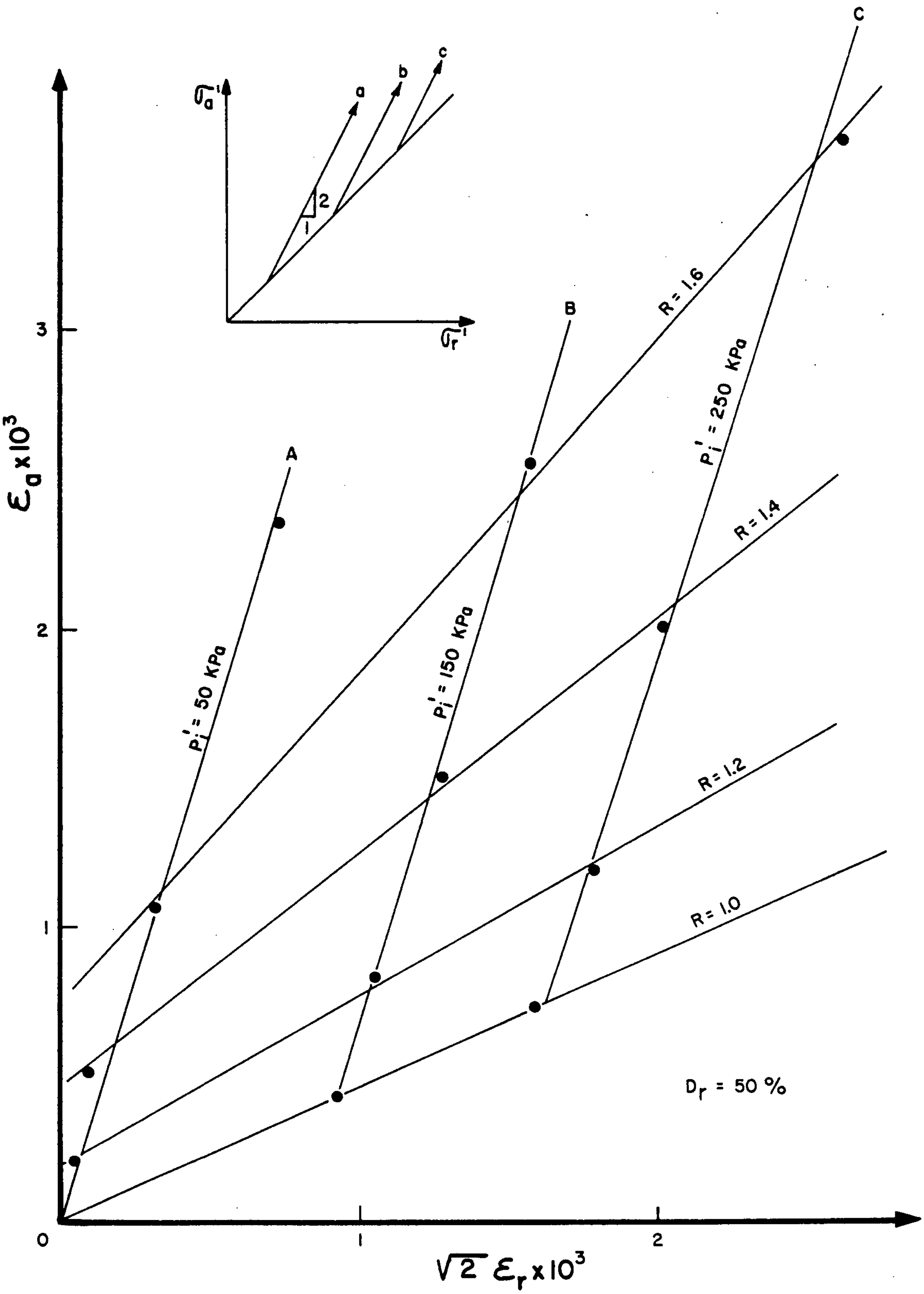

Fig. 6.3c Stress Ratio Potentials in Strain Space for Constant Incremental Stress Ratio of 2 Stress Paths

$$\delta Q = \sigma'_a \delta\varepsilon_a + 2\ \sigma'_r \delta\varepsilon_r \tag{5.7}$$

and since $R = \frac{\sigma'_a}{\sigma'_r}$; Equation (5.7) can be written as

$$\delta Q = \sigma'_r\ \delta\varepsilon_a\ (R + 2\ \frac{\delta\varepsilon_r}{\delta\varepsilon_a}) \tag{6.1}$$

In the experimental results presented previously, it has been shown that at small stress ratio, $\frac{\delta\varepsilon_r}{\delta\varepsilon_a}$, is a characteristic for a given stress path. Therefore the term within the brackets in Equation (6.1) may be considered to represent a path variable, which is relatively independent of confining stress level. Thus, the ratio of energy increments along two parallel stress paths, say a and b in Figure 6.3.a, with identical R history will be

$$\frac{\delta Q_a}{\delta Q_b} = \frac{\sigma'_{r_a}}{\sigma'_{r_b}} \cdot \frac{\delta\varepsilon_{a_a}}{\delta\varepsilon_{a_b}} \tag{6.2}$$

in which a and b refer to path label. As discussed above, the ratio of axial stress increments in parallel stress paths that have the same stress ratio history remains constant. Hence the energy increment ratio along such parallel stress paths would be proportional to the ratio of corresponding confining stresses.

In conventional triaxial paths, σ'_r is constant along the stress path. Therefore, under the assumed conditions of identical stress ratio history and parallel conventional triaxial paths; the energy density increment ratio between two stress paths would remain constant. Along other parallel stress paths, current ratios of confining stress at equal stress ratio states would remain unchanged and equal to the ratio of the initial consolidation stresses. This is because as the current R translates to R + δR along a stress path prescribed by $r = \frac{\delta\sigma'_a}{\delta\sigma'_r}$; a new confining stress of $(\sigma'_r + \delta\sigma'_r)$ is established. However, $R = \sigma'_a/\sigma'_r$ and $R + \delta R = \frac{\sigma'_a + \delta\sigma'_a}{\sigma'_r + \delta\sigma'_r}$; from which $\delta\sigma'_r$ can be expressed in terms of σ'_r, R, δR and r as

$$\delta\sigma'_r = \frac{\sigma'_r \delta R}{(r-(R+\delta R))} \tag{6.3}$$

and

$$\sigma'_r + \delta\sigma'_r = \sigma'_r \cdot \frac{(r-R)}{(r-(R+\delta R))} \tag{6.4}$$

Therefore, so long as r, R and δR between parallel paths are fixed, the ratio of the updated confining stesses will remain equal to the ratio of the consolidation confining stresses. Hence the incremental energy ratio for two parallel stress paths that have the same stress ratio history would also remain unchanged for stress paths other than the conventional triaxial test.

Stress ratio against input energy density at various levels of confining stresses are shown in Figures 6.4.a, b and c for conventional triaxial, constant p' and constant $\delta\sigma'_a/\delta\sigma'_r = 2$ parallel stress paths.

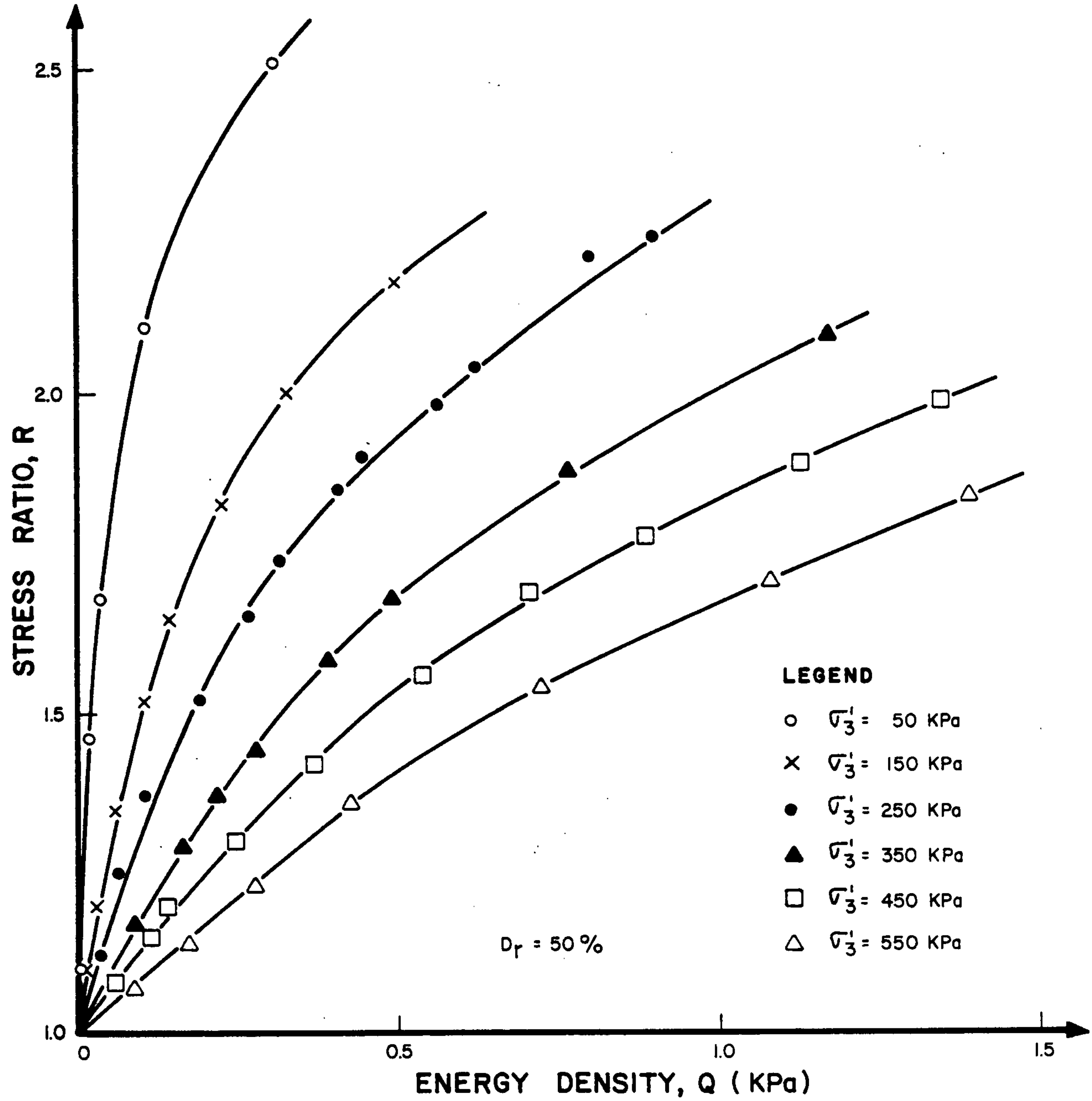

Fig. 6.4a Energy Density with Stress Ratio in Conventional Triaxial Paths

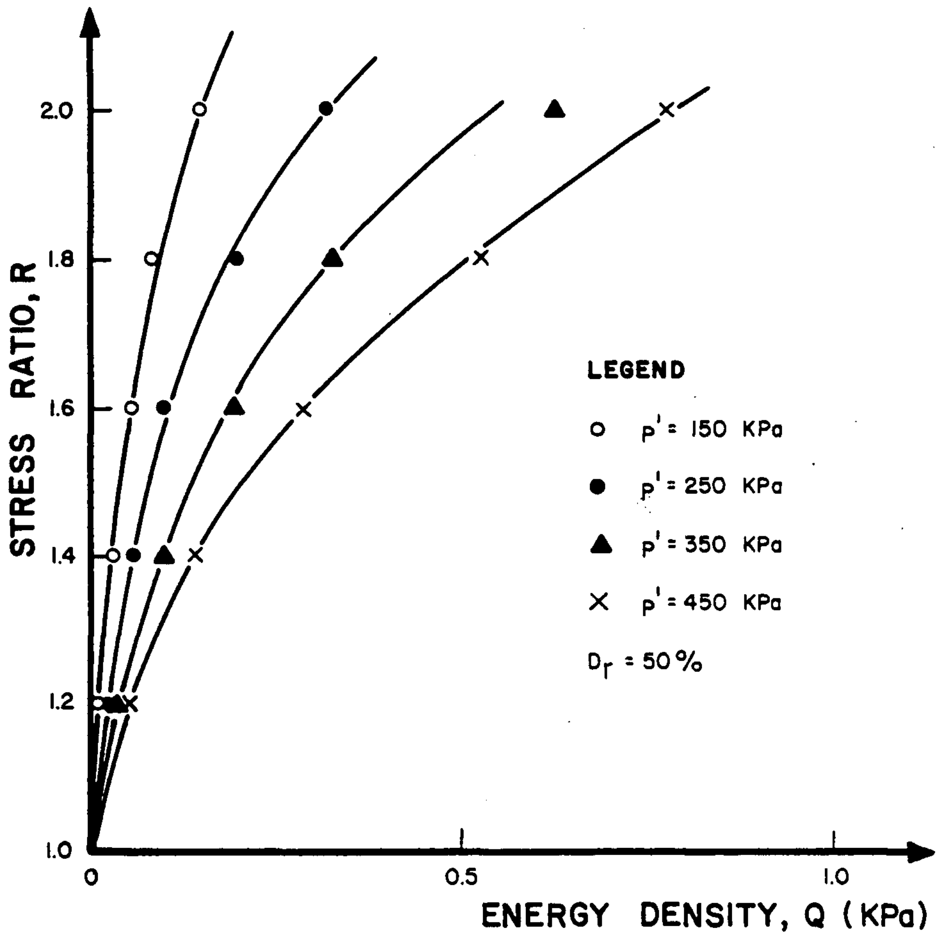

Fig. 6.4b Energy Density with Stress Ratio in Constant Mean Normal Stress Paths

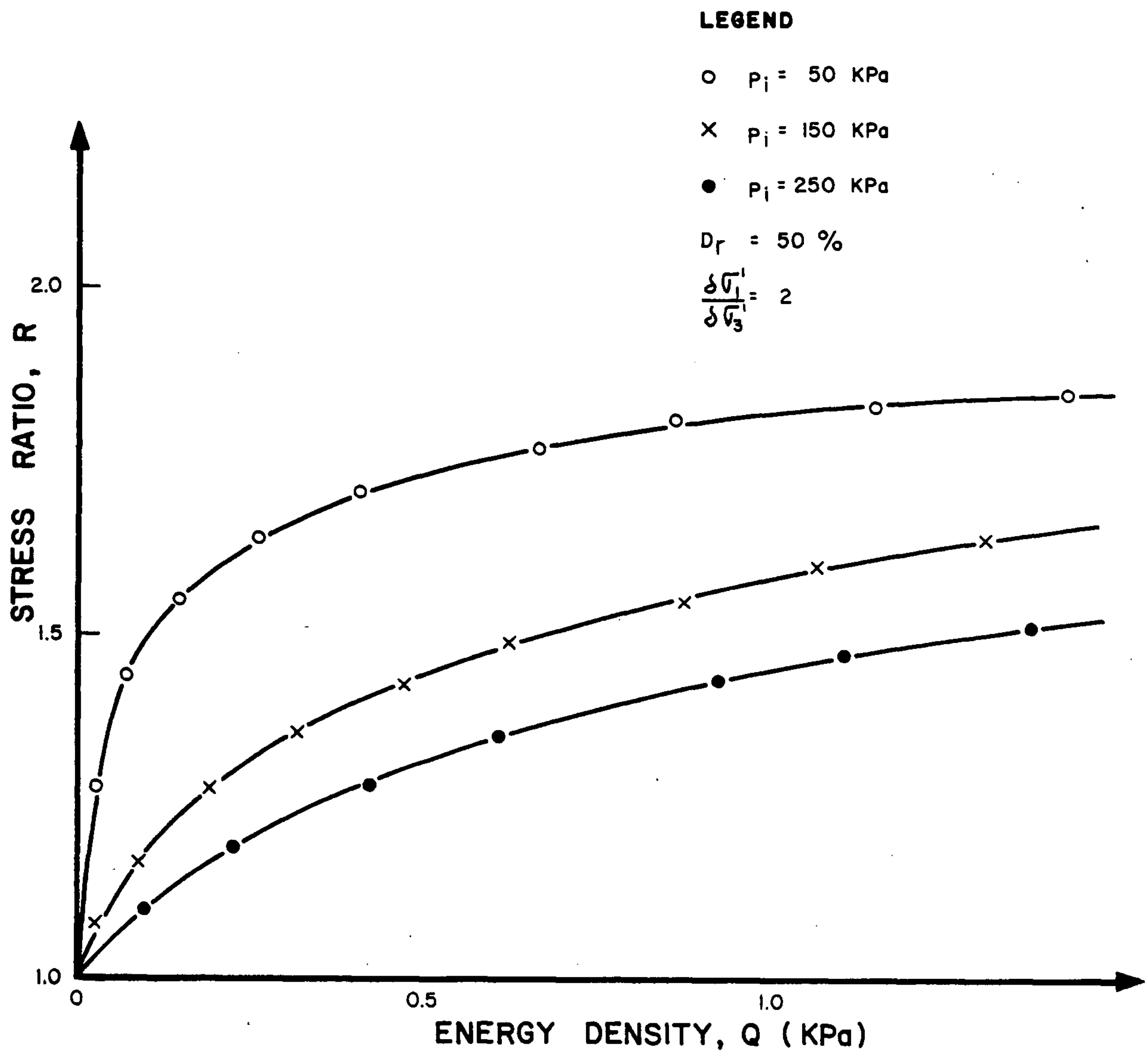

Fig.6.4c Energy Density with Stress Ratio in Constant Incremental Stress Ratio of 2 Stress Paths

Input energy density normalized by corresponding input energy density along paths initiating from a hydrostatic consolidation state of 150 kPa are plotted against stress ratio in Figures 6.5.a, b and c. It may be noted that for each stress path and confining stress, the associated energy ratios are relatively constant. This lends support to the above development which is based on the unique association of strain paths with stress direction. When these constant energy ratios in Figures 6.5.a, b, c associated with each confining pressure are plotted against a normalized value of confining pressure in log - log plot, Figure 6.6, the data points fall close to a straight line which suggests a power relationship that is independent of stress path. This result thus provides a more generalized basis for comparing the energy increment performance of parallel stress paths. A possible use for this observation is discussed in the following section.

6.1.1.4 Quantitative Relationships Between Parallel Paths

The results shown in Figure 6.6 represent a unique relationship between energy density and confining stress ratios along parallel stress paths. This relationship would be described by an expression of the form

$$\frac{\delta Q_a}{\delta Q_b} = \left[\frac{\sigma'_{3a}}{\sigma'_{3b}}\right]^d \qquad (6.5)$$

where a and b identify parallel stress paths that originate from consolidation states σ'_{3a} and σ'_{3b}; and d is the slope of the line shown

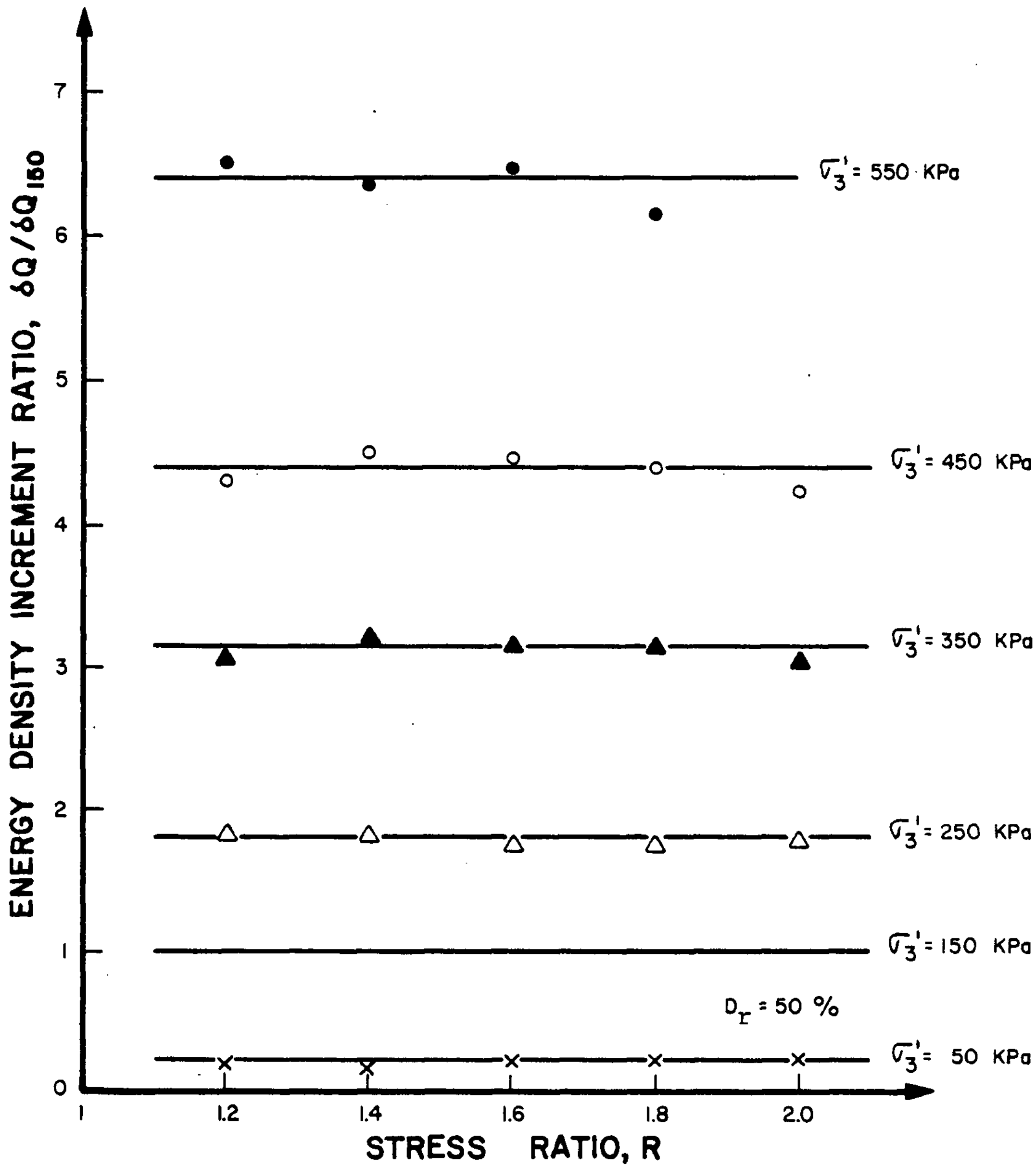

Fig. 6.5a Normalized Energy Density with Stress Ratio for Conventional Triaxial Stress Paths

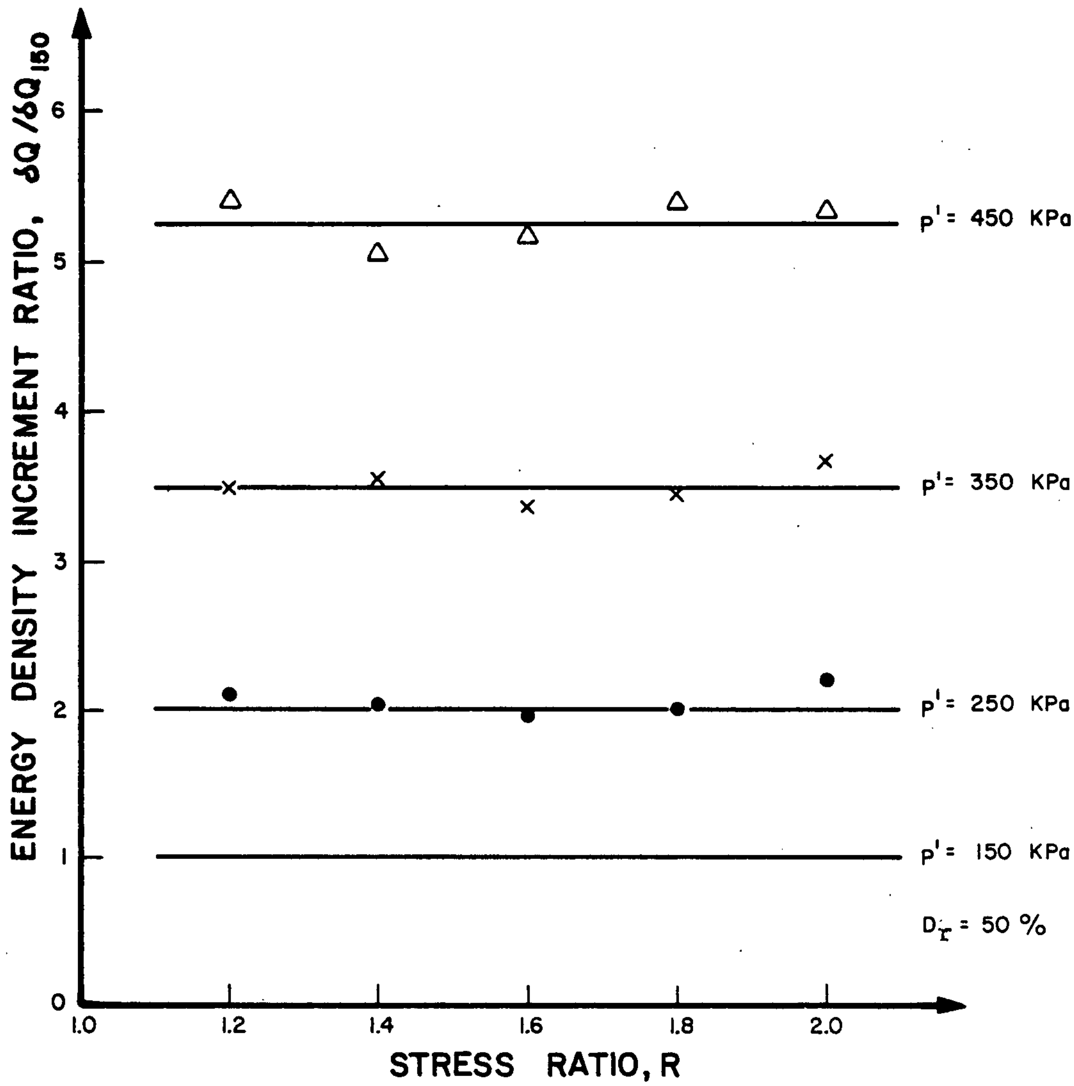

Fig. 6.5b Normalized Energy Density with Stress Ratio for Constant Mean Normal Stress Paths

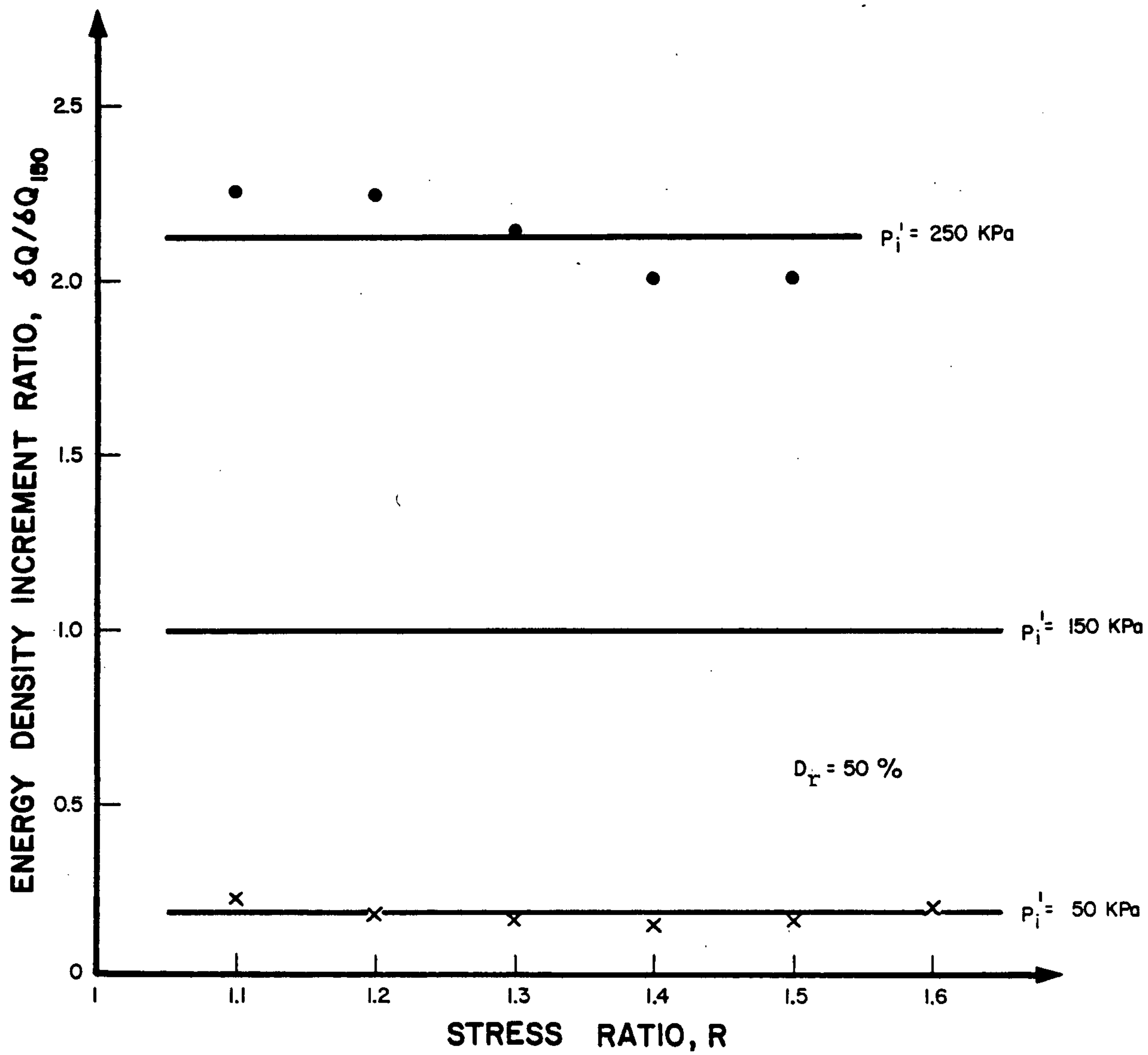

Fig. 6.5c Normalized Energy Density with Stress Ratio for Constant Incremental Stress Ratio of 2 Stress Paths

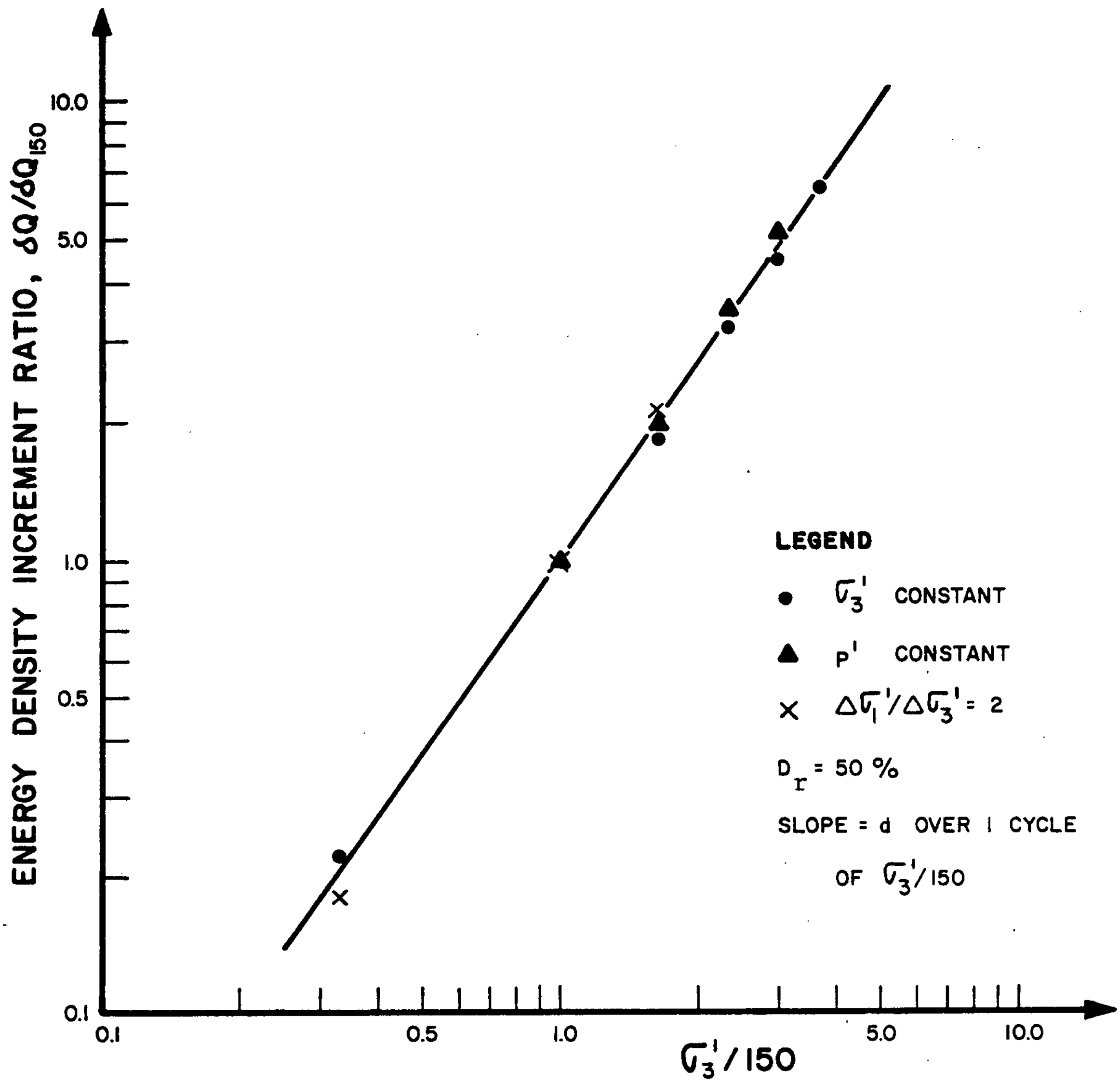

Fig. 6.6 Average Normalized Energy Density with Confining Stress Ratio for All Stress Paths

in Figure 6.6. Using Equations 6.2 and 6.5, corresponding axial strain increment ratios along parallel paths can be expressed as

$$\frac{\delta\varepsilon_{aa}}{\delta\varepsilon_{ab}} = \left[\frac{\sigma'_{3a}}{\sigma'_{3b}}\right]^{d-1} \quad (6.6)$$

which implies that the constant d can be estimated from axial strain and confining stress ratios without having to evaluate actual energy density increments.

Simple stress-strain relationships that are usually used in incremental elastic approximations were examined in Chapter 4. These methods also constitute procedures for relating conventional triaxial results at various confining stress levels and hence involve relationships between parallel stress paths. However, the use of large strain results to describe small strain response was shown to be incorrect. These additional small strain observations in Figure 6.6 for parallel paths are now utilized to seek further improvements to current procedures of incremental elastic representations of soil behaviour.

Considering conventional triaxial test results, in which $\sigma'_r = \sigma'_3$ and constant, axial strain increments would be expressed as

$$\delta\varepsilon_a = \frac{1}{E_t}\,\delta\sigma'_a \quad (6.7)$$

where E_t is tangent modulus at (σ'_3, R or σ_d) and

$$\delta\sigma'_a = \delta R \cdot \sigma'_3 \tag{6.8}$$

Therefore

$$\delta\varepsilon_a = \frac{1}{E_t} \cdot \delta R \cdot \sigma'_3 \tag{6.9}$$

Substituting Equation 6.9 into Equation 6.6; the following relationship is obtained

$$\left[\frac{\sigma'_{3a}}{\sigma'_{3b}}\right]^{d-1} = \frac{\sigma'_{3a}}{E_{ta}} \cdot \frac{E_{tb}}{\sigma'_{3b}} \cdot \frac{\delta R_a}{\delta R_b} \tag{6.10}$$

Considering the same stress ratio history in both paths a and b; (i.e. $\delta R_a = \delta R_b$) E_{tb} would be expressed as

$$E_{tb} = \left[\frac{\sigma'_{3b}}{\sigma'_{3a}}\right]^{2-d} \cdot E_{ta} \tag{6.11}$$

If experimental data was available along any stress path, then it would be possible to represent E_t using parameters derived from a small strain transformed hyperbolic plot as in Figure 4.2.b. From the available data, E_i and the slope m for the small strain, 1×10^{-4} to 1×10^{-2}, range can be determined and E_t at any σ_d would be expressed by

$$E_t = E_i\,(1 - m.\sigma_d)^2 \tag{6.12}$$

or

$$E_t = E_i\,(1 - m\sigma_3'.\ (R-1))^2$$

Thus, for a given test "a", at confining stress σ_{3a}' ; tangent moduli E_{ta} in small strain range would be specified by

$$E_{ta} = E_{ia}\,(1 - m_a\sigma_{3a}'.(R-1))^2 \tag{6.13}$$

On substituting the above relationship in Equation (6.11); the following relationship relating tangent modulus between two paths a and b would be obtained

$$E_{tb} = \left[\frac{\sigma_{3b}'}{\sigma_{3a}'}\right]^{2-d} .\ E_{ia}\ .\ (1-m_a\sigma_{3a}'\ (R-1))^2 \tag{6.14}$$

In this expression, a desired tangent modulus, E_{tb}, at a stress state (σ_{3b}' , R) is determined from a known tangent modulus at a stress state (σ_{3a}' , R).

The expression for tangent modulus given by Equation (6.14), bears some resemblence to the following very popular relationship reported by Duncan and Chang (1970) and Byrne and Eldridge (1982).

$$E_t = \left[\frac{\sigma_3'}{P_a}\right]^n \cdot K_E \cdot P_a \cdot \left(1 - \frac{R_f(1-\sin\phi)(\sigma_1'-\sigma_3')}{2\sigma_3' \sin\phi}\right)^2 \tag{6.15}$$

where;

P_a = atmospheric pressure

(σ_1', σ_3') = current stress state

ϕ = is the failure friction angle corresponding to σ_3'

K_E = the modulus number which represents an E_i for a confining stress equal to atmospheric pressure and divided by P_a

n = the modulus exponent

K_E and n represent the intercept and slope of a log-log linear fit between E_i/P_a and σ_3'/P_a, implying

$$E_i = \left[\frac{\sigma_3'}{P_a}\right]^n \cdot E_{iPa} \tag{6.16}$$

Since $K_E = \frac{E_{iPa}}{P_a}$, Equation (6.16) can also be written as

$$E_i = \left[\frac{\sigma_3'}{P_a}\right]^n \cdot K_E \cdot P_a \tag{6.17}$$

which is identical to the relationship originally suggested by Janbu (1963) from review of experimental results.

According to Equation 6.16, the initial modulus E_i for an arbitrary confining pressure σ'_3 is determined from a reference initial modulus, E_{iPa} at a confining stress equal to atmospheric pressure. This statement is equivalent to Equation 6.11 provided the reference confining stress σ'_{3a} is made equal to atmospheric pressure and n = 2-d. A value of d = 1.43 may be determined from Figure 6.6 and thus n = 0.57. Such a value for n is very close to the mid range of reported n values for sand (Duncan et al, 1980). Hence, the expressions for initial tangent moduli given by Equaiton 6.14 and Equation 6.15, when R = 1, (i.e. loading from an initial hydrostatic stress-state) are of the same form. However, E_i from Equation 6.14 is based on small strain results and with reference to a confining stress at which actual tests were performed. Whereas, E_i that would be given by Equation 6.15 is based on large strain results and is referenced to a confining stress, P_a, which usually corresponds neither to the data base nor the pressures for which predictions are to be made. In both cases, however, a functional relationship between initial modulus, E_i, and confining stress is implied to exist. A useful further development now would be to relate the second hyperbolic parameter, m, to confining stress but without resorting to failure conditions and large strain response.

The squared term in Equation 6.14 contains the stress ratio, R, at which E_{tb} is desired. It also contains the slope m_a in transformed hyperbolic plot and confining stress σ'_{3a} at which the material behaviour has been established experimentally. In this alternative form, m_a represents the best possible fit of data within the small strain range of interest. To facilitate comparison with 6.14, the squared term in Equation 6.15 can be rewritten in the following form.

$$\left(1 - \frac{R_f(1-\sin\phi)(\sigma_1'-\sigma_3')}{2\sigma_3' \sin\phi}\right)^2 = \left(1 - \frac{\sigma_1' - \sigma_3'}{(\sigma_1'-\sigma_3')_{ult}}\right)^2 \tag{6.18}$$

and

$$\left(1 - \frac{\sigma_1'-\sigma_3'}{(\sigma_1'-\sigma_3')_{ult}}\right)^2 = \left(1 - m\ \sigma'_3(R-1)\right)^2 \tag{6.19}$$

in which $(\sigma_1-\sigma_3)_{ult}$ = ultimate asymtotic value of $\sigma_1-\sigma_3$ and m = slope of transformed hyperbolic plot based on large strain data. Thus as was the case for Equation 6.14, the squared term in Equation 6.15 contains the stress ratio, R, at which a tangent modulus is desired. However, a current confining stress, σ_3', is used in Equation 6.15 instead of a reference confining stress σ_{3a}'. The slope m in Equation 6.14, corresponds to results at the reference confining stress σ_{3a}' and would remain unchanged. Whereas, the slope m for Equation 6.15 would correspond to the current confining stress σ_3' and would thus vary with the level of σ_3'. In the presently adopted procedures m is made to vary by adjusting ϕ with reference to current σ_3', as in the case of Equation 6.15. The advantage of using a fixed reference slope and confining stress within the square brackets of Equation 6.21 is that the product of confining stress and slope m remain constant. This is in the same sense of decreasing m with increasing confining pressure as would be implied by current procedure.

The relationships that have so far been determined from experimental observations can be used to express small strain response. Given d, which would be determined from two tests, 'a and b', and also E_{ia} and m_a from a transformed hyperbolic plot for test data 'a' at a confining stress σ'_{3a}; tangent moduli E_{tb} can be determined. The stress state in test b at which E_{tb} is evaluated would be specified by σ'_{3a} and R. Equation 6.14 was used to predict the deviator stress axial srain response shown in Figure 6.7. E_{ia} for σ'_3 = 150 KPa and d = 1.43, (Figure 6.6), were used to make predictions of axial strain response under σ'_{3b} of 50 KPa and 350 KPa. Actual stress-strain response for these stress paths is shown in Figure 6.7 by data points. The observed agreement with prediction is very satisfactory and incorporation of this further refinement in current hyperbolic stress-strain models may prove very useful. This is particularly important because the development proposed does not make use of failure or near failure parameters for describing the deformation response of sand at small strain. Conceptually, there is no basis for linkage of small deformation response and failure conditions in any material. As the stress ratio regime increases, and on approaching failure states use of alternative parameters within this or previous procedure would lead to an improved predictive capability. Thus, as indicated previously, a dual hyperbolic representation of stress strain response has been made possible.

The use of failure parameters for describing dynamic behaviour has also not been found satisfactory. Consequently, modified hyperbolic and reference strain concepts were introduced to enable more realistic

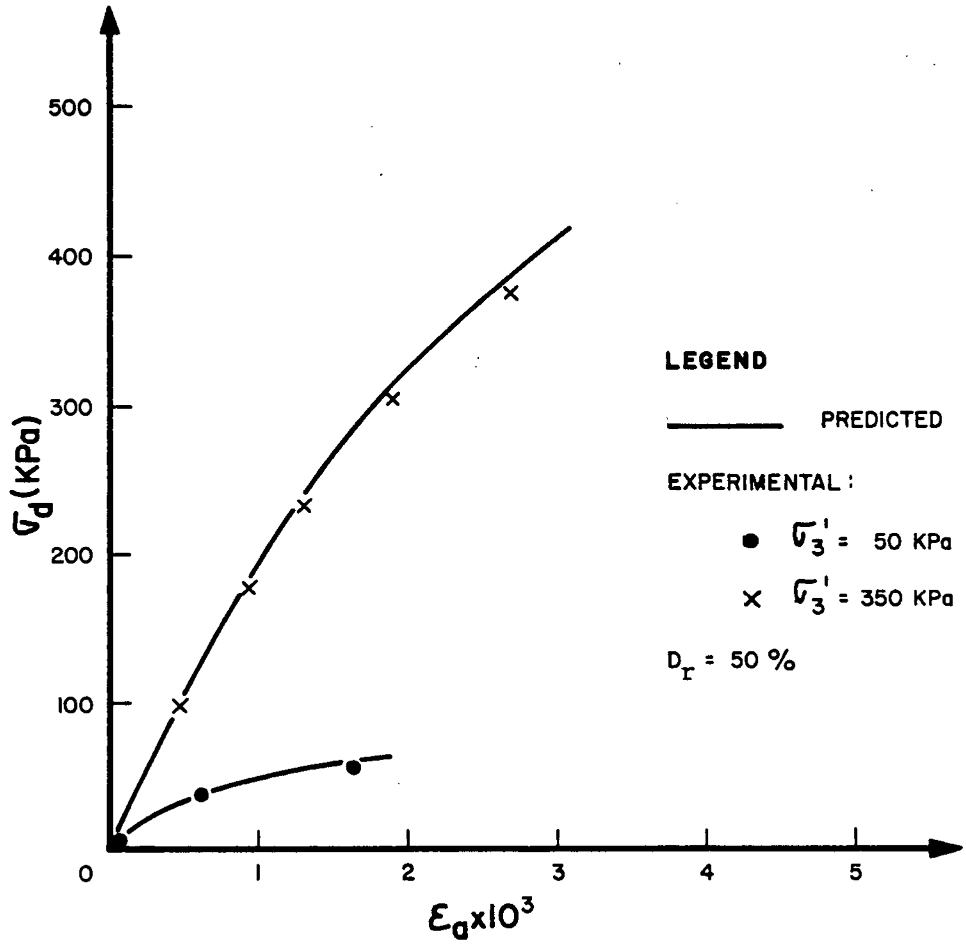

Fig. 6.7 Comparison of Experiment and Prediction in Conventional Triaxial Paths

representation (Hardin and Drenevich, 1972). Separate consideration of small strain response from dynamic tests along lines of development similar to that considered herein would appear to lead to simpler procedures for characterization of dynamic parameters using either stress or strain criteria.

6.1.2 Quantitative Relationships Between Stress and Strain Directions

At small strain, parallel non proportional loading paths have been shown to maintain the same strain direction, Figure 6.1.a,b,c,d. For such paths, actual strain increments have also been interrelated in terms of confining stress and input energy density. Prescription of strain directions in terms of stress directions would be a further development.

For proportional loading, Chapter 5, stress ratio and strain increment direction were associated by the linear relationship shown in Figure 5.2. Furthermore, proportional and corresponding constant incremental stress ratio paths have been found to maintain a common strain direction, Figure 6.1.d. Hence by expressing stress directions in a more general incremental form, it is possible to relate common strain directions to both proportional and nonproportional loading stress paths. Such relationships at a fixed relative density of 50 percent are shown in Figure 6.8.a. Expressions for stress and strain axes in Figure 6.8.a are similar to those used in studies of proportional loading of metals by Rees (1981), except that incremental rather than total stress ratios are utilized and parameters have been adopted to suit triaxial test data. In Figure 6.8.a, the applied

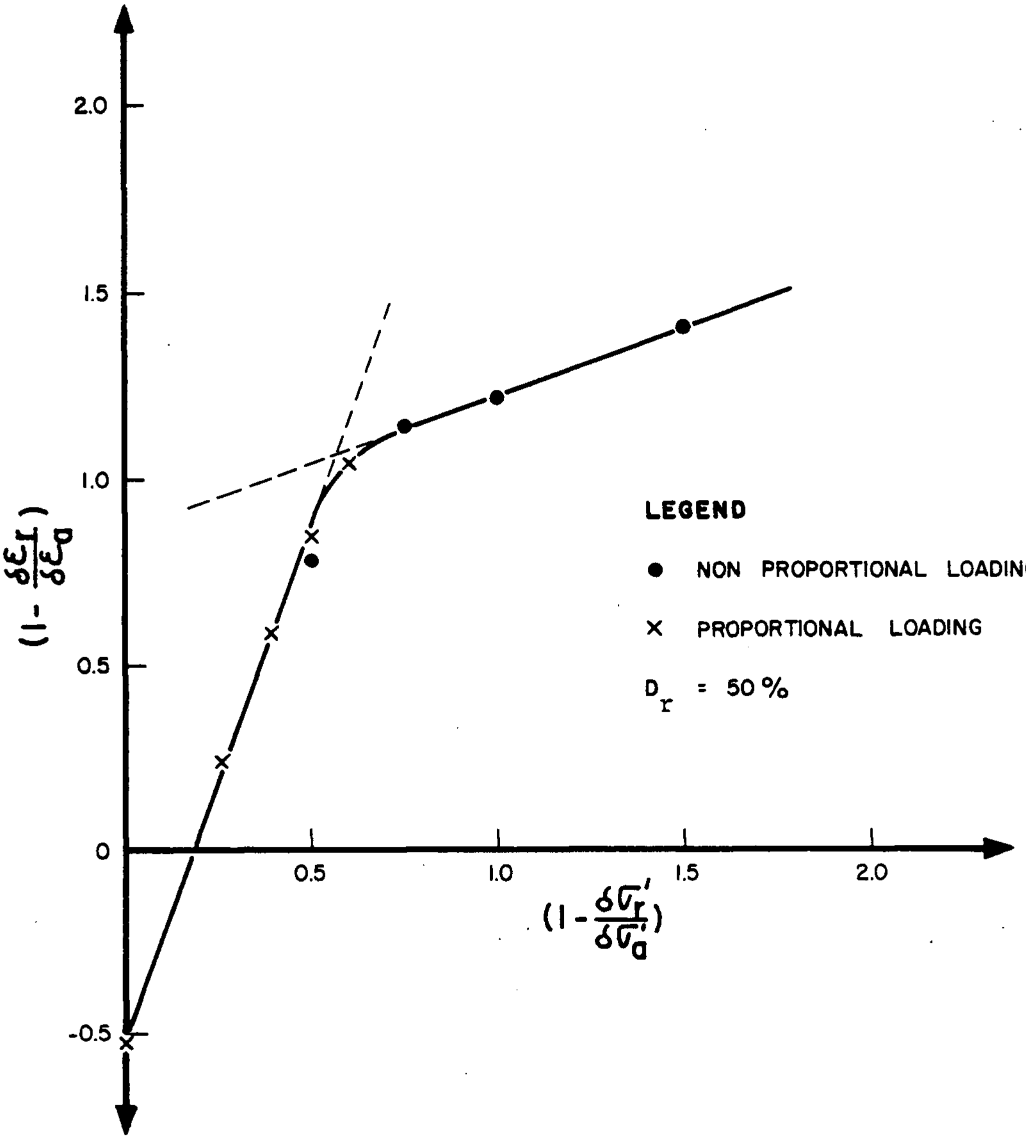

Fig. 6.8a Incremental Stress and Strain Ratio Relationships at 50% Relative Density

conditions of hydrostatic loading, $\delta\sigma'_a/\delta\sigma'_r = 1$, correspond to a horizontal axis stress function value of zero whereas the vertical strain function response is negative. This negative ordinate is a correct reflection of the recognized sense of inherent anisotropy in a pluviated medium dense sand. It may be noted that the results shown in Figure 6.8.a fall along two intersecting lines with a transitional gently curved segment within the intersection. Incrementally proportional loading test results on loose sand, Figure 6.8.b, also show behaviour similar to that observed for medium dense sand. The influence of density is reflected by the different orientations of the intersecting lines, as well as different magnitude of zero intercept.

Key concepts and trends based on results in Figure 6.8.a and b are shown in Figure 6.9. For a given relative density, all stress increments corresponding to contraction in both axial and radial strain fall on the steeper state line A and below a strain function value of about one, which corresponds to a K_o or equivalent K_o path. Strain paths belonging to lower strain function values would be contained within the first quadrant of strain space, (both $\delta\varepsilon_a$, $\delta\varepsilon_r$; positive), and the correspondence between stress and strain directions would remain fixed. Stress paths that are oriented steeper than a K_o stress direction have also been shown to be associated with a unique strain direction within a sizeable initial stress ratio range, Section 6.1.1.1. For such paths, until a threshold stress ratio, whose magnitude varies mainly with relative density, is mobilized; stress and strain path relationships would be described by state line B. The relatively smooth transition between lines A and B appears larger for loose as opposed to dense sand. As stated previously, because loose

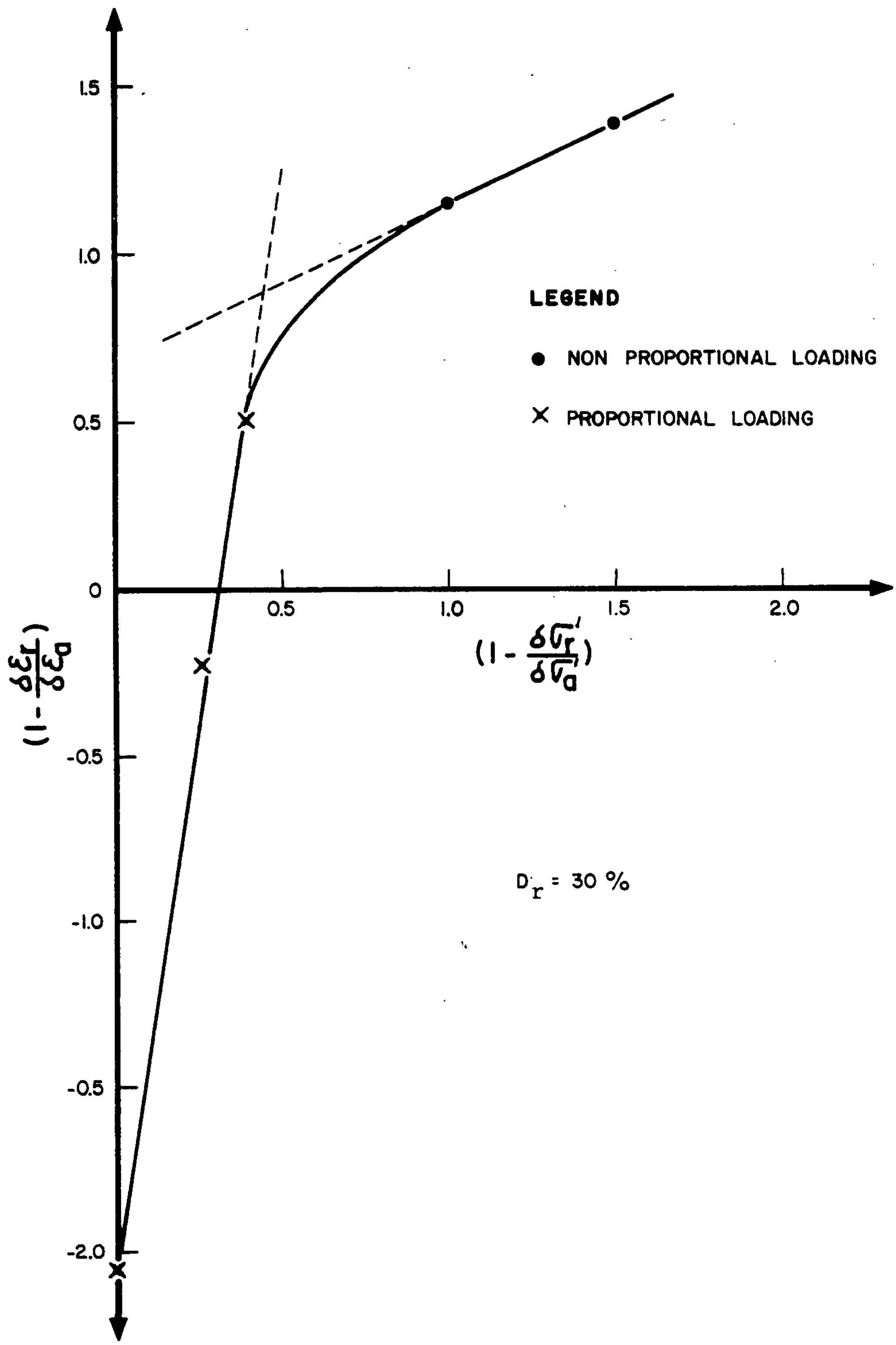

Fig. 6.8b Incremental Stress and Strain Ratio Relationship at 30% Relative Density

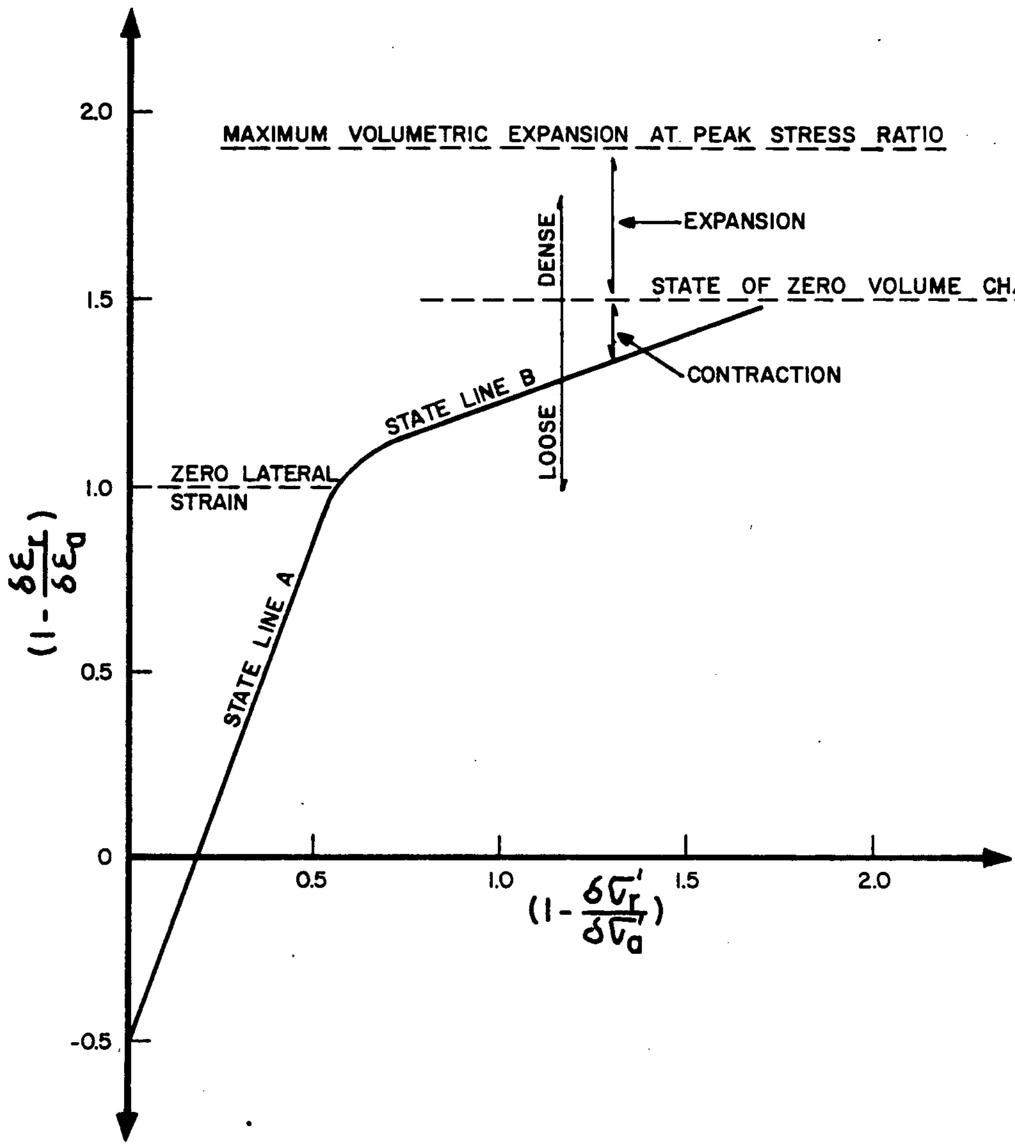

Fig. 6.9 Trends and Features in Incremental Strain and Stress Ratio Relationships

sands deform in smaller clusters; local slip, lack of fit and collapse would be more likely and would occur over a wider range of stress ratios than in dense sand. As the threshold stress ratio is exceeded along the failure paths, strain directions begin to change even though the stress direction is still fixed. Thus the strain function would begin to increase with the stress function remaining constant. At this time, the association of stress state and strain increment ratio in the form of stress dilatancy becomes more relevant as the incremental strain rate progresses to zero, maximum and back to zero rate of volume change. For a given relative density, lines A and B therefore describe an association of stress and strain directions. These state lines would shift lower and to the right with decreasing relative density, (see Figures 6.8.a and 6.8.b). A dense specimen would tend to be isotropic under hydrostatic loading and its state line A would pass through the origin. As discussed previously and comparing Figures 6.8.a and b, inherent anisotropy as reflected by relative density predominates consolidation strain paths. The slope of A and its intercept are functions of D_r; whereas initial strain paths of failure stress paths, state line B, is relatively unaffected by relative density. The orientation of state lines is a function of relative density and perhaps other material and fabric parameters. Until further establishment of basic relationships, at least three tests would be required to determine two points on each of lines A and B at a given relative density.

Association of strain and stress directions is by no means an end. Actual strain increments corresponding to stress increments along the path have to be extracted. To some extent this would be possible using the relationship shown in Figure 6.6, but only so long as strain response in a parallel path is known. Future studies of behaviour across stress paths might enable a more general representation. However, since inherent anisotropy of sand has an important influence on small strain response, rotation of principal axes of stress and strain may have a major impact. Hence, further study of factors not examined herein and assembly of more experimental data in follow up studies of small strain phenomena using torsional hollow cylinder equipment would be more beneficial to the development of comprehensive relationships between stress and strain.

6.2 Other Non Proportional Paths

Considerations were so far restricted to conditions of total loading. A decrease in any of p', q, and η (=q/p') did not occur. The paths so far considered have been labelled as total loading paths. In other stress paths, where one or more of these stress components decrease, the prescription of loading or unloading becomes ambiguous. Out of keeping with this general classification, the small strain behaviour of sand in two other nonproportional paths is examined in this section. In the first part, experimental results under conditions of constant shear, q, are examined. The second part focuses on experimental observations for conditions of stress reversal under constant mean normal stress, p'.

6.2.1 Constant Shear Stress Paths

Stress paths in which a constant shear stress was maintained are associated with an increasing mean normal stress and decreasing stress ratio or a decreasing mean normal stress and increasing stress ratio.

Hence both loading and unloading occur simultaneously and the stress increments constitute an increase or decrease only in mean normal stress. Hydrostatic loading paths are unique in that both q and η remain constant at all times.

When the mean normal stress was increased at constant shear in both compression and extension, and thus decreasing stress ratio, very little change in shear strain was detected. In volumetric and shear strain space, the strain paths for such tests are seen to be linear and nearly vertical (Figures 6.10.a and b).

Also, when mean normal stresses were reduced at constant shear and thus increasing stress ratio, no change in shear strain was observed initially as evidenced by an essentially vertical strain path (Figures 6.11.a and b) and until a limiting stress ratio was approached. The magnitude of volume swelling that occured without shear strain was more for low shear stress levels, Figure 6.11.a. However, the limiting stress ratio at which changeover from a near vertical strain path was initiated was about 1.9 for compression and 1.6 for extension. With further increases in stress ratio, but still at constant shear stress, on the compression side; the initial swelling continues in volume expansion with increasing shear strain, Figure 6.11.b. Whereas in extension mode, the initial swelling is arrested and is followed by volumetric contraction with shear strain. This phenomena is shown in an expanded scale in Figure 6.12 wherein volume contraction and shear strain in extension mode may be noted to precede volume expansion with shear strain or dilation.

The experimental results presented in Figures 6.10, 11 and 12 show that the sense of increasing or decreasing stress ratio along constant

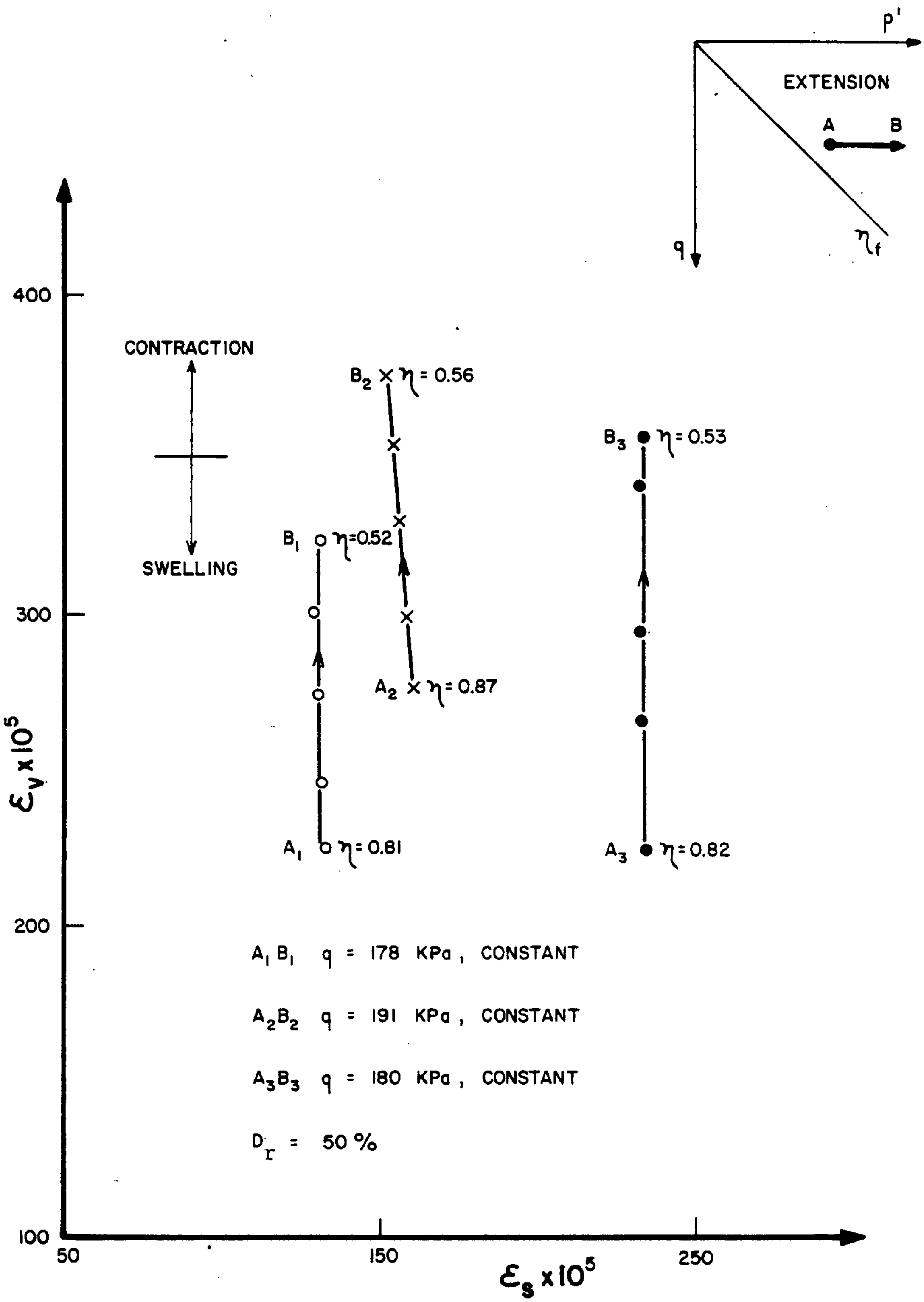

Fig. 6.10a Shear and Volumetric Strain States in a Constant Shear Stress Path for Decreasing Stress Ratio and Increasing Mean Normal Stress Conditions in Extension Mode

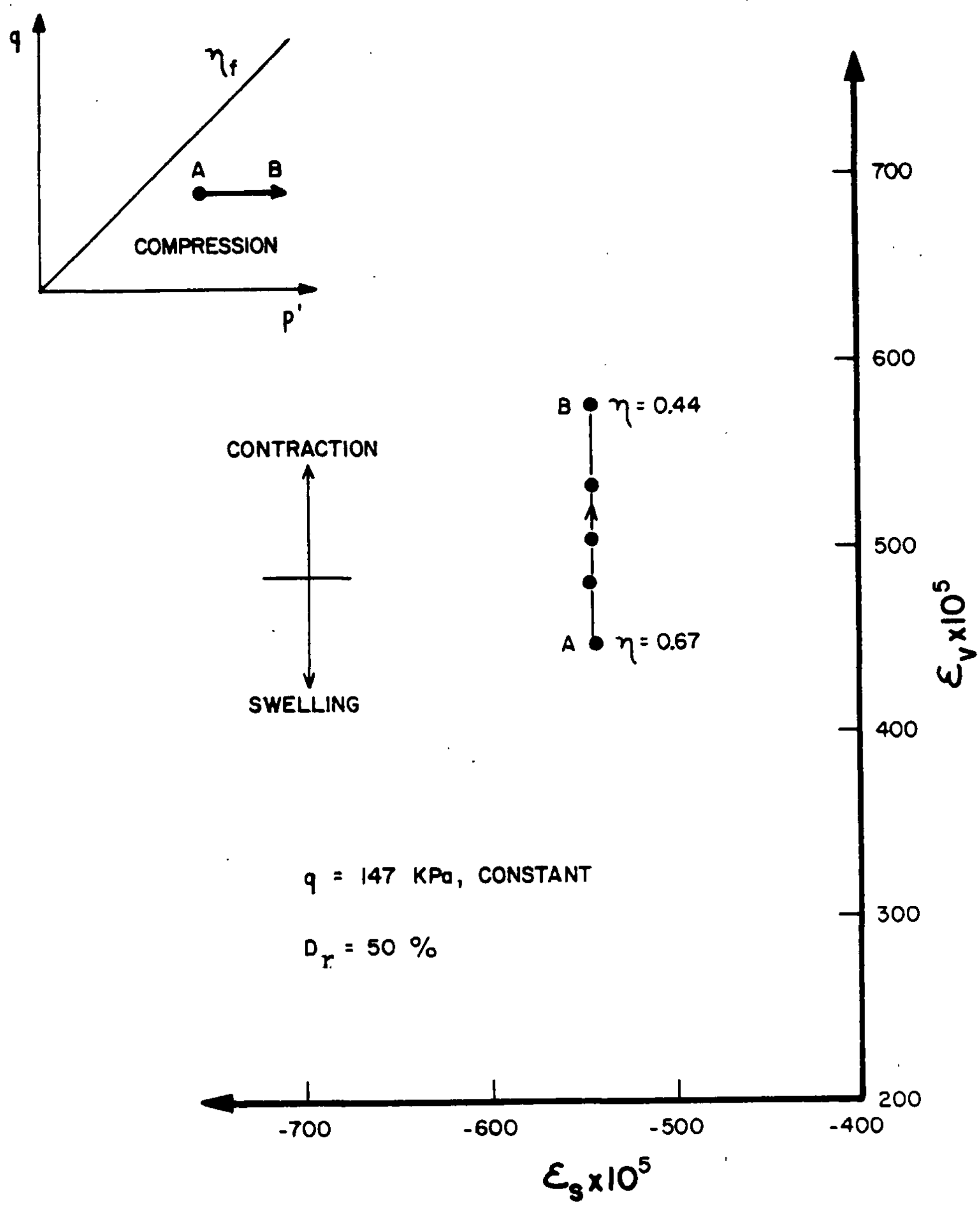

Fig. 6.10b Shear and Volumetric Strain States in Constant Shear Stress Path with Decreasing Stress Ratio and Increasing Mean Normal Stress in Compression Mode

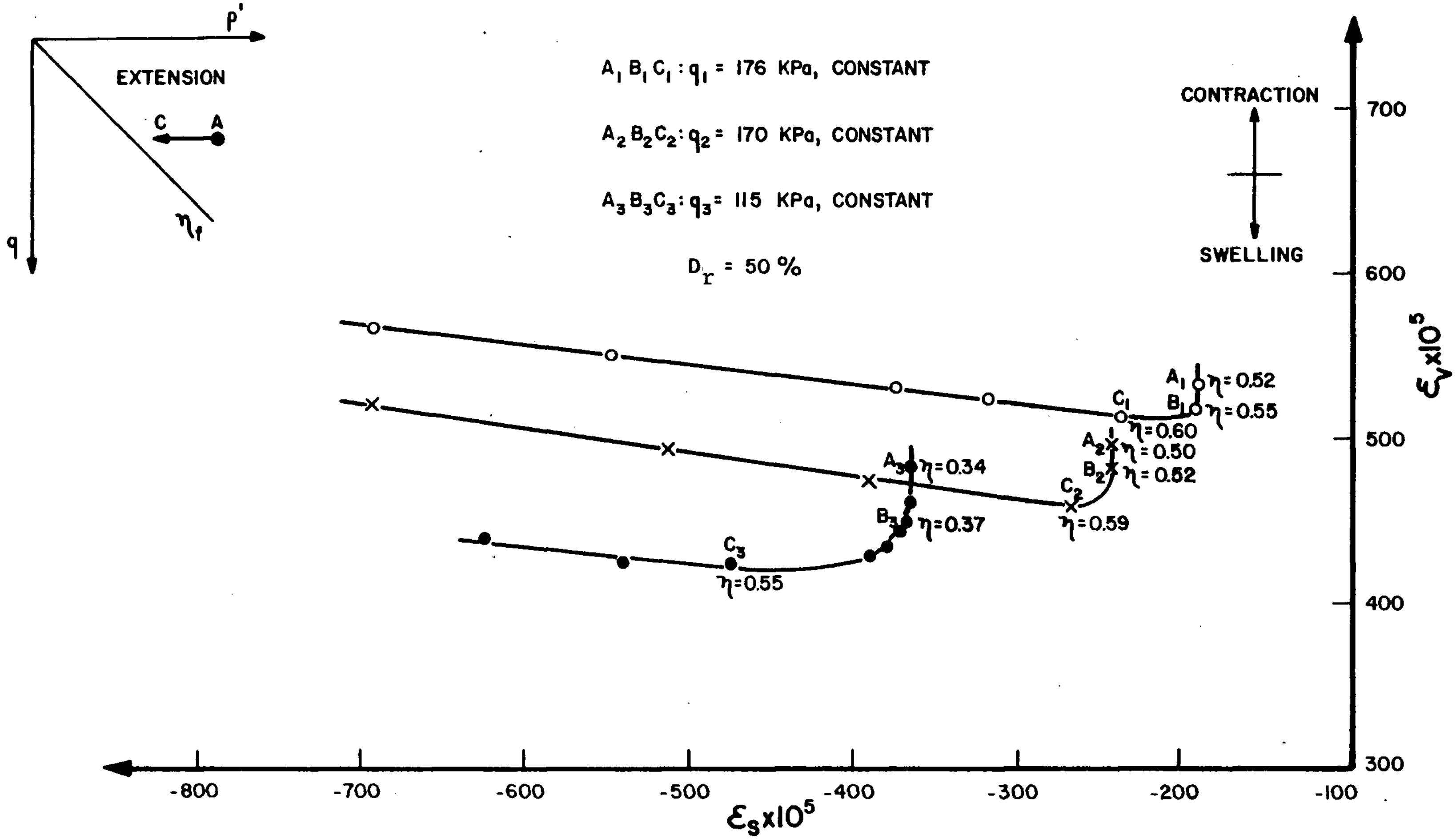

Fig. 6.11a Shear and Volumetric Strain States in Constant Shear Stress Paths with Increasing Stress Ratio and Decreasing Mean Normal Stress in Extension Mode

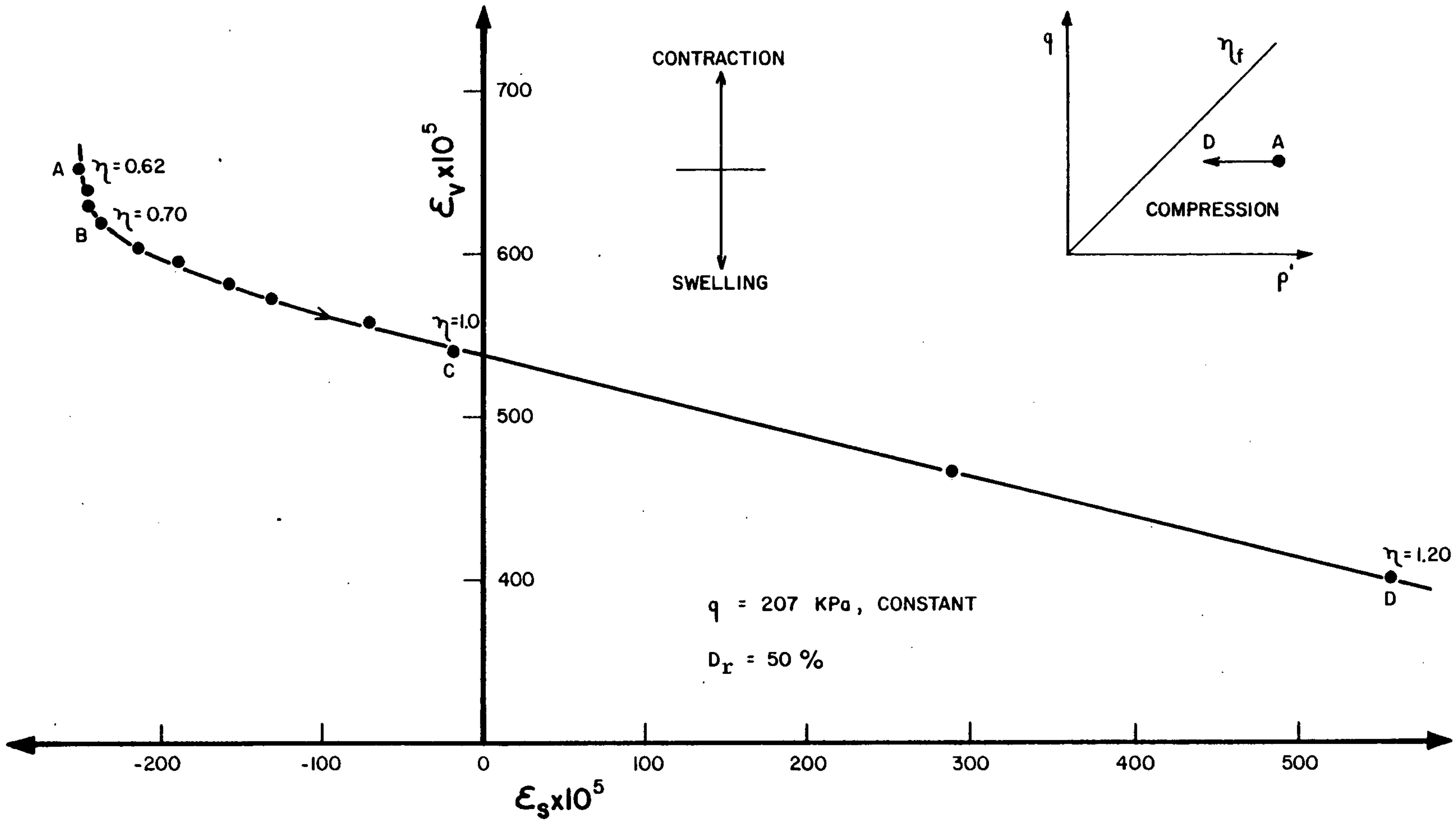

Fig. 6.11b Shear and Volumetric Strain States in Constant Shear Stress Paths with Increasing Stress Ratio and Decreasing Mean Normal Stress in Compression Mode

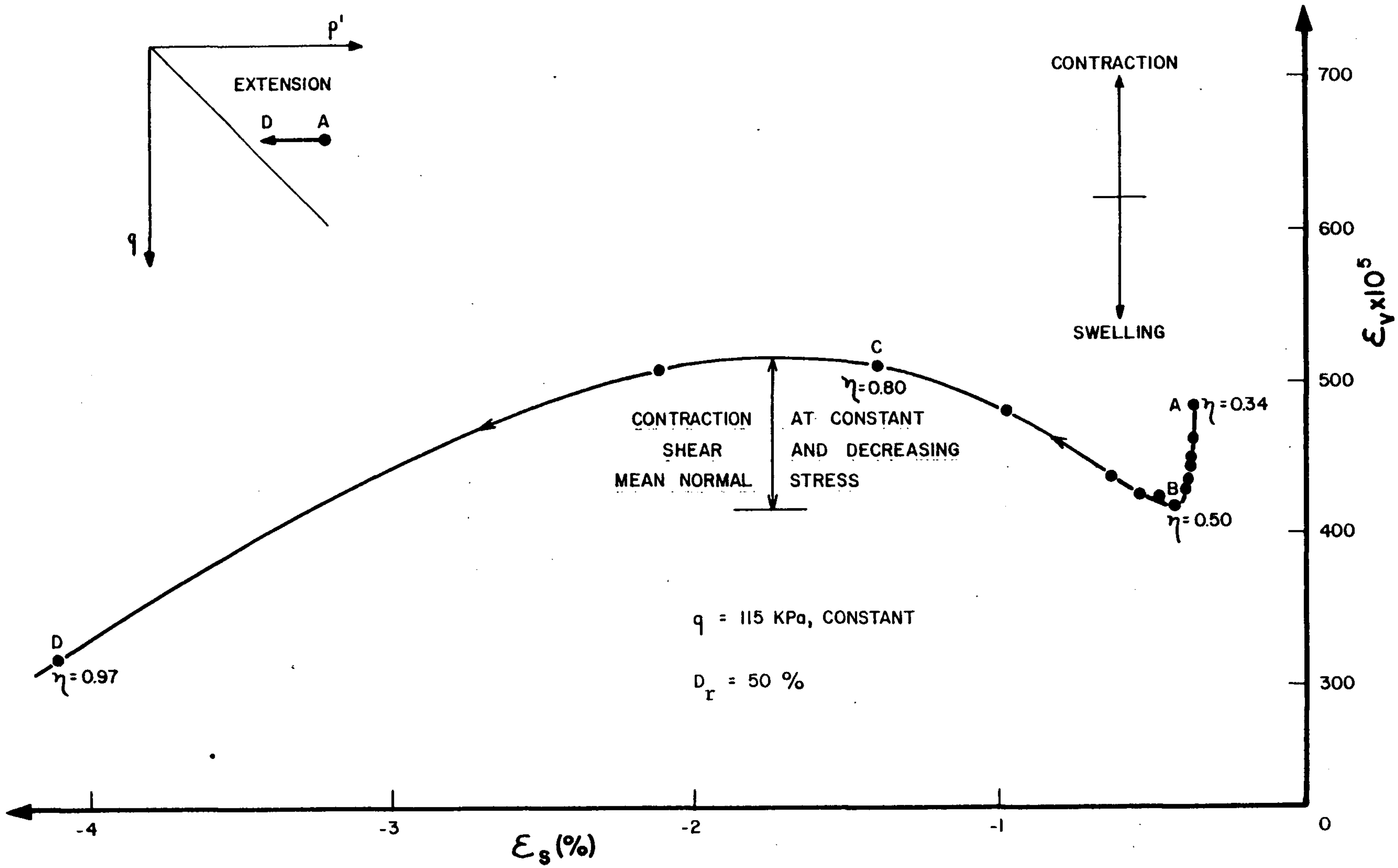

Fig. 6.12 Volume Contraction in a Constant Shear Stress Path Under Increasing Stress Ratio and Decreasing Mean Normal Stress in Extension Mode

shear stress paths does not encourage shear strain development so long as η or R is maintained below a limiting value, appropriate for the density and sense of loading. Inspection of proportional loading test results, Chapter 5, however, shows development of shear strain with increasing shear and at constant stress ratio states. This again implies that shear stress and not stress ratio is instrumental for the development of shear strain when stress states are below a limiting stress ratio. At the same time, fixed strain path orientations are associated with proportional loading paths and with nonproportional loading paths at low levels of stress ratio. Whereas, at constant shear and nonproportional paths that ultimately lead to failure, non linearity and changes in strain path direction develop when limiting stress ratio are exceeded. Hence inherent anisotropy is preserved independent of shear stress state, when stress ratio is held constant or contained to small values. The development of stress induced anisotropy in sand is therefore primarily dependent on stress ratio and not shear stress level.

The tendency for contraction that was observed in the extension mode, Figure 6.12, would contribute to positive pore pressure and reduced strength in an undrained condition. Even though conventional triaxial compression is associated with an increase in mean normal stress whereas conventional triaxial extension involves a decrease; the net volume change at peak strength was invariably found to reflect more volume expansion on the compression side (Green 1969). This somewhat paradoxical phenomena would appear to be due to the intermediate contraction that was observed, Figure 6.12, while in extension. Under undrained conditions, this tendency for contraction and related positive pore pressure lead to a reduced strength in extension as opposed to compression mode, as shown by the experimental results of Chern (1984) and Cheung (1984). Even more, it would imply a reduced potential for contractant volume change with only compression side stress histories as opposed to those involving stress reversal.

Sand formed by pluviation possesses inherent anisotropy because the major principal axes of grain orientation tend to be inclined disproportionately toward the horizontal. In considering conventional triaxial paths, predominant slip would occur at contact planes oriented at $45 + \frac{\phi}{2}$ to horizontal in compression and $45 - \frac{\phi}{2}$ in extension. Therefore, because of the sense of inherent anisotropy and orientation of slip planes, extensional shearing would encourage more closer packing and thus contraction. Such a difference between extension and compression modes is a reflection of inherent limitations of the triaxial test rather than fundamental stress-strain behaviour of sand in that predominant slip planes in the two modes of shearing are entirely separate. However, when rotation of principal axes is permitted and predominant slip planes remain the same for both senses of shearing, such as would be in simple shear tests, separate types of volumetric strain response would not develop. The symmetry of undrained simple shear response as opposed to the nonsymmetry of undrained triaxal results is a clear indicaton of this phenomenon. The conventional triaxial test therefore seems to be less than desirable for the study of cyclic behaviour of sand and such limitations should perhaps be considered in evaluation of test results.

6.2.2 Constant p' Paths

From a review of the test data in constant p' loading paths in compression, corresponding strain paths were observed to be relatively independent of p' and remained linear up to a stress ratio of about 2, Figure 6.3.b. Results of compression side shear unloading at constant p' as well as stress reversal and continued shearing in extension are shown in Figure 6.13. It may be noted that the strain paths follow the same direction both in compression shear unloading and extension shear loading. Similarly unloading from an extensional state and extending into the compression mode at constant p' gives rise to strain paths with essentially the same direction (Figure 6.13). Shear stress and not stress ratio was observed to be mainly responsible for development of shear strain at low values of stress ratio. However, for comparable changes in shear stress, a larger magnitude of shear strain accumulated in extensional as opposed to compressional mode, Figure 6.13.a and b. In both compression and extension modes, the magnitudes of recovered strains were much less than the respective loading counterparts. The rate of volume change with shear strain was greater in compressional unloading and extension loading, (steeper strain paths), as compared to extension unloading and compression loading. The sense of shear strain increment changes in concert with the sense of shear stress increment. However, the sense of volumetric strain increment due to shearing remains contractant whether or not the shear stress is being applied or retracted. Shear volume change only accumulates and does not decrease for both loading and unloading senses of shear stress.

Although strain increment ratios and thus strain directions of compression loading and extension unloading and visa versa were found

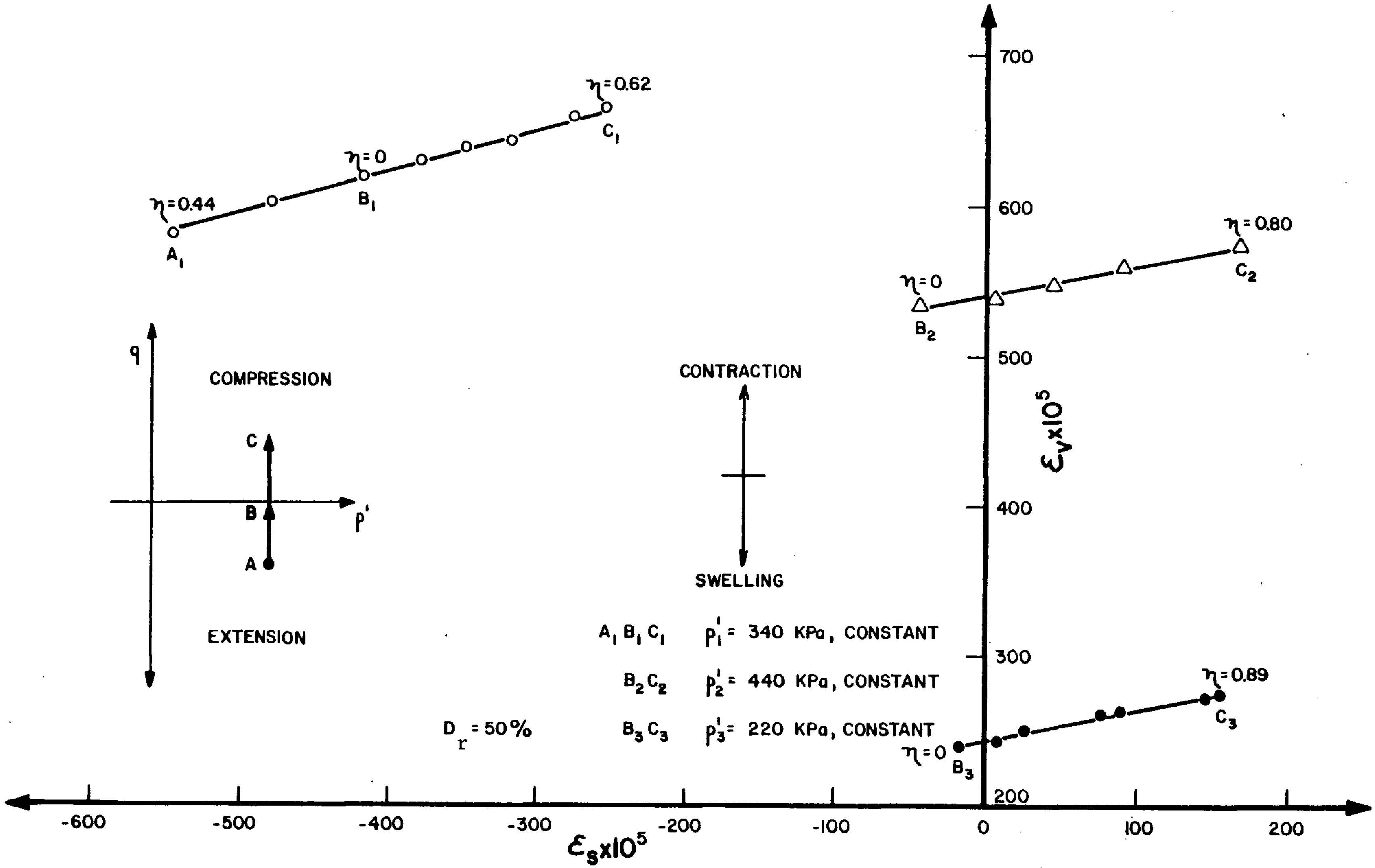

Fig. 6.13a Strain Paths for Extension Side Shear Unloading and Compression Side Shear Loading at Constant Mean Normal Stress

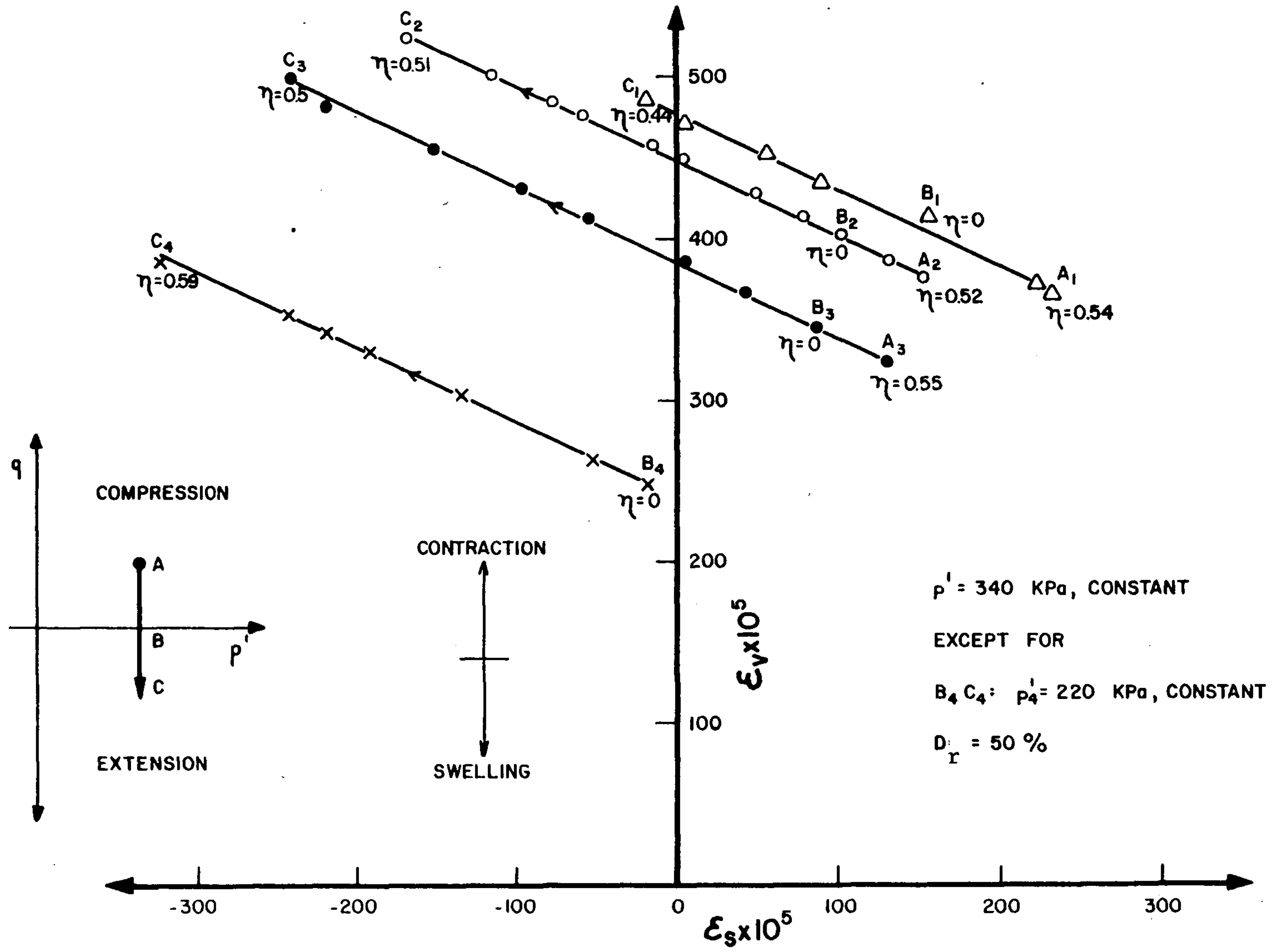

Fig. 6.13b Strain Paths for Compression Side Shear Unloading and Extension Side Shear Loading at Constant Mean Normal Stress

to be identical, magnitudes of actual strain increments vary. Within a region about the hydrostatic stress axis and small stress ratio states, strain directions depend on stress directions regardless of stress reversal and sudden rotation of principal axes of stress, as happens when the stress path crosses the hydrostatic axis. However, softening or stiffening appears to occur simultaneously and in the same sense relative to both axial and radial strain componments preserving strain proportionality.

The stress strain results of compressional unloading and extensional loading at constant p' are shown in Figure 6.14.a. Results for compression loading and extension unloading are presented in Figure 6.14.b. Stress-strain responses to virgin extension and compression loadings are also shown in Figures 6.14.a and b, respectively. It may be noted that compared to response in virgin loading, a stress history in the opposite side has the effect of softening response on the other. In contrast, reloading without stress reversal results in a stiffer response as compared to virgin loading, Figure 4.9. However, it is common knowledge that in a virgin hystereisis loop, reloading in the same sense as virgin loading invariably results in a softer stress strain response when compared to virgin loading.

There are currently two contrasting positions relative to the influence of stress reversal on stress-strain response. Arthur (1971) and Thurairajah (1973) observed that shearing in one direction softens deformation response in the other. In their studies, stress reversal was initiated after mobilization of large strain and from a near failure stress state. Tatsuoka and Ishihara (1974) argued that the

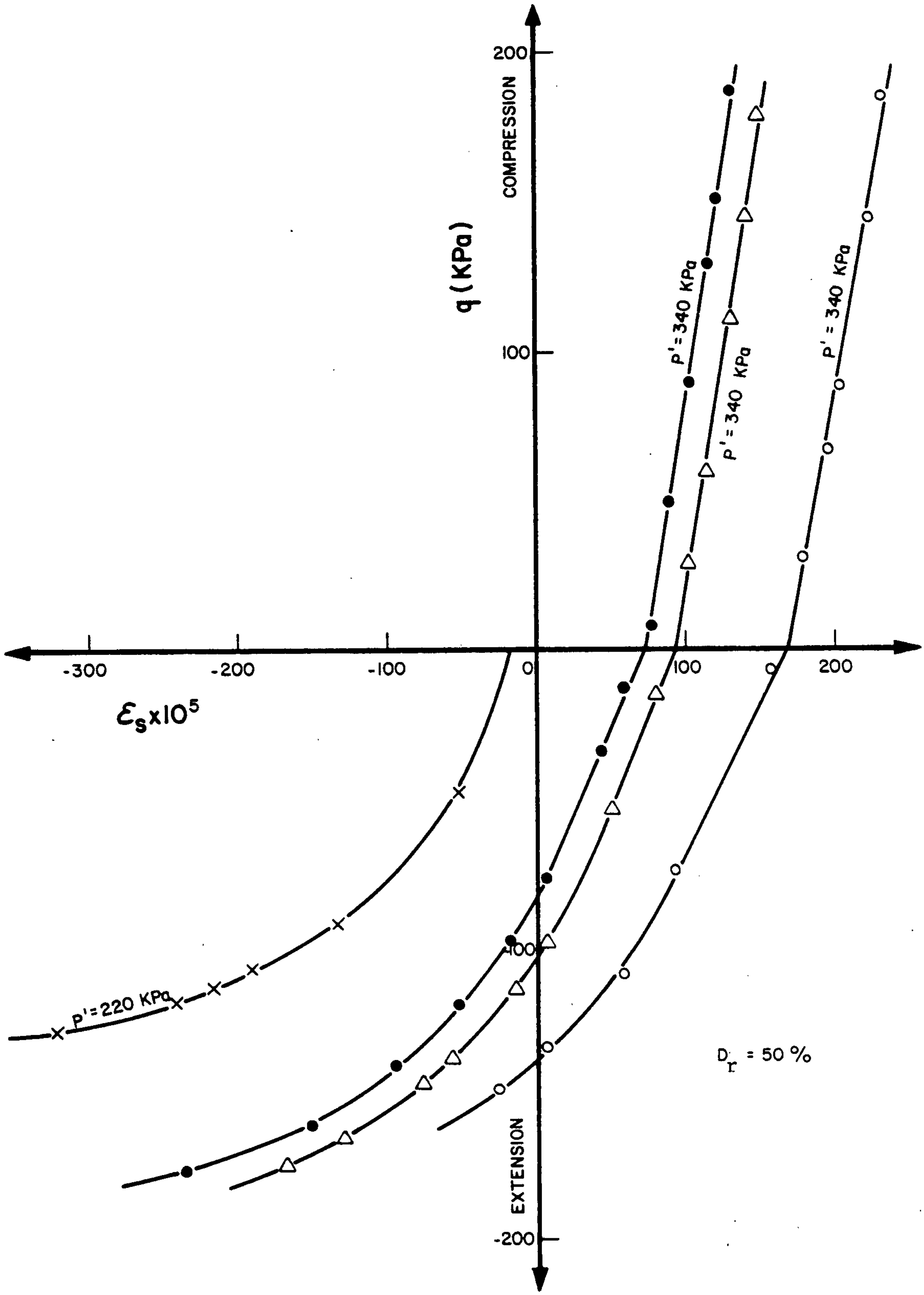

Fig. 6.14a Relationships Between Shear Stress and Shear Strain for Compression Side Unloading and Extension Side Loading of Shear Stress at Constant Mean Normal Stress

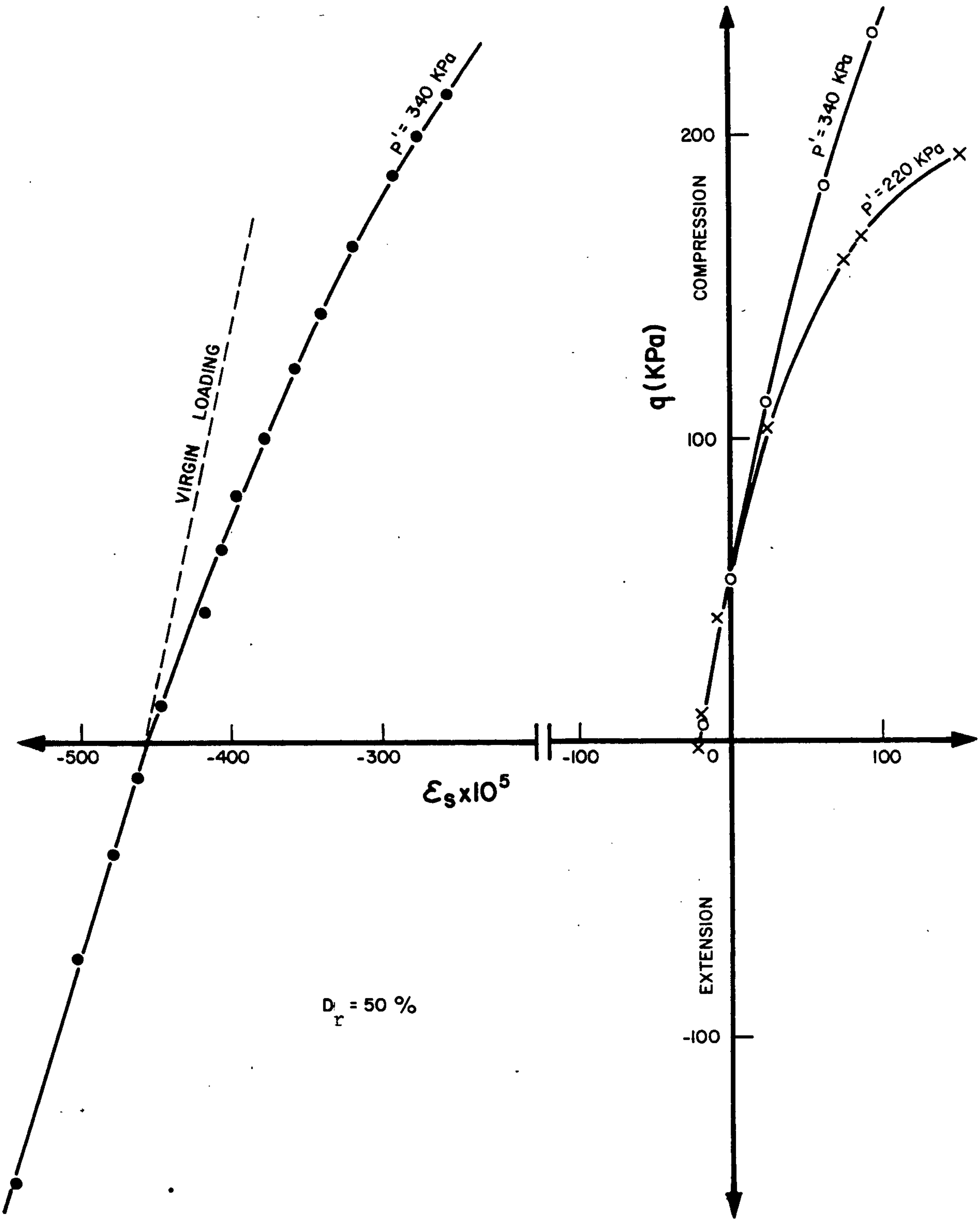

Fig. 6.14b Relationships Between Shear Stress and Shear Strain for Extension Side Unloading and Compression Side Loading of Shear Stress at Constant Mean Normal Stress

observations of Arthur and Thurairajah are due to stress reversal from near failure states and attendant changes of internal structure and grain orientation as a consequence of stress induced anisotropy. They presented experimental results in support of stress reversal and stress history having no influence on response on the opposite side so long as low amplitude shear stress levels are being considered. The experimental results presented herein do not support the findings of Tatsuoka and Ishihara. At the same time, stress reversal in these results was accomplished at small stress ratio and small strain levels. Hence, it would be difficult to justify agreement with the findings of Arthur and Thurairajah on the same basis of a change in internal structure due to stress induced anisotropy.

Stress reversal from both extension and compression modes introduces a distinct change in stress-strain response. Loading following stress reversal and reloading without stress reversal are both initiated from a state of residual shear strain. When the sense of the residual strain is the same as the direction of loading, such as in the case of reloading without stress reversal, a stiffening response is observed. Whereas, the opposite is true when the sense of residual strain is opposite to the direction of loading, as in the case of loading following stress reversal. These observations would appear to be described by the deformation mechanism of linked springs and friction blocks proposed by Zytynski et al (1978).

At small strain, both sliding and elastic deformation of the grains occur with relative importance. On application and removal of a disturbing force in one direction, all of the elastic energy stored would not be released on account of counter sliding resistance.

Consequently, the magnitude of disturbing force necessary to initiate sliding in a direction opposite to the sense of the residual strain would be less than would otherwise be required if motion were to be initiated from virgin loading. On the other hand, a large disturbance would be required to initiate sliding on reloading and in the same sense as the residual strain.

CHAPTER VII - SUMMARY AND CONCLUSIONS

This research is a fundamental investigation of sand behaviour at small strain. Test equipments and procedures were critically evaluated and improved to enable precise load application in different stress paths, accurately measure small deformations and ensure reproduction and consistency of test results. The experimental programme was designed to systematically examine some common frameworks as well as experimental evidence in support of fundamental assumptions necessary for incremental elastic, elasto-plastic and particulate concepts for modelling sand behaviour. New experimental observations are presented. Alternative fundamental interpretation and stress-strain relationships are proposed on the basis of the experimental findings. The present form of the stress-strain model proposed in this research handles contractant proportional loading but includes relative density as a separate parameter. Some common ground between proportional and nonproportional loading behaviour is indicated and future extension of the reported development may be possible through further experimental study.

A value of initial Young's modulus is often used as a key parameter for representing the nonlinear stress-strain response of sand analytically. Initial moduli, E_{max}, determined from resonant column tests are compared with initial moduli from conventional triaxial tests and conditions of virgin loading, E_i; unloading E_{iu} and reloading, E_{ir}. The test results show that E_{max} is unattainable from virgin loading and that suitable initial moduli for characterizing large strain response are generally different from E_{max}. However, initial Young's moduli from unloading, E_{iu}, are close to E_{max}, relatively independent of the deviator stress level from which unloading is initiated and number of cycles of loading. On subsequent reloadings, moduli, E_{ir}, remain intermediate between E_i and E_{max}. Moduli evaluated at common stress points vary depending on the stress path followed in reaching the stress state.

The stress dilatancy equation does not characterize the behaviour of sand at small strain. Nonrecovered strain directions are found to depend on stress direction which leads to intersection of plastic potentials. This is in contrast to large strain behaviour where strain increment directions depend only on stress state and are independent of stress increment direction. As well, the concept of normalized work and suggested fundamental parameter for sand is not valid for describing small strain response.

Because strain increment ratios are associated with stress increment ratios at small strain, proportional loading paths are uniquely related to linear strain increment directions. In strain space, mean normal stress equipotentials are parallel with essentially the same orientation for different relative densities. The ratio of energy density increments between two proportional loading paths that have identical mean normal stress histories remains relatively constant. These observations lead to a framework capable of characterizing proportional loading response within and across relative densities.

Parallel stress paths initiated from different levels of hydrostatic compression result in parallel strain paths. For stress path orientations below an overall stress ratio of $1/K_o$, strain paths remain linear and parallel, essentially without limit. However, in stress paths leading to failure, strain paths become nonlinear at higher stress ratio states. The magnitude of stress ratio above which strain path linearity terminates appears to increase with relative density.

In nonproportional loading paths, stress ratio equipotentials along initial linear strain path segments are linear and appear to radiate from a common point. Initial segments of parallel stress paths can be normalized, with respect to the corresponding hydrostatic compression stress, utilizing this result. The normalized relationship can be considered common for all paths considered.

Paths of constant shear stress, increasing mean normal stress and decreasing stress ratio are found to generate volumetric and no shear strain. However, when constant shear paths in decreasing mean normal stress and increasing stress ratio are followed, initial swelling is observed. The magnitude of rebound decreases with shear stress level. After initial swelling, response is different in compression as opposed to extension modes. On the compression side, initial swelling with zero shear strain is followed by dilation. In extension mode, initial swelling with no shear strain is followed by contraction and then dilation.

Constant mean normal stress paths result in unique strain increment directions. Compression and extension side shear loadings are associated with different strain directions. However, strain paths for compression side shear loading are identical to paths of extension side shear unloading and those for extension side shear loading are the same as for compression side shear unloading. For comparable levels of shear stress increments, more shear strain is generated and the rate of volumetric strain with shear strain during compression side shear unloading and extension side shear loading is much higher than for extension side shear unloading and compression side shear loading.

Within the confines of small strain considerations, accumulated levels of individual strain components reflect a dependence on stress-strain history. However, strain increment directions appear to depend on stress increment direction, independent of stress history or sense of loading or unloading. Small strain shear volume response is contractant for both an increasing and decreasing shear stress increment, whereas the sense of shear strain increment alternates with the sense of the shear stress increment.

The shear strain response of sand, that is in a hydrostatic stress state and subjected to an increment of shear stress, depends on the state of strain. If the sense of shear strain state is opposed to the sense of the stress increment, the stress-strain response is softer than is the case when both the strain state and the stress increment are of the same sense.

REFERENCES

Arthur, J.R.F. (1971) New Technique to Measure New Parameters. Proc. Roscoe Memorial Symposium, Cambridge University, 340-346.

Arthur, J.R.F. and Menzies, B.K. (1972) Inherent Anisotropy in a Sand, Geotechnique, Vol. 22, No. 1, 115-128.

Arthur, J.R.F., Chua, K.S., Dunstan, T. and Rodriguez del C.J.I. (1980) Principal Stress Rotation: A Missing Parameter. ASCE, Journal of the Geotechnical Engineering Division, Vol. 106, No. GT4, 419-433.

Barden, L. and Khayatt, A.J. (1966) Incremental Strain Rate Ratios and Strength of Sand in the Triaxial Test. Geotechnique, Vol. 16, No. 4, 338-357.

Barden, L., Khayatt, A.J. and Wightman, A. (1969) Elastic and Slip Components of the Deformation of Sand. Canadian Geotechnical Journal, Vol. 6, No.3, 227-240.

Barden, L., Ismail, H. and Tong, P. (1969a) Plane Strain Deformation of Granular Material at Low and High Pressures. Geotechnique, Vol. 19, No.4, 441-452.

Bardet, J.P. (1983) Applications of Plasticity Theory to Soil Behaviour: A New Sand Model. Ph.D. Thesis, California Institute of Technology.

Bishop, A.W. (1950) Discussion. Geotechnique, Vol 2, No. 2, 113-116.

Bishop. A.W. (1964) Correspondence. Geotechnique, Vol. 4, No.4, 370-371.

Bishop, A.W. and Green, G.E. (1965), The Influence of End Restraint on the Compression Strength of a Cohesionless Soil. Geotechnique, Vol. 15, No. 3, 243-266.

Budhu, M. (1984) Nonuniformities Imposed by Simple Shear Apparatus. Canadian Geotechnical Journal, Vol. 21, 125-137.

Byrne, P.M. and Eldridge, T.L. (1982) A Three Parameter Dilatant Elastic Stress-Strain Model for Sand. Proceedings International Symposium on Numerical Methods in Geomechanics, Zurich, 73-79.

Chan, C.K. (1975) Low-Friction Seal System. ASCE, Journal of the Geotechnical Engineering Division, Vol. 101, No. GT9, 991-994.

Chaney, R. and Mulilis, J.P. (1978) Suggested Method for Soil Specimen Remolding by Wet-Raining. ASTM, Geotechnical Testing Journal, Vol. 1, 107-108.

Chang, C.S. (1983) Constitutive Modelling for Sand - A Particulate Mechanics Approach. Proceedings of the International Conference on Constitutive Laws for Engineering Materials, Tucson, Arizona, 175-182.

Chen, L.S. (1948) An Investigation of Stress-Strain and Strength Characteristics of Cohesionless Soils. Proceedings, 2nd International Conference on Soil Mechanics and Foundation Engineering, Rotterdam, Vol. 5, 35-43.

Chern, J.C. (1984) Forthcoming Ph.D. Thesis. Department of Civil Engineering, the University of British Columbia.

Cheung, E. (1984) Forthcoming M.A.Sc. Thesis. Department of Civil Engineering, the University of British Columbia.

Cole, E.R.L. (1967) The Behaviour of Soils in the Simple Shear Apparatus. Ph.D. Thesis, Cambridge University.

Coon, M.D. and Evans, R.J. (1969) Discussion. ASCE, Journal of the Soil Mechanics and Foundation Division, Vol. 95, No. SM5, 1281-1283.

Dereswicz, H. (1958) Mechanics of Granular Matter. Advances in Applied Mechanics, Vol. V, 233-306.

Desai, C.S. and Siriwardane, H.J. (1981) Evaluation of Constitutive Parameters for Geological Materials. Symposium on Implementation of Computer Procedures and Stress Strain Laws in Geotechnical Engineering, Chicago.

Duncan, J.M. and Chang, C.Y. (1970) Nonlinear Analysis of Stress and Strain in Soils. ASCE, Journal of the Soil Mechanics and Foundation Division, Vol. 96, No. SM5, 1629-1653.

Duncan, J.M., Byrne, P., Wong, K.S. and Mabry, P. (1980) Strength, Stress-Strain and Bulk Modulus Parameters for Finite Element Analyses of Stresses and Movements in Soil Masses. Report No. UCB/GT/80-01, College of Engineering, Office of Research Services, University of California, Berkeley.

Daramola, O. and Vaughan, P.R. (1982) Discussion. Geotechnique, Vol. 32, No.1, 71-73.

El Sohby, M.A. (1969) Deformation of Sands Under Constant Stress Ratios. Proceedings, 7th International Conference on Soil Mechanics and Foundation Engineering, Mexico City, Vol. 1, 111-119.

El Sohby, M.A. and Andrawes, K.Z. (1972) Deformation Characteristics of Granular Materials Under Hydrostatic Compression. Canadian Geotechnical Journal, Vol. 9, No. 4, 338-350.

El Sohby, M.A. and Andrawes, K.Z. (1973) Experimental Examination of Sand Anisotropy. Proceedings, 8th International Conference on Soil Mechanics and Foundation Engineering, Moscow, Vol. 1, 103-109.

Frydman, S. and Zeitten, J.G. (1969) Some Pseudo-Elastic Properties of Granular Media. Proceedings of the 7 th International Conference on Soil Mechanics and Foundation Engineering, Mexico City, Vol. 1, 135-141.

Ghaboussi, J. and Momen, H. (1984) Plasticity Model for Inherently Anisotropic Behaviour of Sands. International Journal for Numerical and Analytical Methods in Geomechanics, Vol. 8, 1-17.

Ghaboussi, J. and Momen, H. (1982) Modelling and Analysis of Cyclic Behaviour of Sand. Soil Mechanics Cyclic and Transient Loading, Chapter 12, Wiley.

Green, G.E. (1969) Strength and Compressibility of Granular Materials Under Generalized Strain Conditions. Ph.D Thesis, University of London.

Green, GE. (1971) Strength and Deformation of Sand Measured in an Independent Stress Control Cell. Proceedings of the Roscoe Memorial Symposium, Cambridge University, 285-323

Griffiths, D.V. and Smith, I.M. (1983) Experience With a Double Hardening Model For Soil. Proceedings of the International Conference on Constitutive Laws for Engineering Materials, Tucson, Arizona, 553-559.

Hardin, B.O. and Drenevich, V.P. (1972) Shear Modulus and Damping in Soils: Measurement and Parameter Effects. ASCE, Journal of the Soil Mechanics and Foundation Division, Vol. 98, No.SM6, 603-624.

Hardin, B.O. (1983) Plane Strain Constitutive Equations for Soils. ASCE, Journal of the Soil Mehcnaics and Foundation Division, Vol. 109, No.GT3, 388-407.

Hill, R. (1964) The Mathematical Theory of Plasticity. Oxford University Press.

Holubec, I. (1968) Elastic Behaviour of Cohesionless Soil. ASCE, Journal of the Soil Mechanics and Foundation Division, Vol. 94, No. SM6, 1215-1231.

Horne, M.R. (1965) The Behaviour of an Assembly of Rotund, Rigid, Cohesionless Particles, I and II. Proceedings, Royal Society, A286, 62-97.

Ishihara, K. and Towhata, I. (1983) Sand Response to Cyclic Rotation of Principal Stress Directions as Induced by Wave Loads. Soils and Foundations, Vol. 23, No.4, 11-26.

Jaeger, J.C. (1964) Elasticity Fracture and Flow with Engineering and Geological Applications. Methuen, London.

Jakobson, B. (1957) Some Fundamental Properties of Sand. Proceedings 4th International Conference on Soil Mechanics and Foundation Engineering, London, Vol. I, 161-171.

Janbu, N. (1963) Soil Compressibility as Determined by Oedometer and Triaxial Tests. European Conference on Soil Mechanics and Foundation Engineering, Wiesbaden, Vol. 1, 19-25.

Januskevicius, C.K. and Vey, E. (1965) Stresses and Strains in Triaxial Specimens. Instruments and Apparatus for Rock Mechanics, ASTM, STP 392, 37-54.

Kirkpatrick, W.M. and Belshaw, D.J. (1968) On the Interpretation of the Triaxial Test. Geotechnique, Vol. 18, No.3, 336-350.

Kirkpatrick, W.M. and Younger, J.S. (1971) Pattern of Strain in Strength Test Samples. Proceedings of the First Australian-New Zealand Geomechanics Conference, Vol. 1, 377-382.

Kolbuszewski, J.J. (1948) An Empirical Study of Maximum and Minimum Porosities of Sands. Proceedings of the 2nd International Conference on Soil Mechanics and Foundation Engineering, Rotterdam, Vol. 1, 158-165.

Kolbuszewski, J.J. (1948a) General Investigations of the Fundamental Factors Controlling Loose Packing of Sands. Proceedings of the 2nd International Conference on Soil Mechanics and Foundation Engineering, Rotterdan, Vol. 7, 47-49.

Lade, P.V. and Duncan, J.M. (1976) Stress-path Dependent Behaviour of Cohesionless Soil. ASCE, Journal of the Geotechnical Engineering Division, Vol. 102, 51-68.

Ladd, C.C., Foott, R., Ishihara, K., Schlosser, F. and Poulos, H.G. (1977) Stress-Deforamtion and Strength Characteristics, State of the Art Report. Proceedings of the 9th International Conference on Soil Mechanics and Foundation Engineering, Tokyo, Vol. 2, 421-494.

Lambrechts, J.R. and Leonards, G.A. (1978) Effects of Stress History on Deformation of Sand. ASCE Journal of the Geotechnical Engineering Division, Vol. 104, No. GT11, 1371-1387.

Lui, P. (1984) Forthcoming MASc Thesis. Department of Civil Engineereing, The University of British Columbia.

Makhlouf, H.M. and Stewart, J.J. (1965) Factors Influencing Modulus of Elasticity of Dry Sand. Proceedings of the Sixth International Conference on Soil Mechanics and Foundation Engineering, Montreal, Vol. 1, 298-302.

Mehan, R.L. (1961) Effects of Combined Stress on Yield and Fracture Behaviour of Zircaloy-2. Journal of Basic Engineering, Vol. 83, 499-512.

Merkle, J.G. and Merkle, D.H. (1969) Discussion. ASCE, Journal of the Soil Mechanics and Foundation Division, Vol. 95, No. SM5, 1276-1280.

Miura, S. and Toki, S. (1982) A Sample Preparation Method and Its Effects on Static and Cyclic Deformation and Strength Properties of Sand. Soils and Foundations, Vol. 22, No. 1, 61-77.

Momen, H. and Ghaboussi, J. (1982) Stress Dilatancy and Normalized Work in Sands. Proceedings, IUTAM, Symposium on Deformation and Failure of Granular Materials, Delft, 265-274.

NSF/NSERC Workshop 1980, on Limit Equilibrium, Plasticity and Generalised Stress-Strain in Geotechnical Engineering, Montreal.

Moroto, N. (1976) A New Parameter to Measure Degree of Shear Deformation of Granular Material in Triaxial Compression Tests. Soils and Foundations, Vol. 16, No.4, 1-9.

Mroz, Z. (1983) A Constitutive Model for Clays and Sands Applicable for Both Monotonic and Cyclic Loading. Proceedings of the International Conference on Constitutive Laws for Engineering Materials, Tucson, Arizona.

Mulilis, J.P., Chan, C.K. and Seed, H.B. (1975) The Effect of Method of Sample Preparation on the Cyclic Stress-Strain Behaviour of Sand. EERC Report 75-18, University of California, Berkeley.

Newland, P.L. and Allely, B.H. (1959) Volume Changes During Undrained Triaxial Tests on Saturated Dilatant Granular Materials. Geotechnique, Vol. 9, No. 4, 174-182

Nova, R. and Wood, D.M. (1979) A Constitutive Model for Sand in Triaxial Compression. International Journal for Numerical and Analytical Methods in Geomechanics, Vol. 3, 255-278.

Nova, R. (1982) A Constitutive Model for Soil Under Monotonic and Cyclic Loading, Soil Mechanics - Transient and Cyclic Loads. John Wiley & Sons Ltd.

Oda, M. (1972) Initial Fabrics and Their Relations to Mechanical Properties of Granular Material. Soils and Foundations, Vol. 12, No.1, 17-36.

Oda, M. (1976) Fabrics and Their Effects on the Deformation Behaviour of Sand. Department of Foundation Engineering, Faculty of Engineering, Saitama University, Special Issue.

Poorooshasb, H.B., Holubec, I. and Sherbourne, A.N. (1966) Yielding and Flow of Sand in Triaxial Compression, Part I. Canadian Geotechnical Journal, Vol. 3, No.4, 179-190.

Raju, V.S. and Sadasivan, S.K. (1974) Membrane Penetration in Triaxial Tests on Sands. ASCE, Journal of the Geotechnical Engineering Division, Proceedings of ASCE, Vol. 100, No. GT4, 482-489.

Rees, D.W.A. (1981) A Hardening Model for Anisotropic Materials. Experimental Mechanics, 245-254.

Rees, D.W.A. (1981a) A Review of Stress-Strain Paths and Constitutive Relations in the Plastic Range. Journal of Strain Analysis, Vol. 16, No.4, 235-249.

Roscoe, K.H., Schofield, A.N. and Thurairajah, A. (1963) An Evaluation of Test Data for Selection of a Yield Criterion for Soils. ASTM, STP 361, 111-128.

Roscoe, K.H. and Shofield, A.N. (1964) Discussion. ASCE, Journal of the Soil Mechanics and Foundation Division, Vol. 90, No. SM1, 136-150.

Roscoe, K.H. and Burland, J.B. (1968) On the Generalized Behaviour of "Wet" Clay. Engineering Plasticity, Cambridge University Press, 535-609.

Roscoe, K.H. (1970) The Influence of Strains in Soil Mechanics, Tenth Rankine Lecture. Geotechnique, Vol. 20, No.2, 129-170.

Rowe, P.W. (1962) The Stress-Dilatancy Relation for Static Equilibrium of an Assembly of Particles in Contact. Proceedings of the Royal Society, A269, 500-527.

Rowe, P.W. and Barden, L. (1964) Importance of Free Ends in Triaxial Testing. ASCE, Journal of the Soil Mechanics and Foundation Division, Vol. 90, No. SM1, 1-27.

Rowe, P.W., Barden, L. and Lee, I.K. (1964) Energy Components During Shear Tests. Geotechnique, Vol. 14, No.3, 247-261.

Rowe, P.W. (1971) Theoretical Meaning and Observed Values of Deformation Parameters for Soil. Proceedings of the Roscoe Memorial Symposium, Cambridge University, 143-194.

Saada, A.S. and Townsend, F.C. (1981) State of the Art: Laboratory Strength Testing of Soils. Laboratory Shear Strength of Soil, ASTM, STP 740, 7-77.

Saada, A.S., Fries, G. and Ker, C.C. (1983) An Evaluation of Laboratory Testing Techniques in Soil Mechanics. Soils and Foundations, Vol. 23, No.2, 98-112.

Sarsby, R.W., Kalteziotis, N. and Haddad, E.H. (1980) Bedding Error in Triaxial Tests on Granular Media. Geotechnique, Vol. 30, No.3, 302-309.

Sarsby, R.W., Kaltesiotis, N. and Haddad, E.H. (1982) Authors Reply to Discussion. Geotechnique, Vol. 32, No.1, 75.

Seed, H.B. and Idriss, I.M. (1970) Soil Moduli and Damping Factors for Dynamic Response Analyses. Report No. EERC 70-10, College of Engineering, Univesity of California, Berkeley.

Tatsuoka, F. and Ishihara (1974) Drained Deformation of Sand Under Cyclic Stresses Reversing Direction. Soils and Foundations, Vol. 14, No.3, 51-65.

Tatsuoka, F. (1976) Stress Dilatancy Relations of Anisotropic Sands in Three Dimensional Stress Conditions. Soils and Foundations, Vol. 16, No.2, 1-18.

Tatsuoka, F., Muramatsu, M. and Sasaki, T. (1982) Cyclic Undrained Stress Strain Behaviour of Dense Sands by Torsional Simple Shear Test. Soils and Foundations, Vol. 22, No. 2, 55-70.

Taylor, D.W. (1948) Fundamentals of Soil Mechanics. John Wiley & Sons.

Thurairajah, A. (1973) Shear Behaviour of Sand Under Stress Reversal. Proceedings of 8th International Conference on Soil Mechanics and Foundation Engineering, Moscow, Vol. I, 439-445.

Timoshenko, S.P., and Goodier, J.N. (1970) Theory of Elasticity. McGraw Hill, New York.

Tobita, Y. and Yanagisawa, E. (1980) Stress Strain Relationship of Sand and Its Application to FEM Analysis. International Symposium on Soils Under Cyclic and Transient Loading, Swansea, 653-664.

Vaid, Y.P. (1983) Discussion to Cyclic Undrained Stress-Strain Behaviour of Dense Sands by Torsional Simple Shear Test. Soils and Foundations, Vol. 23, No. 2, 172-173.

Vaid, Y.P. and Negussey, D. (1983) A Simple Stress Path Analog for the Triaxial Test. Canadian Geotechnical Journal, Vol. 20, No. 4, 827-832.

Vaid, Y.P., Chern, J.C. and Tumi, H. (1983) Effect of Confining Pressure and Particle Angularity on Resistance to Liquefaction. Fourth Canadian Conference on Earthquake Engineering, Vancouver, 341-351.

Vaid, Y.P. and Negussey, D. (1984) A Critical Assessment of Membrane Penetration in the Triaxial Test. ASTM, Geotechnical Testing Journal, Vol. 7, No. 2, 70-76.

Vaid, Y.P. and Negussey, D. (1984a) Relative Density of Pluviated Sand Samples. Soils and Foundations, Vol. 24, No.2, 101-105.

Varadarajan, A., Sharma, K.G., Mishra, S.S. and Kuberan, R. (1983) Effects of Stress-Path on Stress Strain Volume Change Behaviour of Jumna Sand. Proceedings of the International Conference on Constitutive Laws for Engineering Materials, Tucson, Arizona, 289-296.

Whitman, R.V. (1957) The Behaviour of Soils Under Transient Loadings. Proceedings of the 4th International Conference Soil Mechanics and Foundation Engineering, London, Vol. I, 207-210.

Wu, H.C. and Chang, G.S. (1982) Stress Analysis of Dummy Rod Method for Sand Specimens. ASCE, Journal of The Geotechnical Engineering Division, Vol. 108, No. SM5, 1192-1197

Yamada, Y. and Ishihara, K. (1979) Anisotropic Deformation Characteristics of Sand Under Three Dimensional Stress Conditions. Soils and Foundations, Vol. 19, No.2, 79-42.

Youd, T.L. (1972) Compaction of Sands by Repeated Shear Straining. ASCE, Journal of the Soil Mechanics and Foundaion Division, Vol. 98, No. SM7, 709-725.

Zytynski, M., Randolph, M.F., Nova, R. and Wroth, C.P. (1978) On Modelling the Unloading-Reloading Behaviour of Soils. International Journal for Numerical and Analytical Methods in Geomechanics, Vol. 2, 87-94.